BNWL-1850 PT3
UC-11 50

PACIFIC NORTHWEST LABORATORY ANNUAL REPORT FOR 1973 TO THE USAEC DIVISION OF BIOMEDICAL AND ENVIRONMENTAL RESEARCH

PART 3 ATMOSPHERIC SCIENCES

Battelle
Pacific Northwest Laboratories
Richland, Washington 99352

APRIL 1974

Prepared for the U.S. Atomic Energy Commission under Contract AT(45-1):1830

BNWL-1850 PT3

PACIFIC NORTHWEST LABORATORY
operated by
BATTELLE
for the
U.S. ATOMIC ENERGY COMMISSION
Under Contract AT(45-1)-1830

Printed in the United States of America
Available from
National Technical Information Service
U.S. Department of Commerce
5285 Port Royal Road
Springfield, Virginia 22151
Price: Printed Copy $7.60; Microfiche $0.95

AEC-RL RICHLAND, WASH.

BNWL-1850 PT3
UC-11, Environmental and
Earth Sciences

PACIFIC NORTHWEST LABORATORY
ANNUAL REPORT FOR 1973
TO THE
USAEC DIVISION OF BIOMEDICAL AND ENVIRONMENTAL RESEARCH

PART 3 ATMOSPHERIC SCIENCES

By

C. L. Simpson, Manager
and
Staff of Atmospheric Sciences Program

April 1974

BATTELLE
PACIFIC NORTHWEST LABORATORIES
RICHLAND, WASHINGTON 99352

PREFACE

The Annual Report for 1973 to the U.S. Atomic Energy Commission's Division of Biomedical and Environmental Research represents a change from previous annual reports. For the past 22 years, its composition has reflected our organizational structure--each part of the report was the responsibility of the appropriate research department. In the past several years, research performed for DBER has become more interdisciplinary and more interdepartmental until now only a few projects are conducted wholly within one department. To reflect this change, this report is organized by major program categories according to our schedule-189 submissions. Each part of the Annual Report is comprised of project reports authored by scientists from several research departments. The Annual Report consists of four parts:

Part 1	Biomedical Sciences	Coordinator:	R. C. Thompson
		Editor:	J. L. Simmons
Part 2	Ecological Sciences	Coordinator:	B. E. Vaughan
		Editor:	J. L. Engstrom
Part 3	Atmospheric Sciences	Coordinators:	C. L. Simpson, C. E. Elderkin
		Editor:	J. A. Powell
Part 4	Physical and Analytical Sciences	Coordinator:	J. M. Nielsen
		Editor:	L. L. Lahart

Reports issued are as follows:

Annual Report for	
1951	HW-25021, HW-25709
1952	HW-27814, HW-28636
1953	HW-30437, HW-30464
1954	HW-30306, HW-33128, HW-35905, HW-35917
1955	HW-39558, HW-41315, HW-41500
1956	HW-47500
1957	HW-53500
1958	HW-59500
1959	HW-63824, HW-65500
1960	HW-69500, HW-70050
1961	HW-72500, HW-73337
1962	HW-76000, HW-77609
1963	HW-80500, HW-81746
1964	BNWL-122
1965	BNWL-280, BNWL-235, Vol. 1-4
1966	BNWL-480, Vol. 1, BNWL-481, Vol. 2, Pt. 1-4
1967	BNWL-714, Vol. 1, BNWL-715, Vol. 2, Pt. 1-4
1968	BNWL-1050, Vol. 1, Pt. 1-2, BNWL-1051, Vol. 2, Pt. 1-3
1969	BNWL-1306, Vol. 1, Pt. 1-2, BNWL-1307, Vol. 2, Pt. 1-3
1970	BNWL-1550, Vol. 1, Pt. 1-2, BNWL-1551, Vol. 2, Pt. 1-2
1971	BNWL-1650, Vol. 1, Pt. 1-2, BNWL-1651, Vol. 2, Pt. 1-2
1972	BNWL-1750, Vol. 1, Pt. 1-2, BNWL-1751, Vol. 2, Pt. 1-2
1973	BNWL-1850, Pt. 1-4

W. J. Bair
Program Director, Life Sciences

FOREWORD

At present the Atmospheric Sciences Program is focused on atmospheric cleansing and reinsertion processes. Studies of pollutant interaction with cloud and precipitation droplets and with the earth's surface are being conducted. Accompanying them are the necessary related investigations of aerosol description and behavior, air trajectories, cloud and storm dynamics, turbulence and diffusion. The program in total is aimed at providing a continually improving capability to describe the transport of contaminants released from nuclear facilities which are ultimately delivered to human populations and ecological systems.

This report reflects the emphasis of the program on pollutant removal and resuspension processes, but also demonstrates the continuing research on all aspects of the atmospheric transport problem, from source to receptor. The report is organized in segments which deal with the various phases of the pollutants' history during transport: Characterization of Sources and Ambient Pollutants; Transport Diffusion and Turbulence; Atmospheric Transformation Processes; Removal and Resuspension Processes. The final segment, Special Studies, deals primarily with applied aspects of the research.

Not reported here are applied studies being conducted by our staff which are of concern to the AEC but are not directly related to DBER activities. A concerted effort is made to carry on applied studies concurrently with the research in order to assure that the most effective recent research findings are brought to bear on significant problems and that the most urgent needs for future research are continually being identified.

C. E. Elderkin, Associate Manager
Atmospheric Sciences Department

CONTENTS

(Listing in parenthesis denotes the sponsoring programs under which the research was done.)

CHARACTERIZATION OF SOURCES AND AMBIENT POLLUTANTS

The nature and quantity of radioactive and chemical airborne contaminants must be known before an objective assessment can be made of the consequences of these materials to the environment. Information regarding the characteristics of pollutants is mandatory for estimation of downwind concentrations of particles and gases, the significance of deposition, the probability of resuspension, and the biological significance to the receptor of interest. Atmospheric Sciences and Radiological Sciences have undertaken several studies during the past year in the area of sensitive methods of analysis for trace materials in the atmosphere. An array of low-level analytical methods has been employed to describe the nature and quantity of radioactive material and other contaminants airborne in particular situations. Reports in this section present the findings of this work.

- **PRECIPITATION SCAVENGING***
- **RADIOACTIVE FALLOUT RATES AND MECHANISMS**
- **SURVEY OF RADIOACTIVITY AND CHEMICAL POLLUTANTS**

*This list denotes the sponsoring programs for the research represented by the reports in this section.

POTENTIAL APPLICATION OF ATOMIC ABSORPTION AND ANODIC STRIPPING VOLTAMMETRY TO THE PRECIPITATION SCAVENGING PROGRAM

R. N. Lee

Rain samples from the April 16, 1972 in-cloud scavenging experiment have been analyzed by flameless atomic absorption and anodic stripping voltammetry. These techniques appear to be of potential value to the in-cloud scavenging program. However, more extensive work is required to evaluate the potential of anodic stripping voltammetry.

INTRODUCTION

In general, chemical instrumentation has advanced to the point where several options are available for the analysis of environmental samples. Although it is generally possible to detect trace constituents at and frequently below the nanogram level, the nature of these samples requires that the analyst be alert to possible sources of experimental error. Since each technique may have a unique tolerance for some of the materials which produce interference, high quality results may rest heavily on the method of analysis as well as the caution exercised in securing samples and preparing them for analysis.

This paper describes the results of a brief investigation of the potential application of atomic absorption spectroscopy and anodic stripping voltammetry to the in-cloud scavenging program. Samples acquired during a tracer release on April 16, 1971[1] have been analyzed using flameless atomic absorption for silver detection and anodic stripping voltammetry for indium detection. The results are compared with those obtained earlier using neutron activation.

Since the merits of each technique have been described in earlier reports,[2,3] this paper will be restricted to a description of sample preparation and a listing of the analytical results.

EXPERIMENT

Precipitation samples from the April 1971 in-cloud scavenging experiment had been concentrated to dryness in plastic vials for neutron activation analysis. These vials were placed in 10 ml plastic beakers, filled with distilled concentrated hydrofluoric acid (~0.5 ml) and allowed to stand overnight. The

acid was then evaporated slowly under a heat lamp, the vials rinsed three times with 10^{-2} N nitric acid and the solution brought to 2.0 ml with the dilute acid.

Silver analysis was performed with a Perkin-Elmer Model 306 atomic absorption spectrometer equipped with a HGA-70 graphite furnace and deuterium background corrector. At least two aliquots of each solution were removed for analysis and the remaining solution (at least 1.5 ml) held for the indium analysis.

The contents of the volumetric flasks remaining after silver analysis were poured into 10 ml beakers, the flasks rinsed with 2 to 3 ml of 10^{-2} N nitric acid and the solution evaporated to dryness under a heat lamp. The residue was prepared for anodic stripping voltammetry by dissolving it in 5.0 ml of a solution 2 M in lithium chloride and 0.5 M in sodium acetate. Perchloric acid was added (40 µl) to bring the pH to about 4.5 and the solution allowed to stand overnight. The indium content of these solutions was determined by use of the Model 2014 Anodic Stripping Voltammeter and Model 1014 Cell Holder manufactured by Environmental Science Associates. Following reduction of the electroactive metals into the mercury skin of the composite graphite mercury test electrode, the electrode potential was varied anodically. Oxidation of the dissolved metals occurred at voltages characteristic of the respective metals and with currents directly related to the mass oxidized. Figure 1 illustrates the appearance of a strip chart recording of current versus voltage for Sample 57. The relatively intense peaks observed at the oxidation potentials of cadmium and lead are due in part to the trace metal content of the reagents. The magnitude of this contamination is, however, insufficient to interfere with the indium determination. Instrumental settings used for this analysis are summarized in Table 1 along with those employed for the silver analysis.

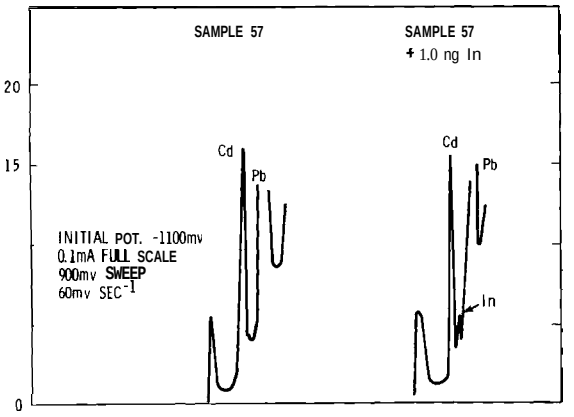

Neg 740938-6

FIGURE 1. Scan of Current Versus Voltage for Sample 57 Before and After the Addition of 1.0 ng Indium

TABLE 1. Summary of the Instrumental Settings Used for the Silver and Indium Analyses

Metal	Analytical Method	Instrumental Settings
silver	flameless atomic absorption	wavelength - 328 nm lamp current - 12 mA atomization temp. - 2250°C
indium	anodic stripping voltammetry	plating potential --1100 MV sweep rate - 60 MV/sec sweep range - 900 MV plating time - 30-45 min

RESULTS

Data acquired from the analysis of eight samples from the April 1971 scavenging experiment are listed in Table 2. Agreement is generally satisfactory although some discrepancies are disturbing. The thermal stress experienced by the vials during neutron activation undoubtedly contributed to the migration of some of the tracer into the container walls. Inability to achieve total recovery of tracer is therefore to be expected. But the poor agreement between the silver results obtained for Sample 6 via neutron activation and atomic absorption cannot be attributed solely to this mechanism.

The data recorded for the ASV analyses are generally in keeping with the expected irreversible loss of indium to the plastic vial. This method of analysis offers no advantage in terms of detection limit although some improvement may be realized. by varying the experimental conditions.

Final appraisal of these techniques must await a more extensive survey of precipitation samples.

TABLE 2. Summary of the Results Obtained from the Dual Analysis of Precipitation Scavenging Samples

Sample	ng Ag		ng In	
	NAA	AA	NAA	ASV
4	<1	0.85	2.93 ± 0.21	∿1
6	30 ± 10	0.10	N.D.	∿1
36	<1	0.53	N.D.	<0.5
48	<1	0.30	N.D.	<0.5
57	<1	0.50	0.68 ± 0.34	<0.5
66	<1	0.30	N.D.	<0.5
75	<1	0.10	1.98 ± 0.99	<0.5
88	<1	0.10	0.46 ± 0.23	∿1

QUILLAYUTE AIR REFERENCE STATION

R. W. Perkins, J. D. Ludwick, C. W. Thomas
M. R. Petersen and J. A. Cooper

The Quillayute Air Base[X] has been selected for the air reference station necessary to sample and monitor air constituents. Installing of appropriate instrumentation there is near completion, and a large variety of air constituents is now under study using sampling and monitoring techniques. High-volume air filtration provides samples for measuring the concentration of a wide spectrum of radionuclides, while their physical size distribution is determined from high-volume impactor samples. Plans for gaseous radionuclide measurements are also being implemented. Monitoring is under way for the gaseous constituents ozone and nitrogen oxides while plans for carbon monoxide and oxides of sulfur are near completion. A constant monitor is kept on the particulate air levels as well as a rather detailed analysis of some 30 stable elements from sampling of these particulates. Size and elemental distributions are continually measured as well. The hemispheric concentrations of certain organic constituents are measured by coordinating the meteorological watch for fresh air masses with certain sampling techniques.

INTRODUCTION

Air pollutants produced regionally not only contaminate their area of origin but also become distributed throughout the hemisphere and transfer between hemispheres. The seriousness of this global air pollution may increase with continued industrialization and fossil fuel and nuclear power generation. It is desirable, therefore, to define current air concentrations of the various gaseous and particulate pollutants present in the atmosphere from these sources. This study will provide basic information on hemispheric pollutant levels; the influence of meteorological conditions; biological hazards to be anticipated; and a basis for assessment of possible worldwide control measures and the establishment of acceptable environmental pollutant levels.

INSTALLATION

A permanent air sampling base for radionuclide measurements has been set up at the Quillayute Air Base in northwestern Washington State. A rather detailed meteorological study indicated that this was the best

---

* Quillayute Air Base, 47° 50'N - 124° 34'W is 3 miles inland of the Pacific Ocean in Northwestern Washington State adjacent to the coastal section of the Olympic National Park near Forks, Washington. The Ouillayute site, controlled by the Washington State Aeronautics Commission, has been decommissioned as an airbase. Their permission to establish the monitoring station and their cooperation have facilitated its expeditious construction and operation, and their help is gratefully acknowledged.

location to meet the overall program objectives. The sampling for non-radioactive pollutants with different requirements took the form of investigating the Aitken nuclei count at four stations along the coast.(4) All of these showed considerable variation and indicated the influence of pollutants of local origin at some times. A rather encouraging bit of information was obtained at the Quillayute sampling station which suggested that sampling somewhat above ground level would reduce and in some instances eliminate local contamination problems encountered. Measurements of Aitken nuclei counts between ground level and the elevated intake at 50 ft are continuing while a new, higher intake at 100 ft is under construction. Meteorological considerations of 18-hr atmospheric back trajectories for the more promising investigated locations indicated a higher probability for persistent westerly, unpolluted air flow near the northern Washington sites. Since data from the four sites studied were somewhat inconclusive and several major operational advantages would be realized at Quillayute, this site was selected as our permanent air monitoring station.

Equipment has been established and we have initiated sample collection for many of the radionuclides of interest. A 600-cfm pump has been installed for the continuous collection of aerosols for radionuclide measurements. Also three Cascade impactors are in operation. One of these operates only when the Aitken nuclei count is below a predetermined level indicative of marine aerosol. Noble gas sampling has not yet been initiated; however, the technology for measuring argon-37 as well as the much more abundant krypton and xenon radionuclides is being developed. Construction of an Oesger-type low background-high pressure counter is near completion and will be used to measure noble gases. Equipment for the continuous measurement of NO_x and ozone is now operational. The specific equipment for continuously monitoring SO_x is as yet unresolved; however, scrubber sampling of SO_2 in the field followed by laboratory analysis is the interim method. Laboratory techniques for analysis of DDT and PCB's which may be adequate for measurement of these chlorinated hydrocarbons have been developed and are in use. Samples are routinely obtained from high-volume filters used in measuring the presence of a large number of stable elements by X-ray fluorescence and neutron activation analysis techniques. Wet and dry fallout samples are obtained from an automated collector loaned to the program by the New York Health and Safety Laboratory.

To meet the basic needs of this program several important factors were given consideration. It was necessary to establish a permanent base at the favored site and to include the necessary facilities anticipated for all types of air sampling and monitoring. Subsequent to this, the permanent station must be equipped for the pollution monitoring purpose in a systematic manner.

The desired pollutant analysis priority must be balanced by availability of equipment suitable for sensitive base line monitoring purposes as well as availability of funding. Emphasis was placed on pollutants whose excess presence may be hazardous to life forms. Particular emphasis must also be placed on the individual isotope and/or overall radiation dose to the human community.

The permanent monitoring station at Quillayute consisted of a large, 10 ft wide × 60 ft long mobile trailer. This is shown in Figure 2. It is located on the western edge of the base, some distance from the few personnel activities that still remain. The trailer has been provided with all the necessary facilities anticipated for its complete operation as an independent air pollutant monitoring station. This includes the necessary power for instrumental operation and internal environmental controls. An air stack was constructed which allows air sampling and monitoring from the 50 ft level by instruments located within the station. A security fence enclosure protects the high-volume impactor samplers and all other equipment that must be external to the trailer for effective pollutant measurement. A 1000-ft extension of

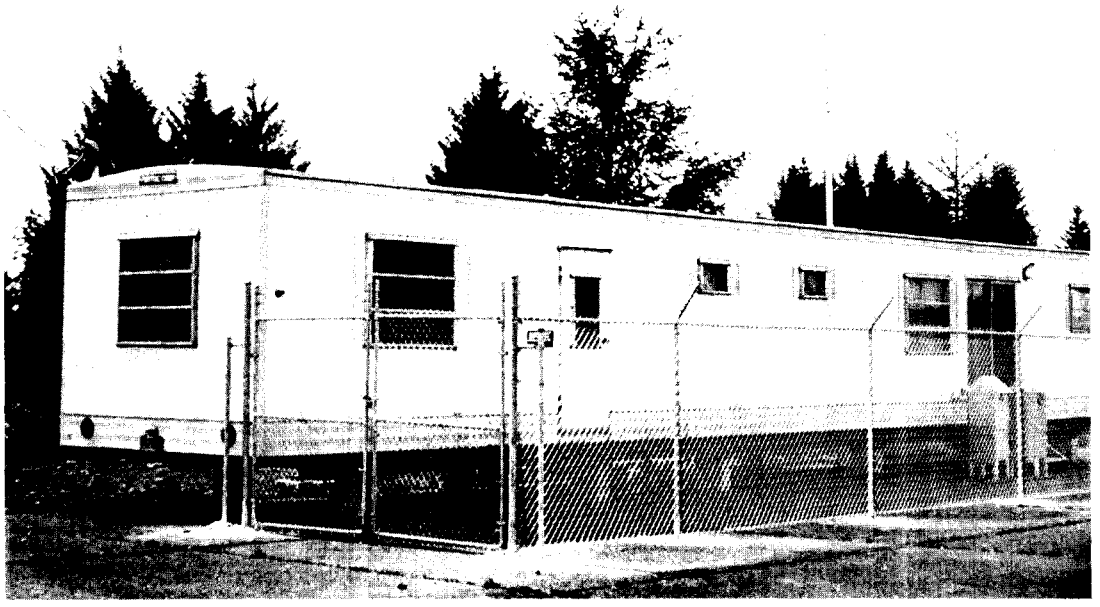

Neg 735833-5

FIGURE 2. Permanent Monitoring Station at Quillayute

the existing three-phase power line was necessary to position the trailer so that the westward fetch would be unobstructed. As previously noted, construction is under way on a 100-ft sampling stack including high-volume sampling capability to replace the existing shorter version.

Table 3 illustrates the sampling periods used for various collectors.

TABLE 3. Particulate Air Sampling Devices at Quillayute

Materials Measured	Collector	Standard Collection Interval
Radionuclides (gross)	600-cfm Pump	14 days
Radionuclides Size Distribution	40-cfm Andersen Impactors	7 days
Stable Elements	1-cfm Pump	1 day
Stable Elements Size Distribution	1-cfm Andersen Impactor	7 days
Organic Particulates	600-cfm Pump	8 hr to 2 days

PARTICULATE LEVELS

A condensation nuclei monitor (Environment/one, Model Rich 100) was used to constantly monitor the particulate levels of air entering the 50-ft sampling stack. This instrument was equipped with an automatic range changing feature so as to allow unattended operation over long periods of time. There are seven instrumental ranges whose specific position is indicated by a 1 to 7-volt level applied to an output terminal. The instrumental output as well as this voltage level is monitored by a multipoint recorder. The lowest scale of this instrument is 0 to 1000 nuclei/ml. When the particulate level exceeds 75% of any scale the instrument moves to the next higher scale, i.e., 750 nuclei/ml. This particular point is of importance since the 1-V level is also used to actuate a relay whose primary contacts control the flow of 110 V to a bank of receptacles. Any instrumental or pumping operations using 110 V can then be made to operate only when the particulate levels are low or in other words, only during periods of relatively clean air. In certain selected instances the operation of the 1 cfm Andersen 7-stage impactor was so controlled.

At this time a full year of particulate monitoring data is available from the station. The most prominent feature of the data is the recurring short-term sharp increases in the levels, probably due to pollutant sources. No pronounced seasonal changes were observed; however, typical summer levels were higher than other seasons. Although average values may be somewhat misleading since daily fluctuations were often severe, the rural particulate levels observed were about 1000 condensation nuclei/ml with summertime levels of 2000-3000 CN/ml. Rarely and only for short time intervals did the levels exceed 10,000 CN/ml during the year.

When a fresh western air mass entered the region, considerable change was noted. The average levels dropped dramatically with typical frontal passage to values between 10 and 200 CN/ml. This decrease was evident even when no precipitation

accompanied frontal passage. These "clean air" levels were observed to persist for several days on some occasions. Although onshore air flow in itself generally produced levels somewhat below the 1000 CN/ml average values, the particulate levels were more indicative of the recirculatory history of the air parcel in the general air mass than that of any "clean air" nuclei concentrations. Figure 3 illustrates the particulate levels before and after a "clean air" mass passed into the monitoring region. The sharp delineation of particulate levels appears appropriate for interpreting time of frontal passage.

QUILLAYUTE OZONE CONCENTRATIONS

On July 1, 1973 an ozone monitor (Bendix Series 8000) was added to the high-level air intake stacks.

Local ozone levels were observed to fluctuate with low values observed daily from 2300 to 0700. During these hours the ozone concentration was typically below 10 ppb (12 $\mu g/m^3$). During a typical day (0700 to 2300 hr) air concentrations varied between 20 and 40 ppb. (See Figure 4.) The maximum observed value during July 1973 was 45 ppb while the overall maximum value, 55 ppb, observed through November 1 occurred October 19. Twice during July the values exceeded 40 ppb, each time at the rear of cyclonic conditions and some 200 miles from the pressure center. Both this effect and the diurnal effect have been previously reported. Figures 5 and 6 illustrate the maximum observed daily ozone-air concentrations.

Clean air ozone levels were about 30 ppb during July, assuming that the highest values obtained during the day are most representative of the tropospheric concentrations. This is based on the assumption that best mixing occurs during the day, particularly late in the thermal uplifting period, and extends into evening. At that time a minimum of surface and low-level ozone depletion occurs. The average ozone concentrations for October exceeded those for the summer months and, in addition, very high daily levels were recorded. The onset of these higher levels appeared to coincide with the onset of vigorous fall weather activity in early October. At that time there was a southerly shift in the jet stream air pattern from its usual more northerly deflection to a position in the vicinity and south of the monitoring station. Consequently, the usual fall reduction in ozone levels reported by worldwide observers has not been observed this fall at Quillayute.

The diurnal effect has been attributed to the increased stability of the air during the nighttime period. It has been shown that in stable air with small eddy diffusion, ozone increased rapidly above the ground (indicating a downward flux). Ozone is probably destroyed in the stable air layer not only by ground contact, but within the stable layer as the result of accumulated pollution. The data indicate ozone depletion even with

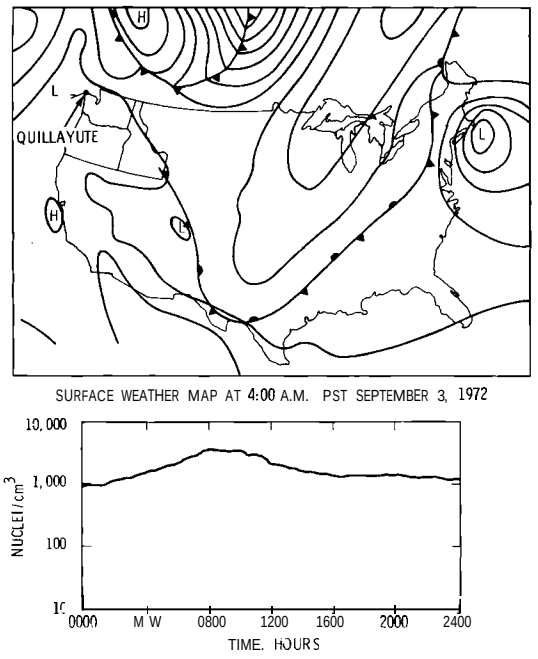

Neg 740040-2

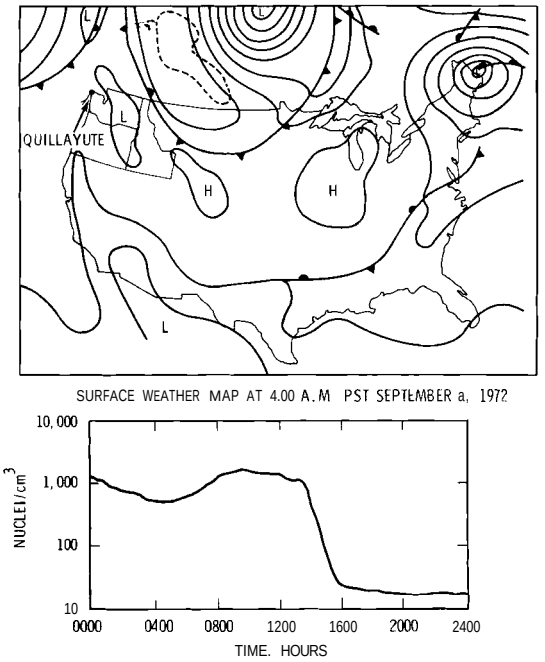

Neg 740040-3

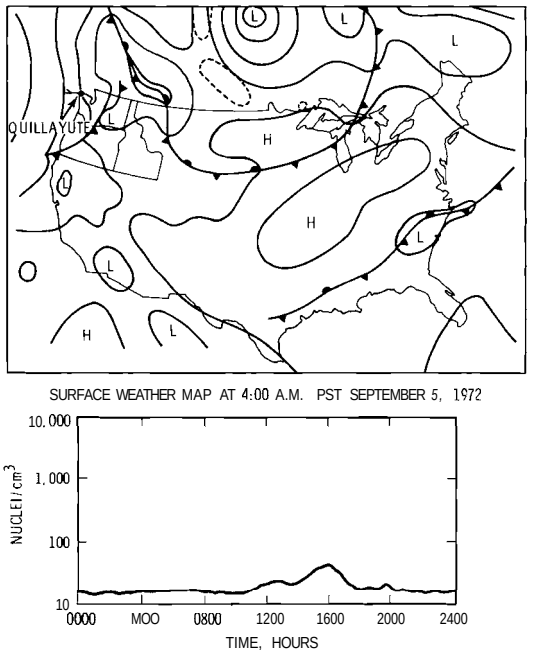

Neg 740040-1

FIGURE 3. Comparison of Surface Air Mass Position with Particulate Levels

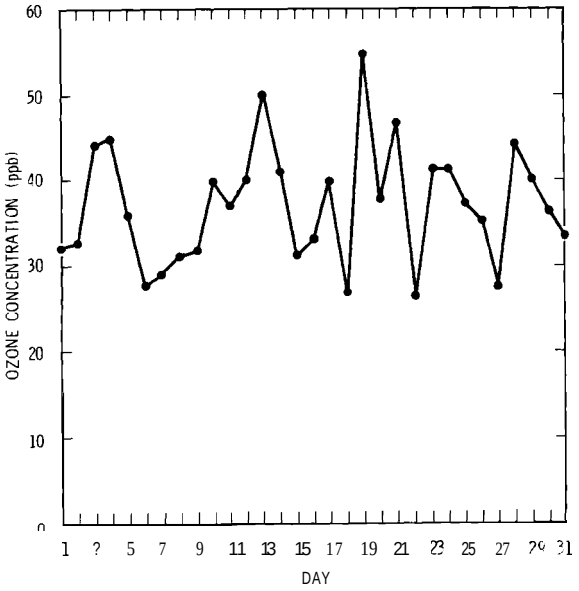

Neg 740040-6

FIGURE 4. Typical Daily Quillayute Ozone Levels, October 1, 1973

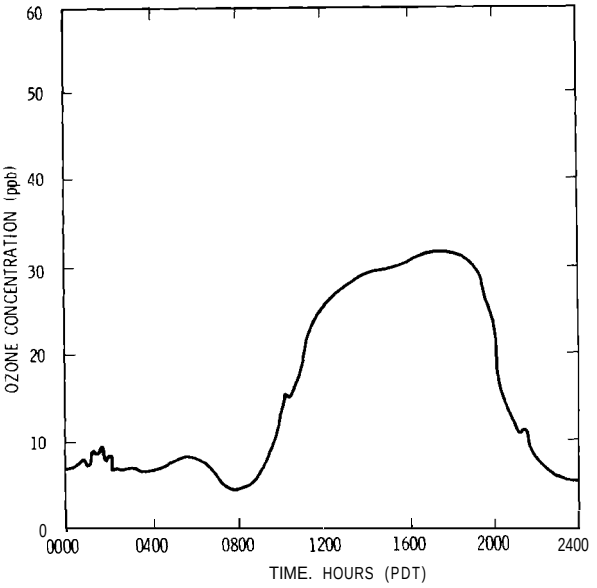

Neg 740040-4

FIGURE 6. Maximum Daily Quillayute Ozone Levels, October 1973

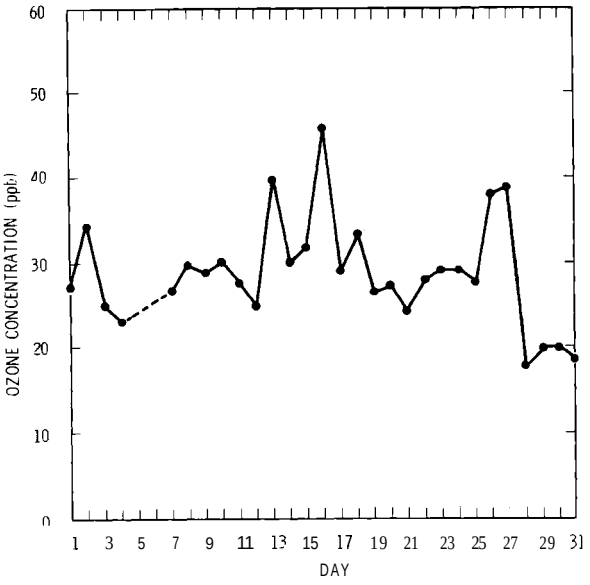

Neg 740040-5

FIGURE 5. Maximum Daily Quillayute Ozone Levels, July 1973

the sampling port at 17 m. It is obvious that the stable layer is many times this level during the night.

Correlations were observed between increasing particulate levels and decreasing ozone concentrations. These were due presumably to reaction of the ozone with the particulate or other pollutants which accompany this prime indicator of contaminated air. This phenomenon was most discernible when particulate levels approached or exceeded 10^4 nuclei/cm^3 or when unusually high particulate levels occurred during early morning periods. This latter case resulted in a further reduction of the already decreasing ozone concentration in the early morning and was clearly evident.

Air concentrations as low as 2 ppb were observed during such periods.

QUILLAYUTE NO_x LEVELS

October 1, 1973 a nitrogen oxide analyzer (REM Mode 642) was added to the instrumentation measuring the high-level stack input air. This instrument is capable of independently measuring NO and NO_2 air concentrations. Data through November 1, 1973 indicate that most of the material occurs as NO_2 with about 10 to 20% being NO. The basic air concentrations vary from 1 to 4 ppb with occasional rises to 10 ppb when local rural contamination is present. The measured levels at Quillayute are equal to or higher than those observed on Hawaiian and coastal Florida locations.

ATMOSPHERIC ORGANIC CONSTITUENTS

Both gaseous and organic pollutants absorbed on particulates have been investigated in the urban atmosphere where air pollution, especially photochemical smog, exists. Some organic compounds, though pollutants, are potentially useful as tracers of air mass movements. At the research station in Quillayute, Washington, particulate and gaseous samples are being collected to establish the background atmospheric concentrations of selected organic compounds and the usefulness of these compounds as tracers.

Whole gas samples were collected in evacuated gas bottles (~0.5ℓ vol) and returned to the laboratory for analysis of trichlorofluoromethane (Freon-11) by gas chromatography using an electron capture detector.

Particulate samples were collected on various filter materials using high-volume air pumps. Initial samples collected on Millipore^{C} filters were not suitable for organic analysis due to contamination from the Millipore^{C} substrate. Adequate samples were obtained when specially cleaned fiberglass filters were used as collectors and the sampling interval of the 600-cfm pump extended to 2 days.

The 600-cfm pump (17 m^3/min) operates with a filter head containing eight 1-ft^2 filter surfaces. Membrane filters were normally used as absolute filter surfaces. However, during selected periods of onshore flow from trans-Pacific trajectory air masses, special efforts were made to change the filter surface to the treated glass material. Definitive "clean air" samples were obtained in a minimum of time by maintaining a meteorological watch on the station site and forecasting the expected duration of any onshore flow. The prebaked filters were then returned to their original container and delivered to the Richland, Washington laboratory for analysis.

Benzene extracts of the particulate samples on the glass filters were concentrated and initially subjected to chromatographic separation on alumina using benzene as the elutant. Recoveries for the compound classes of interest were: 80 to 90% for n-alkanes and chlorinated

pesticides and 50 to 60% for polycyclic aromatic hydrocarbons. The results obtained show that the air during onshore flow at Quillayute contained less than 40×10^{-12} g particulate n-alkanes ($C_{12}H_{26}$ - $C_{32}H_{66}$) /m^3 air (reported concentrations in American urban atmosphere = 2-77 × 10^{-9} g/m^3) and less than 80×10^{-15} g particulate p,p'-DDT or p,p'-DDE/m^3. (Reported concentrations over the Atlantic Ocean = 78×10^{-15} g/m^3 and 212×10^{-15} g/m^3.)

The volume ratio of CCl_3F in onshore air was just detectable at a160×10^{-12} (reported concentration over the Atlantic Ocean at 45°N = 80×10^{-12}). Further sampling methods are being planned to obtain larger particulate samples and to analyze larger gas samples, thus improving the overall sensitivity for organic constituents at the background levels in oceanic air.

RADIONUCLIDE CONCENTRATIONS SAMPLED

The concentrations of some 19 radionuclides were measured in air at the Quillayute monitoring station during 1973. Samples were obtained by passing large volumes of air (17 m^3/min) through Millipore membrane filters for 2-week sampling periods. Shorter sampling periods were occasionally used in special circumstances. The Millipore filter membranes have been shown to be essentially absolute for removing atmospheric aerosols associated with radionuclides. The radionuclides were measured using large Ge(Li) diodes and the concentration of the gamma-emitting radionuclides determined. The radionuclide concentrations measured at Quillayute during 1973 were from 1/2 to 1/10 the concentration measured at Richland, Washington. This relatively large difference is believed due to the orographic lifting by the Olympic and Cascade Mountains with subsequent vertical mixing of higher altitude and surface air prior to Richland sampling. Since the radionuclide concentration increases with altitude, the vertical mixing of the air mass by the Cascade Mountains results in higher radionuclide concentrations east of the range.

To observe any differences that might result in radionuclide contact from masses of different origin, special experiments were occasionally scheduled. One such period was from October 10, 1973 to October 12, 1973 during which time differential sampling was in effect. "Maritime air" of trans-Pacific origin was forecast and obtained for this interval. At this time the concentration of radionuclides showed a significant increase of some two to four times the average concentration measured during September 1973. This indicates that during this special sampling period significant contributions of higher altitude air were transported to surface levels, increasing the concentration to values comparable to the Richland area's.

Two high-volume Andersen Cascade impactors were operated at Quillayute to measure the radionuclide distribution of aerosols. Their combined flow allowed collection of a total

of 40 cfm. Significant samples were obtained from these impactors using a weekly changeout period. The high-volume samplers separated the atmospheric aerosol into five fractions of >7 μm, 3.3 to 7 μm, 2.0 to 3.3 μm, 1.1 to 2.0 μm, and a backup filter of 0.01 to 1.1 μm size ranges. For radionuclide measurements 8 weeks of samples were normally combined. These data showed that 83% of the ^{7}Be activity, 58% of the ^{137}Cs activity, and 44% of the fresh medium-lived nuclear debris (from the June 1973 Chinese nuclear test) were associated with particles less than 1.1 micron.

Since most of the ^{7}Be measured at ground level is produced in the stratosphere and enters the troposphere through the "tropopause gap" from late winter through early spring, it should be associated with stratospheric aerosols. Cesium-137 is produced during nuclear testing, but since 1954 surface air concentrations have shown seasonal variation indicating stratospheric origin. Therefore, ^{137}Cs should be associated with both stratospheric aerosols and tropospheric aerosols that were produced during detonation. Fresh fission products are, however, mainly of tropospheric origin and are associated with the larger tropospheric aerosols. These data would tend to confirm these suggestions. The data from the Quillayute monitoring station are summarized in Tables 4 and 5.

b.

June 26, 1973 the Chinese conducted an atmospheric nuclear test with a reported yield of "several megaton." The radioactive debris was detected in air samples collected starting on July 5, 1973 and reached peak concentrations 2 to 3 days later. Fresh fission products enriched with relatively large amounts of ^{237}U and ^{239}U characterized this test as a fission-fusion-fission type device. The concentration of fresh radioactive debris was considerably lower than from the previous Chinese nuclear test of March 1972. High-volume Andersen Cascade impactors (20 cfm) samples showed that approximately 60% of the initial fresh debris was associated with particles larger than 3.3 μm diam while only 25% was associated with particles of less than 1.1 μm diam. This pattern reversed itself on the subsequent weekly sample taken between July 10 and 19. Here approximately 60% of the total activity was associated with the very small particles collected on the membrane backup filter. Iodine-131 was found to be consistently associated with the very small particles.

TABLE 4. Distribution of Atmospheric Aerosols at Quillayute, Washington During 1973

Particle Size*	Fresh Fission Products ^{103}Ru	^{141}Ce	^{95}Nb	$\bar{X}$
	July - August			
1	12.3	15.0	19.9	15.7
2	6.5	14.7	15.6	12.3
3	17.7	12.6	14.7	15.0
4	11.6	17.0	9.2	12.6
5	51.8	40.6	40.5	44.3

* 1 = greater than 7 μm
2 = 3.3 to 7
3 = 2.0 to 3.3
4 = 1.1 to 2.0
5 = less than 1.1 (0.01 to 1.1)

TABLE 5. Distribution of Atmospheric Aerosols at Quillayute, Washington During 1973

Particle Size*	Percent Distribution: Cosmogenic ^{7}Be				Long-Lived Fission Product ^{137}Cs			
	Mar-Apr.	May-June	July-Aug.	$\bar{X}$	Mar-Apr.	May-June	July-Aug.	$\bar{X}$
1	1.8	2.8	2.1	2.2	5.5	4.2	6.0	5.2
2	2.6	2.8	3.3	2.9	5.7	5.8	9.2	6.9
3	3.2	4.5	3.6	3.8	8.4	7.2	13.6	9.7
4	8.6	7.4	7.8	7.9	22.4	20.5	18.5	20.5
5	83.9	82.5	83.1	83.2	58.0	62.3	52.7	57.7

*1 = greater than 7 μ
2 = 3.3 to 7
3 = 2.0 to 3.3
4 = 1.1 to 2.0
5 = less than 1.1 (0.01 to 1.1)

STABLE ELEMENTS IN AIR SAMPLES

Multi-element analysis of atmospheric particulates at the Quillayute reference station provides information useful in identifying aerosol sources, tracing air masses, evaluating potential health hazards and establishing a reference level to evaluate the effect of man's future activities. Neutron activation and X-ray fluorescence analysis are providing the highly sensitive and selective multi-element analyses required to measure the small amount of material collected on many of the samples. The high sensitivity provided by these techniques is especially important for studies of the clean air masses associated with onshore winds and submicron particles separated with impactors.

Measurements have been made on total filters and Andersen impactor stages collected at ground level and from a 50-ft tower. The ground-level measurements showed contributions from local sources while the measurements on samples collected from the tower during onshore winds exhibited concentrations comparable to other remote locations. The concentration of Pb averaged about 29 ng/m^3 in the ground level samples collected during March 1973. The Pb concentration in samples collected with the 50-ft tower was less than 3 ng/m^3, a value comparable to the worldwide background Pb estimate of about 1 ng/m^3. (See Tables 6 and 7.)

Many of the measurements of aerosols collected from the 50-ft tower during onshore airflow are less-than-values which are approximately equal to or less than those values reported at isolated sites such as Greenland, the North Central Pacific, and the Antarctic. (See Table 8.) The sampling methods are being modified to collect larger air samples to provide definitive measurements of these ultra low concentrations found in aerosols from maritime air masses.

TABLE 6. Weekly Data from Andersen Impactor

Date	Stage Number	Elemental Concentration (ng/m^3) Al	Br	Cl	Cu	Mg	Mn	Na	Ti	V
5-27-73 to 6-3-73										
	1	400 ± 40	<3	160 ± 20	<6	430 ± 150	2.7 ± 0.5	86 ± 20	<10	0.4 ± 0.2
	2	260 ± 30	<1	220 ± 30	<6	340 ± 100	1.7 ± 0.4	220 ± 30	<10	0.4 ± 0.2
	3	168 ± 20	<1	750 ± 90	<10	130 ± 100	1.4 ± 0.3	420 ± 40	<20	<0.2
	4	51 ± 7	<3	570 ± 70	<8	<100	0.5 ± 0.2	390 ± 40	<20	<0.2
	5	26 ± 6	<1	680 ± 80	<9	<100	0.4 ± 0.2	440 ± 40	<20	<0.2
	6	<3	<1	120	<5	<70	<0.2	96 ± 25	<10	<0.2
	7	<3	<1	<10	<4	<70	<0.2	44 ± 10	<6	<0.1
	BUF	<3	<3	40	<4	<70	<0.2	<10	<6	<0.06
7-2-73 to 7-8-73										
	1	<3	<1	<10	<3	<70	<0.2	<10	<5	<0.03
	2	<3	<2	<10	<3	<70	<0.2	<10	<5	<0.03
	3	<3	<1	<10	<3	<70	<0.2	<10	<5	<0.03
	4	<3	<1	<10	<3	<70	<0.2	<10	<5	<0.03
	5	<3	<1	<10	<3	<70	<0.2	<10	<5	<0.03
	6	<3	<1	<10	<2	<70	<0.2	<10	<5	<0.03
	7	<3	<1	<10	<2	<70	<0.2	<10	<5	<0.03
	BUF	<3	<1	<10	<3	<70	<0.2	<10	<5	<0.03
North Central Pacific		<100		5000	<2	<1000	<3		5	<2
Antarctic		0.5	1.0							0.001
Nord Greenland		240		300	3.4	160	1.6		9.2	

TABLE 7. Comparison of Aerosol Pb Concentrations Measured at the Quillayute Reference Station and Other Remote Locations

Location	ng/m^3	
Pristine Atmosphere	0.6	
North Central Pacific	1.0	
Windward Oahu	1.7	
South Indian Ocean	1.0	
North Indian Ocean	4.0	
Novaya Zemlya (USSR)	0.2	
Greenland	0.5	
Antarctic	0.5	
Laguna Mountain, Calif. (Min)	4.0	
White Mountain, Calif. (Min)	1.2	
North Central Pacific (BNW)	<4	
Remote Continental U.S. (Avg. of 10 Sites)	22	
Quillayute, Wash. (BNW, Ground Level)	29	March 1973
Urban Location (Typical)	2000	
Quillayute, Wash. (BNW, 50 ft Tower)	<3	October 1973

TABLE 8. Comparison of Aerosol Stable Element Concentrations Measured at the Quillayute Reference Station and Other Remote Locations

Element	Typical Urban	Quillayute, Washington Hi Vol (2 wk) 3-5-27	Andersen (1 wk) 7-5-73	1 cfm Total (1 day) 10-10-73	Typical North Central Pacific	Typical Antarctic	Nord Greenland	Mauna Loa Hawaii
Al	4000	>90	<9	--	<1000		160	360
Br	150	7.6	<5	<2		1.0	3.2	5.9
C1	500	>1040	<40	--	5000		300	350
Cu	200	2.1	<9	<6	<2		3.4	4.8
Fe	4000	172	--	<5	9	0.5	166	430
Mg	2000	>120	<200	--	<1000		160	360
Mn	100	4.5	<0.6	<4	<3		1.6	7.6
Mo	3	<0.1	--	<1			0.17	0.077
Na		--	<40	--				
Pb	1300	27		<3	1	0.5	22	1.5
Rb	10	<0.5		<1				
Sr	20	2.3	--	<1	<5		0.87	2.7
Ti	300	22	<20		5		9.2	30
V	50	<2	<0.1	--	<2	0.001		
Zr	10	<0.3		<1				

THE PARTICLE SIZE DISTRIBUTIONS OF MANMADE AND NATURAL RADIONUCLIDES

J. A. Young

At Richland, Washington greater than 90% of the short-lived radon and thoron daughters and 88% of the cosmogenic ^{7}Be were present on particles too small (1.1 μm) to have appreciable settling velocities. The percentage of nuclear weapons radionuclides present on particles larger than 1.1 μm is fairly large soon after a nuclear test, but decreases fairly rapidly with time

Aerosol particles larger than about 1 μm diam have appreciable settling velocities. Therefore, measured atmospheric transport and deposition rates for one material may not be applied to another material unless they are both primarily present on particles smaller than 1 μm. One of the prime goals of the Radioactive Fallout Rates and Mechanisms program is to determine atmospheric transport and deposition rates from measurements of natural and manmade radionuclides. Therefore, Andersen 20-cfm

cascade impactors are being operated at Richland and Quillayute, Washington to determine the fractions of the various radionuclides present on particles larger than 1 μm. This impactor separates particles into size ranges of >7 μm, 3.3 to 7 μm, 2.0 to 3.3 μm, and 1.1 to 2.0 μm, and uses a backup filter to collect particles smaller than 1.1 pm.

At Richland 94% of the thoron daughter, ^{212}Pb, and 91% of the radon daughters, ^{214}Bi and ^{214}Pb, in the atmosphere were attached to particles smaller than 1.1 μm. At Richland and Quillayute the percentages of the cosmic-ray-produced radionuelide, ^{7}Be, on particles smaller than 1.1 μm were 88% and 84%, respectively. It is evident that settling can have only a minor effect on the total transport and deposition of these radionuclides. However, a considerably larger fraction of the nuclear weapons-produced radionuclides was present on particles larger than 1.1 pm. One week after the Chinese thermonuclear test of June 26, 1973, only 25% of the radioactive debris was present on particles smaller than 1.1 pm. By September 1973 the percentages of several nuclear weapons-produced radionuclides present on particles smaller than 1.1 μm averaged around 60 to 65%. Shleien et al.[5] have reported that 400 days after the last weapons test, 88% of the debris was present on particles smaller than 1.75 μm diam. Therefore, settling may appreciably affect the transport and deposition of nuclear weapons-produced radionuclides soon after a test, but the effect of settling decreases with time and eventually becomes negligible.

TRACE POLLUTANT EMISSIONS IN FOSSIL FUEL COMBUSTION

L. A. Rancitelli, K. H. Abel and W. C. Weimer

Measurements of trace elements in coal and flyash indicate that substantial amounts of the potentially toxic elements Se, Hg, and As are emitted into the atmosphere by the Centralia coal-fired electric plant.

Electric power generation in the next decade will rely to a large degree on fossil fuel electric plants. Federal standards regulate the releases of total particulate matter and the gaseous by-products NO_x and SO_2 to the environment. While these substances are by far the most abundant pollutants and have been shown to have detrimental effects, potentially toxic trace elements including Hg, Se, As, Sb, Pb, Cd, F, U, Cu, Ni,

Zn, Be, U and Th are also being emitted in unknown amounts. The consumption of millions of tons of coal per year at these electrical generation facilities may release significant amounts of these trace constituents in the coal to the environment.

A detailed characterization of the emitted materials, including evaluations of the chemical composition of both gaseous and particulate by-products, chemical composition of the particulate fraction versus particle size, and the availability of the toxic materials to the biosphere, is necessary before environmental impact can be established. Therefore a program has been initiated to characterize the emissions and to evaluate the levels and environmental impact of these trace constituents at the Centralia Steam Plant in Centralia, Washington.

The initial step was to perform a mass balance using coal and flyash samples collected from the Centralia facility. An estimate of the emission levels for most elements was obtained using flyash concentrations and the assumption of 99% efficiency for the electrostatic precipitators. Table 9 indicates these outputs in kg/yr for operation at peak capacity and shows that substantial quantities of Se, Hg, As, Co, Cr and Fe are released. For the very volatile elements Se and Hg, a better estimate could be obtained through comparison of coal and flyash concentrations to determine the amount lost during combustion. The loss for Hg was approximately 90% and for Se approximately 50%. Both loss factors were included in the calculated estimates for Se and Hg in the table.

TABLE 9. Estimated Annual Emission of Trace Elements from the Centralia Power Plant

Element	Output - Kg/yr
As	155
Br	850
Co	290
Cr	720
Cs	15
Eu	20
Fe	220×10^3
Hf	125
Hg	2,250
La	520
Sb	30
Sc	205
Se	8,300
Sm	90
Ta	85
Tb	15
Th	100
Yb	40

Particulate flyash samples have also been taken from the various stages of the electrostatic precipitators and in the stack beyond the precipitators. Analyses of these samples indicate that at least As and Se are condensing onto flyash particles as the combustion gases cool. Other elements may also condense onto the flyash, and in this way some of the toxic trace elements may be concentrating on the fine particulates which escape the electrostatic precipitators.

The potential trace metal depositions from the Centralia stack effluents to the surrounding environment have been estimzted based upon

the elemental discharges presented in Table 9 and assuming a complete deposit of these materials within a defined area. The maximum limit of deposition was assumed to be 11.2-km from the power plant. Investigations by Dana et al.[6] during rainstorms indicated that the maximum removal of SO_2 occurred between the plant and this 11.2-km distance. Two geometries were used to estimate the trace metal inputs to the surface environment; both of these geometries assumed 100% deposition of particulate materials within the designated boundaries. The first deposition geometry is that of a semi-circle with an 11.2-km radius. The second geometry is that of a segment of a circle with an 11.2-km radius and an arc length of 10 km. The length of this arc corresponds to the maximum plume spreading that Dana et al.[6] were able to detect by ground-level SO_2 measurements at the 11.2-km distance from the stacks.

TABLE 10. Estimated Annual Elemental Deposition Around the Centralia Power Plant

Element	Deposition - $mg/m^2/yr$ Semi-Circle (192 km^2 area)	Segment (56 km^2 area)
As	0.8	2.8
Br	4.3	15.1
Cs	1.5	5.2
Cr	3.7	12.9
Cs	0.08	0.3
Eu	0.1	0.4
Fe	1115	3930
Hf	0.6	2.2
Hg	12.7	44.6
La	2.6	9.3
Sb	0.2	0.5
Sc	1.0	3.7
Se	42.1	148.2
Sm	0.5	1.6
Ta	0.4	1.5
Tb	0.08	0.3
Th	0.5	1.8
Yb	0.2	0.7

The annual elemental depositions for each of these geometries are presented in Table 10. While it is unlikely that any of the elements listed will be deposited in quantities great enough to be detected (above ambient levels) in the soils, some of these trace metals could significantly increase the ambient concentrations in vegetation. Even though the ambient elemental concentrations in soil may not be signficantly increased by these deposition rates, the impact to this phase of the environment cannot be dismissed. If the elements in flyash are more readily available for biological uptake than their soil-derived counterparts, they can still present an environmental hazard even though the flyash may increase the natural levels by a few percent. The more volatile elements such as Hg, As, Sb, and Zn, which might be expected to condense on the surface of flyash particles, are prime examples of pollutants readily available to the biosphere.

ATMOSPHERIC NATURAL AEROSOLS AND FALLOUT PARTICULATES DURING 1973 AT RICHLAND, WASHINGTON AND POINT BARROW, ALASKA

C. W. Thomas

Radionuclide concentration at Richland decreased two- to tenfold during 1973, reflecting the lack of high-yield testing during 1971 and 1972. Time variations in the atmospheric concentrations of ^{238}Pu and ^{239}Pu at Richland and Point Barrow since 1964 have been typical of nuclear weapons-produced radionuclides except for the increase in the ^{238}Pu concentration from 1965 to 1968 resulting from the SNAP-9A burnup.

The concentration of stable elements and radionuclides was measured in atmospheric samples collected in 1973. As indicated in Figure 7, the concentration of radionuclides associated with weapons testing decreased two- to tenfold during 1973 at Richland, Washington, reflecting the lack of high-yield weapons testing during 1971 and 1972. For the period 1971 through 1973 the atmospheric radionuclide concentrations decreased with a residence half-time of 11 months similar to that measured from 1963 to 1966.

Atmospheric weapons testing in the northern hemisphere during 1971 and 1972 consisted of a 20-kiloton device detonated in November of 1971, and 20- and 200-kiloton devices in January and March 1972, respectively. In June of 1973 the Chinese tested a device of several megatons, and fresh fission product debris was detected on July 3, 1973. The concentration of short and medium-lived radionuclides were much lower than those associated with the March 1972 tests. However, unlike 1972, the insertion of debris into the stratosphere should be relatively large and will be reflected in the 1974 spring maximum. In April 1964, a SNAP-9A generator containing 17 K Ci of ^{238}Pu burned at an altitude of 46 km in the southern hemisphere over the Indian Ocean, tripling the global atmospheric inventory for this radionuclide.

Measurements of ^{238}Pu in air samples collected at Richland, Washington (46° N latitude) during the period 1966-1972 were reported in 1972. During 1973 the atmospheric concentration of ^{238}Pu and ^{239}Pu were measured in surface air samples collected at Pt. Barrow, Alaska (71° N latitude) from late 1964 to 1972 as a part of a program to define the rates of long-term stratospheric processes in the northern hemisphere as well as the rates of interhemispheric mixing. The seasonal variation in the concentration of ^{238}Pu and ^{239}Pu in samples collected at 71° N latitude were similar to those of other nuclear weapons-produced radionuclides of stratospheric origin, with maximum concentrations occurring in the early

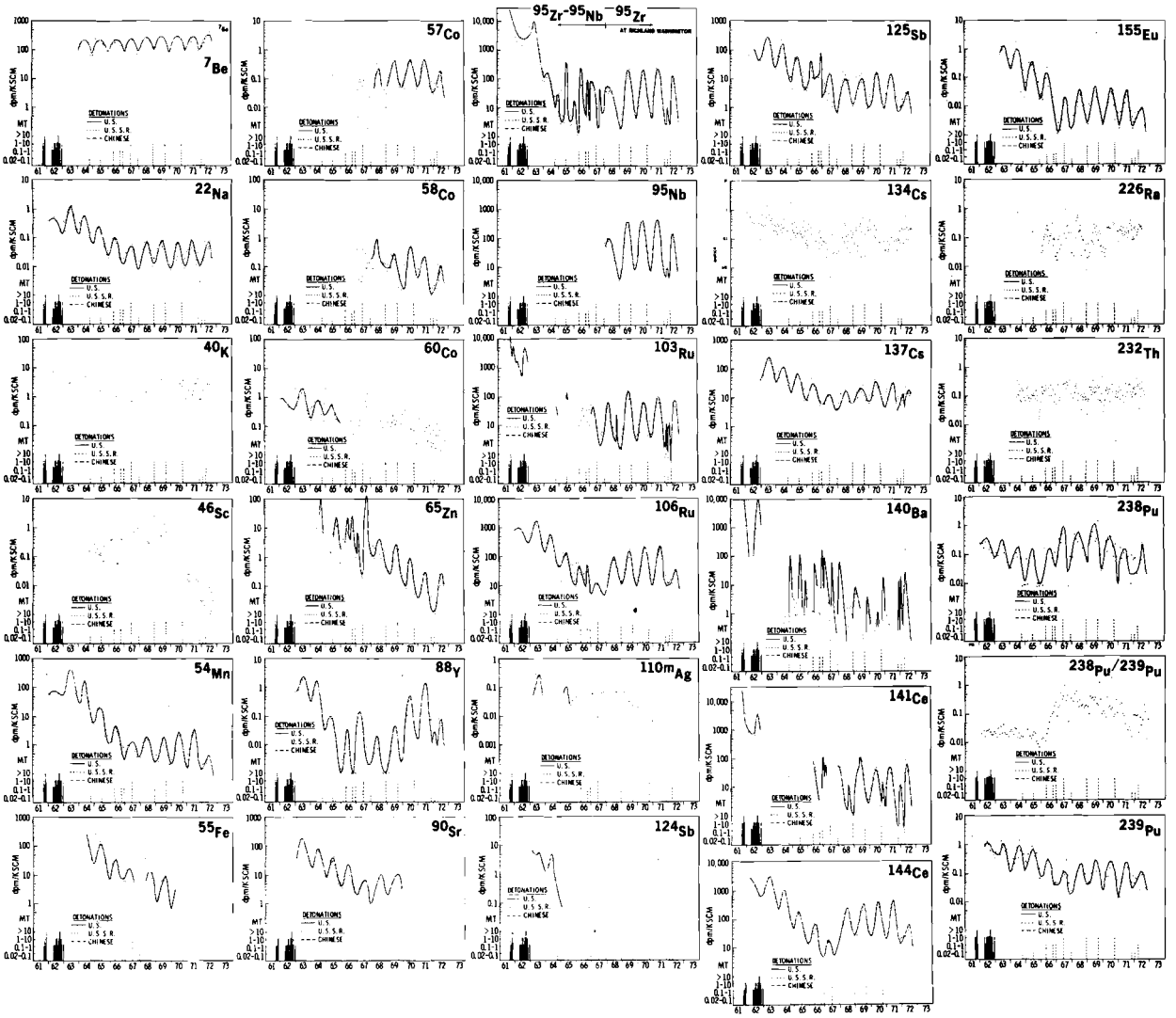

Neg 736612-1

FIGURE 7. Radionuclide Concentration in Surface Air at Richland, Washington

spring and minimums in the fall. From 1965 to 1967 the ^{239}Pu concentration decreased similarly to that measured at Richland, showing a residence half-time of about 11 months and an origin primarily from the 1961-1962 U.S.-Russian test series. From 1967 through 1970 the ^{239}Pu concentration remained relatively constant, reflecting contributions from other atmospheric tests, primarily those conducted by the Chinese and the French. The ^{238}Pu concentration in the atmosphere from 1965 to 1968 increased steadily, indicating that ^{238}Pu from the SNAP-9A burnup had reached high northern latitudes.

The ^{238}Pu/^{239}Pu concentration ratio measured at Pt. Barrow followed

a pattern similar to measurements made at Richland. From 1967 through 1969 the concentration of SNAP-9A plutonium at Pt. Barrow remained fairly constant, indicating ^{238}Pu was being transferred across the equator into the northern hemisphere at a rate comparable to the rate at which ^{238}Pu was being deposited on the earth's surface in the northern hemisphere. The ^{238}Pu concentration showed seasonal variation typical of radionuclides of stratospheric origin, indicating the transfer was taking place primarily in the stratosphere. The comparison of ^{238}Pu concentrations at Pt. Barrow and Richland showed concentrations at Richland about threefold higher than those at Pt. Barrow. (See Table 11.) This comparison was also noted for other weapons-produced radionuclides of stratospheric origin.

The trace element concentrations in the air filter samples collected at Richland in 1973 (shown in Table 12) were determined using X-ray fluorescence analysis to study background concentrations and the sources of the trace elements. The ratio of the concentration of each element to that of iron was calculated and compared to the ratio in diabase (basalt) to determine if the atmospheric concentrations of the element resulted primarily from material from the earth's crust. The calcium, titanium, chromium and manganese in the air probably were due primarily to basaltic dust. Nickel, zinc, arsenic, bromine, molybdenum and lead demonstrated large contributions from other sources. The bromine-to-lead ratio of 0.15 is about what would be expected from automobile exhaust. The concentrations measured in 1973 were similar to those measured in 1972. Monthly averages showed the concentrations of those elements attributed to basalt reached maximum

TABLE 11. ^{239}Pu and ^{238}Pu Concentrations in Air at Richland, Washington and Pt. Barrow, Alaska

	Richland			Alaska		
	^{239}Pu	^{238}Pu	$^{238}Pu/^{239}Pu$	^{239}Pu	^{238}Pu	$^{238}Pu/^{239}Pu$
1962	10.32	0.2367	0.02292			
1963	6.423	0.1698	0.02644			
1964	5.646	0.1886	0.03340			
1965	4.740	0.07114	0.01501	1.3142	0.0256	0.01948
1966	1.719	0.1073	0.06271	0.6003	0.0576	0.09595
1967	0.9629	0.3672	0.3722	0.1622	0.0856	0.5277
1968	1.3667	0.3361	0.2459	0.4300	0.1289	0.2998
1969	1.3920	0.4983	0.3580	0.3941	0.0987	0.2504
1970	1.5744	0.2268	0.1441	0.3024	0.4976	0.1646
1971	1.6357	0.0952	0.0582			
1972	0.8924	0.0735	0.0823			

TABLE 12. Comparison of Aerosol Chemical Composition at Richland, Washington with Diabase (All values normalized to iron)

	Aerosol		Diabase	Aerosol	
	1972	1973		1972	1973
Ca	0.38	0.397	1.01	0.377	0.393
Ti	0.114	0.101	0.082	1.39	1.23
Cr	0.0034	0.0027	0.0015	2.24	1.80
Mn	0.018	0.018	0.017	1.05	1.06
Fe	1	1	1	1	1
Ni	0.032	0.012	0.001	31.7	12
Cu	0.005	0.0051	0.0014	3.57	3.64
Zn	0.018	0.0162	0.00	17.1	14.7
As	0.0018	0.0045	0.000028	62.9	161
Br	0.0184	0.0141	0.000006	3066	2350
Sr	0.007	0.0048	0.0023	3.17	2.09
Mo	0.0003	0.00024	0.0000006	533	400
Pb	0.113	0.0928	0.0001	1130	928

values in the summer and minimum values during the winter, while those elements associated with lead attained maximum values in the late fall and winter and minimum values in the summer.

BEHAVIOR AND CHARACTERISTICS OF RADIOACTIVE DEBRIS FROM THE CHINESE NUCLEAR WEAPONS TEST OF JUNE 26, 1973

C. E. Jenkins and R. W. Perkins

Debris from the Chinese test of June 26, 1973 was first observed at Richland 8 days later. The maximum radioiodine dose from the grass-milk-child-thyroid chain was estimated to be only 1 mrem on the west coast and 12 mrem in Minnesota.

Fallout debris from the Chinese People's Republic thermonuclear test of June 26, 1973 has been studied with the aim of providing a better basis on which to estimate hazards from radioactive fallout. This test, detonated at 0855 PST, was first observed at our laboratory in Richland,

Washington on July 3, 8 days later. Peak atmosphere concentrations occurred 14 days after detonation. The high concentrations of ^{237}U and ^{239}Np indicate that it was a fission-fusion-fission device. The ratios of the various fission products indicated very little fractionation relative to fission yields. The ^{131}I was approximately 17% in particulate form with the remaining 83% being divided about equally between inorganic and organic gaseous forms. Particle size analysis showed that during the first week approximately 60% of the particulate debris was associated with particles of >3.3 μ, while 25% was associated with particles of <1.1 μ. During the second week greater than 60% was associated with particle sizes of <1.1 μ. The air concentrations and concentrations on vegetation along the west coast, were 2 to 3 orders of magnitude lower than those resulting from the last Chinese nuclear test of March 1972. Fission product ratios were very close to those produced in normal fission yield indicating very little fractionation. A few grass samples from Minnesota showed about an order of magnitude higher fallout than maximum fallout on the west coast. The maximum dose estimate for the grass-milk-child-thyroid chain is calculated to about 1 mrem on the west coast and 12 mrem in Minnesota.

REFERENCES

1. D. G. Atkinson, W. E. Davis, L. F. Radke, B. C. Scott, W. G. N. Slinn, T. M. Tanner, J. M. Thorp, N. A. Wogman and J. A. Young, "Precipitation Scavenging of Tracers Released into Frontal Storms," Pacific Northwest Laboratory Annual Report for 1971 to the USAEC Eivision of Biology and Medicine, Volume II: Physical Sciences, Part 1, Atmospheric Sciences, BNWL-1651, PT1, Battelle, Pacific Northwest Laboratories, Richland, WA, pp. 1-19, December 1972.

2. J. D. Ludwick, "Polarographic Techniques Applied to Prospective Atmospheric Particulate Tracers," Pacific Northwest Laboratory Annual Report for 1967 to the USAEC Division of Biology and Medicine, Volume II: Physical Sciences, Part 3, Atmospheric Sciences, BNWL-715, Battelle, Pacific Northwest Laboratories. Richland, WA, pp. 63-64, October 1968.

3. R. N. Lee, "Trace Metal Analysis by Atomic Absorption Spectrometry Using a Graphite Furnace Atomizer," Pacific Northwest Laboratory Annual Report for 1972 to the USAEC, Division of Biology and Medicine, Volume II: Physical Sciences, Part 1, Atmospheric Sciences, BNWL-1751, PT1, Battelle, Pacific Northwest Laboratories, Richland, WA, pp. 85-88, April 1973.

4. J. D. Ludwick, J. A. Young, L. A. Rancitelli and W. E. Davis, "A Comparison of the Particulate Pollutant Levels at Proposed Baseline Monitoring Stations," Pacific Northwest Laboratory Annual Report for 1972 to the USAEC, Division of Biology and Medicine, Volume II: Physical Sciences, Part 1, Atmospheric Sciences, BNWL-1751, PT1, Battelle, Pacific Northwest Laboratories, Richland, WA, April 1973.

5. B. Shleien, N. A. Gaeta and A. G. Friend, "Determination of Particle Size Characteristics of Old and Fresh Airborne Fallout by Graded Filtration," Health Physics, vol. 12, pp. 633-639, 1966.

6. M. T. Dana, J. M. Hales, W. G. N. Slinn and M. A. Wolf, Natural Precipitation Washout of Sulfur Compounds from Plumes, Final Report to the Environmental Protection Agency, Division of Meteorology, EPA-R3-73-047, 1973.

TRANSPORT, DIFFUSION AND TURBULENCE

The following reports focus on modeling the physical behavior of the atmosphere and its contaminants in or near the planetary boundary layer. This boundary layer extends from the surface, where eddies on the order of a few centimeters transport material and energy, through a layer on the order of 1 km where large eddies effect this transport. Because it is the major receptor and conveyor of energy and matter emanating at the surface, certain aspects of the planetary boundary layer must be understood in order to provide an improved basis for assessing the environmental costs of national policy or the lack of it.

In the past Battelle's boundary layer research focused on the lowest 10% of the layer as the logical starting point for describing the behavior of effluents near the ground and stack gases of low buoyancy. Studies of turbulence, transport, diffusion, and deposition have aimed at providing models to evaluate effects of postulated reactor accidents over relatively short downwind distances. With increased number and size of nuclear power and fuel handling facilities, it is now more important to deal with a greater number of large potential sources distributed over broader geographic areas. Concurrently an increased desire to assess low-level radiation effects is requiring more realistic atmospheric models where conservative models were adequate before.

Research reported in this section represents a transition between past and future needs—a transition of emphasis rather than to new topics. Current topics of importance such as regional transport, long-range diffusion and deposition, and resuspension are all ones that have been part of the Hanford program at different times in the past to meet particular needs. Consequently, the new emphasis is more accurately a reemphasis building on past Hanford work.

The following reports show that attention in the last year has centered around these areas:

1) Modeling diffusion and deposition in terms of models of turbulence intensity and scale. The effort of the past year has focused on developing better techniques for obtaining the turbulence parameters necessary for input to the Hanford turbulent diffusion model under development.
2) Developing a basic understanding and models of surface layer turbulence for determining energy and mass transfers to and from the surface as applicable to diffusion, deposition and resuspension.
3) Determining and modeling deposition velocities through experimental field studies with diffusing nondepositing and multiple depositing tracers.
4) Integration and evaluation of models for diffusion, deposition and resuspension.
5) Mesoscale transport and diffusion over Hanford (primary support by ARHCO) and regional transport over the northwest.
6) The development and testing of improved measurement and analysis techniques.

All these efforts, some directly and others indirectly, constitute research necessary to formulate the planetary boundary layer portion of any atmospheric assessment model. This in turn can be used by environmental impact and cost/benefit models for application to regional planning assessments.

- **ATMOSPHERIC DIFFUSION, DEPOSITON, AND TRANSPORT PHENOMENA**
- **FUNDAMENTAL TURBULENCE**
- **PARTICLE RESUSPENSION AND TRANSLOCATION**
- **FALLOUT PHENOMENOLOGY**
- **ATLANTIC RICHFIELD HANFORD COMPANY**

A METHOD FOR DETERMINING MONIN-OBUKHOV L's FROM PROFILES OF SUBJECTIVELY ESTIMATED MEAN WIND SPEEDS AND TEMPERATURES

D. C. Powell

A method has been developed for calculating Monin-Obukhov L values using wind and temperature data from the four lowest levels of the Hanford 400-ft tower. The L values computed by this method are compared to L values computed from flux data from sonic anemometers. For one unstable case and for one stable case the agreement is quite good. For a slightly stable case, where the estimates of L differ by an order of magnitude, other logic favors the L as estimated from the 400-ft tower data.

OBJECTIVE

A description is given of a method of calculation of Monin-Obukhov L values independent of the heat and momentum flux measurements that are included in the definition of the L:

$$L = \frac{-u_*^3\,\Theta}{kg\,\overline{w'\Theta'}} \qquad (1)$$

where u_* is the friction velocity, related to the momentum flux, Θ is the absolute temperature, k is Von Karman's constant, g is the gravitational constant, and $\overline{w'\Theta'}$ is the heat flux correlation. Such a method may be useful at sites where reliable flux measurements are not available and where L values are wanted for particular times or for climatologies.

METHOD

Businger et al.[1] have endorsed the computation of gradients of wind and potential temperature by the use of second order polynomials in ln(z). The equations are

$$\overline{U}(z) = A_u + B_u\,Ln(z) + C_u\,Ln^2(z) \qquad (2)$$

$$\overline{\Theta}(z) = A_\Theta + B_\Theta\,Lnz + C_\Theta\,Ln^2(z) \qquad (3)$$

where $\overline{U}$ is the mean wind speed, $\overline{\Theta}$ is the mean potential temperature relative not to 1000 mb but to the lowest level of measurement, and z is the height. The gradients are found by differentiating (2) and (3):

$$d\overline{U}/dz = B_u/z + 2\,C_u\,Ln(z)/z \qquad (4)$$

$$d\overline{\Theta}/dz = B_\Theta/z + 2\,C_\Theta\,Ln(z)/z. \qquad (5)$$

From these gradients the Richardson number may be obtained and thence z/L since there is a one-to-one relation between these two stability parameters. The relations used were also taken from Businger et al.[1] For unstable conditions the approximation

$$z/L = Ri \quad (6)$$

was used, where Ri is the Richardson number. For stable conditions the equation used to relate the two parameters was

$$\frac{z}{L} = \frac{-0.74 + 9.4\ Ri + \sqrt{4.9\ Ri + 0.55}}{9.4 - 44\ Ri} \quad (7)$$

This equation cannot be used for values of Ri greater than 0.21 since the denominator must remain positive for the results to be meaningful. Mention should be made of the fact that a value of 0.35 for Von Karman's constant is involved in the derivation of (7). Busch[2] points out that this value obtained by Businger et al.[1] does not agree with the value of 0.4 obtained by other investigators.

The coefficients in (2) and (3) are obtained by a regression method when data from more than three heights are used. The data input for the calculations reported here were:

1. the hourly average wind speeds estimated from strip charts to the nearest mph by an observer for the 7, 50, 100, and 200-ft levels of the tower;
2. the instantaneous temperature prevailing at the middle of the hour and read to the nearest tenth of a Farenheit degree for the 3, 50, 100, and 200-ft levels of the tower.

The wind speed measurements were taken from Bendix-Friez Aerovane 3-blade anemometers. The guaranteed accuracy is ±1.5 mph. The temperature is measured with copper shielded resistance thermohms placed in a radiation shield and aspirated at the rate of 10 cfm. The guaranteed accuracy is ±0.5°F.

COMPARATIVE RESULTS

Three comparisons will be given between L values from the gradient calculation method and from concurrent flux measurements from sonic anemometers. In each case the sonic anemometer was operated as part of an AEC-sponsored turbulence test. The tests, known as EB-1, EB-11, and EB-6, were taken under unstable, stable, and slightly stable conditions, respectively. The L values quoted from the gradient calculation method are those from the value of z/L, computed from the Richardson number where z is 15 m.

For the unstable case the L values from the gradient calculation method and from the sonic-measured fluxes are shown in Figure 1. The L values from the gradient calculation method apply at the half-hour, while those from the fluxes apply at the midpoint of the test period analyzed. Elderkin[3] has given values of -98 m and -225 m for L for two periods of the EB-1 data analyzed. When compared with the L values calculated by the gradient method, the comparison is obviously quite good considering the type of data used for the gradient calculation method.

A similar comparison for the stable case is given in Figure 2 for two periods of EB-11 data analyzed by Powell and Horst in another report in this volume. This figure shows two

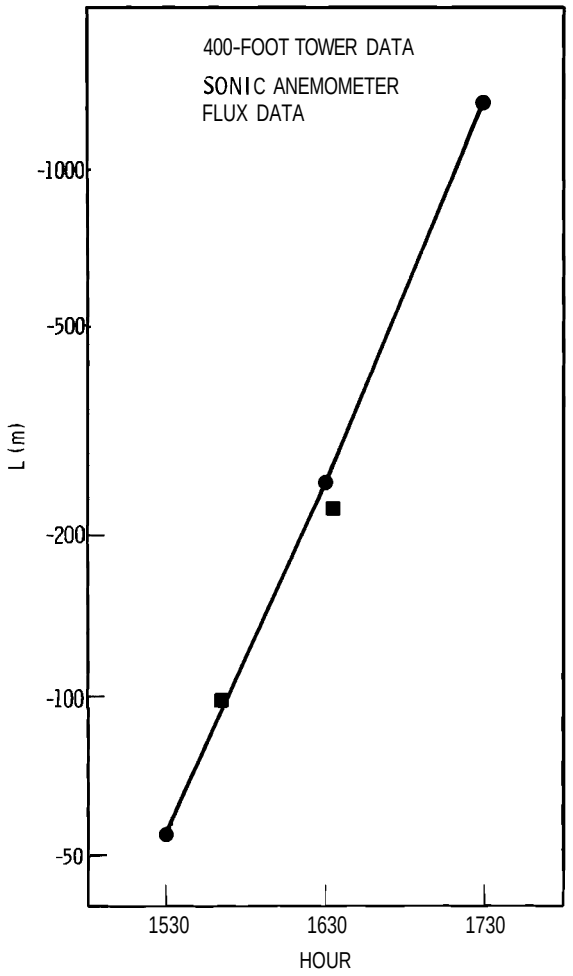

Neg 740226-3

FIGURE 1. Comparison of Monin-Obukhov L Values Computed from Sonic Anemometer Flux Data with Those Calculated from Profile Data - Unstable Conditions

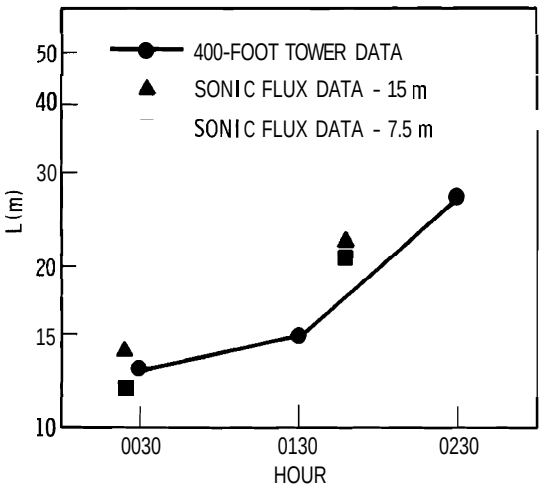

Neg 740226-4

FIGURE 2. Comparison of Monin-Obukhov L Values Computed from Sonic Anemometer Flux Data with Those Calculated from Profile Data - Stable Conditions

independent values of L from flux measurements from each experimental period. The L values were independently computed using the flux data from the anemometers at 7.5 m and 15 m rather than by averaging information from the two levels as was done to compute the L values Elderkin quotes. Here the comparison of the three independent calculations of L again is quite close, especially the calculations from the two sets of sonic anemometer data.

For the slightly stable test, EB-6, Elderkin[3] quotes a value of 4400 m for L. Here the agreement with the L from the gradient calculation method is not as good. The L's computed for the 15-m level for the half-hour times before and after the mid-time of the data sample were 435 m and 425 m, respectively. However, there is also a question about the accuracy of the flux method of calculation. Kaimal and Businger[4] have shown that to calculate the true heat flux correlation, $\overline{w'\theta'}$, from sonic anemometer data, a correction term must be added which has a negative value if the momentum flux is downward. The raw $\overline{w'\theta'}$ value from the EB-6 analysis was positive, which is true only for unstable conditions. The corrected

heat flux was negative only because the correction term added was of greater magnitude than the original sonic anemometer heat flux. Therefore, considering the fact that the test period was about 10:00 p.m., an L indicating definitely stable conditions, as was obtained from the gradient calculation method, seems more credible than the nearly neutral L obtained from the corrected sonic heat flux measurement that was positive in uncorrected form.

DEPENDENCE OF SITE EVALUATION OF ROUGHNESS LENGTH AND DISPLACEMENT LENGTH ON VALUE CHOSEN FOR VON KARMAN'S CONSTANT

D. C. Powell

By using sets of values of Von Karman's constant, roughness length, and displacement length, the gradient calculation method developed in the preceding paper may be extended to calculate values of the friction velocity. The criterion for validation is agreement of friction velocity values so calculated with those calculated from concurrent sonic anemometer data. When this is done using 0.35 or 0.40 for Von Karman's constant, the associated sets of values of roughness length and displacement length differ significantly. These results indicate that a new value of Von Karman's constant should not be adopted for profile analysis of data for a particular site unless the roughness length and displacement length values assumed for the site are reevaluated. This information will be used in diffusion-deposition models at Hanford.

SUMMARY

The gradient calculation method described in the previous paper may be used to estimate values of the friction velocity, u,, which may be compared to the value of u, calculated by analyzing data taken concurrently from a sonic anemometer. For this purpose observations taken in nearly neutral conditions are required. The observations used were the 400-ft tower data recorded at the time of the AEC turbulence test, EB-8, previously analyzed in some detail by Elderkin et al.[5] During this test the value of u, calculated from the $\overline{u'w'}$ correlation was 0.48 mps. Values very closely approximating this were calculated using the gradient calculation method with either of the following inputs

k	z_o	d
0.40 m	0.03 m	0.4 m
0.35 m	0.05 m	0.2 m

where z_o is the roughness length, d is the displacement length, and k is Von Karman's constant.

The value of 0.03 m for z_o agrees with that previously published by Horst and Elderkin[6] for the homogeneous area on the Hanford diffusion grid. At the time of their analysis, Von Karman's constant was considered to be 0.4 without equivocation. But since Von Karman's constant has been reevaluated at 0.35 by Businger et al.[1] and since other current investigators do not agree on a common value [see Busch[2]], the possibility of using either or some intermediate value in analysis exists. The result above shows that this cannot properly be done without reconsidering values of z_o and d.

If the input wind speed data from the Hanford 400-ft tower consisted of three significant figures, the analysis procedures of the gradient could be extended to indicate a preference for the first set of values given. However, in view of the fact that the input wind speeds were the integers: 11, 17, 19, and 21, the indicated preference for the first row of figures cannot be considered as a significant result.

Horst and Elderkin[6] computed a displacement length of 1.4 m for the homogeneous area. This figure differs from that calculated from the 400-ft tower data because the sagebrush has been cut down over a small area surrounding the tower. On the other hand, the value of z_o indicated for the two locations is the same. Therefore, the displacement length is indicated to depend on local roughness, while the roughness length is indicated to depend on integrated roughness over the upwind fetch.

When a displacement length is used, the zero extrapolation height of the wind profile is $z_o + d$, which is much closer to d than to z_o. On the other hand, z_o is important in the equations as a turbulence-generating parameter since the predicted value of u_* is very sensitive to the value of z_o used. If different values of z_o prevailed at the tower and over the homogeneous area, there would be different amounts of turbulence over the two areas.

A final point to bring out is that Monin-Obukhov L values calculated from the tower data are not very sensitive to the differences in assumed values of displacement length. The variation of L is less than 10% when d varies as described above.

DETAILS

The primary equations used in this analysis are the expansion of the mean wind speed, $\overline{U}(z)$, in second order polynomials of $\ln(z-d)$, and the wind profile law in terms of z-d. These may be written

$$\overline{U}(z) = A_u + B_u \, \mathrm{Ln}(z-d) + C_u \, \mathrm{Ln}^2(z-d) \tag{1}$$

$$\overline{U}(z) = \frac{u_*}{k} \mathrm{Ln} \frac{1}{z_o} + \frac{u_*}{k} \mathrm{Ln}(z-d) + \Psi\left(\frac{z-d}{L}\right). \tag{2}$$

For very nearly neutral conditions C_u and $\Psi[(z-d)/L]$ should be nearly zero. Therefore like terms from (1) and (2) may be equated:

$$u_* = \frac{}{\mathrm{Ln} \frac{1}{z_o}} \quad \text{and} \tag{3}$$

$$u_* = B_u \, k. \tag{4}$$

The z_o value in (3) should also be the value of (z-d) in (1) for which $\bar{U}(z)$ extrapolates to zero.

When the value of k may be anywhere from 0.35 to 0.4, it is possible for distinctly different sets of values for z_o and d to satisfy all these conditions. As a final condition we may require the nondimensional shear defined by

$$\Phi_m = \frac{k(z-d)}{u_*} \frac{d\bar{U}}{dz} \quad (5)$$

to approximate the value given by Businger et al.[1] for nearly neutral conditions. When a displacement length is added to the concept, their equation reads

$$\Phi_m = 1.0 + 3.0 \frac{z-d}{L} + 10.2 \left(\frac{z-d}{L}\right)^2. \quad (6)$$

The values for the variance coefficients and parameters from the analysis of the EB-8 data are given in Table 1. The value of u_* from the sonic anemometer data to be matched by calculations using the 400-ft tower mean wind and temperature data was 0.48 mps. The 400-ft tower temperature data showed a very slight increase of potential temperature with height--above 0.003°K/m. Therefore, the second order coefficient, C_u, in the expansion should be a small positive number and Φ_m should be greater than unity. For these reasons the numbers in the table show a preference for a value of 0.4 for Von Karman's constant along with the associated values of z_o and d.

TABLE 1. Analysis of 400-ft Tower Wind Profile Data at the Time of Turbulence Test EB-8

	k = 0.35	k = 0.40
A_u	4.04	4.24
B_u	1.33	1.23
C_u	-0.0072	0.0064
z_o(m)	0.05	0.03
d(m)	0.2	0.4
$u_* = \frac{A_u k}{\text{Ln } \frac{1}{z_o}}$ (mps)	0.47	0.48
$u_* = B_u k$ (mps)	0.47	0.49
$^*\Phi_m = \frac{k(z-d)}{u_*} \frac{d\bar{U}}{dz}$	0.96	1.04
$^*\Phi_m$ (Eq. 6)	1.07	1.07
$^*(z-d)/L$	0.0214	0.0234

*Using z = 15 m.

POWER SPECTRAL ANALYSIS OF TWO PERIODS OF TURBULENCE DATA FOR VERY STABLE CONDITIONS

D. C. Powell and T. W. Horst

Sonic anemometer data from heights of 60, 15, and 7.5 m have been analyzed for two 55-min periods during which the critical Richardson number was attained at heights between 15 and 30 m. The best organization of the spectra was achieved by plotting dimensionless spectra, normalized by individual variances, as functions of dimensional frequency. For the less stable 55-min period the spectra from the 60-m level organize well with the spectra from the Zower levels except at the lower frequencies which are not included in the normalizing variances. The frequencies of maximum spectral energy at 15 and 7.5 m for the three components average less than 60% of the values predicted by previous modeling. The parameterization of the data achieved by using the dimensionless frequency of maximum spectral energy f_m is found to be in no way inferior to that using the dimensionless frequency f_o proposed by the A.F.C.R.L. investigators.

SUMMARY

Atmospheric turbulence analysis is neither as objective nor as exact as it appears to a non-meteorologist reading turbulence literature because of his interest in a particular application. This paper illustrates that fact with the analysis of stable turbulence data which differs in certain important details from the state-of-the-art model set forth by Kaimal in 1973.(7)

The values of the dimensionless frequency of maximum spectral energy predicted by Kaimal's model average about 1.7 times the measured values from Hanford data taken at heights of 15 and 7.5 m. This ratio is 1.54 for the 15-m level and 1.84 for the 7.5-m level.

On the other hand, height dependency is not found for the dimensional frequencies of maximum spectral energy. The dimensionless spectra plotted as functions of dimensional frequencies collapse in the middle and high frequencies for the lowest two levels for the first 55-min period and for all three levels for the second 55-min period. The spectral energy at low frequencies at the 60-m level is not predictable from the spectra at the lower levels, other than to say that there is considerably more low-frequency energy at the 60-m level.

The principal application of spectral models in current departmental research is for use in diffusion-deposition-resuspension modeling. On the basis of the information set forth in this paper, it seems reasonable to strip from the transport model the provisions for scaling the spectrum to correspond to a particular height under stable conditions.

DATA DESCRIPTION

The data analyzed for this report were taken during two 55-min periods in 1970:

2358 July 30 to 0052 July 31

0122 July 31 to 0216 July 31.

The array consisted of six logarithmically spaced sensors mounted on a 62-m tower of the Hanford diffusion grid. Sonic anemometers were mounted at 60, 15, and 7.5 m. Gill anemometers were mounted at 30, 3.75, and 1.875 m. For this report only the data from the three sonic anemometers were analyzed.

During the first period non-stationarity prevailed in the form of large meanders, particularly in the lateral component. Conditions were considerably more stationary during the second period.

Profile Analysis

The profile analysis is given so that the spectral analysis to follow may be appropriately related to existing literature. The Richardson numbers for various heights from the 400-ft tower data (see paper by Powell entitled "A Method for Determining Monin-Obukhov L's from Profiles of Subjectively Estimated Mean Wind Speeds and Temperatures" in this volume) encompassing the time span of both runs, were supercritical over part of the height span. The computed Richardson numbers are as follows in Table 2.

The Monin-Obukhov L values computed from the fluxes of heat and momentum from the sonic anemometer data at 15 and 7.5 m are in remarkably good agreement considering the independent sources of the data. These values along with $\overline{U}$ at 60, 15, and 7.5 m are given in Table 3. The times associated with the parameter values are the mid-points of the analysis periods.

An L value computed from the fluxes at 60 m during the second period turned out to be less than 0.05 m. During the first period the heat flux at 60 m was even more difficult to evaluate; therefore no L calculation was made. The good agreement of the L values at 7.5 and 15 m with those computed from the 400-ft tower data is illustrated in the report by Powell referenced above.

TABLE 2. Richardson Numbers for the Test Period

Time	2330	0030	0130	0230
Level (m)				
60	2.27	0.55	0.80	0.34
30	0.87	0.31	0.37	0.22
15	0.33	0.17	0.17	0.14

TABLE 3. L Values from Sonic Flux Data and Mean Wind Speeds

Time	0025		0149	
Level (m)	$\overline{U}$ (mps)	L (m)	$\overline{U}$ (mps)	L (m)
60	7.0	--	7.3	--
15	3.7	12	3.6	21
7.5	2.5	14	2.5	22

SPECTRAL COMPARISON WITH MODEL BY KAIMAL FOR 0.05 < Ri < 0.20

The model with which the power spectra will be compared is that given by Kaimal.[1] Kaimal's equations are:

$$\frac{n\,S_{\alpha(n)}}{\sigma_\alpha^2} = \frac{0.164\ f/(f_o)_\alpha}{1 + 0.164\ [f/(f_o)_\alpha]^{5/3}}, \quad (1)$$

$$\alpha = u,v,w,$$

$$(f_o)_u = 0.5\ Ri, \quad (2)$$

$$(f_o)_v = 1.5\ Ri, \text{ and} \quad (3)$$

$$(f_o)_w = 2.8\ Ri \quad (4)$$

where $nS_\alpha(n)$ is the logarithmic power spectrum at frequency n, a_a^2 is a turbulence variance, f is the dimensionless frequency $nz/\bar{U}$, and $(f_o)_\alpha$ is the value of f for which the straight line of the inertial subrange extrapolates to a normalized spectral value of unity. Ri is the Richardson number.

Other investigators have given their spectral models as functions of f_m, the value of f for which a smoothed version of the sample spectrum has its maximum value, rather than f_o. The disadvantage in using f_m is that it must be subjectively estimated due to lack of smoothness in the sample spectra. There are two disadvantages in using f_o. In the first place the value of the parameter depends on the normalizing variance, which in turn depends on the frequency range used for calculation. Secondly the -2/3 slope of the inertial subrange may not be well defined.

Kaimal relates f_o and f_m with the approximate equation:

$$(f_o)_\alpha \approx 0.26\ (f_m)_\alpha. \quad (5)$$

Substituting (5) into (1) yields an equation of a more standard form:

$$\frac{nS_{\alpha(n)}}{\sigma_\alpha^2} = \frac{0.63\ f/(f_m)_\alpha}{1 + 1.5[f/(f_m)_\alpha]^{5/3}}. \quad (6)$$

The initial comparison consisted of two parts. First the values of f_m were estimated and compared to the predictions from (2), (3), (4) and (5) for each 55-min period and for the 15 and 7.5-m levels. Secondly the same comparison was made for f_o using the variances which correspond to the frequency range stipulated by Kaimal, i.e., 0.0045 Hz to 10 Hz.

The result of this comparison, using 12 spectra in each case, was that both f_m and f_o were significantly lower than the predicted values. In fact the mean ratio of predicted values to measured values was 1.7 in each case. Among the three components, the ratios were 1.3 for u, 1.7 for v, and 2.0 for w. For the individual spectra the highest and lowest such ratios were 2.60 and 0.93. The mean ratios for the two periods were 1.5 and 1.9--the higher ratio being for the more stationary period.

No physical explanation for these ratios can be offered at present. One computational check was made. Since Kaimal divided his hour-long data samples into 16 equal parts and averaged the spectra to get his results, additional analysis was done with the Hanford data using segments

of this length. The values of f_m obtained were essentially the same as for the 55-min segments.

Results indicate in two ways that f_o is not preferable to f_m as a scaling parameter. In the first place, the interchangeability given by (5) is upheld by the present analysis provided that the variance used for normalizing the spectra is for the frequency range 0.0045 Hz to 10 Hz. Secondly the standard deviation of the 12 f_o values from the mean of 1.7 was 0.44 while the standard deviation of the 12 f_m values was 0.30. Thus the subjectivity associated with smoothing the discrete spectral estimates is at least as great in estimating f_o as in estimating f_m. Therefore, in light of the need to choose an arbitrary frequency band for its specification, f_o appears to have no distinct advantage over f_m for parameterizing this data set.

COLLAPSE OF DIMENSIONLESS POWER SPECTRA AS FUNCTIONS OF DIMENSIONAL FREQUENCY

The dimensionless power spectra for u', v', and w' were plotted as functions of dimensional frequency and are given in Figures 3 and 4 for each of the two 55-min periods. For each component the dimensionless spectra for the three heights, 60, 15 and 7.5 m, are superimposed. The normalizing variances are for the same frequency range as that used to compute the f_o values. Therefore the attempted collapse of the spectra is for the middle and high frequencies but not for the low frequencies.

For the second 55-min period the spectra from all three levels collapse remarkably well to the same general curve for the middle and high frequencies. For the first 55-min period the spectra for the 15 and 7.5-m levels are in close agreement, but there is some separation of the spectra for the 60-m level from the others. Most important of all, in neither case can the collapse be improved by using a frequency shift factor that changes with height according to similarity theory.

It will be noticed that although the Richardson number at 60 m is supercritical for all times during the two periods, the 60-m spectra fail to collapse with the spectra

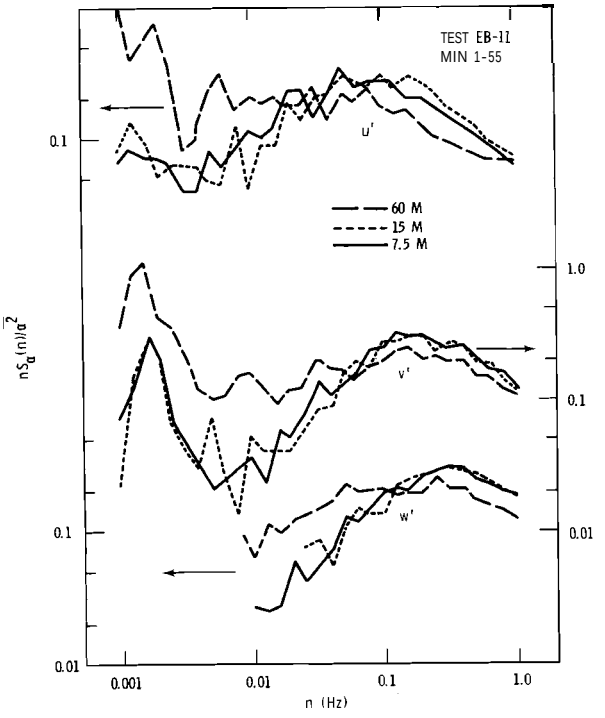

Neg 740681-2

FIGURE 3. Logarithmic Power Spectra Normalized for the Frequency Band 0.0045 to 10.0 Hz - 1st 55-min Period

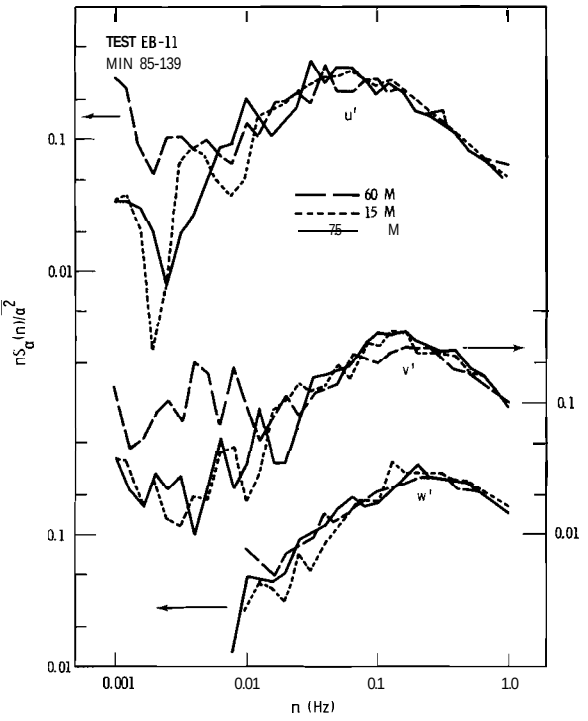

Neg 740681-1

FIGURE 4. Logarithmic Power Spectra Normalized for the Frequency Band 0.0045 to 10.0 Hz - 2nd 55-min Period

from the lower levels only for the first 55-min period. However, during the first part of this period, the stability was much greater than at any time during the second period.

Also attention must be called to the fact that the low-frequency portions of the spectra, the parts important for diffusion modeling, are quite dissimilar when the 60-m spectra are compared with those for the two lower levels.

THE EFFICACY FOR STABLE CONDITIONS OF A FREQUENCY-SHIFT FACTOR THAT CHANGES WITH HEIGHT

The dimensionless frequency used in Kaimal's model is

$$\frac{f}{(f_m)_\alpha} = \frac{nz}{\bar{U}(z)\ (f_m)_\alpha} \qquad (7)$$

where

$$(f_m)_\alpha = C_\alpha Ri(z) \qquad (8)$$

and where $\bar{U}(z)$ and Ri are the functions of z/L given by Businger et al..[1] for stable conditions. The frequency shift factor is $z/\bar{U}(z)(f_m)_\alpha$. Since both numerator and denominator increase with z, it is possible that the change of the shift factor with height is not greater than the uncertainty of the absolute value of the shift factor. To examine this possibility we hold L constant and compare the frequency shift factor as z varies from 6 to 60 m. The result is shown in Figure 5 for the special case where the roughness height, z_o is 3 cm. It turns out that for L = 20 m, which is representative of the test periods, the shift factor varies over a ratio of 1.75 from 6 to 60 m. This is about the same as the

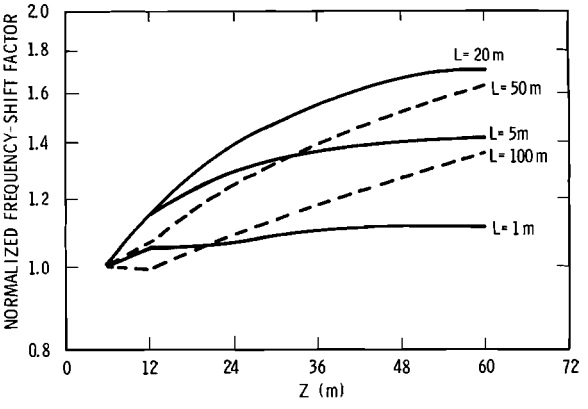

Neg 740787-6

FIGURE 5. Frequency Shift Factor Normalized by its Value at 6 m for Selected Values of the Monin-Obukhov L

factor by which our measured f_m values miss the predicted values. It seems reasonable to state that if the change of the shift factor with height is a significant part of the model, then the ratio within which it occurs theoretically should be much greater than some standard deviation of uncertainty regarding application to particular cases. According to this reasoning, the change of shift factor with height does not seem significant in view of the observed discrepancy (which, however, may have a physical basis) between the predicted and measured f_m.

COMPARISON OF DIFFUSION-DEPOSITION MODEL COMPONENTS WITH EXPERIMENTAL RESULTS

C. E. Elderkin, D. C. Powell,
G. H. Clark* and P. W. Nickola

Estimations of crosswind integrated exposures (CIE) are made with the Hanford diffusion-deposition model using a measured vertical velocity spectrum and a Hay-Pasquill β value from analysis of concurrent turbulence data. The crosswind integrated exposures of both depositing and nondepositing tracers are modeled reasonably well by the measured spectrum and the experimentally indicated β value of 8, although both these components differ significantly from the model-derived values. The model for deposition velocity is extended, the application of which supports the parameterization given in previous reports.

INTRODUCTION

Previous Hanford tracer dispersion experiments have been compared with a model of vertical diffusion and deposition in order to evaluate the deposition velocities of particulates under varying meteorological conditions and to verify the description of the combined processes of diffusion and deposition.[8,9] The model utilizes surface roughness, wind speed, and stability determined from profiles provided by a routinely operationing meteorological tower. These serve as inputs to descriptions of the turbulence spectrum, the ratio of Lagrangian to Eulerian time scale, β (required for the Hay-Pasquill diffusion calculation), and the deposition velocity, as segments of the model.

More recently experiments have been performed to provide independent

* Australian AEC representative on temporary assignment at Battelle, Pacific Northwest Laboratories.

field evaluations of these three segments of the model while simultaneously providing the concentration data necessary for overall model verification. The turbulence was measured directly so that the true spectrum of vertical velocity would be provided. A line of turbulence measurements along the mean wind direction gave the quasi-Lagrangian time scale[10] as well as the Eulerian scale for β estimates. Depositing (zinc sulfide particulates) and nondepositing (Krypton-85 gas) tracers were simultaneously released for direct determination of deposition. One of these experiments, Test V-6, is discussed here and comparisons are made between measured and modeled results.

MEASURED VERSUS MODELED SPECTRA

Comparisons were made between the vertical velocity spectrum generated by the model for a height of 15 m and the spectrum measured at the release height of 26 m (adjusted to represent the spectrum at 15 m by increasing the amplitude 14%). No scale change was made, based on recent turbulence analyses (see paper by Powell and Horst in this volume) showing that for cases of similar stability virtually no change in the scale of turbulence with, height occurs because the expected shift to larger eddy sizes with increased height is offset by a shift to smaller eddy sizes resulting from increased stability with height. The height of 15 m was considered the representative height for diffusion and transport. It was found that the spectrum generated by the model was similar in shape to the measured spectrum with the exception that at high frequencies the measured spectrum falls off more rapidly than the -2/3 slope of the model spectrum. More importantly, the modeled spectrum is shifted to higher frequencies than the measured spectrum by about 40% and also is about 20% smaller in amplitude.

INDEPENDENT ESTIMATES OF β

The modeled Lagrangian to Eulerian scale ratio is given as β = 19 for the stability length L = 40 of Test V-6. The value of β estimated from correlations of turbulence measurements spaced along the mean wind in this test was about 6, however. The method of determining β was that followed in (11). It has been noted by N. Z. Ariel and E. K. Byutner,[12] however, that variability in both speed and wind direction about the mean values tends to reduce the quasi-Lagrangian correlation coefficient estimated in this manner because of the dispersal of trajectory end points for a given time lag, about the mean position where the turbulence data were measured. To evaluate this effect shorter time increments were selected where this dispersion was reduced. As shown in Table 4, β for the vertical wind component was largest when determined over the shortest time increment of 7 min, ranging from 6 to 10. In the table, w_3 and w_4 are w' measured at the third and fourth towers of the turbulence array; $\rho_{3,4}(\tau_m)$ is the

TABLE 4. Estimates of β from Correlation Data for w Measured at Two Towers

Time Interval, min	$\rho_{3,4}(\tau_m)$	τ_m, sec	τ_{Em}		$\beta = \tau_m/\tau_{Em}$	
			w_3	w4	w3	w4
45-99	0.282	7.2	1.33	1.27	5.41	5.67
45-72	0.264	7.2	1.42	1.11	5.07	6.49
59-72	0.325	7.4	1.00	1.00	7.4	7.4
59-65	0.281	7.2	1.24	1.20	5.81	6.0
66-72	0.385	7.4	0.72	0.84	10.3	8.8

maximum cross-correlation value between w_3 and w_4; τ_m is the time lag at which the maximum cross-correlation occurs; τ_{Em} is the time lag at which this same cross-correlation value occurs on the Eulerian autocorrelation functions of w_3 and w_4, as indicated. A more reasonable estimate of β than the average value of 6 would appear to be β = 8, an average value for the 7-min calculations. This is still considerably lower than the value of 19 generated by the model.

ESTIMATION OF CIE - NONDEPOSITING TRACER

When the model calculates the CIE through the bivariate normal diffusion equation, the modeled vertical velocity spectrum and the modeled β value serve as inputs to σ_z as it is determined by the Hay-Pasquill technique. Though the modeled Eulerian turbulence spectrum, which is shifted to higher frequencies than the measured spectrum, tends to produce less diffusion, this is offset by the modeled β shifting the Lagrangian spectrum to lower frequencies than allowed by the actual β, as determined by measurements. Thus in Figure 6, the crosswind exposure curve produced by the model compares reasonably well with the curve determined from the measured spectrum and the experimental value of 8 for β and very closely for β = 10. In the figure the curves for β = 6, 8, and 10 are for estimation with the measured spectrum. The curve for β = 19 is for estimation with the modeled spectrum. Furthermore, comparison in Figure 6 of measured exposures of nondepositing Krypton 85 with these calculated exposure curves where deposition has not yet been included also shows good agreement, particularly with the curve resulting from the measured spectrum and the best estimate of β = 8.

Modeling of turbulence spectra underway in ongoing turbulence studies is consistent with the spectrum observed during this experiment and is leading to an improved turbulence description in the diffusion-deposition model. Ongoing measurement of spatial and temporal turbulence correlations should also provide the needed improvement in the model's description of β as a function of stability.

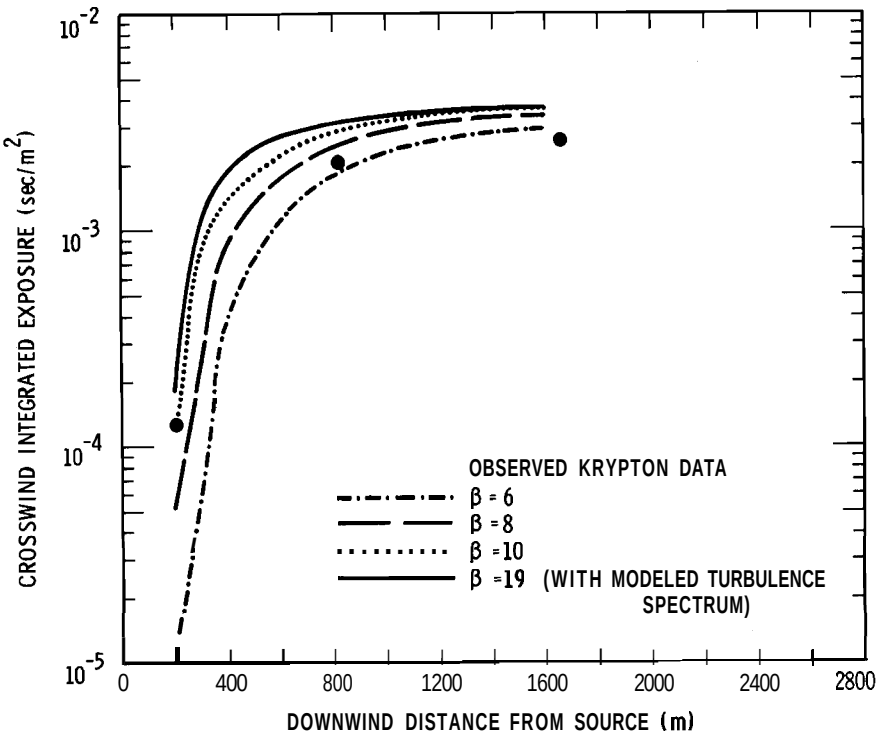

Neg 740787-5

FIGURE 6. Estimated and Measured CIE for Non-depositing Tracer

ESTIMATION OF CIE - DEPOSITING TRACER

When deposition is included in the model, using the observed turbulence and Lagrangian to Eulerian scale ratio, the calculated crosswind integrated exposures compare reasonably well with the measured exposures of depositing particulate zinc sulfide tracer when a value of 8 for β is used. Ratios of calculated to observed exposures for distance from the source where measurements were made are given in Table 5. At the first two distances, the surface measurements were on the tails of the vertical distributions, the surface exposure being less than 2% of the elevated centerline exposure at 200 m, but at 800 m and beyond, the plume had significantly intersected the surface, with exposures at 800 m being more than 25% of the elevated centerline value. At 800 m and beyond, the ratio of calculated to observed exposures was consistently near 0.5, suggesting that the particulate tracer calibration yields exposures too high by about a factor of 2 and needs improvement. Along-wind mass fluxes of the particulates calculated through cross sections of the plume reported by Nickola and Clark (see "Measurement of Particulate Plume Depletion by Comparison with Inert Gas Plumes" in this volume) confirm the overestimation of the particulate exposures. However, Nickola and

TABLE 5. Comparison of Diffusion-Deposition Model Exposures with Measured Exposures

Downwind distance (m)	200	400	800	1200	1600	3200
Calculated exposure / Observed exposure	0.064	1.78	0.556	0.685	0.464	0.501

Clark are able to estimate that the fraction of the plume lost at 800-m distance from the source is 3 to 6% of the quantity released in Test V-6. The model estimates that 6% has been lost at this distance, agreeing reasonably well with observation.

MODELING OF DEPOSITION VELOCITY

The deposition velocity was assumed in the model to be $V_d = 3.0\ u_*^2/\bar{U}$. This was found to give most consistent results in evaluating a set of dispersion data from over the Hanford Grid characterized by stabilities ranging from neutral to very stable. This expression works well again for Test V-6, where the calculated deposition velocity of 8 cm/sec gives consistent comparison between modeled and measured surface exposures at distances where the plume strongly intersected the ground. But it must be questioned whether the coefficient 3.0 would continue to be appropriate for deposition over a significantly different surface. To comment on this, a slight extension is made here of the initial simple deposition model used, which assumed: that (1) the eddy diffusivity for momentum and matter are the same or at least have a constant ratio, (2) at z_o the surface serves as a perfect sink for particulates and (3) the flux of particulates as well as momentum is constant with height through the lowest few meters of the plume. Strictly the latter is not true for the early stages of the plume where diffusion still controls the shape of the concentration profile near the surface. The transfer is now considered to take place through two regions: one the canopy of vegetation extending to a height z_1 and the other the layer of turbulent air above extending to z_2, the breathing height or the height at which the exposure measurements were taken.

Since the flux of matter is

$$F = K(z)\ \frac{\partial \bar{\chi}}{\partial z}$$

where K(z) is the eddy diffusivity and $\bar{\chi}$ the average concentration, integrating from the top of the canopy to the exposure measurement height gives

$$\int_{z_1}^{z_2} \frac{dz}{K(z)} = \frac{\bar{\chi}_2 - \bar{\chi}_1}{F}$$

if the flux is considered constant with height. Similarly for the wind profile,

$$\int_{z_1}^{z_2} \frac{dz}{K(z)} = \frac{\bar{U}_2 - \bar{U}_1}{u_*^2}$$

Then, if the diffusivities in this region are equal,

$$\frac{\bar{U}_2 - \bar{U}_1}{u_*^2} = \frac{\bar{\chi}_2 - \bar{\chi}_1}{F} = \frac{1}{V_d} - r_1$$

where r_1, the concentration at the top of the canopy layer divided by the flux into the canopy, is considered the resistance of the canopy layer. Considerable investigation of this resistance has been done by Sehmel et al.[13] in a wind tunnel for a limited number of surface types. His work suggests that for particle sizes comparable to the mean diameter of the zinc-sulfide tracer particles used in the field experiments discussed here the resistance to transfer is low and that the transfer resistance of the turbulent air above is approached as the limiting factor in determining the deposition velocity. For smaller particles this is not the case; the resistance of the canopy to transfer of the particulates becomes dominant. The deposition velocity, then, is

$$V_d = \frac{1}{\frac{\bar{U}_2 - \bar{U}_1}{u_*^2} + r_1},$$

and if the canopy resistance is small compared to the resistance of the air above, for the particulates of interest at the moment,

$$V_d = \frac{u_*^2}{\bar{U}_2 - \bar{U}_1}$$

Measurements of the wind during Test V-6 gave 2.9 mps and 2.6 mps for $\bar{U}_2$ at 1.5 m and $\bar{U}_1$ at 0.8 m respectively. The deposition velocity can then be estimated as

$$V_d = 10 \frac{u_*^2}{\bar{U}_2}.$$

This is clearly too large, most likely because of the difficulty in measuring a representative $\bar{U}_2 - \bar{U}_1$ (the wind profile was measured in an area with lower and sparser sagebrush than typically found over the diffusion grid so that the measured $\bar{U}_2 - \bar{U}_1$ was smaller than a characteristic value) and because some canopy resistance still remains. Yet this result corroborates the reasonableness of a factor of 3 rather than 1 in the deposition velocity expression which was found to give the best results with diffusion-deposition experiments.

Expressing the deposition velocity as

$$V_d = \frac{1}{\frac{\bar{U}_2}{u_*^2} - \frac{\bar{U}_1}{u_*^2} + \frac{\bar{\chi}_1}{F}},$$

we can see that the first term in the denominator, $\bar{U}_2/u_*^2$, is the total atmospheric resistance to momentum transfer below z_2, the second term $\bar{U}_2/u_*^2$, is the resistance to momentum transfer below the top of the canopy, and the third term, $\bar{\chi}/F$, is the resistance to particulate transfer below the top of the canopy.

In general then the deposition velocity will deviate from $u_*^2/\bar{U}_2$ as momentum and particulates are transported and removed in differing ways through different canopies. For example, if $\bar{U}_1/u_*^2$ and $\bar{\chi}_1/F$ are equal

or if both are small (as with dense, porous, leafy vegetation strongly absorptive of both momentum and particles) the deposition velocity would approach $u_*^2/\bar{U}_2$. But if $\bar{U}_1/u_*^2$ is large while $\bar{\chi}_1/F$ is small (as in open, somewhat sparse vegetation, offering less resistance to momentum but still serving as a good filter especially for large, easily impacted particles) the deposition velocity would exceed $u_*^2/\bar{U}_2$. If, on the other hand, canopy resistance to particle transfer, $\bar{\chi}_1/F$, is larger than the canopy resistance to momentum transfer, $\bar{U}_1/u_*^2$, then deposition velocity will be smaller than $u_*^2/\bar{U}_2$. Such might occur where a rugged canopy offers much mechanical roughness, increasing momentum transfer, but sparsity of leaves and total surface area minimizes particle removal by the canopy, particularly for sub-micron particles with poor impaction properties.

For a thorough description of deposition much more information must be developed regarding diffusivities of momentum and matter for a variety of surface canopy types and a variety of pollutant materials.

ESTIMATION OF MEAN CROSSWIND CONCENTRATION PROFILES FROM "INSTANTANEOUS" CROSSWIND TRAVERSES

P. W. Nickola and G. H. Clark*

Detailed real-time concentration histories available from use of the ^{85}Kr inert gas tracer system permit the simulation of aircraft crosswind traverses through a diffusing plume. The results of such simulations are presented for a tracer release in a thermally stable atmosphere. The standard error of estimate of the peak crosswind exposure was found to be in excess of 100% of the true value for a single traverse at either 800 or 1600 m from the source. This error is reduced to 25 to 30% if 6 traverses are presumed to have been flown. For crosswind integrated exposures standard errors are found to be about 40% and 15% for one and six traverses respectively. Standard errors for other numbers of traverses are presented graphically.

In field measurements designed to define dimensions and concentrations of plumes of atmospheric pollutants (or tracers simulating pollutants), a fixed sampling grid has one great advantage over mobile sampling approaches. Fixed samplers monitor continuously and hence integrate the total impact of a tracer or pollutant at each sampling location. Moving samplers depend upon "grab" samples

* Australian AEC representative on temporary assignment at Battelle, Pacific Northwest Laboratories.

to estimate the integrated concentration of a tracer or pollutant at a series of locations.

Conversely, mobile samplers have several advantages over fixed samplers. As the need to sample extends to large distances and relatively large elevations above the surface, fixed samplers become impractical. Rugged terrain, bodies of water or other physical barriers may preclude establishment of fixed samplers. If the sampler required is reasonably sophisticated, the cost of obtaining and operating more than a few can be prohibitive. Mobility here is an asset. In contrast to the fixed sampling grid., mobile samplers may be taken to a specific site with relative ease.

The Battelle Cessna 411 aircraft has been instrumented and is being further instrumented* for measurement of atmospheric tracers. It is intended that the aircraft be flown in a series of crosswind traverses through a diffusing tracer plume in order to define plume dimensions and concentrations at various distances from the release point. A question remains as to how applicable the measurements made on these short duration crosswind traverses can be in efforts to model the mean plume. The detailed real-time histories of plume concentration generated on the Hanford ^{85}Kr field grid offer some insight in this problem area.

Currently 127 sensors are deployed on the krypton field grid. Samplers are located on sectors of arcs located at 200, 800 and 1600 m from the release point.

During the field experiment of interest, krypton was released from an elevation of 26 m for a period of 30 min beginning at 0516 PST on September 13, 1973. Concentration measurements made at an elevation of 1.5 m on the 800 and 1600-m arcs were used in compiling the results reported in this paper. In the lowest 100 ft of the atmosphere, the initial temperature inversion of about 2.0°F decreased to about 1.5°F during tracer release. Wind speeds during the experiment remained quite constant. Speeds were 2.9, 5.3 and 6.8 mps at elevations of 1.5, 15 and 30 m respectively.

Atmospheric concentrations of krypton were monitored continuously at each sensor and were recorded as a series of 10-sec mean concentrations. During Test V-6 the tracer remained within the crosswind bounds of the sensors as it traversed the 800 and 1600-m arcs. It is assumed that if an aircraft had been able to pass crosswind at an elevation of 1.5 m, it would have "seen" the crosswind distribution measured by the krypton detectors during a 10-sec time increment. This assumption may be moot, but such factors as the mixing of sampled air within the aircraft sampler intake tubing, and the finite

* See accompanying reports entitled "Elevation of an Airborne Fluorescent Particle Counter for Atmospheric Tracer Studies," by M. M. Orgill and P. W. Nickola and "A Real-Time System for Detection of the Atmospheric Tracer Sulfur Hexafluoride," by M. C. Miller and R. N. Lee.

response time of the aircraft detection and recording systems contribute to a smoothing effect on tracer concentrations that may originally be present at the aircraft sensor intake.

Figure 7 plots crosswind integrated exposures (CIE) at 800 m as a function of time after onset of release of tracer. Data have been normalized to unit source strength. Each dot represents a 10-sec CIE measured by the continuously monitoring krypton detectors. Each traverse crosswind through the plume by the aircraft would result in one CIE measurement, i.e., one dot.

An aircraft is presumed to have traversed crosswind through the plume periodically for a total of 3, 6, 12, and 24 traverses, and crosswind distribution of exposures is deduced from these traverses. These traverses were restricted to the period from 5 to 29 min after tracer release began. No leading or trailing edge effects should be present during this period.

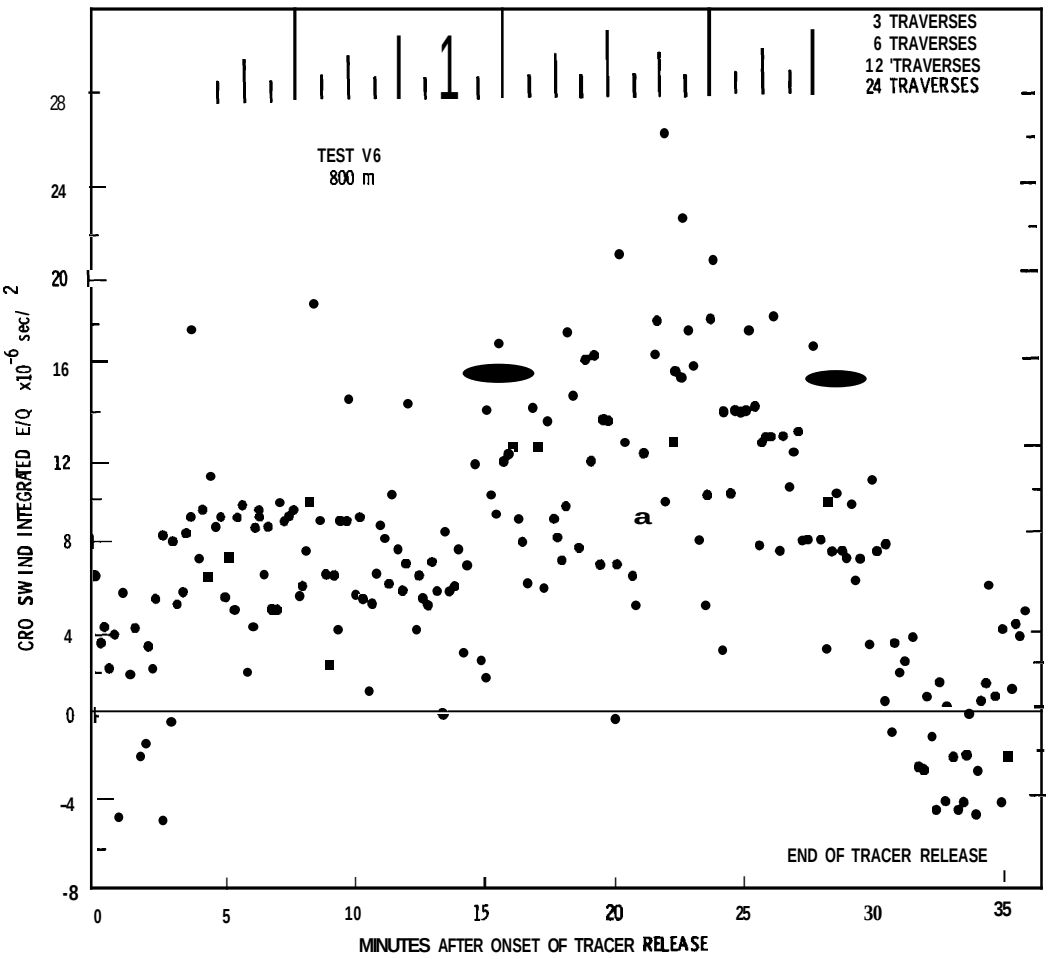

Neg 740787-1

FIGURE 7. Crosswind Integrated Exposure as a Function of Time, Test V-6, 800-m Arc

In other words, this period of plume equilibrium should give statistics identical to those which would be observed had the plume been emitted continuously instead of over a period of only 30 min. (In fact, it is obvious from Figure 7 that these integrated concentrations increase with time. This increase is likely due to the enhanced vertical diffusion from the aloft plume which, in turn, results from the slight erosion of the temperature inversion during the tracer emission period.)

The actual times of presumed aircraft traverses are indicated at the top of Figure 7. Figures 8 and 9 show the crosswind profiles resulting from these assumed traverses at 800 m from the source. The measured true profile as determined from the continuously operating samplers is also presented. It is trite but true that 12 or 24 traverses result in a better estimate than do 3 or 6 traverses.

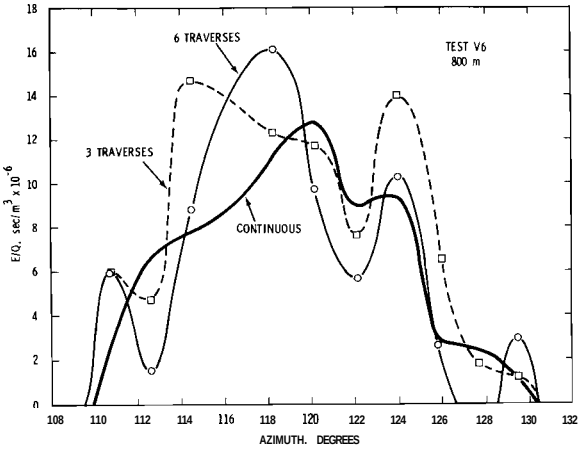

Neg 740787-4

FIGURE 8. Observed Crosswind Distributions of Exposure and Similar Distributions Based on "Instantaneous" Crosswind Traverses, Test V-6, 800-m

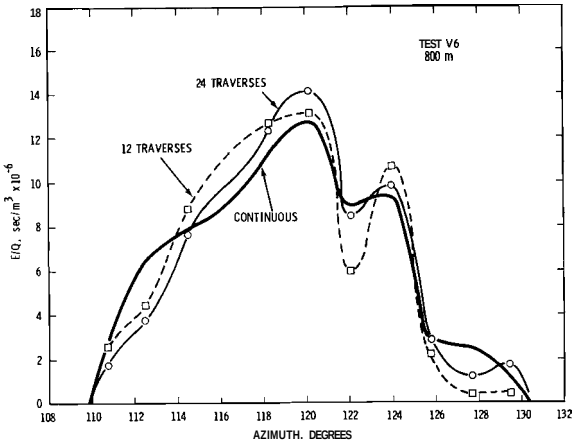

Neg 740787-3

FIGURE 9. Observed Crosswind Distributions and Similar Distributions Based on "Instantaneous" Crosswind Traverses, Test V-6, 800-m

Of course, all these curves are only samples of a great number of similar combinations of traverses that could have been employed to construct crosswind estimates. It is not necessary that the traverses be evenly spaced in time as is suggested at the top of Figure 7. However, it is necessary to avoid the bias that could be introduced by repeating sampling over an interval short enough to result in sampling the same short-term "eddy" twice. This difficulty would likely not arise in actual aircraft sampling procedure since there is finite length of time involved in turning the aircraft to return for another sampling traverse.

As stated above, Figures 8 and 9 give only example distributions. The question still remains as to how many traverses are required to obtain a reasonable approximation of the true profile. Figure 10 gives some guidance toward making that decision.

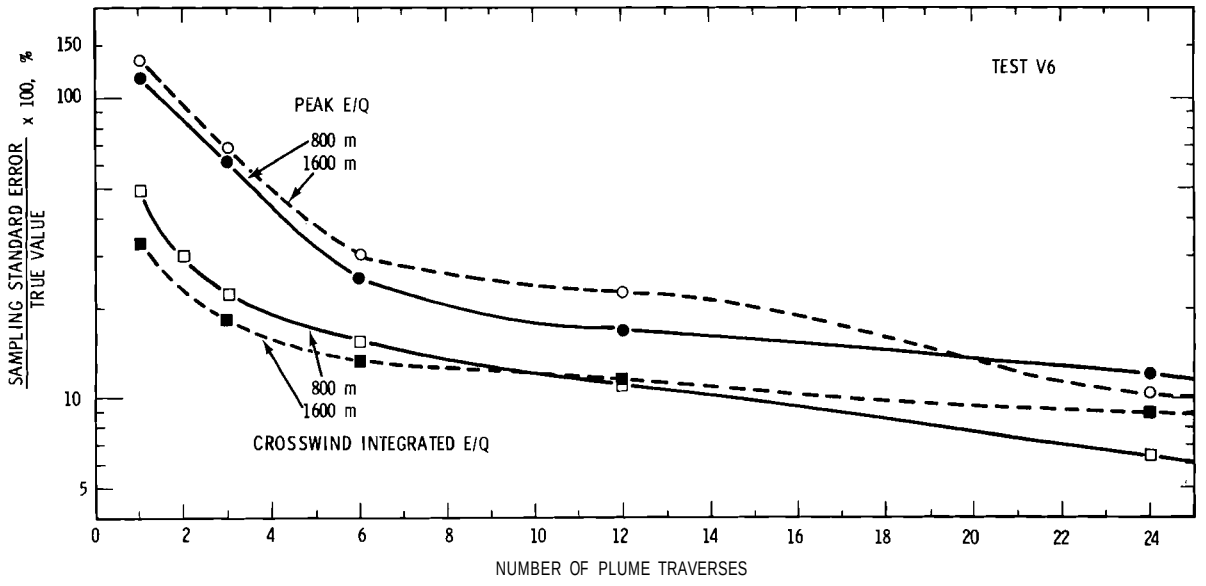

Neg 740787-2

FIGURE 10. Standard Error in Measurement as a Function of the Number of Traverses Through the Continuous Plume, Test V-6, 800 and 1600-m

Here data are presented for the 1600-m arc as well as the 800-m arc. The standard error of measurement is given as a function of the number of traverses through the continuous plume.

For the peak exposure (E/Q), Figure 10 indicates that if only one traverse were made, the standard error is about 120% of the actual value. Thus on the basis of one traverse there is about one chance in three of estimating the peak E/Q too high or too low by more than 100%. It would require six traverses to reduce the standard error on the peak E/Q to less than 30%. For CIE values, one traverse results in a standard error of about 40%, while six traverses result in a standard error of about 15% of the true value. The added dividends in accuracy accruing to repeat traverses decreases after six or seven traverses.

On the basis of this one experiment there appear to be minimal differences in the standard errors for the computed parameters for 800 and 1600 m.

As mentioned earlier, the atmosphere was thermally stable during this test. (Based on temperatures and winds measured at 2 and 15 m, the Richardson number was 0.06.) For other stabilities, the efficiency of a given number of traverses as predictors will likely vary from those reported here. Further, since tracer release was from an elevation of 26 m during experiment V-6, the peak exposure experienced at the 1.5-m elevation is unlikely to approximate that at the centroid of the plume. The standard error statistics would likely vary with distances from the

centroid. Such values should be developed for tower samples nearer the centroid. However, the data presented here were to a large extent hand generated and therefore rather limited in number. A computer program is envisioned which will routinely generate standard errors for each sampling location. Better estimates of the error versus the number of traverse statistics should then be available.

MEASUREMENT OF PARTICULATE PLUME DEPLETION BY COMPARISON WITH INERT GAS PLUMES

P. W. Nickola and G. H. Clark*

The successes and shortcomings of the 1972-73 series of multi-tracer releases are reviewed. Tracers were dispersed to the atmosphere simultaneously from an elevation of 26 m. Although the particulate tracer, zinc sulfide, showed strong evidence of depletion in the near-ground layers, problems in calibration of the tracer assay technique complicate the specification of the magnitude of this depletion. Estimation of the zinc sulfide deposition was accomplished through comparison with the nondepositing, inert gas tracer, krypton-85. The krypton displayed strong evidence of "reflection" from the ground on one of the three experiments examined. The density of vertical samplers on the field measurement grid is currently not great enough to permit mass balance computation of high confidence. Following release into an unstable atmosphere, about 1% of the particulate zinc sulfide is estimated to have deposited before the plume reached 200 m. During one release into a stable atmosphere, 0 to 1% of the tracer deposited during movement to 812 m. During release into a somewhat less stable atmosphere, from 3 to 6% of the particulate zinc sulfide was deposited during traversal to 842 m.

INTRODUCTION

A prime purpose of the series of tracer field releases on the Hanford field diffusion grid during the 13 months beginning October 1972 was to make measurements permitting estimates of deposition from particulate plumes. Analysis of the field results available to date does not justify a firm quantitative description of particulate plume depletion due to contact with the ground and vegetative surfaces. However, evidence suggests that the approach of this investigation holds promise of success. The main purpose of this note is to present this evidence and

* Australian AEC representative on temporary assignment at Battelle, Pacific Northwest Laboratories, Richland, Washington.

to present a minor amount of information on the magnitude of particulate plume depletion.

The field technique employed entails the simultaneous release of an inert gas, krypton-85, and one or more particulate tracers from the same location. The downwind air concentrations of the depleting particulate plumes are compared with concentrations of the nondepleting krypton. The expected deficit of the particulates can be ascribed to deposition and other unspecified depleting mechanisms which occur primarily at the earth-air interface. One admitted difficulty with this technique is that measurement and analysis procedures which may be perfectly adequate for atmospheric diffusion studies may lack the accuracy and precision required in detection of (potentially) small differences in concentration. The adequacy of the currently used field tracer techniques is also considered in this report.

FIELD GRID AND EXPERIMENTS

The multitracer field approach has several logistic or practical restrictions when contrasted with more conventionai single tracer diffusion studies. It requires simultaneity in dispersion and sampling for the number of tracers involved and, hence, additional manpower. Further, if the field sampling grids for the various tracers do not extend over the same range, the frequency of opportunity of field experiments is limited by the restrictions imposed by the smallest grid. In the current situation, the krypton sampling grid, with its relatively sophisticated but limited array of samplers, dictates a lesser range of wind directions acceptable for field experiments than would be permissible with the particulate sampling grid.

During the 17 times the multi-grid system was activated during the current test series, weather and equipment "cooperated" sufficiently to justify actual tracer releases on eight occasions. All releases were from the 26-m elevation on the Hanford 125-m meteorology tower. Test identification, tracer released, and some pertinent meteorology are listed in Table 6. Abbreviations employed in this text to identify specific tracers are footnoted at the bottom of Table 6.

Field sampling for the particulates took place on filters placed on a grid of sectors of six arcs concentric (or nearly so) about the tracer release tower. The angle embraced by the sampling arcs was approximately 80°. The basic sampling elevation was 1.5 m. Distances of the sampling arcs from the release point were approximately 0.2, 0.4, 0.8, 1.2, 1.6 and 3.2 km.* Additionally five towers spaced at 8° increments were found on each of the arcs at 0.2, 0.8, 1.6 and 3.2 km. Samplers on these towers reached to elevations of 33, 42, 62 and 62 m,

* Arcs at 0.8, 1.6 and 3.2 km are actually concentric about a point 100 m due south of the release point. Thus, the distance from release point to arc varies with azimuth.

TABLE 6. Time, Tracer and Meteorology Pertinent to Multi-Tracer Releases from 26-m Level, 1972-1973

Test	Date	Period of Release	Tracers Released	Mean Wind Speed at 2 m	Mean Wind Speed at 30 m	A Temp 30 m - 6 m	Ri (2,15)[a]
V-1	10/26/72	0930-1000	FP,[b] Kr,[c] Rhod[d]	4.0 m/sec	5.8 m/sec	-1.7 °F	-0.22
V-2	11/09/72	1030-1100	FP, Kr, Rhod	2.6	4.2	-0.9	-0.03
V-3	11/16/72	0955-1025	FP, Kr, Rhod	2.7	3.8	-1.4	-0.08
V-4	12/12/72	1049-1120	FP, Kr, Rhod	1.2	2.7	-0.9	0.28
V-5	09/05/73	0601-0631	FP, Kr, Rhod	1.4	4.6	1.5	0.08
V-6	09/13/73	0516-0546	FP, Kr, Rhod	2.0	6.7	0.9	0.06
V-7	09/25/73	1201-1231	FP, Kr	3.3	4.3	-2.2	-0.31
V-8	11/28/73	1125-1142	FP, Indium[e]	1.7	2.8	-1.0	-0.29

a. Ri (2,15) Richardson number for layer between 2 and 15 m.
b. FP Fluorescent particulate ZnS, with mass median diam of about 5 μm.
c. Kr Krypton-85, an inert radioactive gas.
d. Rhod Rhodamine B particulate, with mass median diam of about 0.8 μm.
e. Indium Indium particulate, with mass median diam estimated at 0.1 μm.

respectively. Vacuum for sampling was supplied by pumps powered by small internal combustion engines.

The grid instrumented with 127 krypton-85 detectors was restricted to three arcs. Basic sampling level again was at a height of 1.5 m. The azimuths embraced by krypton detectors were 58, 40 and 15° at 0.2, 0.8 and 1.6 km respectively. Tower-mounted detectors were operative only at 0.2 and 0.8 km.

Vertical profiles of wind speed, wind direction and temperature were measured on the 122-m tower at the source point and on a nearby 24-m tower.

DATA REDUCTION

The two field sample assay techniques felt to be best "in hand" at the onset of this test series were for FP[14] and Kr.[15,16] All filters from each of the eight experiments have been assayed for FP. However, the assay procedure used was one developed about 13 years ago. It is now seen that to attain the more accurate mass measurement required by this test series the FP assay procedure is in need of refinement and that the Rankin counter used in assay is in need of recalibration. Steps are currently under way to effect these improvements. Once they are completed, all filters will be reassayed for FP.

Two problems have disturbed the smooth reduction of the Kr measurements. The first involved a malfunction of a tape recording system during the four 1972 tests. The result was the interjection of a considerable number of spurious signals

between or over meaningful Kr concentration measurements. A long and frustrating iterative process of editing tape output, reprogramming, and generating new output has only recently resulted in the retrieval of a complete set of valid data for test V-2. Indications are that a similar approach will obtain valid V-1 data. However, retrieval of Kr data from tests V-3 and V-4 is in considerably greater doubt.

The second problem with the Kr data involved possible faulty control of a high voltage. This may have caused a reduction in Kr detector count rate (and resultant indicated concentrations of Kr) during some periods of field operation. A careful examination of operational notes taken during field experiments and of accompanying background count rates may permit diagnosis of the samplers affected and of the magnitude of the effect.

Since the analysis of a filter for rhodamine is a destructive assay technique, it will be delayed until after the filters are reassayed for FP. (The FP assay is nondestructive.) Although our chemists feel that filter assay for indium will be feasible, the specific procedure has not yet been developed.

For completeness, Table 6 lists all eight field tests in the current series. However, the analysis and discussion which follow result from Kr and FP measurements made during field tests V-5, V-6 and V-7 only. As mentioned earlier, recording problems have precluded the decoding of Kr measurements from tests V-1 through V-4. (The valid Kr data from test V-2 became available too late for inclusion in this report.) Since it was raining at the onset of test V-8, it was decided not to chance exposing the krypton system Gieger-Müller detectors during that experiment.

ANALYSIS AND DISCUSSION

Despite awareness of the limitations imposed by calibration uncertainties, a mass balance was attempted on tracer passing the 200 and 842-m arcs during test V-6. This test was selected since all tracer (above the 1.5-m elevation) was contained within the crosswind dimension (y) delineated by the five towers on each arc. The procedure entailed specification of normalized exposures (E/Q, with units of sec/m^3) at all measurement points on the vertical surface. Isopleths of E/Q were then drawn on the basis of these data points. Figures 11 and 12 show isopleths of E/Q at 842 m for Kr and for FP. The dashed isopleths are extrapolations above the tops of the 42-m towers.

After isoplething, a value of E/Q was interpolated for each box in a grid with dimensions of one meter in height (z) and one degree in crosswind width. The interpolated E/Q values were summed crosswind and multiplied by their crosswind spacing increment (Ay, with units of meters) to obtain crosswind integrated exposures (CIE/Q, with units of sec/m^2).

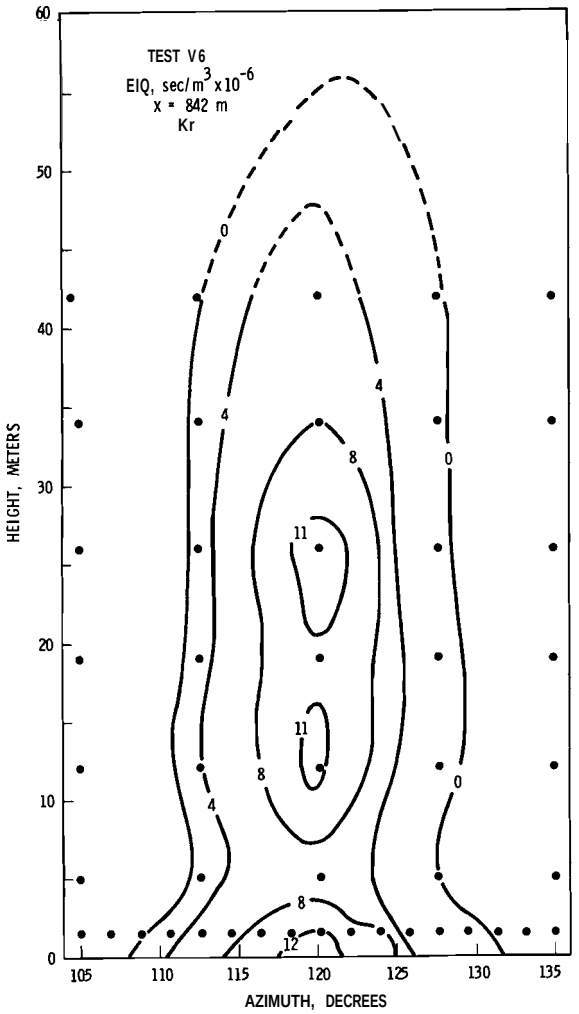

Neg 741011-2

FIGURE 11. Isopleths of Normalized Exposure for Krypton on the Plane x = 842 m During Test V-6. Vertical exaggeration 28:1.

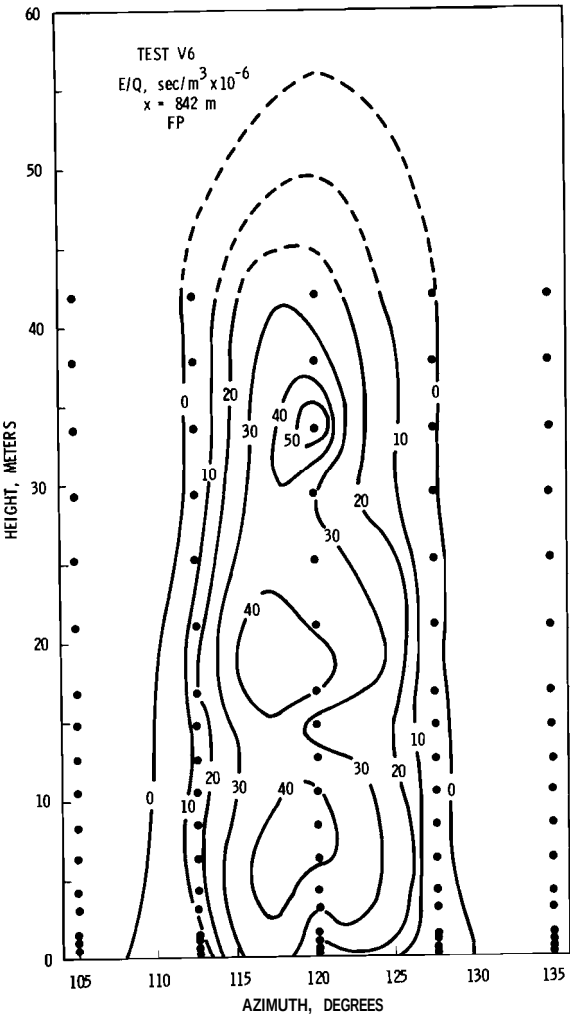

Neg 741011-1

FIGURE 12. Isopleths of Normalized Exposure for Zinc Sulfide FP on the Plane x = 842 m During Test V-6. Vertical exaggeration 28:1.

Examination of vertical wind profiles measured during tracer release provided wind speeds (with units of m/sec) which, when multiplied by 100 (CIE/Q) gave the percentage of tracer passing through the vertical surface per meter increment in height (P, with units of %/m).

It is obvious from a cursory examination of the isopleths on Figures 11 and 12 that the exposures of FP are considerably greater than those for Kr. This fact is reflected by the summation of P over all levels. This sum (Σ, with units of %)will total to 100% for a perfect mass balance. At 842 m for test V-6, Σ_{Kr} = 37% and Σ_{FP} = 133%. Although the graphics are not presented for the similar procedures performed at the

200-m arc, the sums found there are Σ_{Kr} = 57% and Σ_{FP} = 198%.

There are several potential reasons for the large discrepancy from the ideal. As has already been mentioned, a miscalibration in assay technique is one possibility. Mismeasurement of the amount of tracer dispersed is another. Poor isoplething (whether due to ineptness or paucity of data points) is a third possibility. Mismeasurement of the wind speed profile could introduce an error, though hardly one of the magnitude displayed.

In any event, if it is presumed that the measurements made of tracer concentration were correct in a relative sense (as opposed to absolute), the percentages actually observed can be normalized to total to 100%, and the vertical profiles of Kr and FP can be compared. This normalization procedure led to the profiles shown on Figure 13. Here there is reasonable agreement between tracers. Cumulatively summing tracers from the ground level upward reveals 50% of the tracer below 25.6 m for both Kr and FP at the 200-m arc. At 842 m, the fiftieth percentile is reached at 24.8 m for the Kr and at 24.2 m for the FP. Extrapolation above tops of the towers at 200 m accounted for 18% of the Kr and for 14% of the FP. At 842 m above-tower measurements accounted for 10% of the mass in both cases.

Probably the most encouraging point made on Figure 13 is the increase in Kr percentage observed in the lowest 5 m of the 842-m curve.

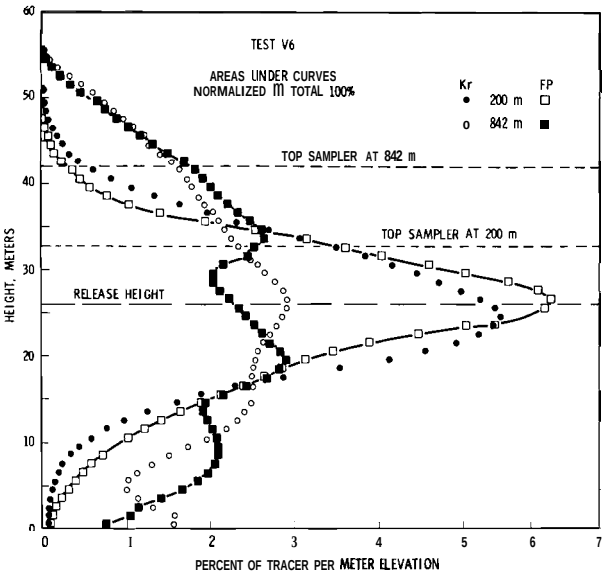

Neg 741011-4

FIGURE 13. Vertical Profiles of Fraction of Tracer per Unit Height for Test V-6. Total amounts of tracers were normalized to 100%.

This increase is very likely due to the (so-called) reflection from the ground of this inert gas. Contrast this increase with the sharp decrease in percentage of the particulate FP in the lowest 5 m. This contrast in near ground-level exposures is also evident in the examination of Figures 11 and 12. These differences suggest strongly that the experimental approach has good chance of success if the mass or concentration measurements can be better quantized.

Although the isoplething and subsequent computations of tracer per unit increment in elevation are amenable to computer processing, the results presented above were tediously generated by hand. The question arises as to how much better is this careful approach than a simpler quick-and-dirty (QAD) approach.

Hence, for test V-6, the fraction of tracer per meter of elevation was computed for the seven Kr measurement levels and for the 17 or 18 FP measurement levels. Here only five data points were used for computing the crosswind integrated exposures. (In test V-6 the end data points were zero since no tracer was observed on the towers at the extremities of the crosswind distribution.) The vertical profiles generated from this QAD approach are shown by the solid curves on Figure 14. No extrapolations were made above the tops of the towers. The current calibrations (miscalibrations?) for determining Kr and FP were used. By weighting the proportion of the total tracer by the vertical spacing of data measurement points, the total tracer passing each arc--up to the top measurement level--could be com-- puted. These sums are indicated at the appropriate elevations on Figure 14.

The individual dots and X's plotted on Figure 14 are those generated by the careful isoplething approach. (The values plotted here were not normalized to force a total of 100%.) The close agreement in the profiles suggests that the effort involved in the detailed approach was largely wasted.

The QAD approach was also used in the computation of profiles of tracer for tests V-5 and V-7. Since the tracer plumes were not contained

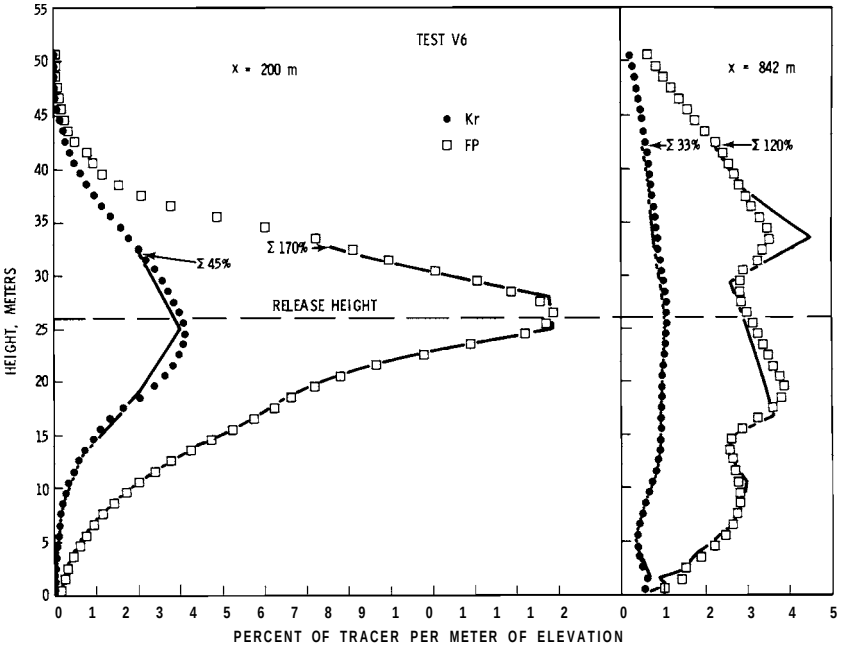

Neg 741011-4

FIGURE 14. Vertical Profiles of Measured Fractions of Tracer per Unit Height for Test V-6. Solid curves from QAD technique. Individual points from careful isoplething.

crosswind within the bounds of the towers on tests V-5 and V-7, some estimate of the proportion of the tracer outside these bounds was required. The only hint of this proportion was afforded by the basic 1.5-m samplers on the FP grid. (The Kr grid at 1.5 m did not encompass the crosswind tracer distributions.) Estimates of tracer beyond that represented by the tower grid during test V-5 were 25% at 200 m and 43% at 812 m.* Corresponding values during test V-7 were 51% and 47% for 200 m and 867 m respectively. As mentioned earlier, the percentages were zero for both 200 m and 842 m during test V-6.

The amount of tracer within bounds of the towers was corrected for that estimated to be beyond, and the results are plotted on Figures 15, 16 and 17. The figures at the top of each curve are sums of tracer percentage up to that topmost measurement point. Plotting of the percentages on a logarithmic scale emphasizes that with the exception of the lowest 5 m or so, the profiles for Kr and FP are reasonably parallel. If attention is restricted to the curves above 5 m, the implication is that although calibrations used in generating either or both curves were in error, the ratio of indicated Kr to indicated FP was consistent. Thus the individual curves are likely valid in a relative sense. If the FP and Kr curves can be superimposed so that the one essentially overlies the other in the 5-m-and-above elevations, the discrepancies between the curves below 5 m can be used to investigate the effects of deposition.

Before proceeding with the deposition investigation, another point can be made regarding relative agreement of the Kr and FP data. Table 7 presents the ratio of the computed sums of Kr to that for FP by test and sampling arc. There is little variation from sampling arc to sampling arc in this ratio (0.64 to 0.60 for test V-5 for instance)

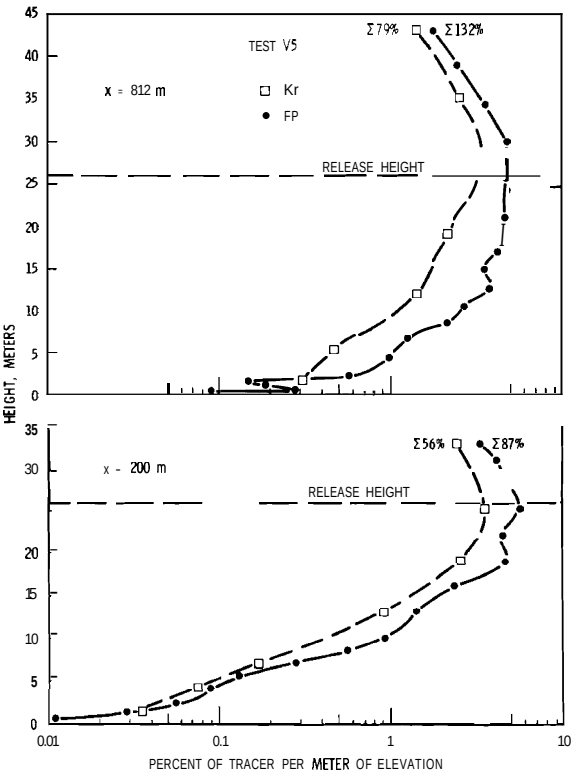

Neg 741011-8

FIGURE 15. Vertical Profiles of Measured Fraction of Tracer per Unit Height for Test V-5 as Determined by QAD Technique

* The source-to-sampler distances reported are those of the mean of the E/Q distribution of FP at the 1.5-m elevation.

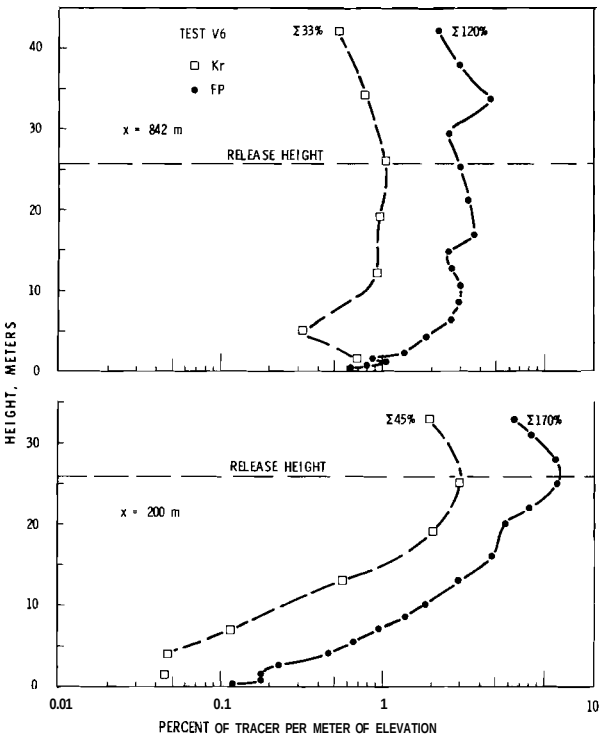

Neg 741011-3

FIGURE 16. Vertical Profiles of Measured Fraction of Tracer per Unit Height for Test V-6 as Determined by QAD Technique

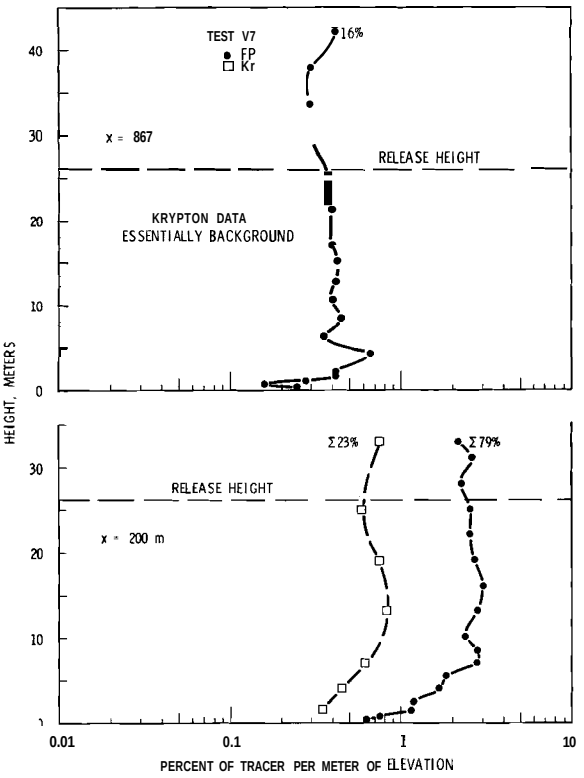

Neg 741011-7

FIGURE 17. Vertical Profiles of Measured Fraction of Tracer per Unit Height for Test V-7 as Determined by QAD Technique

TABLE 7. Ratios of Σ_{Kr} to Σ_{FP}. (Sums from ground to top of towers.)

Distance from Source	Test V-5 QAD	Test V-6 QAD	Test V-6 Isoplethed(a)	Test V-7 QAD
200 m	$\frac{56\%}{87\%} = 0.64$	$\frac{45\%}{170\%} = 0.26$	$\frac{57\%}{198\%} = 0.29$	$\frac{22\%}{79\%} = 0.28$
800 m	$\frac{79\%}{132\%} = 0.60$	$\frac{33\%}{120\%} = 0.28$	$\frac{37\%}{133\%} = 0.28$	$\frac{Bkgd}{16\%} = ?$

a. Percentages here include data extrapolated above top of towers, i.e., include the entire distribution.

although there is considerable variation in the amount of tracer computed as passing the arcs (87% to 132% for Σ_{FP} on test V-5, for instance). The implication here is that the calibrations for FP and Kr are consistent for a specific test, but that the large differences in the total mass computed as passing different arcs during the same test are due to insufficient sampling density. It is recognized that the somewhat different fractions of the plumes can be above the tops of the towers, but in the stable atmospheres observed during tests V-5 and V-6 the bulk of the tracer should have remained below the tops of the towers. Furthermore, the isoplethed percentages listed in Table 2 for test V-6 include extrapolations to embrace the entire vertical distributions, and here also the ratios remain conservative while the percentages vary.

Estimates of the fraction of FP tracer depleted from the plumes have been made graphically for three locations: test V-5 at 812 m, test V-6 at 842 m, and test V-7 at 200 m. Tracer concentrations were too near background to consider analysis in the other three possible cases (V-5 and V-6 at 200 m, and V-7 at 867 m). The appropriate Kr profiles of Figures 15, 16 and 17 were extrapolated above tower tops to zero, and the summed percentages under these curves were normalized to 100%. Then, on the basis of the relatively constant FP to Kr mass ratios above 5 m (where depletion effects were missing or less significant), the FP profiles were normalized to match the general profile of the Kr. Thus the areas of the curves above 5 m should total to the same value.

The lower portions of these profiles are displayed on Figure 18. Since test V-6 shows the most dramatic depletion, it will be used to illustrate the graphic approach employed. The heavy curves are the previously described normalized profiles of Kr and FP percentage. The deficiency of FP in the lowest 5 m is proportional to area ABC less area DEB. This converts to 2.8% of the tracer depleted during the plume traversal to the 842-m arc.

An alternate approach is to presume that the shape of the FP profile below 5 m would have been that of the Kr profile had deposition not occurred. The area describing depletion then becomes AEF, and this area corresponds to a 5.7% depletion.

The same approach was employed for tests V-5 and V-7. The range of estimates of depletion is given in Table 8.

An areal plot of FP exposures based on measurements made at the 1.5-m level could be employed with the deposition estimates presented, and estimates of deposition velocity could be developed. However, the confidence in the absolute value of the measurements currently reported does not justify this effort.

If a complete mass balance is to be attempted following future field experiments, the evidence presented suggests that a much more dense sampling network than that currently in use is needed. To "fill in" the

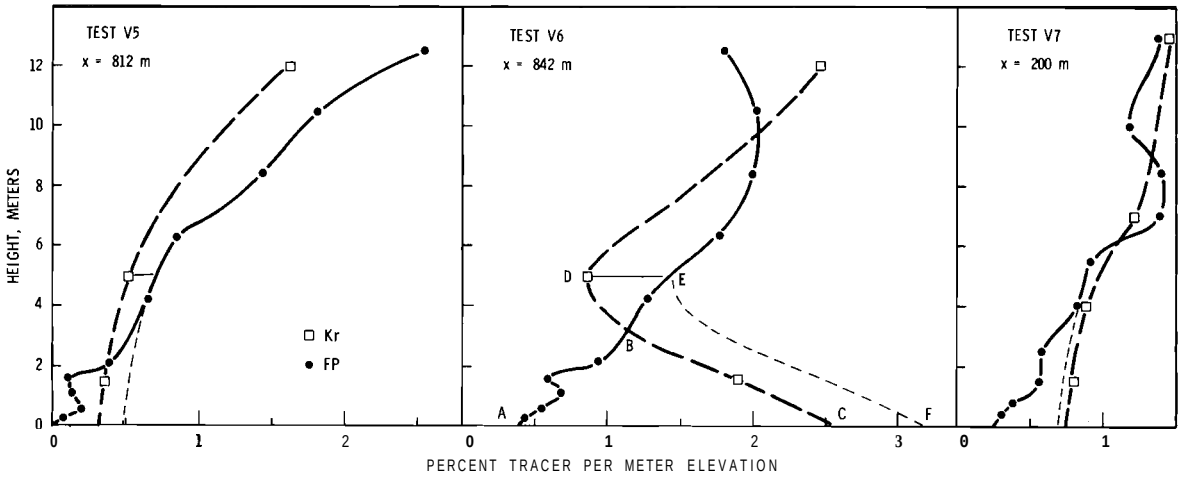

Neg 741011-10

FIGURE 18. Near-Ground Vertical Profiles of Fraction of Tracer. Total Kr for each complete distribution was normalized to 100%.

TABLE 8. Estimates of FP Plume Depletion

Test	Proportion of Plume Depleted During Traversal to- 200 m	812 m	842 m
V-5	--	0 to 0.8%	--
V-6	--	--	2.8 to 5.7%
V-7	0.7 to 1.0%	--	--

holes with many more towers and samplers becomes impractical from budgetary and manpower considerations. Presuming high confidence in the accuracy of tracer concentration measurements can be attained, the compromise of comparison of tracers within a restricted but intensely instrumented grid offers possibilities. For instance, a relatively low-elevation aloft release during stable atmospheres might be instrumented only up to the level of release with the assumption made that a "half-mass" balance would be performed.

CONCLUSIONS

The field measurement techniaues currently employed for Kr and FP produce good relative concentrations of these tracers, but better definition of absolute concentrations is required in deposition studies. Better calibration of the measurement techniques is in order.

For the field experiment examined in greatest detail (test V-6), the median elevation for the mass of tracer passing arcs at 200 and 800 m from the source was within 2 m of the release height of 26 m.

In all three field experiments examined, at distances where significant amounts of tracer intersected the ground, the vertical profiles showed a decrease of the FP tracer

with respect to the Kr at elevations near the ground. Test V-6 displayed strong evidence of reflection from the ground by the inert Kr gas.

The density of field sampling at elevations above 1.5 m precluded confident mass balance computations. Careful isoplething of exposures and subsequent crosswind summing of mass by small vertical increments gave small differences when compared to a more gross "quick-and-dirty" crosswind summing approach.

Following release into the unstable atmosphere of test V-7, about 1% of the released FP tracer is estimated to have been deposited before the plume traversed a distance of 200 m. During a release into a quite stable atmosphere, 0 to 1% of the tracer was deposited during plume traversal to 812 m; and during release into a somewhat less stable atmosphere, 3 to 6% of the tracer was deposited during traversal to 842 m.

FITTING AN ANALYTICAL CURVE TO SOME EXPERIMENTAL DIFFUSION DATA

G. H. Clark* and P. W. Nickola

A technique has been developed for fitting a Gaussian curve to crosswind concentration distributions observed in atmospheric plumes. Effects are presented of truncating of observations to successively smaller portions of the crosswind distribution. comparison of statistics (σ_z and $\bar{z}$) generated from a truncated observed distribution and from the "complete" (observed plus extrapolated) crosswind integrated distribution reveals minor differences.

INTRODUCTION

An attempt has been made to develop an analytical approach to fitting a Gaussian curve to experimental atmospheric diffusion data in order to eliminate some subjectivity from analyses. During periods of startup or carrying out of atmospheric diffusion field tests, meteorological conditions frequently do not remain completely stationary. This deviation causes the tracer plume to shift away from the main axis of the sampling grid. In these cases, the measured horizontal distribution of tracer, rather than being fully defined, is likely to be truncated. In a similar manner, the vertical distribution of tracer is limited by the height of the tower samplers.

* Australian AEC representative on temporary assignment at Battelle, Pacific Northwest Laboratories, Richland, Washington.

The approach used initially in this study was to test several hypothetical distributions of ground-level tracer exposures and to successively truncate points. This simulated the effect of the tracer moving further away from the sampling grid. The influence of this truncation on the derived standard deviation and mean value statistics can be studied. Data from the current series of atmospheric diffusion field tests were also subjected to similar computer analysis.

MATHEMATICAL MODEL

In order to fit a Gaussian curve to the experimental data, a program called REEP (Reduction of Error in the Estimation of Parameters), from the Share program library, was used with the following analytical expression:

$$\text{Tracer exposure} = \frac{\Theta_1}{\sqrt{2\pi}\,\Theta_2} \exp\left[-\frac{1}{2}\left(\frac{x-\Theta_3}{\Theta_2}\right)^2\right]$$

where Θ_1 is an amplitude,
Θ_2 is a standard deviation,
Θ_3 is a mean value, and

Θ_1, Θ_2, and Θ_3 are unknown variables determined for each distribution of data using REEP.

REEP, a Fortran IV coded package, is designed to solve unconstrained nonlinear estimation problems by combining the modified Marquardt method[17,18,19] and a gradient search technique[20] with the projection method of Rosen.[21] This program has proven very flexible in handling some of the more unusual tracer dispersion data, especially under neutral to unstable atmospheric stability conditions.

TEST RESULTS

To investigate the effect of truncating a Gaussian distribution on the derived estimates of standard deviation and mean value statistics, two cases were considered--a platykurtic (flat) distribution and a leptokurtic (pointed) distribution of hypothetical diffusion data. These effects are seen as a family of curves in Figures 19 and 20. In the platykurtic test case, even with the full contingent of 22 data points, the curve fitting routine slightly overestimates the tracer exposures both near the peak and in the tails of the distribution. Only when greater than eight (36%) of the points are truncated do the curves deviate significantly from the curve fitted through all the data points. It is somewhat surprising to note that the trend in the derived standard deviation statistics reverses, with the value calculated after a 36% truncation being approximately equal to the complete Gaussian curve (Table 9).

In the case of the leptokurtic diffusion data, there is good agreement to the point where only one half of the Gaussian curve is defined (see Figure 20). Thereafter there is a significant departure in the computed standard deviation and mean value statistics.

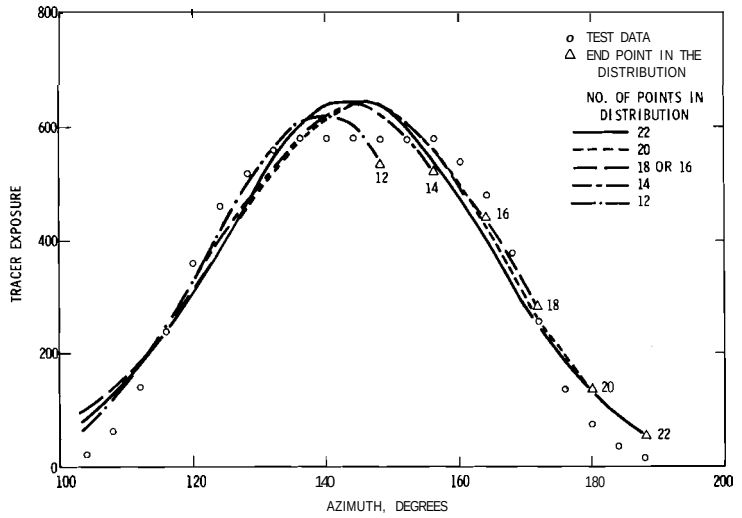

Neg 741011-9

FIGURE 19. Curve Fitting to a Platykurtic (Flat) Distribution of Test Data

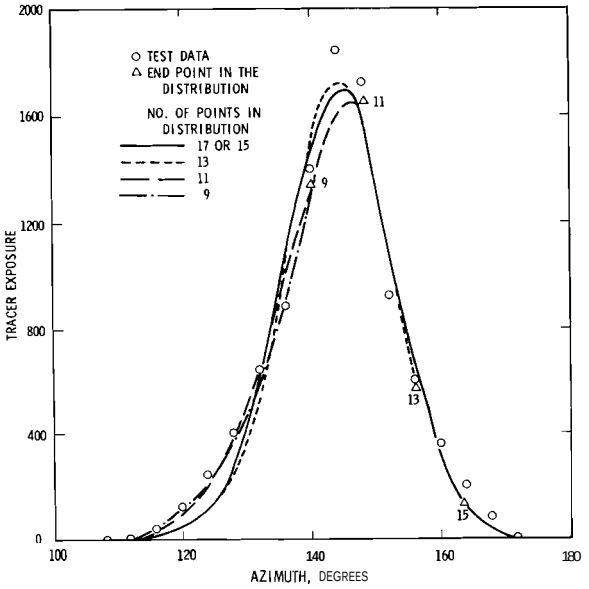

Neg 741011-6

FIGURE 20. Curve Fitting to a Leptokurtic (Pointed) Distribution of Test Data

As a final case in point, the crosswind integrated exposures of ZnS tracer taken from the tower sampler array during Test V-6 were input to the REEP computer code analysis program. In Table 10 the results are presented for the observed truncated distribution of data points and also for the distribution including extrapolation beyond the tower limits. There is a similar trend in both the observed and extrapolated values of σ_z with downwind distance x. The average difference between the two sets of numbers is only 8%, with the observed (truncated) σ_z values being slightly higher.

CONCLUSIONS

All atmospheric diffusion data needs to be subjected to cautious interpretation prior to any statistical analysis. A similar situation applies when trying to analytically fit a Gaussian curve to both the horizontal and vertical tracer exposures from the field experiments. It has been shown that use of the REEP program results in some success in statistically describing a truncated Gaussian distribution of data.

TABLE 9. The Effect of Truncating Data Points on the Gaussian Curve Fitting Statistics

	Platykurtic Data						Leptokurtic Data				
Number of Data Points	22	20	18	16	14	12	17	15	13	**11**	9
Θ_1	32463	32819	33704	33988	30923	25745	36229	36166	35390	49487	189847
Θ_2 (σ_y) (degs.)	19.9	20.3	21.1	21.3	19.4	16.5	8.5	8.5	8.2	**11.1**	17.6
Θ_3 ($\bar{y}$) (degs.)	144.5	144.7	145.3	145.5	143.2	139.2	144.3	144.3	144.2	147.8	166.7

TABLE LO. Statistics from the Crosswind Integrated Exposures of ZnS During Test V-6

	Observed (Truncated)				Observed plus Extrapolated			
x(m)	200	800	1600	3200	200	800	1600	3200
Θ_1	4527	8443	10242	4784	4174	8122	9705	4461
Θ_2 (σ_z) (m)	9.1	16.0	16.5	18.9	8.5	15.0	15.3	17.3
Θ_3 ($\bar{z}$) (m)	26.5	19.7	20.8	18.4	25.6	21.0	21.6	19.7

A SURFACE FLUX MODEL FOR DIFFUSION, DEPOSITION AND RESUSPENSION

T. W. Horst

A model of the diffusion-deposition-resuspension transport process is developed which accounts for the effect of deposition and resuspension on the airborne concentrations by representing the net vertical flux of material at the surface due to these processes as an areal source of material for further downwind diffusion. The diffusion process is modeled by the standard Gaussian plume. This model is used to show that the assumptions of the source depletion model of deposition overestimate surface air concentrations and, hence, the deposition flux by factors of 2 to 4 for moderately strong deposition, $V_d/\bar{u} = 10^{-2}$. These results can be used to define the limits within which the source depletion model may be used with acceptable accuracy.

The resuspension into the air of hazardous material previously deposited on the ground presents a danger which is currently difficult to assess due to a lack of both quantitative physical facts and models to accurately simulate many common situations. At the same time, realistic environmental experiments to determine the physics of resuspension also necessarily include the processes of diffusion and deposition, and a

model including all of these processes is needed to separate the effects of diffusion, deposition and resuspension in the measurements.

To this end, a simple model of the diffusion-deposition-resuspension transport process has been programmed for use on the CDC 6000 computer. This program calculates the evolution of air and ground concentrations of a tracer or pollutant emanating from a specified source and having a given initial distribution on the ground surface. Since the distribution of material on the ground is a source for downwind air concentrations through resuspension, the calculations are considerably simplified by assuming homogeneity in the crosswind direction. Thus the calculations are exact for an infinite line source and closely approximate the crosswind-integrated concentrations from a point source.

MODEL DESCRIPTION

The diffusion process is represented by the standard Gaussian model, assuming perfect reflection of the plume at the ground. Thus a diffusion function can be defined as the downwind air concentration $\chi(x,z)$ of a nondepositing tracer, normalized by the source strength Q,

$$D(x,z,h) \equiv \frac{\chi(x,z)}{Q} = \frac{1}{\sqrt{2\pi}\,\bar{u}\,\sigma_z(x)} \left\{ \exp\left[\frac{-(h-z)^2}{2\,\sigma_z^2(x)}\right] + \exp\left[\frac{-(h+z)^2}{2\,\sigma_z^2(x)}\right] \right\}. \quad (1)$$

(All symbols are defined at the end of this article.) Presently one primary source $Q(t)$ is assumed to be located at the point ($x = 0$, $z = h$). The net flux of material from the ground to the air due to the processes of deposition and resuspension, however, is a secondary, areal source of material,

$$S(x,t) \equiv \frac{\delta Q}{\delta x} = -V_d\,\chi(x,z=z_d,t) + \Lambda G(x,t). \quad (2)$$

Here the deposition and resuspension fluxes are respectively assumed to be directly proportional to the air and ground concentrations through a deposition velocity V_d and a resuspension rate Λ.

Using these definitions, the equation for the evolution of the air concentration χ can be written as the sum of the diffusion from the primary source and from all upwind areal sources,

$$\chi(x,z,t) = Q(t-x/\bar{u})\,D(x,z,h) + \int_0^x S\left(\zeta, t-\frac{x-\zeta}{\bar{u}}\right) D(x-\zeta,z,h=0)\,d\zeta. \quad (3)$$

Note that this formulation accounts for the finite transport time $d/\bar{U}$ between a source and a point which is a distance d downwind. To complete the model we also need to calculate the evolution of the available (for resuspension) ground concentration G due to the processes of deposition, resuspension, and fixation by the soil,

$$\frac{dG(x,t)}{dt} = V_d\ \chi(x,z = z_d,t)$$

$$- (\Lambda + \alpha)\ G(x,t). \qquad (4)$$

The soil fixation rate constant a describes the rate at which material on the ground becomes bonded to the surface in such a way that it is no longer available for resuspension.

COMPARISON TO SOURCE DEPLETION MODEL

A simpler model, for the deposition process only, is described by Van der Hoven.[22] It accounts for the loss of material due to deposition by correspondingly reducing the source strength used to calculate the air concentration at any given distance from the source. The model presented here, which more appropriately depletes the portion of the plume adjacent to the surface, can be used to test the probable magnitude of the errors caused by the source depletion assumption. For the special case of a time-independent source and no resuspension, (2) and (3) can be combined to give

$$\chi(x,z) = Q\ D(x,z,h) -$$

$$\int_o^x V_d\ \chi(\zeta,z_d)\ D(x-\zeta,z,h = 0)\ d\zeta. \qquad (5)$$

In contrast, the assumptions of the source depletion model give

$$\chi(x,z) = Q\ D(x,z,h) -$$

$$\int_o^x V_d\ \chi(\zeta,z_d)\ D(x,z,h)\ d\zeta, \qquad (6)$$

which reduces to

$$\chi(x,z) = Q\ D(x,z,h)$$

$$\exp\left[-\int_o^x V_d\ D(\zeta,z_d,h)\ d\zeta\right]. \qquad (7)$$

It is readily apparent that (7) is more easily solved than (5) and is therefore a more desirable model when the results are acceptably accurate. To assess the accuracy of (7) relative to (5) they were both solved for $1\ m < x < 10^5\ m$; $h = 0$, 10 m, 100 m; $z_d = 1$ m; $z = z_d$, h; and $V_d/\bar{u} = 10^{-2}$, 10^{-3}. Solutions were obtained for unstable, neutral and stable thermal stratification (Pasquill categories A, D and F), using the rural diffusion coefficients amalgamated by Briggs.[23] While these σ's may already include the effects of deposition, they are entirely adequate for the present purposes.

Figure 21 shows the airborne concentrations at heights of 1 m and 10 m, normalized by the corresponding airborne concentration without deposition, due to a source at a height of 10 m. As expected, the surface depletion model in general predicts smaller air concentrations at the surface than does the source depletion model. Consequently, however, the surface depletion model also predicts less deposition. This finally produces the result seen for Pasquill F and $x > 8$ km: smaller total deposition leads, at large downwind distances, to greater surface air concentrations for the surface depletion model than for the source depletion model. It is also interesting to note that for the stable case the air concentration

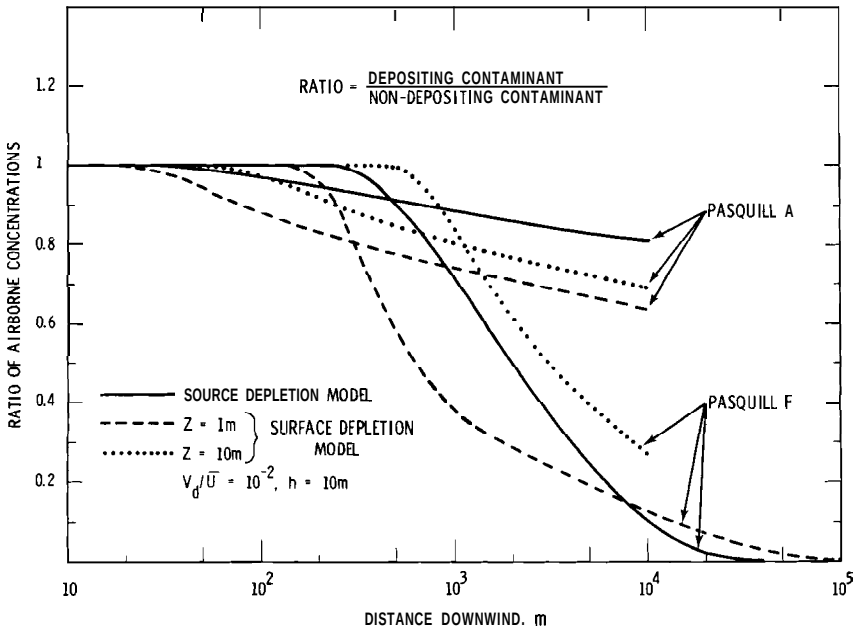

Neg 740226-2

FIGURE 21. Ratio of Airborne Concentrations for a Depositing Versus a Nondepositing Tracer as Calculated by Both the Source Depletion and the Surface Depletion Models

ratio at source height is greater for the surface depletion model than for the source depletion model, while the opposite is true for the unstable case. This is due to the much smaller vertical mixing between the surface and 10 m for the stable case than for the unstable case: the plume depletion due to deposition at the surface is not as readily communicated to the air concentration at 10 m. Since the deposition at short distances is less for the surface depletion model, a height can always be found above which the air concentration is greater for the surface depletion model. This height will decrease with stability.

While Figure 21 shows the effect of deposition on the air concentrations as predicted by the two models, Figure 22 displays a better measure of their relative accuracy, the ratio of the air concentrations as predicted by the two models. In general, the source depletion model overestimates the surface air concentration, by factors of 2 to 4 in some cases. Further, as noted above, at greater distances the source depletion model underestimates the surface air concentration, eventually by extremely large factors. Since the deposition is directly proportional to the surface air concentration, these same errors also apply to the deposition flux to the surface. Thus this figure demonstrates that care must be taken to use the source depletion model only at distances small enough to keep the error due its simplifying assumptions within a tolerable limit.

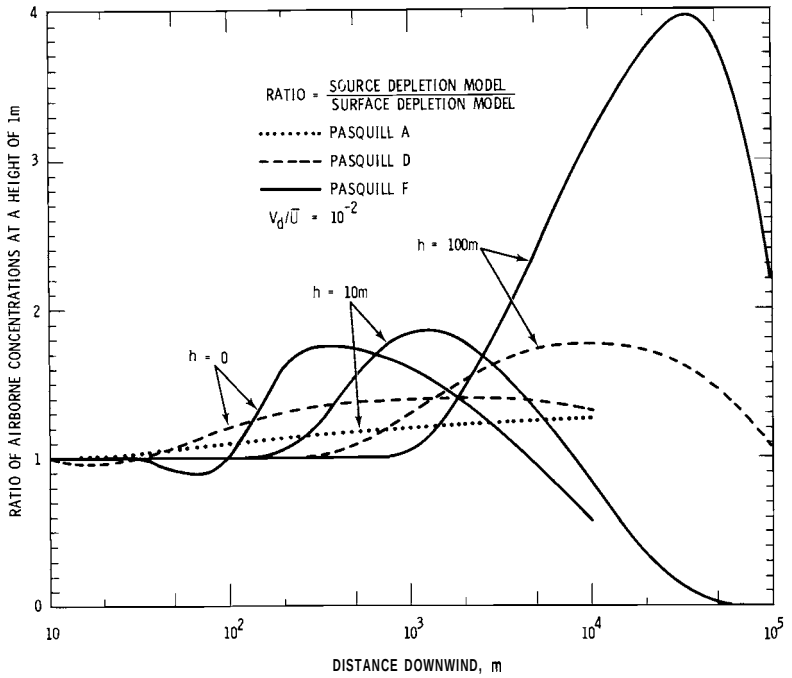

Neg 740226-1

FIGURE 22. Ratio of Airborne Concentrations at Ground Level as Calculated by the Source Depletion Model Versus the Surface Depletion Model

As would be expected, both the amount of deposition and the differences between the source and surface depletion models increase with $V_d/\bar{U}$. The data presented here is for $V_d/\bar{U} = 10^{-2}$, a case of moderately strong deposition. For the source depletion model it can be shown from (7) that the ratio presented in Figure 21 is easily modified for a new value of $V_d/\bar{U}$:

$$(\text{Ratio}_1)^{(V_d/\bar{U})_2} = (\text{Ratio}_2)^{(V_d/\bar{U})_1} \quad (8)$$

The surface depletion model cannot be directly modified in this manner, but the change will be in the same direction as indicated by (8).

DEFINITION OF SYMBOLS

- D diffusion function $\equiv \chi/Q$ (sec m^{-2})
- χ crosswind-integrated air concentration (units m^{-2})
- Q source strength (units sec^{-1})
- $\bar{u}$ mean wind speed (m sec^{-1})
- σ_z vertical diffusion coefficient (m)
- h height of diffusion source (m)
- z height of receptor (m)
- x downwind distance coordinate (m)
- t time (sec)
- V_d deposition velocity (m sec^{-1})
- z_d height of air concentration used to define V_d (m)
- A resuspension rate (sec^{-1})
- G surface concentration available for resuspension (units m^{-1})
- ζ downwind coordinate of surface source, variable of integration (m)
- a rate of soil fixation (sec^{-1})

MESOSCALE TRANSPORT AND DIFFUSION STUDIES

L. L. Wendell and W. F. Sandusky

In progress is an investigation of the validity of using the single-point wind in mesoscale radiological assessments on and around the Hanford site. Work at another AEC Site has shown the practice to be unreliable. Tower data are being analyzed and used to construct wind field trajectories for comparison with constant-volume balloon trajectories and trajectories constructed with a single-point wind. The appropriateness of the use of constant-volume balloon trajectories as an indication of mesoscale transport is being tested by aircraft sampling of an SF_6 plume in the vicinity of the balloons along their trajectories.

INTRODUCTION

Current assessment procedures for estimating radiological doses to distances up to 50 miles involve the use of a wind measured at a single location. A mesoscale wind field and transport study, over a 21-station network of wind towers on and around the National Reactor Testing Station (NRTS) in southeast Idaho, demonstrated that mesoscale boundary layer flow can be too complex for single-station approximation (Wendell 1972).[24] This was shown to be true for the sustained long-term release (Start and Wendell 1974)[25] as well as the accidental short-term release. The local topographic variability seems to be the primary cause of the horizontal spatial variation of the boundary layer flow. Since the terrain variation on and around the Hanford site has more complexity than that of the NRTS, one would expect as much or more mesoscale horizontal variability to prevail. Thus, to provide information which would improve the transport and dispersion estimates for the Hanford site, initial analyses along the lines of those done at the NRTS have been undertaken.

WIND FIELD AND TRAJECTORY STUDIES

A field experiment was conducted during April and May 1973 with eight telemetered stations and 13 supplemental stations providing tower-based wind data. Twelve constant-volume balloons were released during the period and tracked by double theodolites. The balloon trajectories were compared with trajectories constructed for hypothetical particles released at the same time and location and carried by the winds derived from those measured at the tower locations. The average separation between balloons and corresponding particles was 1.2 miles at a travel distance of 5 miles. The longest balloon track was 10 miles, and the separation from the hypothetical particle at this distance was 0.5 mile. These comparisons are few and the distances not long enough to be conclusive, but

they represent about the longest tracks practicably obtained with double theodolites. Test tracks with aircraft have been carried out to as far as 30 miles. Further work with the longer tracks is proceeding and is discussed in the next section.

Analyses in progress on this data set are the computer plotting of the wind fields in synoptic fashion as was done with the Idaho data. A sample of four hourly plots is shown in Figure 23. Also terrain features are to be superimposed onto the flow patterns to see if any obvious correlations are evident. The NRTS style trajectory plots of serially released particles are also being generated several times with various combinations of stations removed to check the sensitivity of the trajectories to network configuration. Figure 24 shows an example of this type of plot. Also planned are comparisons of wind field and single-station generated trajectories.

TRANSPORT AND DISPERSION

It has been implicitly assumed that the trajectories derived from the wind fields or constant-volume balloon flights are representative of the true motion of the air in the planetary boundary layer. This is an assumption that should be subjected to considerable verification. This is being done in cooperation with another program using the constant-volume balloon, the aircraft and a tracer (SF_6). One test run has been completed successfully. A balloon was released into the SF_6 plume under stable conditions and wind speed about 9 m/sec. The aircraft followed the balloon downstream and made sampling runs perpendicular to the track of the balloon. The SF_6 was sampled and analyzed in real time with a gas chromatograph. The balloon was tracked for about 30 miles with positive indications of SF_6 along the whole track. This shakedown run was conducted before the sampler was calibrated. Therefore quantitative concentration calculations await this calibration. This technique should not only provide valuable information on long-range plume dispersion but also on the validity of using constant-volume balloons as indicators of mesoscale range transport.

DISCUSSION AND RECOMMENDATIONS

The preliminary effort with the wind network described above should provide an insight into the spatial variability of the winds and resulting transport patterns in the near-surface layer. Another very important aspect of boundary layer transport is wind direction and speed shear in the vertical. Dramatic examples of this have been observed on towers at both the NRTS and Hanford sites. This phenomenon seems to be induced by local terrain variation in both locations. The causes and frequency of occurrence should also be determined and factored into transport and dispersion models to make them as realistic as practicable for assessment problems.

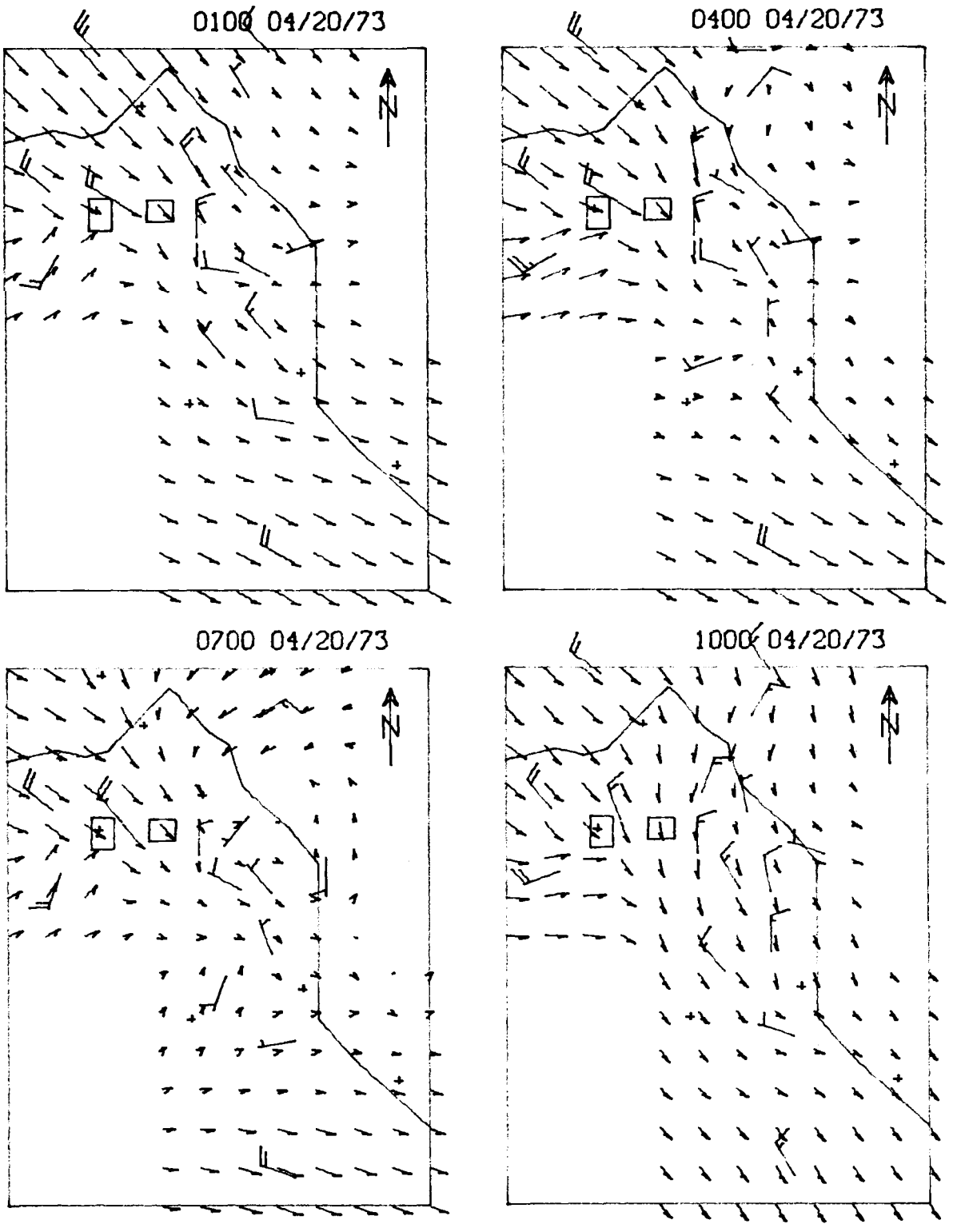

FIGURE 23. Examples of Wind Field Plots over a Grid Covering the Hanford Site. The long solid line represents the Columbia River. The small boxes represent the 200 West and 200 East areas. The wind data from each station are plotted in standard form, and the interpolated winds are plotted as vectors at the grid points.

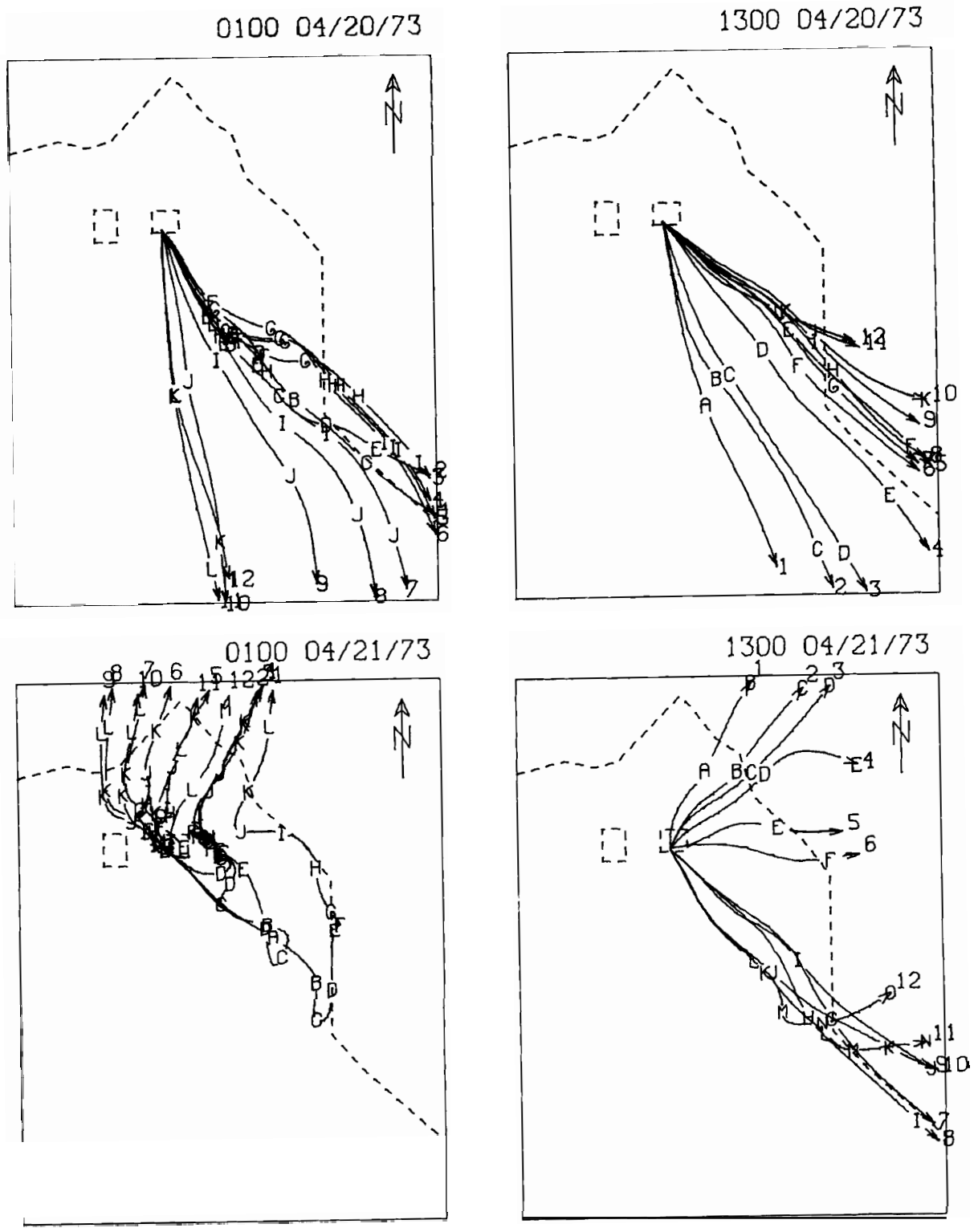

FIGURE 24. Examples of Trajectory Plots Showing the Paths of Hypothetical Particles Released Hourly and Transported by Time Series of Objectively Interpolated Wind Fields. The numbers at the ends of the trajectories indicate the order of release. The letters along the trajectories represent hourly positions.

A MODEL TO COMPUTE LOW-LEVEL MONTGOMERY STREAM FUNCTIONS

W. E. Davis

The model to compute Montgomery stream functions was improved by incorporating water vapor. An error analysis was performed on the model comparing radiosondes taken at three sites in the grid. Results indicated errors in the Montgomery stream function with a standard deviation greater than $\pm 0.05 \times 10^7$ cm^2 sec^{-2} would be exceeded at ~100 mb less than the sfc pressure at all sites for November 1972 data.

INTRODUCTION

In last year's annual report, Davis[26] indicated that a mesoscale model for computing Montgomery stream functions from surface data had been developed and comparisons between stream functions computed from data produced by the model and from observed data for August 1972. Conclusions, based on the comparisons, indicated that the model should be changed to incorporate water vapor effects in the computation of stream functions.

MODEL

The model was developed to compute Montgomery stream functions from a vertical pressure versus potential temperature distribution. The sounding was arrived at by assuming a bilinear variation of pressures on potential temperature surfaces as derived from four radiosonde reports. A linear time change was computed between two time periods when the four radiosonde reports were available. Stream functions were computed for each hourly reporting station in an array. With the basic model in mind, we can now move on to the changes incorporated this year in the model.

As noted last year,[26] this model tended to have a mean difference which was attributed to the lack of inclusion of water vapor effects. This was arrived at when comparing a limited number of soundings with and without water vapor. Thus it was decided to include in the computer program these effects. Water vapor effects, expressed in terms of mixing ratio, were added to the model in the same way pressure was calculated with one change. The change was that because of large horizontal and time changes in mixing ratio the model would on occasion compute negative mixing ratios. Values of the mixing ratio in the model were not allowed to decrease less than 1 g/Kg.

RESULTS

An analysis was made for November 1972 data on days when radiosondes were taken at any of the three sites. With the exception of a couple of days where data is yet to be reduced, the data is shown in Table 11.

TABLE 11. Model Comparison Results

	Bilinear Mean Difference in $\psi(X10^{-7}cm^{-2}sec^2)$			SMP Mean Difference in $\psi(X10^{-7}cm^{-2}sec^2)$		
mb	HMS	PDX	SEA	HMS	PDX	SEA
1000	0	0.002	0.01	0.02	0.005	0.017
950	0.014	0.010	0.012	0.095	0.006	0.001
900	0.029	0.020	0.014	-0.007	0.008	-0.007
850	0.031	0.023	0.024	-0.041	0.009	-0.005
	Standard Deviation in ψ			Standard Deviation in ψ		
mb	HMS	PDX	SEA	HMS	PDX	SEA
1000	0.012	0.010	0.028	0.014	0.027	0.036
950	0.020	0.016	0.035	0.016	0.026	0.045
900	0.032	0.029	0.045	0.022	0.036	0.055
850	0.042	0.043	0.052	0.059	0.052	0.059

As can be seen, the data results are similar to the results arrived at in last year's report except that in general the mean difference for Seattle, Washington; Portland, Oregon; and Hanford, Washington, was improved by the addition of Stampede Pass hourly data (see Davis 1973).(26) However, when computing the standard deviation only, the HMS data for 950 mb and 900 mb were improved.

In comparing November's Seattle results with the Seattle results in the August study in last year's report, the standard deviations were found to be larger for the November case. However, the height, over which the error value of ±0.05 was exceeded, was about the same pressure of ∿100 mb above surface. Again the addition of Stampede Pass, which reduced the standard deviation in the August study, did not do the same in the November study.

Work is continuing on the reduction of data for December 1972 and February 1973 when radiosonde comparisons will be made for Seattle and Portland but not Hanford since no radiosondes were taken at that site during these periods. Also, a changeover has been completed with the model working on the CDC 6600.

THE DEVELOPMENT OF A SONIC ANEMOMETER SYSTEM FOR AIRCRAFT USE

T. W. Horst and T. J. Bander

A three-dimensional sonic anemometer was designed for mounting on an aircraft, constructed and laboratory tested. A noseboom for mounting the anemometer was also constructed and flight-tested. Further testing of both elements of this system is required prior to operational use.

A basic understanding of atmospheric diffusion requires knowledge of the structure of the turbulent eddies which effect the diffusion. Currently there is a great deal more known about turbulence in the lowest

tens of meters of the atmosphere than in the remaining 90% of the planetary boundary layer. There are two reasons for this: first, this constant flux layer adjacent to the surface is less complex than the entire boundary layer, and second, it is much more accessible to measurements from towers. Since diffusion to the distances of interest to the AEC is effected to a large extent above the surface layer, a capability is being developed at PNL for the study of the structure of the planetary boundary layer from an instrumented aircraft.

A sonic anemometer sensor array specifically designed for the measurement of turbulent wind fluctuations from an aircraft[27] was constructed and tested, both in the laboratory and in the environment (Figure 25). Final laboratory testing will be performed in a high-speed (~150 mph) wind tunnel prior to actual flight testing on the aircraft. One major goal of the wind tunnel work will be an evaluation of several fairing designs for the transducers. These smooth the air flow around the transducers themselves in order to minimize environmental noise which may interfere with the reception of the sonic signal.

A boom, extending 1 m in front of the aircraft nose, was constructed and mounted on the Cessna 411 in order to place the anemometer in air undisturbed by the passage of the aircraft. This boom was static tested, FAA approved, and flight tested. Figure 26 shows the boom instrumented with a package to measure the vertical and lateral vibrations

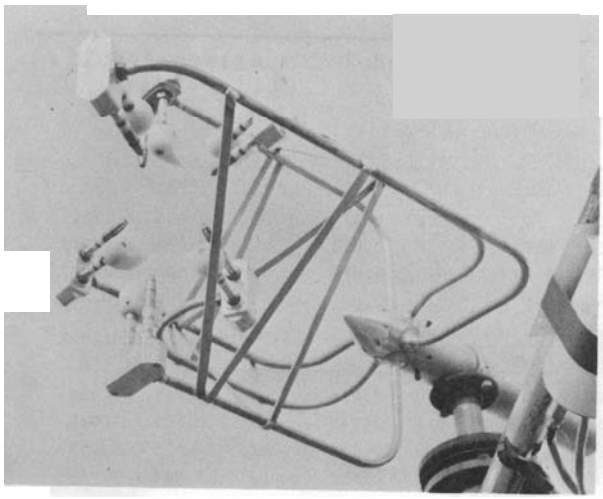

Neg 741390-2

FIGURE 25. For "The Development of a Sonic Anemometer System for Aircraft Use": Aircraft Anemometer Mounted on Tower for Environmental Testing

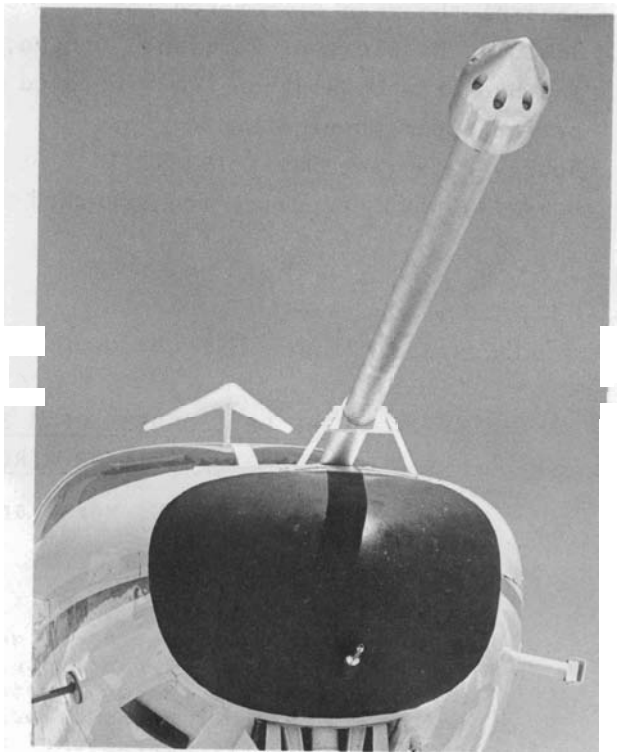

Neg 732762-1

FIGURE 26. For "The Development of a Sonic Anemometer System for Aircraft Use": Aircraft Anemometer Boom Instrumented to Measure Boom Vibrations

of the boom and to simulate the weight of the anemometer.

These two elements of the anemometer system will be combined with the aircraft motion system[27] in CY-1974 for final testing and initial data collection.

EVALUATION OF AN AIRBORNE FLUORESCENT PARTICLE COUNTER FOR ATMOSPHERIC TRACER STUDIES

M. M. Orgill and P. W. Nickola

A Model 220 automatic fluorescent particle counter is being evaluated in an aircraft for utilizing the instrument in field dispersion, transport and deposition studies. Results to date indicate that typical crosswind and downwind concentration profiles can be obtained, but tracking of plumes beyond 7 km has not been totally successful.

A Cessna 411 aircraft is being instrumented for conducting airborne measurements of particulates and gases important to our present AEC diffusion, transport and dry deposition research programs. The first phase of this study is evaluating sampling instruments which promise to meet requirements of a reliable airborne sampling system, i.e. fast response time, high sampling rate, real time capability and good sensitivity. The second phase, beginning next fiscal year, will utilize the airborne instrumentation to conduct field experiments of atmospheric dispersion, transport and deposition within 5 to 50 km.

The sampling instruments presently under evaluation are the MEE Model 110 automatic fluorescent particle counter, an SF_6 airborne gas chromatograph and a MEE Model 140 ice nucleus counter. Other sampling instrumentation may be added depending on the needs and scope of the program.

During the past year most of the effort has been directed toward evaluation of the automatic fluorescent particle counter (AFPC). The AFPC is a portable sampling unit which detects and counts fluorescent zinc sulfide particles commonly used in atmospheric diffusion and transport studies. The counter automatically samples, counts and determines concentration of fluorescent particles in real time.

A schematic of the AFPC in Figure 27 illustrates the operation of the instrument. An air sample is continuously drawn through the intake at approximately 1 liter per second by a

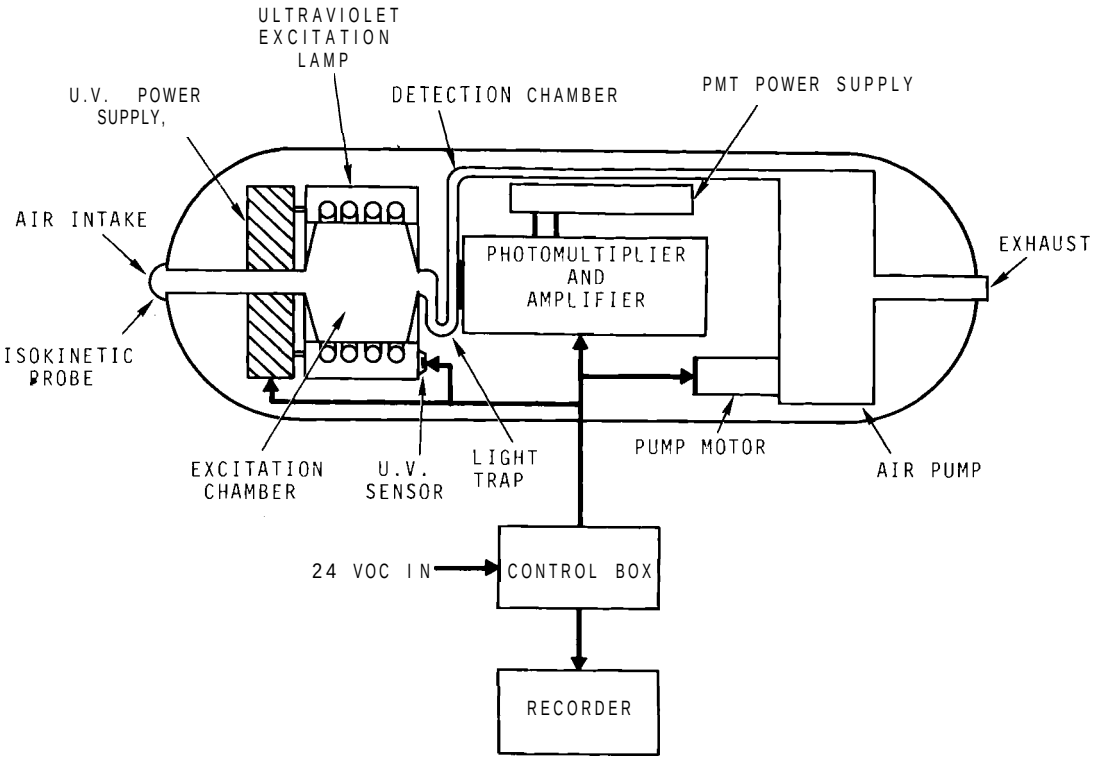

FIGURE 27. Schematic Diagram of Model 110 Automatic Fluorescent Particle Counter

positive displacement pump. For airborne operation the diameter of the intake orifice is sized to obtain isokinetic sampling.

The sample air plus entrained tracer particles passes into an excitation chamber designed to retain the sample for approximately 500 msec. At least 300 msec are required to excite the fluorescent material to a maximum fluorescence. The excitation source consists of a tightly coiled spiral lamp with a peak output of 3650 Å. The lamp spectrum closely matches the excitation spectrum of the zinc sulfide, which peaks at 3700 Å.

The fluorescing tracer particles then pass through a light trap into a detection chamber. The light trap is designed so that the time of passage is less than 5 msec to assure that the particles are still as bright as possible when passing through the detection chamber. A sensitive photomultiplier detector detects each zinc sulfide particle, and the resultant signal is amplified and processed in the electronics unit to give a digital readout of total counts or counts per unit volume. The data output can be monitored visually and recorded by a digital strip-chart recorder, tape system or digital printer.

Evaluation of the AFPC has consisted of ground tests, airborne background readings and airborne measurements of FP2210 and FP3206, commercially available fluorescent

particulate tracers. The ground tests were preliminary operational checks to assure that the instrument was working properly. Airborne background sampling has consisted of flights over the Hanford Project and surrounding regions. Smoke, dust and industrial smoke have also been sampled for background readings.

A summary of the experimental flights including natural airborne background measurements is shown in Table 12. Natural airborne background over the Hanford Project has varied from 1 to 24 particles/liter with an average between 3 and 6 particles/liter. Natural background away from the Hanford Project has varied from 1 to 15 particles/liter with an average of 2.4. Sampling of smoke, dust and industrial type plumes has shown elevated (10 to 200 particles/liter) background levels near the source. The reason the AFPC responds to these other particulates is not entirely known at this time but may be the result, in part, of natural fluorescent materials and spurious scattering effects within the AFPC sensor pod. However, this particular characteristic of the instrument has not seriously affected any field experiment because of the low natural background levels over and near the Hanford area.

Six flights following tower release of FP3206 and FP2210 have been conducted over the Hanford diffusion grid (Table 12). The first three experimental flights were conducted with the AFPC inside the aircraft with the isokinetic inlet connected to the aircraft sampling probe by a plastic tube. This arrangement appeared unsatisfactory due to the high probability of deposition of the FP material in the aircraft sampling probe and connecting tube. The last three experimental flights were completed with the AFPC sensor pod attached underneath the aircraft's fuselage as indicated in Figure 28. This position of the sensor pod minimizes the possibility of extraneous deposition of the FP tracer.

Airborne sampling of FP3206 and FP2210 from tower releases and under stable to unstable conditions has shown the following tentative results:

1. The AFPC is relatively more sensitive to FP3206 than to FP2210. The difference in sensitivity is about a factor of nine.
2. Typical crosswind downwind concentration profiles with distance have been observed during sampling flights. Figure 29 shows an example of the airborne concentration as a function of crosswind distance in a case where the FP3206 plume was relatively narrow.
3. Sampling of the fluorescent particle plumes for distances over 7 km has been disappointing to this time. A distance of 13 km has been the limit for detecting a plume above natural background readings.

In the future, work will proceed toward further ground and airborne evaluation of the AFPC and also of an airborne SF_6 gas chromatograph. If evaluations of these two instruments show promising results, then the next step will be to conduct simultaneous airborne measurements of fluorescent

TABLE 12. Experimental Flight Data Obtained with Automatic Fluorescent Particle Counter

Date	Source	Emission Rate (gm/min)	Type of Plume	Stability	400 ft Wind Speed (mph)	Range of Maximum Counts (counts/sec)	Maximum Distance Plume Tracked (km)
3/9/73	Hanford		Background	Unstable	12-20	5-24	
	Stacks(Hanford)		Smoke	Unstable	12-20	39-44	
	Al Smelter		Industrial	Unstable	12-20	55-100	
	Ground		Dust	Unstable	12-20	109-159	
3/14/73	Hanford		Background	Unstable	2-4	4-22	
	*Tower (85 ft)	24	FP2210(Wet)	Unstable	2-4	4-25	
	Burningfield		Smoke	Unstable	2-4	5-12	
	Pasco		Smoke & Haze			6-32	
	Boise-Cascade		Industrial			76-105	
3/19/73	Hanford		Background	Unstable	4-8	6-11	
	*Tower(400 ft)	152	FP2210(Dry)	Unstable	4-8	74-95	3.2
		285	FP3206(Dry)	Unstable	4-8	552-885	9
3/30/73	Hanford		Background	Unstable	2-7	2-5	
	*Tower (400 ft)	10.5	FP3206(Dry)	Unstable	2-7	232-645	7
6/11/73	Columbia River		Background			2-15	
	Boise-Cascade		Industrial			10-14	
	Al Smelter		Industrial			14-236	
6/14/73	Hanford		Background	Unstable	25	1-5	
	*Tower (400 ft)	94	FP3206(Dry)	Unstable	25	20-30	3.2
6/15/73	Hanford		Background	Stable-Neutral	14-16	1-3	
	*Tower (400 ft)	100	FP3206(Dry)	Stable-Neutral	14-16	11-956	7
6/18/73	Hanford		Background	Stable-Neutral	4-11	1-3	
	*Tower (400 ft)	152	FP3206(Dry)	Stable-Neutral	4-11	20-927	13
10/10/73	SE Washington		Background			1-3	
	Boise-Cascade		Industrial			11-15	
	Pulp Mill		Industrial			8-18	

*Releases from towers.

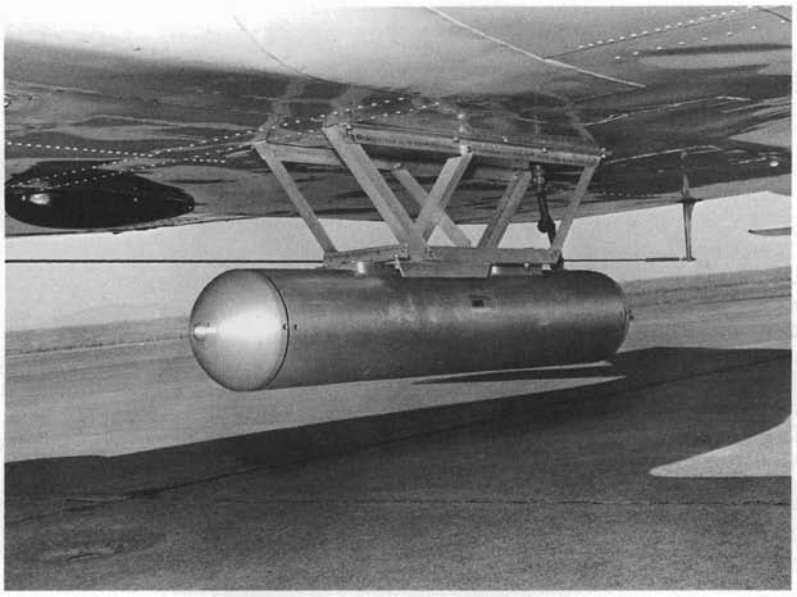

Neg 61169-3

FIGURE 28. Airborne Location of Automatic Fluorescent Particle Counter Sensor Pod

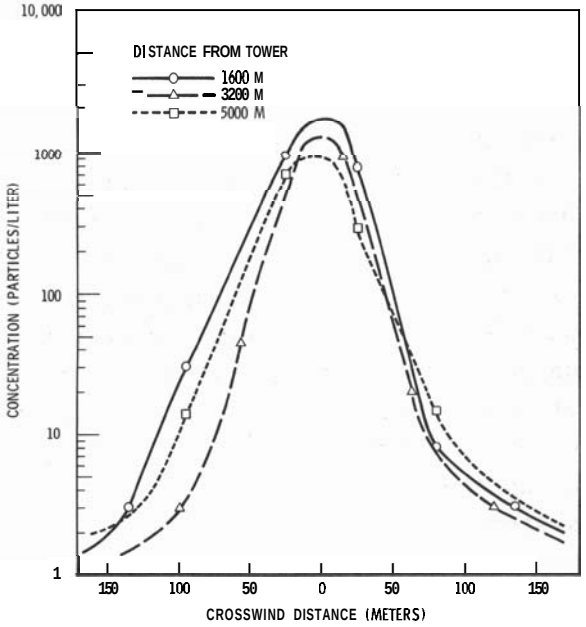

Neg 740681-3

FIGURE 29. FP3206 Concentration as a Function of Crosswind Distance. Altitude 137 meters (450 feet) above ground, June 18, 1973.

particles and SF_6 as tracers. Experiments with silver iodide in conjunction with the ice nucleus counter will provide another size range (submicron) of particulate to be included in the study.

ACKNOWLEDGMENTS

F. O. Gladfelder, J. M. Baily, K. M. Busness and J. C. Draper have assisted with the evaluation of the AFPC.

A REAL-TIME SYSTEM FOR DETECTION OF THE ATMOSPHERIC TRACER SULFUR HEXAFLUORIDE

R. N. Lee and M. C. Miller

An SF_6 tracer gas detection system built for aircraft operation has undergone tests to determine its qualitative performance. The primary component of this system is a gas chromatograph equipped with an electron capture detector. During operation, continuous flow of an atmospheric sample through a column possessing an affinity for oxygen allows real-time description of an SF_6 plume before arrival of the oxygen frontal. The column, which is rejuvenated by an argon backflush, permits sampling for 1-min intervals during each 6 to 8 min of flight time.

INTRODUCTION

While the total impact of the fuel shortage is difficult to predict, it is apparent that recently established air quality standards may be relaxed as we become increasingly dependent on our relatively abundant reserves of coal and high sulfur oil. If these standards are not to be compromised, advances must be realized in air pollution control technology and in the understanding of atmospheric diffusion processes. While the first is surely required to reduce emissions from industrial sources faced with the use of dirtier energy sources, the second is essential to the siting of new facilities.

The atmospheric scientist is thus confronted with the need to formulate and develop atmospheric models which will furnish input for assessing the impact of these facilities on the surrounding environment. To achieve this end, research aircraft and aircraft sampling techniques will play an important experimental role. The use of atmospheric tracers has furnished valuable information on plume behavior although it has not been generally possible to follow such materials beyond 15 km. Sulfur hexafluoride is, however, remarkably well suited for long-range studies due to its very low water solubility, passive chemistry and ready detection via the electron capture detector. Dietz has made a significant contribution to the study of atmospheric diffusion with the development of a portable gas chromatographic system capable of detecting this material at concentrations as low as 4×10^{-13} cc/cc.[28,29,30] This report concerns the performance of a similar system.

DETECTOR DESIGN AND OPERATION

The schematics appearing in Figures 30 and 31 illustrate the operation of the real-time sulfur hexafluoride detector being developed for application to the diffusion programs of the Atmospheric Sciences

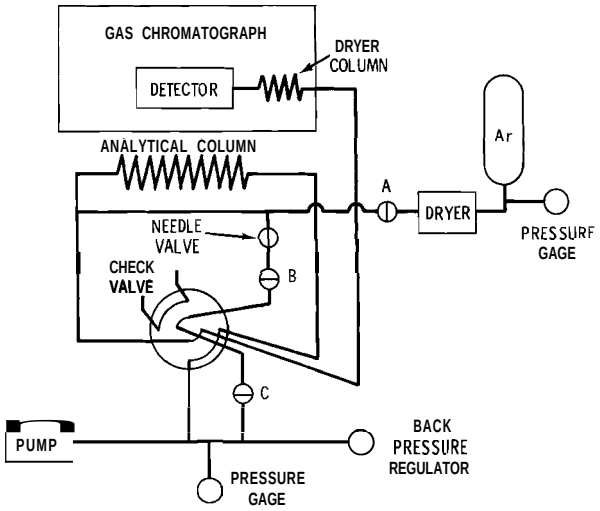

Neg 740938-4

FIGURE 30. SF_6 Detection System - Sampling Mode

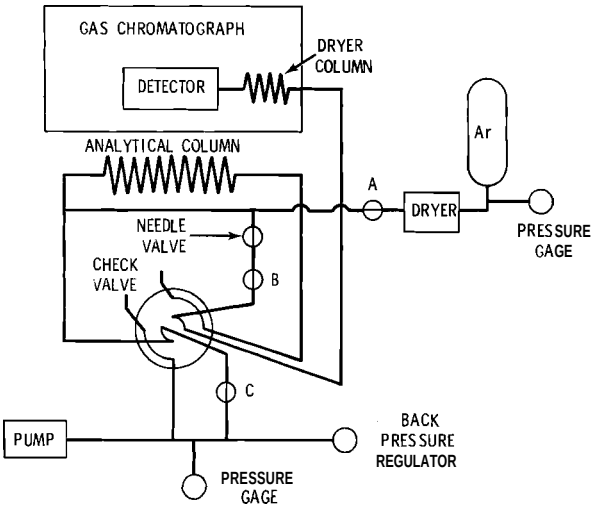

Neg 740938-5

FIGURE 31. SF_6 Detection System - Backflush Mode

Department. This unit is basically the same as that built by Dietz. It consists of an Analytical Instrument Development Model 511 portable gas chromatograph equipped with an electron capture detector, a Gast Model 0531 pump, Veriflo Model PN-4180115 back pressure regulator and a 6-ft analytical column external to the chromatograph.

The molecular sieve column employed with this system was conditioned in a slightly different manner from that used by Dietz.[31] A 6-ft section of 1/8-in. stainless steel tubing was packed with 5A molecular sieve. Helium gas was first passed through the column for 4 days while maintaining a temperature of 250 to 290°C. Oxygen and water were thus removed from the column. Nitric oxide was then introduced for 3.5 hr. During this period column temperature was held at 250 to 300°C for 3 hr and then allowed to fall to room temperature. Loosely bound nitric oxide was removed with a stream of helium before conversion of the more tightly bound gas to the dioxide. This was accomplished by exposing the column to a stream of oxygen gas. During this final stage of conditioning the column was maintained at room temperature for 30 min and then brought to 100°C.

Valves A, B, and C are solenoid valves which are activated during sampling. Unlike the Dietz system, air is directed to the analytical column and hence to the electron capture detector by manual operation of an 8-port valve.

Sampling is initiated following a purge of the detector and the analytical column with argon. After this brief backflush period (~5 min), valves A, B, and C are closed simultaneously with activation of the pump. The back-pressure regulator is then adjusted to provide the desired column pressure before switching the 8-port valve to the

sampling position. Tests described in the next section were conducted with a column pressure of between 10 and 13 psi. Under these conditions, approximately 75 and 135 sec are required for the respective transit of sulfur hexafluoride and oxygen from the sampling probe to the detector. Thus a 1-min real-time description of the plume profile is achieved, via frontal chromatography with recorder response to the plume offset approximately 1 min from the time the aircraft enters the plume. Portrayed graphically in Figure 32 is the long response time, which is a necessary consequence of the column separation of sulfur hexafluoride from oxygen. The response of the electron capture detector to oxygen appears at the end of the chromatogram.

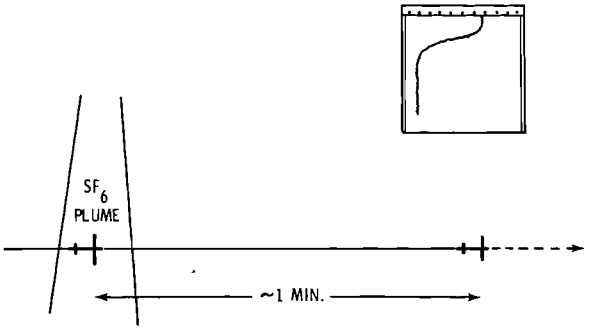

Neg 740938-3

FIGURE 32. Relative Position of the Aircraft During Sampling and Detector Response to the SF_6 Plume

RESULTS

Qualitative tests of the system's response to a sulfur hexafluoride plume were obtained by operating the detector both in the field at ground level and in the aircraft over the Hanford reservation. Although recorder response has not been calibrated, results of these field tests have provided encouraging evidence for potential application of this system to long-range diffusion studies. The chromatogram shown in Figure 32 was recorded from a moving truck 1.6 km downwind of a continuous ground level release of approximately 0.01 cfm. Meteorological conditions at test time were characterized by northwesterly winds at speeds 16 to 20 mph and neutral stability conditions.

Figure 33 shows the plume profile at an altitude of 700 ft, 3.2 km from the source. During this test, sulfur hexafluoride was released at approximately 0.7 cfm from the 400-ft level of the Hanford meteorological tower. Superimposed on the chromatogram in Figure 34 is the recorder response to a background air sample.

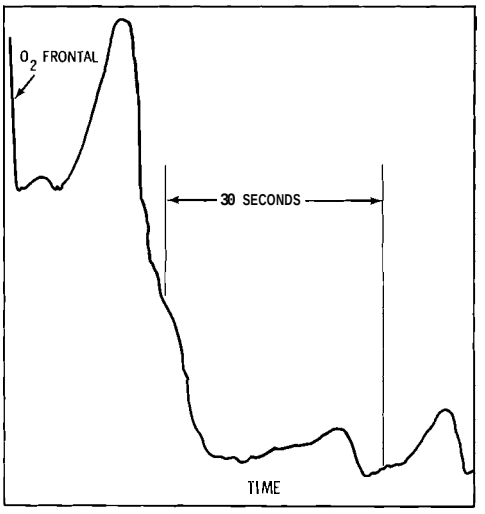

Neg 740938-2

FIGURE 33. Frontal Chromatogram of Air Sample 1.6 km from Source

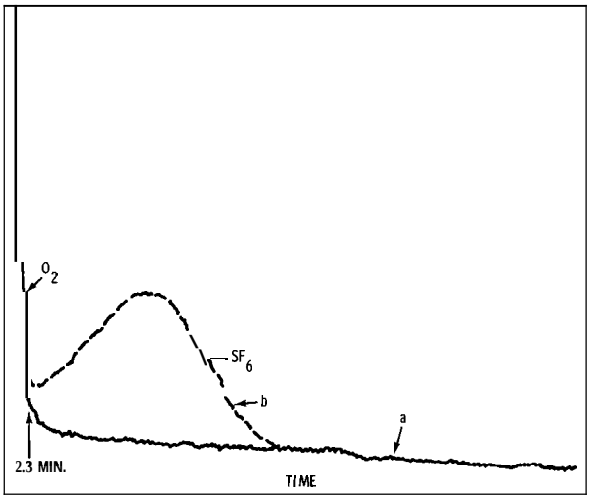

Neg 740938-1

FIGURE 34. Superimposed Frontal Chromatograms of Air Samples: a = background; b = 700-ft altitude

Throughout this early test period the major difficulty has been locating the plume at the distances of interest. All releases for aircraft sampling have been from the 400-ft level of the meteorological tower with a source strength of less than 1 cfm. During these tests we have been able to see the plume at distances of up to 29 km. With the current design, however, we are limited to a sampling time of approximately 1 min for every 6 to 8 min of flight time. Under this constraint, we are restricted to a sampling path of about 3 km before backflushing in preparation for the next sample. We have therefore investigated the use of a tetroon to provide a visual indication of the approximate plume location. The success of this trial promises to enhance the applicability of this tracer detection system.

REFERENCES

1. J. A. Businger, J. C. Wyngaard, Y. Izumi and E. F. Bradley, "Flux-Profile Relations in the Atmospheric Surface Layer," J. Atmos. Sci., vol. 28, pp. 181-189, 1971.

   N. E. Busch. "The Surface Boundary Layer," Boundary-Layer Meteor., vol. 4, pp. 213-240, 1973.

3. C. E. Elderkin, "Diabatic Effects on Atmospheric Turbulence Spectra," Pacific Northwest Laboratory Annual Report for 1970 to the USAEC, Division of Biology and Medicine, Volume II: Physical Sciences, Part 1, Atmospheric Sciences, BNWL-1551, Battelle, Pacific Northwest Laboratories. June 1971.

4. J. C. Kaimal and J. A. Businger, "A Continuous Wave Sonic Anemometer-Thermometer," J. Appl. Meteor., vol. 2, pp. 156-164, 1963.

5. C. E. Elderkin, D. C. Powell and T. W. Horst, "Modeling of Wind Component Spectra," Pacific Northwest Laboratory Annual Report for 1970 to the USAEC, Division of Biology and Medicine, Volume II: Physical Sciences, Part 1, Atmospheric Sciences, BNWL-1551, Battelle, Pacific Northwest Laboratories, Richland, Washington, June 1971.

6. T. W. Horst and C. E. Elderkin, "Turbulence Studies in the Atmospheric Boundary Layer," Pacific Northwest Laboratory Annual Report for 1969 to the USAEC, Division of Biology and Medicine, Volume II: Physical Sciences, Part 1, Atmospheric Sciences, BNWL-1307, Battelle. Pacific Northwest Laboratories, Richland, Washington, June 1970

7. J. C. Kaimal, "Turbulence Spectra, Length Scales and Structure Parameters in the Stable Surface Layer," Boundary-Layer Meteor, vol. 4, pp. 289-309, 1973.

8. D. C. Powell and C. E. Elderkin, "Profile-Derived Estimation of Crosswind Integrated Exposures from Elevated Releases: Initial Model," Pacific Northwest Laboratory Annual Report for 1971 to the USAEC Division of Biology and Medicine, Volume II: Physical Sciences, Part 1, Atmospheric Sciences, BNWL-1651, Battelle, Pacific Northwest Laboratories, Richland, Washington, pp. 161-170, December 1972.

9. C. E. Elderkin and D. C. Powell, "Profile-Derived Estimation of Crosswind Integrated Exposure from Elevated Sources: Model Revisions and Applications," Pacific Northwest Laboratory Annual Report for 1971 to the USAEC Division of Biology and Medicine, Volume II: Physical Sciences, Part 1, Atmospheric Sciences, BNWL-1651, Battelle, Pacific Northwest Laboratories, Richland, Washington, pp. 171-173, December 1972.

10. F. A. Gifford, "Variation of the Lagrangian-Eulerian Time Scale Relationship with Stability," USAEC Meteorological Information Meeting, Chalk River, Canada, September 11-14, 1967, AECL-2787, pp. 485-499, 1967.

11. C. E. Elderkin and D. C. Powell, "Measurements and Graphs of Turbulence Autocorrelations in Space and Time," Pacific Northwest Laboratory Annual Report for 1971 to the USAEC Division of Biology and Medicine, Volume II: Physical Sciences, Part 1, Atmospheric Sciences, BNWL-1651, Battelle, Pacific Northwest Laboratories, Richland, Washington, pp. 155-161, December 1972.

12. N. Z. Ariel and E. K. Byutner, "Relation between the Lagrangian Functions for the Atmospheric Layer Near the Earth Surface," Izv., Atmos. and Oceanic Phys., vol. 2, pp. 993-996, trans. J J. Gollob, 1966.

13. G. A. Sehmel, S. L. Sutter and M. T. Dana, "Dry Deposition Processes," Pacific Northwest Laboratory Annual Report for 1972' to the USAEC Division of Biomedical and Environmental Research, Volume II: Physical Sciences, Part 1, Atmospheric Sciences, BNWL-1751, Part 1, Battelle, Pacific Northwest Laboratories, Richland, Washington, pp. 43-49, April 1973.

14. J. J. Fuquay, Progress in Atmospheric Physics: A Summary of Hanford Laboratories Work on the Program Under General Electric, 1959-1964, HW-83602, General Electric, Richland, Washington, September 1964.

15. J. D. Ludwick, J. J. Lashock, R. E. Connally and P. W. Nickola, "Automatic Real-Time Air Monitoring of ^{85}Kr Utilizing the 4096 Memory of a Multiparameter Analyzer," Rev. Sci. Instr., vol. 39, pp. 853-859, 1968

16. P. W. Nickola, J. D. Ludwick and J. V. Ramsdell, "An Inert Gas Tracer System for Monitoring the Real-Time History of a Diffusing Plume," J. Appl. Meteor., vol. 9, no. 4, pp. 621-626, 1970

17. Donald W. Marquardt. "An Algorithm for Least-Squares Estimation of Nonlinear Parameters," SIAM Journal, vol. 11, no. 2, pp. 431-441, June 1963.

18. David F. Sanno, "An Algorithm for the Solution of Nonlinear Estimation Problems with Linear Constraints," Technical Memorandum No. 161, File CAO1, October 27. 1965.

19. David F. Sanno, A Modified Newton-Raphson Technique for Constrained Nonlinear Estimation Problems, Doctoral dissertation submitted to Carnegie Institute of Technology in partial fulfillment of the requirements for the degree of Doctor of Philosophy.

20. Thomas L. Saaty and Joseph Bram, Nonlinear Mathematics, McGraw-Hill, New York, pp. 70-90, 1964.

21. J. B. Rosen, "The Gradient Projection Method for Nonlinear Programming, Part I, Linear Constraints," SIAM J., vol. 8, no. 1, pp. 181-217, March 1960.

22. I. Van der Hoven, "Deposition of Particles and Gases," Meteorology and Atomic Energy, 1968 (D. Slade, ed.), USAEC, TID-24190, pp. 202-208, 1968.

23. G. A. Briggs, Diffusion Estimation for Small Emissions, ATDL Contribution 79 (Draft), Air Resources Atmospheric Turbulence and Diffusion Laboratory, Oak Ridge, Tennessee, May 1973.

24. L. L. Wendell, "Mesoscale Wind Fields and Transport Estimates Determined from a Network of Wind Towers," Monthly Weather Review, vol. 100, pp. 565-578, 1972.

25. G. E. Start and L. L. Wendell, "Regional Effluent Dispersion Calculations Considering Spatial and Temporal Meteorological Variations," NOAA Technical Memorandum (in press).

26. W. E. Davis, "A Model for Near Surface Computation of Montgomery Stream Functions," Pacific Northwest Laboratories Annual Report for 1972 to the USAEC, Division of Biomedical and Environmental Research, Volume II: Physical Sciences, Part I, Atmospheric Sciences, BNWL-1751, Pt 1 UC-53, Battelle Pacific Northwest Laboratories, April 1973.

27. T. W. Horst and K. M. Busness, "Aircraft Instrumentation for the Measurement of Turbulent Wind Fluctuations," Pacific Northwest Laboratory Annual Report for 1972 to the USAEC, Division of Biology and Medicine, Volume II: Physical Sciences, Part 1, Atmospheric Sciences, BNWL-1751, Pt 1, Battelle Pacific Northwest Laboratories, Richland, Washington, April 1973.

28. R. N. Dietz and E. A. Cote, "Tracing Atmospheric Pollutants by Gas Chromatographic Determination of Sulfur Hexafluoride," BNL-16642, Brookhaven National Laboratory, Brookhaven, New York, February 1972.

29. R. N. Dietz, E. A. Cote and G. J. Ferber, "Evaluation of an Airborne Gas Chromatograph for Long Distance Meteorological Tracing," 165th Amer. Chem. Soc. Meeting, Dallas, Tex., Div. Water, Air and Waste Chem., vol. 13, no. 1, p. 5, 1973.

30. R. N. Dietz and E. A. Cote, "Tracing Atmospheric Pollutants by Gas Chromatographic Determination of Sulfur Hexafluoride," Environmental Science and Technology, vol. 7, no. 4, p. 338, 1973.

31. R. N. Dietz, "Gas Chromatographic Determination of Nitric Oxide on Treated Molecular Sieve," Anal. Chem. vol. 40, no. 10, p. 1576, 1968.

ATMOSPHERIC TRANSFORMATION PROCESSES

Contaminants, once released to the atmosphere, can be altered in many ways. Gases may become adsorbed on particles and particles may coagulate. Many chemical processes occur, frequently promoted by light and catalyzed by trace substances in the air. Understanding of transformation is essential in making material balances of air pollutants and accounting for observed downwind concentrations.

During the past two years our program on atmospheric transformations has proceeded essentially through three stages of development. The first began with our acquisition of the Cessna 411 aircraft, where the primary task was to acquire trace gas and aerosol instrumentation and incorporate it for airborne analysis. The second stage of the program was to utilize this newly developed facility for airborne observation and to relate these observations qualitatively to atmospheric transformation phenomena. The third stage of this program—beginning at the present time—is to develop mathematical models for quantitative diagnosis and analysis of atmospheric phenomena observed using the aircraft facility. It is anticipated that subsequent comparison between transformations models and observation will result in improved models which will be useful as input to other DEBR programs—particularly those involving wet- and dry-deposition processes.

The contributions in this section, corresponding largely to the second phase of research, indicate our key emphases in this area the past year. Of special interest in research this year have been the changes in particle sizes with height and downwind location from major sources. As part of the studies in St. Louis during METROMEX, account was taken of the chemical transformations of some pollutants. Inert pollutants were used as indications for exclusively diffusion processes. This section includes those reports concerned with transformations of aerosols and gases.

AIRBORNE LABORATORY FOR AIR POLLUTION STUDY*

A. J. Alkezweeny

A description is given of air pollution and cloud physics instrumentation aboard a Cessna 411 aircraft. The aircraft is capable of continuously measuring and recording aerosol particle size distributions and concentrations of Aitken nuclei, cloud condensation nuclei, ice nuclei, and concentrations of trace gases, as well as meteorological and aircraft parameters. All the data are measured and recorded automatically on magnetic tape and/or strip-chart recorders.

The aircraft is currently in use for characterization of aerosol and trace gases in polluted and unpolluted atmospheres.

INTRODUCTION

During the past 2 years Battelle, Pacific Northwest Laboratories has been adapting and instrumenting a Cessna 411 aircraft to perform airborne measurements of parameters important to the understanding of the characteristics and behavior of aerosols and trace gases in the atmosphere.

The all-weather, radar equipped, twin-engine aircraft is capable of cruising at speeds between 110 and 230 mph for a period of 5 hr and up to altitudes of 25,000 ft. The following sections describe the electrical power distribution, the air sampling probe, measuring instruments, data recording, and data processing.

ELECTRICAL POWER DISTRIBUTION

The instrumentation presently installed in the aircraft requires both 28 VDC and 115 VAC-60 Hz. The aircraft 28 V bus is supplied by two 100-ampere (A) alternators. The bus supplies power directly to certain instruments and also to a 115 VAC-60 Hz inverter which provides up to 1 kW output to the remaining instruments.

Power distribution to the instruments is controlled via a central power control panel. The control panel is divided into three functional areas: inverter control, AC power, and DC power. Selection of

* This paper presents a continuation of the project reported on in "Aircraft Instrumentation for Atmospheric Research," Pacific Northwest Laboratory Annual Report for 1971 to the USAEC Division of Biology and Medicine, Volume II, Part I Atmospheric Sciences, BNWL-1651 PT1, Battelle Northwest Laboratories, Richland, Washington, pp. 91-99, December 1972.

the inverter, application of the inverter load, and selection of an external AC source are provided in a manner which prevents the application of inverter and external AC power simultaneously. A switch selects an external AC source supplied via an external AC jack at the rear of the control panel chassis and is used for ground operations (maintenance, calibration, etc.). A pair of switches and relays applies the 28 VDC to the inverter and connects the inverter output load. The AC power is distributed to the instrumentation via a group of standard AC outlets protected by individual circuit breakers.

Distribution of 28 VDC power is also controlled by a group of circuit breakers. A main 15-A circuit breaker/switch feeds five branch circuit breakers which service the DC outlets for instrument power.

Metering is provided for visual monitoring of the DC input current to the inverter, AC and DC volts and total AC and DC current load. All the power to the inverter and the instruments can be disconnected by a main 60-A breaker/switch accessible to the pilot. All breakers can be manually operated and are MIL and FAA approved.

SAMPLING PROBE

The sampling probe consists of two parts, one located primarily outside and the other inside the aircraft. The outside component is made of stainless steel and is located on the upper left-hand side of the aircraft (Figure 1). The probe extends about 10 in. from the fuselage and has an area expansion ratio of 16 to decrease the flow velocity before the stream is deflected inside the aircraft. The inside component is made of aluminum with five stainless steel tubes. It is connected to the outside probe at the point where it extends inside the aircraft by means of a rubber hose and clamps. A detailed design of the outer portion of the probe is shown in Figure 2.

To maintain isokinetic sampling, the 1/2-in. tube may be connected to a pump whose pumping rate can be adjusted so that the air velocity at the probe's orifice is the same as the aircraft speed. Unfortunately there is insufficient data to determine the loss of particles to the inside wall of the probe resulting from the probe's 90° bend. However, in view of recent wind tunnel data by Sehmel,[1] we can assume that for particles less than 5 μm in diameter, the loss is less than 10%.

INSTRUMENTATION

The number of instruments carried aboard the aircraft is limited by the useful weight and the available power of the aircraft. Normally with pilot, copilot and one observer aboard, the total weight available for instrumentation is 575 lb. Reduction in flight time increases the useful weight by 200 lb/hr. Total power available for instrumentation is 2360 W DC and 800 W AC. Typical placement of equipment onboard the aircraft is shown in Figure 3. The

Neg 720804-1

FIGURE 1. The Locations of the Various Sensors on the Aircraft

1) Sampling Probe
2) Dewpoint Sensor
3) Temperature and Relative Humidity Sensor
4) Turbulence Sensor

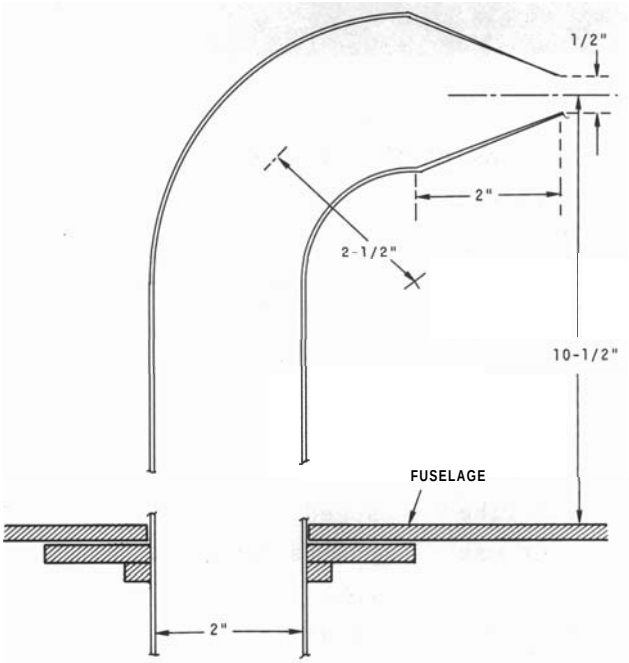

Neg 721419-5

FIGURE 2. The Sampling Probe

Neg 725129-11

FIGURE 3. The Locations of the Instrumentations Inside the Aircraft

1) End of Sampling Probe
2) Ice Nuclei Counter
3) Metrodata Magnetic Tape Recorder
4) Power Control Panel
5) Condensation Nuclei Counter
6) Turbulence Indicator System
7) SO_2 Monitor
8) Royco Recorder
9) Pulse Converter
10) Royco Optical Sensor
11) Royco Display Unit
12) Pulse Height Analyzer
13) Paper Tape Printer

following paragraphs briefly describe the instrumentation available for use aboard the aircraft.

Meteorological and aircraft parameters are measured via three different systems. The first is a Metrodata Systems, Inc., Model M8. This system measures temperature, humidity, air speed, altitude, bearings from two points (VOR), distance from one point (DME), and compass heading. The temperature and humidity are obtained from sensors in a probe mounted on the nose of the aircraft (Figure 1). The temperature sensor uses a shielded, linear-response thermistor

head, and the humidity sensor uses a carbon-strip hygristor similar to that used in radiosondes. The aircraft's Pitot-static system is connected to a potentiometric transducer to measure air speed and altitude. The VOR and DME data are derived from the navigational receivers of the aircraft. These and the altitude are used to determine the exact position of the aircraft at any time.

The second system is a Cambridge Systems Model 137-C3 aircraft hygrometer manufactured by EG&G for measuring the dew point temperature. The sensor is mounted on the left hand side of the aircraft nose (Figure 1).

The third system is a Universal Indicated Turbulence System, Model 1120, manufactured by Meteorology Research, Inc. It measures the turbulence intensity of a specific frequency band which lies within the inertial subrange. It also measures the air speed. The location of the sensor on the outside of the aircraft is shown in Figure 1.

A number of trace gas and aerosol measurement systems have been adapted for use onboard the aircraft. These include:

A Condensation (Aitken) Nucleus Counter (General Electric): This unit is capable of detecting particles larger than 0.001 μm by measuring the light scattered from water droplets formed on particles which are exposed to a high supersaturation achieved by sudden expansion. The intensity of light scattering is automatically related to the particle concentration; response time is about 2 sec.

A Whitby Aerosol Analyzer, Model 3030 (Thermo Systems, Inc.): This unit samples air at the rate of 5 liters/min and measures the concentrations of particles in the range of 0.01 to 0.5 μm in 10 size classes. Typical mass concentrations measured by this unit range from 6 to 600 $\mu g/m^3$.

A Royco Optical System: In this system the aerosol particles are drawn into a Royco Model 220 optical sensor (Royco Instruments, Inc., Menlo Park, California), and light scattered at 90° from the individual particles is detected by a photomultiplier tube and pre-amplifier, generating corresponding voltage pulses. The voltage pulses are fed into a modified pulse converter Model 171 manufactured by TII (Technical Instruments, Inc., North Haven, Connecticut), then to a TII Model 401-D pulse height analyzer (PHA) operated in the Mossbauer mode, and a TII Model 500-A paper tape printer. This system is capable of simultaneously measuring the size distribution in the range of 0.3 to 5 μm in about 100 channels. The pulses from the sensor are also fed into a two-channel pulse height analyzer where the concentrations of particles in the size range 0.3 to 1 μm and greater than 1 μm are recorded.

A Chemiluminescent NO-NO_x Monitor (REM Model 642): This analyzer measures light emitted from the chemiluminescent reaction between NO and

ozone. Employing a reducing catalyst, this is capable of detecting both NO and NO_x at levels below 0.1 ppm with a 5 ppb sensitivity.

An SO_2 Monitor (Sign-X Laboratories, Inc., Model 604B): In this instrument the sampled air is mixed with deionized water. SO_2, in the air sampled, is dissolved and ionized in the water. The resultant increase in conductivity is measured and related to the SO_2 concentration in the sample. CO_2 is known to interfere with the SO_2 measurement; however, a scrubber included with the instrument can be used to remove the SO_2 from the sample and hence establish a baseline for the measurement.

A Cloud Condensation Nucleus Counter (Meteorology Research, Inc.): This unit is capable of measuring cloud condensation nucleus concentrations at adjustable supersaturations in the range 0.2 to 2%.

An Ice Nuclei Counter (MEE Industries): This unit is a fast-response counter for detecting and recording ice nuclei in the concentration range between 0.1 and 10^4 nuclei/liter over any activation temperature from 0°C to -30°C.

DATA RECORDING SYSTEM

A recorder input panel built into the data acquisition system functions as a convenient connecting point for all signal inputs to an onboard Metrodata Model DL620 magnetic tape data logger. Precision 10-turn potentiometers at each input terminal permit the operator to attenuate and/or calibrate each data input signal to a full-scale range appropriate to the Metrodata recorder. All data lines utilize coaxial or shielded, twisted pair cable, and, insofar as is possible, all lines and interconnections external to the various instruments are shielded to preserve data integrity. Auxiliary coaxial connectors are available for simultaneous recording of the analog signals on chart recorders.

The Metrodata recorder may be used in several input configurations ranging from ±10 mV to ±5 V full scale with a 2000-point resolution. The instrumentation presently installed utilizes ±10 mV and ±1 V ranges. The recorder samples 18 analog inputs (plus two real-time channels) at rates up to 48 channels/sec. At the minimum sampling interval, 4 hr of recording may be accomplished on a single tape cartridge. Analog inputs are converted to digital form and recorded as four-character BCD digits (sign plus three digits). Hours, minutes and seconds data from a real-time clock are recorded at the beginning of each 20-channel scan.

DATA ANALYSIS

Upon recording of data, the magnetic tapes from the Metrodata recorder are brought to the Battelle, Pacific Northwest Laboratories' computer facility for further processing and analysis. The central processor in the facility is a Systems Engineering Laboratories SEL

840A. The magnetic tape records acquired in-flight are read into the computing system via a Metrodata Model DL 622 tape reader. By means of a high-speed electrostatic printer/plotter, the tape record can be output either as a numerical record or as a graphic representation as a function of time. If more detailed analysis of the recorded data is required, the Metrodata tapes can be read into the 840A computer, preprocessed and/or formated, and rewritten onto industry-compatible magnetic tape for processing on more extensive computer systems.

CONCLUSIONS

A Cessna 411 aircraft has been instrumented for use as an airborne laboratory for studying the behavior and characteristics of aerosol and trace gases above the ground level. It is capable of determining the particle size distribution in the range of 0.001 to 5 μm and the concentration of several trace gases as well as some cloud physics parameters. Meteorological and aircraft parameters are also measured. A magnetic tape and a strip-chart recorder are provided for data recording.,

ACKNOWLEDGMENTS

The author wishes to acknowledge the contributions of K. M. Busness, who designed the power distribution and data recording system, F. O. Gladfelder, pilot, and J. M. Baily, copilot/aircraft mechanic, who constructed the mounting racks for the equipment, and the valuable suggestions of C. L. Simpson, C. E. Elderkin, W. G. N. Slinn, and J. M. Hales.

CHARACTERISTICS OF AEROSOLS FROM ST. LOUIS

A. J. Alkezweeny

Aerosol particle size distributions were measured over St. Louis. It was found that the concentrations of particles of all sizes generally decrease with an increase in altitude and that the size distributions in the same location show a considerable daily variation. The volume distribution measured with time peaked around 0600 for particles greater than 0.45 μm. At noon an increase in the particles less than 0.45 μm and in the Aitken nuclei concentrations was observed. Even though a decrease in the Aitken nuclei count was measured downwind of St. Louis, it was associated with an increase in the concentrations of larger particles.

INTRODUCTION

For modeling the behavior and the change in the characteristics of atmospheric pollutants four parameters should be considered: 1) the meteorology of the area, 2) the sources, 3) the removal processes, and 4) the interactions between the component of the pollutant, i.e., gas-to-particle conversion, coagulation of particles, and particle growth by condensation. Removal processes are strongly linked to the characteristics of the aerosol and trace gases. The long-range objective of the USAEC-DBER program on Atmospheric Aerosol and Trace Gases is to study these interactions experimentally and theoretically and to construct submodels for inclusion in general atmospheric response models. Another objective is to determine the effect of air pollution on cloud formation and precipitation development through nucleation, which is important in the wet removal process.

A segment of this program was conducted in St. Louis under the 1973 METROMEX project, which involved airborne assessment of trace constituents using an instrumented aircraft. The results of this study are presented and discussed in this report.

EXPERIMENT

The measuring instrumentation was mounted inside a Cessna 411 aircraft described by Alkezweeny.[2] Specific instrumentation included a General Electric Aitken Nuclei Counter, a Mee Ice Nucleus Counter, and a Royco Optical System. The latter consisted of a Royco Model 220 Optical Sensor, a pulse converter, a pulse height analyzer, and a digital printer, capable of simultaneously measuring size distributions of aerosol particles in the range from 0.3 to 5 μm diam in about 100 channels. Another two-channel pulse height analyzer and recorder were connected to the optical sensor to record continuously the concentrations of particles in two size ranges, 0.3 to 1 μm and greater than 1 *pm*.

The first two flights were made on July 27 and 28. Several penetrations were made through nine individual plumes along the Mississippi River. Later in the flight, about 12:00 noon local time, the particle-size distributions were measured at several altitudes from 1500 ft to 5500 ft MSL over the city center, west of the river.

The third flight, made on August 1, concentrated on simultaneously measuring the concentrations of particles in three size ranges, Aitken nuclei range, 0.3 to 1 μm and greater than 1 μm, at a constant altitude (1500 ft MSL) along the wind trajectory. The flight path, totaling about 120 miles, started upwind of the city, over the city and downwind of it.

The last four flights consisted of measuring particle size distributions and concentrations of Aitken nuclei at 2000 ft and 4000 ft MSL over the city and 50 miles downwind of it. They were made on August 2 and 3, about 6 hr apart, starting at 0600, 1200, 1800 and 2400. During all flights the sky was either clear or there were a few scattered clouds, and the wind speed was estimated at less than 5 mph.

RESULTS AND DISCUSSION

Aircraft penetrations through the plumes along the Mississippi River showed no drastic increase in the count of ice nuclei above the surroundings. The area along the river, however, was observed to have high concentrations of ice nuclei (about 50 to 200 nuclei/liter active at -20°C), especially near the St. Louis Arch. It was initially suspected that the high count might be caused by noise from the instrument; however, when the aircraft climbed to higher altitudes the count dropped to zero. This observation is consistent with our previous aircraft measurement over the city,[3] when a high concentration of the nuclei was observed in the same general area.

Figure 4 shows the size distributions of aerosol particles over St. Louis at four different altitudes for July 27. The results indicate that

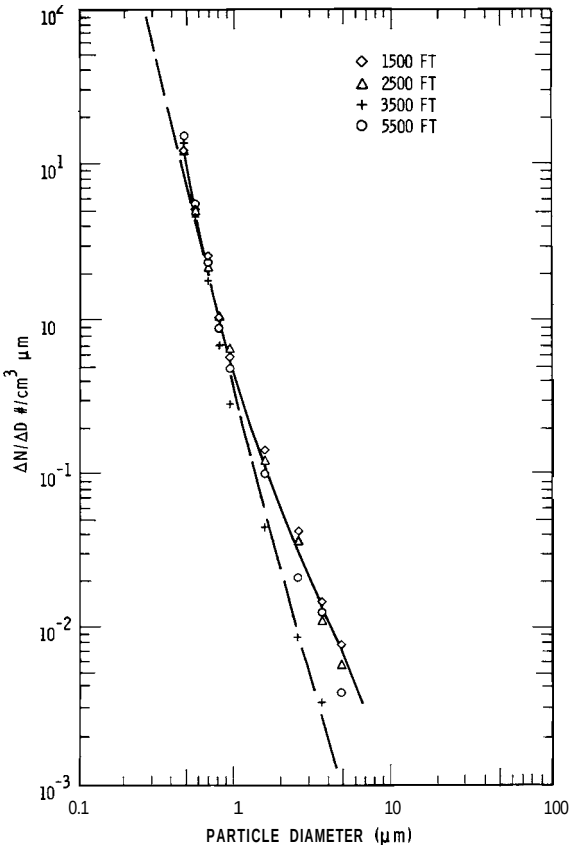

Neg 740225-3

FIGURE 4. Particle Size Distributions over St. Louis at Different Altitudes for July 27

the concentrations of particles larger than 1 µm decrease faster with altitude than do smaller ones. It is possible that plumes near the sampling site may have contributed to the measurement at the lower altitudes. The distributions at 1500 ft and 5500 ft are plotted in Figure 5 as a volume distribution, along with the distributions obtained on July 28. It is interesting to note that results are quite different even though they were taken at the same location and altitude, but 24 hr apart. For instance, the total volume of particles in any size range for the 28th is much higher than that for the 27th at 1500 ft.

Figure 6 shows the concentrations of Aitken nuclei at a different location along the flight path of August 1.

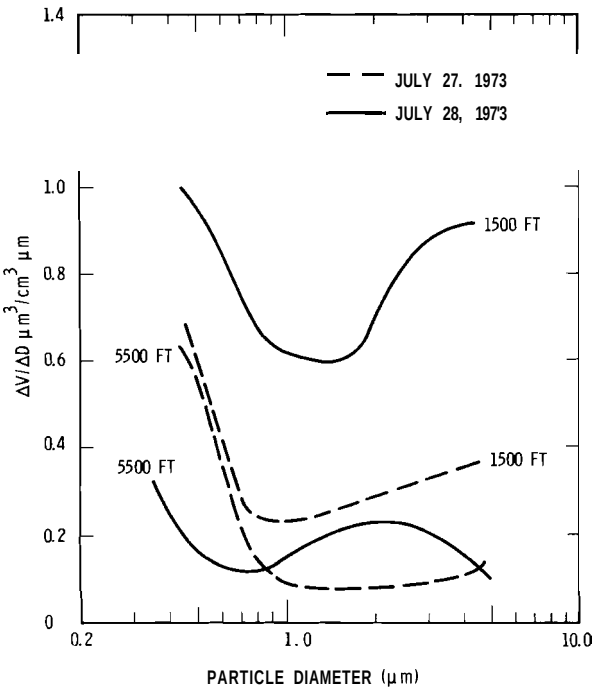

Neg 740225-6

FIGURE 5. Particle Volume Distributions over St. Louis

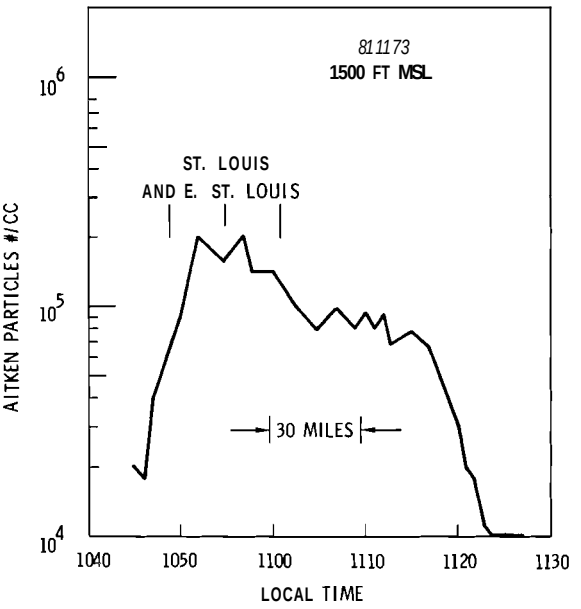

Neg 740225-10

FIGURE 6. Concentrations of Aitken Nuclei at Different Locations Along the Flight Path of August 1

The concentration increases sharply over St. Louis and East St. Louis then slowly decreases for about 30 miles, followed by a faster decrease. This behavior can be assessed by visualizing a parcel of air moving over St. Louis. The rate of change of the nucleus concentration within the parcel can be represented by the following equation

$$dN/dt = -KN^2 + Q \qquad (1)$$

where N is the particle concentration, K is the coagulation constant and Q is a source term that takes into account particle sources within the parcel, such as generation by photochemical reaction. When Q is larger than KN^2, an increase in the particle concentration should be observed as in the case over St. Louis and East St. Louis. However, at a later time

when the two terms are about equal, the rate of change of N will be small. When the concentrations of gases responsible for the photochemical reaction are depleted and the parcel is far from particle source (assuming other source mechanisms to be small), the coagulation term becomes dominant. The result is a faster decrease in the nucleus concentration. In this range an increase in the concentrations of larger particles should be observed, an effect which can be seen in Figure 7. The concentrations of large particles in the two size ranges increase to about double their value over St. Louis.

If the Aitken nuclei were coagulating only with themselves, an increase in the concentration of particles only in the range 0.3 to 1 μm should be observed. Since the concentration of particles larger than 1 μm is detected, it is indicated that the Aitken nuclei are coagulating with the larger particles as well.

The increase in the concentration of particles larger than 1 μm may have an important implication in inadvertent weather modification. The injection of these particles into a cloud is expected to lead to the formation of large cloud droplets which could enhance precipitation.

During the measurement, the wind speed was estimated to be about 5 mph. If we assume that the wind speed and direction were steady in the past several hours, then we may approximate the change in the concentration of Aitken nuclei, in Figure 7, with Equation 1 and neglecting Q. The value of K, for which the equation

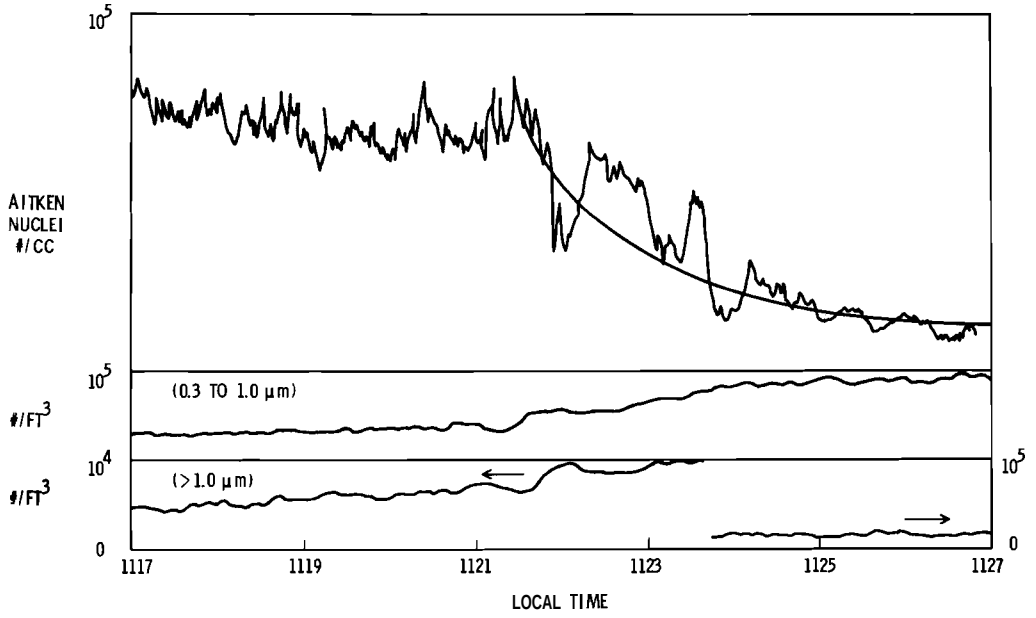

Neg 740225-1

FIGURE 7. Concentrations of Aitken Nuclei and Larger Particles Along the Last 30 Miles of the August 1 Flight Path

visually fits the data is 5.5×10^{-9} cm^3/sec (see Figure 7). This value of K is rather high for only self coagulation of the Aitken nuclei. However, considering that they are coagulating with larger particles, this value of K is reasonable.

Figures 8a through 8d represent the particle-volume distributions measured at 6 hr apart over St. Louis and 50 miles downwind of it. The distributions obtained at 2000 ft MSL show an interesting feature. Early in the morning the distribution peaks around 0.45 pm, and the volume concentration is higher than at the later time. This is probably caused by the relative humidity, usually high at this time. Around noon there was a decrease in the volume concentrations for particles larger than 0.45 pm. This effect may be attributed to the decrease in the relative humidity and an increase in the photochemical activity. Measurements of the Aitken nuclei during the same period (see the figure caption) over St. Louis shows a peak around noon.

CONCLUSIONS

Measurements of the particle size distributions show generally that the concentrations of particles of all sizes decrease with an increase in altitudes. The distributions measured 24 hr apart in the same location show a considerable daily variation. The volume distribution measured with time over St. Louis peaked around 0600 and has a peak around 0.45 μm. At noon an increase in the particles less than 0.45 μm in diameter and in the Aitken nuclei were observed, reflecting the effect of photochemical reaction.

The decrease in the concentration of Aitken nuclei with distance downwind of St. Louis was associated with an increase in the concentrations of particles in the range 0.3 to 1 μm. The rate of decrease in the nuclei concentration was fitted by the Smoluchowski coagulation equation.

Finally, the ice nucleus measurement indicated that the city is a source of ice nuclei, but we were unable to determine the sources of the nuclei.

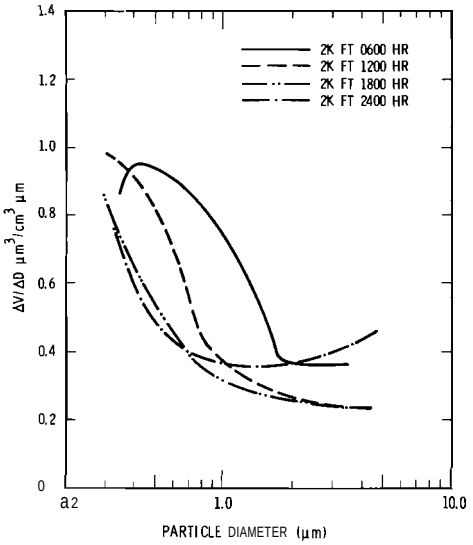

Neg 740225-7

FIGURE 8a. Particle Volume Distributions Measured over St. Louis on August 2. Aitken nuclei concentrations for the 0600,1200, 1800 and 2400-hr flights were 2.2×10^4, 4×104, 6.75×10^3 and 2×10^3 #/cm^2, respectively.

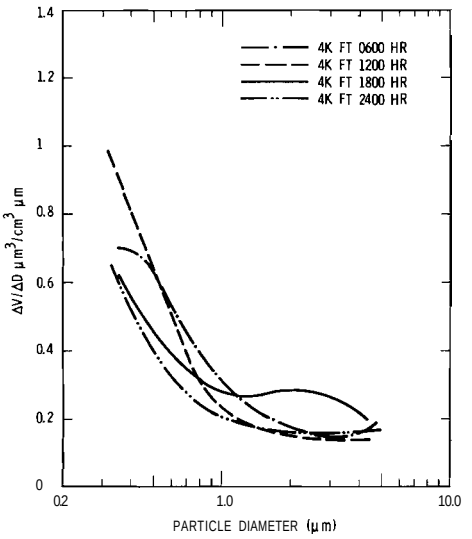

Neg 740225-4

FIGURE 8b. The Same as Figure 8a, but at 4000 ft MSL. The corresponding Aitken nuclei concentrations were 1.4×10^4, 3×104, 6×103 and 10^3 #/cm^3, respectively.

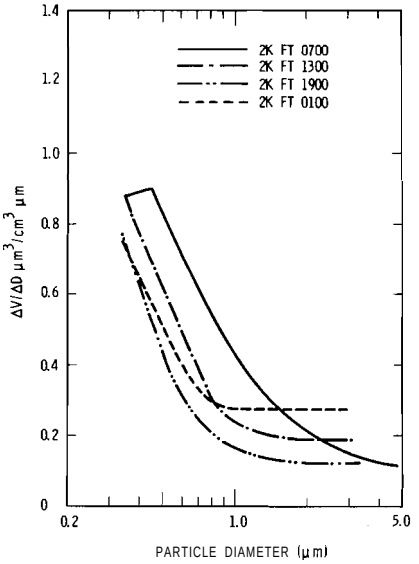

Neg 740225-9

FIGURE 8c. The Same as Figure 8a, Obtained 50 Miles Downwind of St. Louis. The corresponding Aitken nuclei concentrations were 2×10^4, 6×10^3, 3.8×10^3, and 1.4×10^3 #/cm^3, respectively.

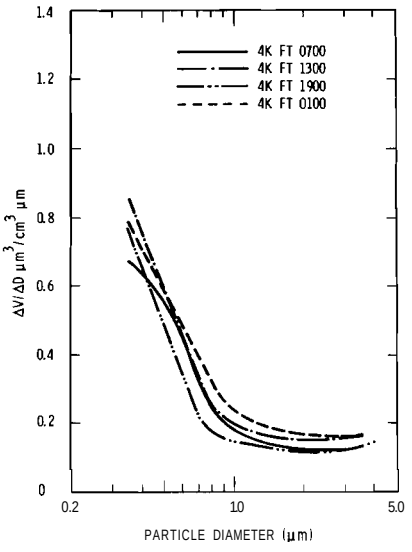

Neg 740225-8

FIGURE 8d. The Same as Figure 8c, but at 4000 ft MSL. The corresponding Aitken nuclei concentrations were 2.5×10^4, 5×10^3, 3.1×10^3 and 10^3, respectively.

PRELIMINARY IN-PLUME MEASUREMENTS NEAR CENTRALIA

A. J. Alkezweeny

Preliminary in-plume measurements of trace gases and particulates were conducted near Centralia, Washington. A maximum of 0.28 ppm NO, concentration was detected. The measurement suggested that aerosol particles leaving the stack undergo significant coagulation.

Industrial plumes offer some distinct advantages in studying the interaction between aerosol particles and the transformation of gases to aerosols. Leaving a stack, gases and aerosol particles in a parcel of air may undergo several transformations, including gas-to-particle conversion, particle coagulation, and sedimentation as the parcel travels further from the source. These processes depend upon the meteorological conditions as well as the types of gases and sizes of particles emitted from the stack and can be investigated by monitoring the concentrations of gases and particulates of different sizes at different locations within a plume.

A program has been initiated to study the feasibility of conducting in-plume measurement for these purposes, involving use of an instrumented Cessna 411 aircraft. The instrumentation carried onboard the aircraft consists of a General Electric Condensation (Aitken) Nuclei Counter, a Royco Optical Sensor connected to a two-channel pulse height analyzer, and a recorder to record the concentrations of particles in the size ranges 0.3 to 1 μm and greater than 1 μm in diameter, and a chemiluminescent NO-NO_x monitor. Initial feasibility tests were conducted during the fall of 1973 in the plume of the Centralia steam plant located near Centralia, Washington.

The first penetration through the Centralia plume was made on September 27, 1973 at 0930. The sky was clear and a low fog was dissipating. The plume from the stack was mixed with another plume from an adjacent forced draft cooling tower. Therefore the result was a mixture of gases, particulates and water droplets. The flight path started upwind of the plume to about 15 miles downwind at about 1500 ft MSL. The results are shown in Figure 9.

Although the results are preliminary and no conclusion will be drawn from them, a few interesting observations may be derived. For example, the concentration of aerosol particles in the size range 0.3 to 1 μm is greater than 10^6 particles/ft^3. This is the upper limit for the instrument. The maximum concentration of NO_x was about 0.28 ppm. The figure also reflects plume-height fluctuations as the plume travels downwind.

Finally let us compare the peaks in the concentrations of particles greater than 1 μm to the peak in the

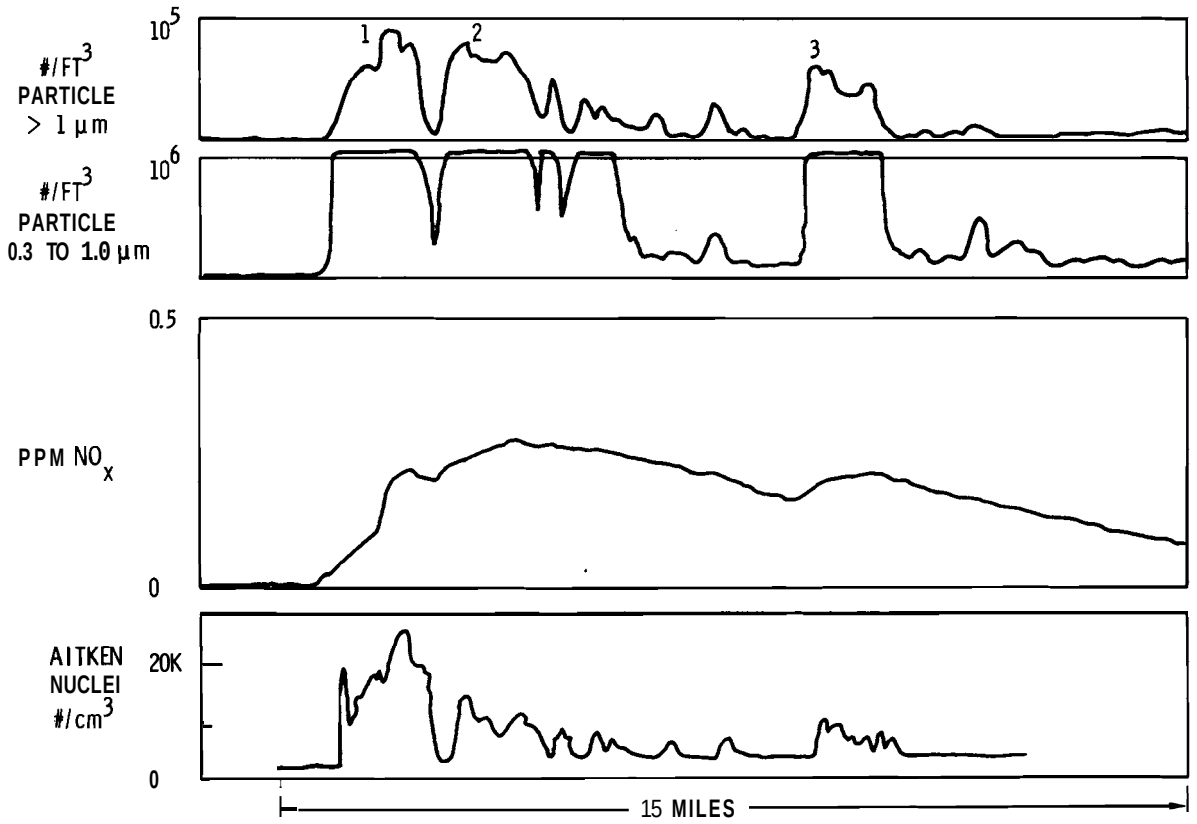

Neg 740225-2

FIGURE 9. NO_X and Particulate Concentrations Obtained at Different Locations in the Centralia Plume

concentrations of Aitken nuclei. If it is assumed that the change in the particle concentration due to plume diffusion is independent of the particle sizes, the ratios of the concentrations at peak 2 (see Figure 9) to those at peak 1 and 3 to 1 for the larger particles should be the same as for the Aitken particles. However, the results show the ratios to be higher for the large particles, indicating coagulation of the Aitken nuclei.

In conclusion, this scoping experiment has indicated that it is feasible to conduct in-plume measurement to understand the behavior of aerosol particles and trace gases emitted from a stack. It further suggests the need for the sampling system to dilute the aerosol before it enters the measuring instrumentation. Further, more quantitative tests are planned for the coming year.

CONCENTRATIONS AND RATES OF REMOVAL OF CONTAMINANTS FROM THE ATMOSPHERE IN AND DOWNWIND OF ST. LOUIS

J. A. Young, T. M. Tanner, C. W. Thomas,
N. A. Wogman and M. R. Petersen

The atmospheric concentrations of trace elements, sulfates, SO_2, freons and CO were measured upwind, in, and downwind of St. Louis to determine the rates at which these contaminants are removed from the atmosphere by dry deposition and chemical reactions.

The St. Louis metropolitan area generates large numbers of pollutant materials, some of them toxic, into the atmosphere. These contaminants are carried large distances by the prevailing winds and may affect regions considerably downwind of St. Louis. The downwind decreases in the atmospheric concentrations of these contaminants with time and distance depend upon atmospheric mixing processes, wet and dry deposition on the earth's surface, and in some cases chemical conversion processes.

The relative importance of mixing processes versus removal processes in decreasing the contaminant concentrations downwind of St. Louis may be determined by comparing the concentrations of conservative contaminants with the concentrations of reactive contaminants. The Freons released into the atmosphere by the St. Louis metropolitan area are essentially conservative, having residence times in the atmosphere of several years. Freon-11, CCl_3F, is released into the atmosphere primarily by aerosol spray cans, while Freon-12, CCl_2F_2 is released primarily by air conditioners. Carbon monoxide is often also considered to be essentially conservative, although it is known to react at appreciable rates with soil microflora, especially at warmer temperatures.

The concentrations of trace elements, sulfates, SO_2, CO, and Freons are being measured in air samples collected upwind, in, and downwind of St. Louis during July 1973 to determine the atmospheric concentrations of these contaminants produced by St. Louis and to determine the rates at which the concentrations are decreased downwind by atmospheric mixing processes, dry deposition on the earth's surface, and, in the case of SO_2, chemical reactions.

The aerosol samples that are being analyzed for trace elements by X-ray fluorescence and neutron activation were collected using HiVol pumps to draw air through 2-in. diam IPC filter papers at flow rates of about 1.2 m^3/min. Samples were collected for SO_2 analysis by bubbling air through sodium tetrachloromercurate solutions at rates of 1 liter/min.

Evacuated 460 cm^3 capacity gas cylinders were used to collect whole air samples for analysis for CO and Freons.

On 6 days air samples were collected on three arcs downwind of St. Louis. The three sampling arcs were set up 20, 40, and 60 miles downwind of St. Louis on 4 of the 6 sampling days; 20, 40, and 80 miles downwind on 1 day; and 20, 50, and 80 miles downwind on the other day. The sampling arcs were set up by five people equipped with completely mobile sampling apparatus. On each day the first arc consisted of five sampling locations arranged more or less equidistant on a 30- to 50-mile line perpendicular to the predicted wind 20 miles downwind of St. Louis. The length of the line was varied according to the uncertainty in the expected wind. The sampling sites were located on side roads away from towns and highways. At each of the sites an aerosol sample and an SO_2 sample were collected over a period of about 1 hr, and a whole air sample was collected at the beginning of the sampling period. The samples were collected, as much as possible, at approximately the same time at each location. After collecting one set of samples at the first site, the five people moved usually 20 miles downwind where they set up a second site and again collected a complete set of samples over a period of usually about 1.5 hr. They then again moved usually 20 miles farther downwind and collected a third set of samples over a period of usually 2 hr.

The spacing of sampling arcs was chosen so that the sampling sites were moved downwind at about the same speed as the predicted wind. The elapsed time between the start of sampling at the 20-mile arc and the start of sampling at the 60-mile arc varied from 5 to 6 hr on the days the wind speed was predicted to be 5 to 10 mph. Because on July 27 the predicted wind was 10 mph, the third arc was set up 80 miles downwind.

On each sampling day at least one set of air samples was collected upwind of St. Louis to determine the contaminant concentrations in the air entering St. Louis. Sequential samples were also collected on the roof of the 10-story Federal Building in downtown St. Louis to determine the concentrations inside the city. On 2 days sequential samples were also collected just east of the Mississippi near Granite City. On 3 days vertical profiles were taken using the Battelle Cessna 411. Contaminant concentrations as functions of particle size will be determined from Lundgren impactor samples collected upwind of St. Louis, on the roof of the Federal Building, and at two other sites in the St. Louis area.

At present, analysis of the air samples for SO_2 and the Freons has been completed, and the X-ray fluorescence analysis for primarily lead, bromine, and particulate sulfur (presumably primarily sulfates) is nearly completed. Lead and bromine result from automobile exhaust, while SO_2 is also produced in large quantities by fossil fuel-fired power plants. The SO_2 released into the atmosphere is

converted fairly rapidly into sulfates. The neutron activation analysis for other trace elements is just starting, while the analysis for CO has not yet begun, due to a delay in the delivery of a CO analyzer.

The concentrations of lead, bromine, SO_2, and particulate sulfur were reasonably uniform along each sampling arc and also in sequential samples taken at a given location. However, the Freon-11 and Freon-12 concentrations varied widely. Probably this large variation was at least partially due to the very short 2 or 3 sec sample collection period. The wide variability of the measured Freon concentrations will cause difficulties in the interpretation of the measurements. In future experiments a method will be devised to collect whole air samples over a period of an hour or two.

The concentrations of lead, bromine, and. SO_2 in downtown St. Louis averaged 20 times higher than the upwind concentrations. Freon concentrations were also considerably higher in downtown St. Louis. The lead, bromine, and Freon-11 concentrations at the 20-mile arc averaged only 20, 13, and 60%, respectively, of their downtown concentrations. However, the SO_2 concentrations at the 20-mile arc averaged higher than the downtown concentrations, presumably because of the presence of large SO_2 sources along the Mississippi east of St. Louis. On days with westerly winds the SO_2 concentrations at the 20-mile arc east of St. Louis averaged 2.5 times higher than those at the Federal Building. On days with easterly winds, however, the SO_2 concentrations at the 20-mile arc west of the city averaged only 65% of those at the Federal Building. The large decreases in lead, bromine and Freon concentrations between the Federal Building and the 20-mile arcs probably result from vertical mixing of these materials through the boundary layer. The smaller decrease in the Freon-11 concentration may result from a larger average distance of the Freon-11 sources from the Federal Building. Lead and bromine should be produced in large amounts by the downtown traffic, while Freon-11 is probably released in large amounts in the suburbs. However, it is also possible that some of the decrease in lead and bromine concentrations could be due to the settling of large particles. The particle size distributions of the lead- and bromine-bearing particles will be determined from Lundgren impactor samples collected on the roof of the Federal Building to determine whether particle settling can be a major deposition mechanism for the lead and bromine.

The lead, bromine, and Freon-11 concentrations decreased slowly with distance beyond the 20-mile arc. The lead and bromine concentrations at the outer arc (60 or 80 miles) averaged 68 and 74%, respectively, of the concentrations at the 20-mile arc. If the occasional very high Freon-11 concentrations are ignored, the calculated average Freon-11 concentration of outer arc becomes 90% of the average concentration at the 20-mile

arc, suggesting that atmospheric mixing processes decreased the contaminant concentrations around 10%, and that dry deposition processes removed around 20% of the lead and bromine between the 20-mile arc and the outer arc.

The average SO_2 concentrations decreased with distance much more rapidly, decreasing to 27% of the 20-mile arc concentration at the outer arc. If it is assumed that the SO_2 concentration was decreased 30% by mixing and deposition processes, as was the case for lead and bromine, then the conversion of SO_2 to sulfates alone would have been sufficient to decrease the SO_2 concentration to about 40% of the 20-mile arc concentrations at the outer arc. If it is assumed that the average wind speed was 7 mph on days when the outer arc was at 60 miles and 10 mph when it was at 80 miles, then the calculated half residence time for SO_2 before being converted to sulfate or deposited becomes 3.5 hr. As might be expected, the decrease in SO_2 concentration with distance was accompanied by an increase in the sulfate concentration. The sulfate concentration at the outer arc averaged 125% of the concentration at the 20-mile arc. Unfortunately, the measured sulfate concentrations are only relative numbers, due to problems in calibrating the X-ray fluorescence analyzer for the low energy sulfur X-rays. Therefore, at present, it can not be determined whether the concentration in the sulfate concentration is equal to that expected from the decrease in SO_2. At least some of the aerosol samples will be analyzed chemically for sulfate to obtain a calibration factor so that this calculation can be made.

The concentrations of lead, bromine, and Freon-11 at the outer arc averaged about twice the upwind concentrations, and SO_2 averaged seven times the upwind concentration.

VERTICAL PROFILES OF TRACE GASES IN ST. LOUIS

A. J. Alkezweeny

Airborne and ground measurements of NO, and NO have shown their concentrations at 2,000 ft above the ground to be higher than those at the ground and to decrease with altitude above that eZevation.

During the 1973 METROMEX program, an investigation was conducted to determine the vertical profile of trace gases over St. Louis and to compare the results with those simultaneously obtained on the ground. The ground

measurements were performed in the Battelle Columbus air pollution trailer located near the St. Louis University campus. Above the ground an instrumented Cessna 411 aircraft was used.[3] The concentrations of NO_x and NO were measured with a REM Chemiluminescence NO-NO_x Monitor. Samples of other gases were collected in plastic bags for a later chemical analysis.

In this report a summary of the NO_x and NO measurements is presented. The results of the other trace gases measurements, details of the experiment, and interpretation of the results will be reported later.[4] A total of three flights was made during the period of July 30 to August 1, 1973. Times of the measurements were 1525 to 1535 on July 30, 1105 to 1140 on July 31, and 1055 on August 1. The results of these measurements are shown in Table 1.

The concentrations of NO_x and NO at 1,000 ft above the ground were observed to be higher than those on the ground and decreased with altitude. Furthermore, the concentrations in the afternoon were higher than in the morning for all altitudes. The results ostensibly reflect the significance of above-ground sources of these gases.

TABLE 1. Vertical Profile of Trace Gases and Temperature in St. Louis

Date	Altitude, ft	Temperature, °C	NO_x, ppm	NO_2, ppm	NO, ppm
7/30/73	Ground Level	32.0	0.060	0.036	0.024
	1500	27.7	0.100	0.030	0.070
	2100	25.3	0.080	0.020	0.060
	3500	22.5	0.060	0.010	0.050
	4500	19.2	0.045	0.010	0.035
7/31/73	Ground Level	26.5	0.022	0.014	0.008
	1000	23.6	0.041	0.009	0.032
	2500	12.1	0.040	0.014	0.026
	4000	15.7	0.030	0.007	0.023
	5500	15.9	0.022	0.003	0.019
8/1/73	Ground Level	21.8	0.020	0.011	0.010
	1000	--	0.045	0.007	0.038

REFERENCES

1. G. A. Sehmel, "Particle Sampling Bias Introduced by Anisokinetic Sampling and Deposition Within the-Sampling Line," J. Amer. Ind. Hyg. Assoc., vol. 31, pp. 758-771, 1970.

2. A. J. Alkezweeny, "Airborne Laboratory for Air Pollution Study," in this report.

3. A. J. Alkezweeny, "Concentrations of Aerosol and Trace Gases over St. Louis," Pacific Northwest Laboratories Annual Report for 1972 to the USAEC, Division of Biology and Medicine, Volume II: Physical Sciences, Part 1, Atmospheric Sciences, BNWL-1751 PT1, Laboratories. Richland. WA. April 1973.

4. A. J. Alkezweeny and C. W. Spicer, "Vertical Profile of Pollutants in St. Louis," under preparation.

REMOVAL AND RESUSPENSION PROCESSES

WET REMOVAL PROCESSES

Washout and in-cloud scavenging are important processes by which air pollutant particles and gases are removed from the atmosphere. The primary objective of the precipitation scavenging research at Battelle-Northwest is to develop methods for modeling and predicting of wet removal processes in the atmosphere.

This year several significant new findings in the precipitation scavenging program have substantially altered our research emphasis. These have also caused us to reassess our studies, leading to what could well be termed the "year of reappraisal" in precipitation scavenging. Some important findings in this regard are listed:

- We have demonstrated mathematically that field and laboratory experiments of washout using polydisperse aerosols, while suitable for determining the washout characteristics of certain well defined aerosols, are of limited value as tests of particulate washout theory; our below-cloud scavenging efforts are being revised accordingly.
- An in-cloud tracer scavenging experiment performed at Quillayute resulted in removal rates much lower than anticipated from previous results. This finding appears to indicate that inter- and intra-cloud transport is more significant to scavenging than expected previously. Consequent modifications of experiment plans are being made.
- Substantial evidence suggests that under some conditions scavenged gases may desorb significantly subsequent to the raindrops' impact on the surface. This finding has strong implications to delivery-rate assessment and sampler design. As a result a no-resuspension sampler is being fabricated and future tests of this effect are anticipated.

- **PRECIPITATION SCAVENGING**
- **FALLOUT PHENOMENOLOGY**
- **ATMOSPHERIC AEROSOLS AND TRACE GASES**
- **ENVIRONMENTAL PROTECTION AGENCY SCAVENGING STUDIES**
- **TRACER STUDIES IN THE METROMEX EXPERIMENT**
- **TRACER STUDIES IN THE NATIONAL HAIL RESEARCH EXPERIMENT**
- **RADIOACTIVE FALLOUT RATES AND MECHANISMS**
- **BATTELLE MEMORIAL INSTITUTE PHYSICAL SCIENCES PROGRAM**

PROGRESS REPORT ON IN-CLOUD SCAVENGING IN FRONTAL STORMS

W. E. Davis, J. A. Young and J. M. Thorp

A report is made on the successful in-cloud release of tracers in a storm on December 5, 1973 near Quillayute, Washington. Suggestions are made for work to be completed before the nsxt test series.

INTRODUCTION

The relative importance of meteorological and aerosol parameters affecting in-cloud scavenging is presently under investigation. Meteorological parameters such as temperature, lapse rate, wind speed, wind shear, liquid water and vertical velocity are being considered in in-cloud scavenging test series.

The dependence of the rate and efficiency of in-cloud scavenging of aerosol particles upon aerosol particle characteristics such as their size distribution, their wettability or solubility, and their droplet nucleating ability is poorly understood at the present time (Slinn).[1] A series of tracer experiments was planned for the fall of 1973 to test some of these effects. One experiment designed to study the effects of particle size distribution was the simultaneous release of indium by means of pyrotechnic flares and iridium by means of aerosol generators. The generators produce particles smaller than 0.01 μm by burning acetone solutions of the tracer, while the flare particle size distribution peaks on the order of 0.1 μm (Dingle).[2] The larger flare particles should act as better condensation nuclei and might be expected to be scavenged more rapidly than the smaller generator particles.

The effect of particle solubility was to be studied by the simultaneous release of a soluble tracer such as lithium and a nonwettable tracer such as iridium or indium. A water-soluble tracer should act as a much better CCN than a nonwettable tracer and therefore might be scavenged more rapidly (Semonin).[3]

In addition to the above primary experiments, it was planned to conduct a few secondary experiments. One was the burn of a rhenium-europium mixture in the acetone generators to determine whether the two tracers would behave identically, showing the same deposition patterns. A second experiment was the release of lithium between the main bands of a frontal storm to determine whether there was significant precipitation

scavenging between bands. It was also planned to release osmium into a precipitating cell to determine the suitability of osmium as a tracer.

EXPERIMENT

On December 5, 1973 the PPI radar at Makah AFB near Neah Bay, Washington showed a cell imbedded in a frontal storm moving toward the planned release area near Quillayute. The decision was made to release tracers into this cell, and the Battelle Cessna 411, equipped with indium flares on one wing and two aerosol generators on the other, was directed to this cell. As the transponder signal from the Cessna was displayed on this radar scope, it was possible to position the aircraft rather accurately within the precipitating cell.

When the Cessna reached the proper position, an attempt was made to burn the europium-rhenium solution in the aerosol generators. But the generators refused to light, possibly because the burner nozzles had been clogged by a precipitate which later was found to have formed in the tracer solution. The indium flares were then burned from 0950 to 0956, and a second attempt was made to light the aerosol generators. This time one of the generators fired and the other did not. Hence, lithium, iridium, osmium, and the remaining rhenium-europium solution were released sequentially with only one burner firing. The burn of the last tracers was completed at 1025. The tracers were all released at 5000 ft at an ambient temperature of 2°C and in a stable layer. Pictures of the scope displays of the RHI and PPI radars at Makah AFB were taken before, during, and after the tracer release. Following the passage of the cell, samples of rain were collected from the 190 rain collectors of the rain sampling network. Thirty-five sequential samples were also collected at several locations. The samples are now being analyzed with neutron activation for indium, iridium, osmium, europium, and rhenium, and will later be analyzed by atomic absorption and anodic stripping for lithium and indium, respectively.

CONCLUSIONS

The positioning of the aircraft using the PPI scope was highly successful. When the scope showed the plane moving toward the edge of the cell, the pilot reported a decrease in precipitation, and when the scope showed the plane at the center of the cell, the pilot reported maximum precipitation. It is unfortunate that generator malfunction prevented the simultaneous release of indium and lithium. However, because the release of the water-soluble lithium was immediately preceded by the release of nonwettable indium and immediately followed by the release of nonwettable iridium and osmium, the results of the sample analysis should indicate the relative scavenging rates and efficiencies for the soluble and nonwettable particles. The

fact that one burner failed to light will make it difficult to determine the effect of particle size upon the scavenging by comparing the deposition of the indium from the flares with the deposition of iridium, osmium, rhenium, and europium since some large particles were certainly produced by the raw release through the unlighted burner. Even though the rhenium-europium solution was partly burned and partly released raw, the deposition pattern should indicate whether the two tracers can be expected to behave indentically.

FUTURE WORK

Once the analysis of this storm is completed, the results will be used to update experiments planned for the next test series. Determination of particle size in the indium flares will be carried out as well as experiments to determine the variation of the size distribution with concentration in the acetone burners.

A SUMMARY OF CURRENT FINDINGS FROM THE ANALYSIS OF 1972 QUILLAYUTE SCAVENGING EXPERIMENTS

W. E. Davis*

The results of two in-cloud releases of tracer in two frontal storms at Quillayute, Washington are reported: on March 21, 1972, In and AgI were released with little or no deposition; on March 31, 1972 a rhodamine release showed values to 5x background detected in ground samples.

INTRODUCTION

Precipitation scavenging of particular pollutants by storms has been of interest for some time, since scavenging is probably the main method by which the atmosphere is cleaned of pollutants (see Precipitation Scavenging, 1970).[4] Research is presently under way to identify variables which affect deposition of tracers released in-cloud by precipitation in frontal storms. Various factors, such as chemical and physical characteristics of the particles, i.e. particle size, solubility, etc., (see Slinn)[1] have been proposed as affecting the removal efficiency of material in-cloud. To test these factors as well as meteorological

* This research was conducted by members of the Atmospheric and Radiological Sciences Departments too numerous to include in a comprehensive author's list.

variables, i.e. stability, temperature, wind shear, etc., a series of experiments has been carried out at a test site on the Olympic Peninsula. The following reports the results of ongoing analysis of tests run during two storms conducted during calendar year 1972.

March 21, 1972 Storm

On March 21, 1972, a storm was seen approaching the coast of Washington, and a decision was made to release two tracers into the storm. The object was to test two tracers of different solubilities. At 1738-17492, 10 indium flares containing 45 g In/flare and 10 flares containing a total of 2 kg of AgI were released at 6800 ft at 0°C. Near the time of release, the RHI radar at Neah Bay, Washington, which was being used in the experiment to identify cells into which the tracer was to be released, became inoperative. However, since the plane was in the air, the decision was made to release the tracer in a region noted previously as an area of echo return. The release was made within an echo region satisfying estimated conditions for deposition of the tracer over the arcs (see Figure 1). The expected deposition pattern was determined from the wind field. Subsequent analysis of collected samples indicated that neither Ag nor In was greater than background. Additional samples both east and west of the pattern were analyzed with the same negative result.

The postanalysis of photographs of the PPI at Neah Bay, Washington

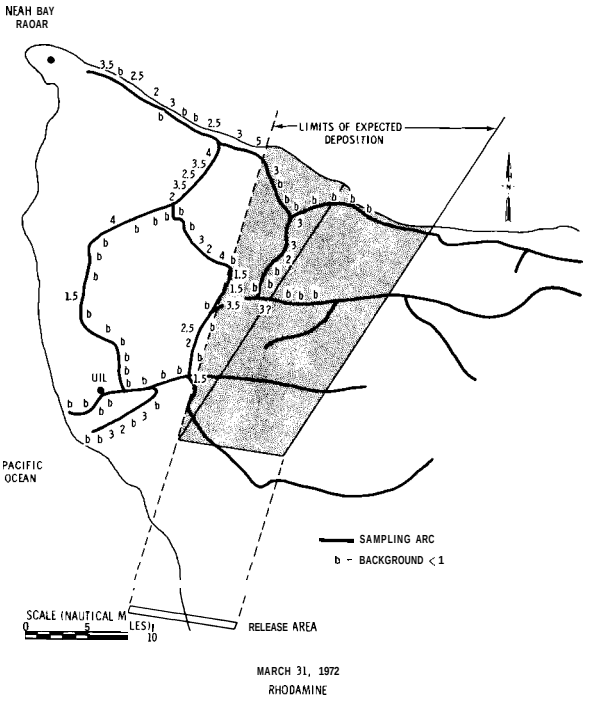

Neg 740788-1

FIGURE 1. Deposition of Rhodamine in ng/sample

indicated no echos of any size or consistency in the area of release. Gladfelder[5] aboard the aircraft noted areas of visual ground contact during the release and also areas with thin spots in the overcast. He also noted that the release was made in a precipitating cloud. Thus it appears that although the release was made in the frontal storm and in-cloud, it was in a region with insufficient precipitation to deposit In or Ag of detectable quantities.

March 31, 1972 Storm

On March 31, 1972, with a storm seen approaching the coast, a decision was made to release three tracers, AgI, In, and the organic dye rhodamine (see Slinn).[1] The objective in releasing rhodamine was

to test the feasibility of using this tracer for future in-cloud scaveng- experiments.

The release on March 31 was the second attempt to release rhodamine. The first, on March 21, was unsuccessful due to a dispenser spray nozzle being clogged by the solution. In the second attempt the spray nozzle was removed and the material released by opening a valve, resulting in a free release of the tracer. The speed of the aircraft was relied upon to break up the stream into drops. Release occurred at an altitude of 6200 ft at a temperature of 2°C over an 18-min period. The dispersed solution consisted of rhodamine dissolved in 15 liters of methanol, resulting in a concentration of 40 g/liter. No attempt was made to measure the size distribution resulting from the release. However, Dana[6] estimates that the release can be characterized by mass medium particle diameter of 12 ± 5 μm. This estimate was based on work by Wolf and Dana[7] in their studies of air-blast particle generation. To produce a better estimate of particle size range, additional work is necessary more closely approximating the actual release conditions than those of a ground-based generator used by Wolf and Dana.

The results of the scavenging experiment are shown in Figure 1 where the concentrations were plotted after analysis in a fluorimeter. The main result of the analysis is that the maximum values are at best 5x background. Thus, some of the deposition is probably masked in the background values. Further work is necessary using a spectrofluorimeter to separate background contributions from the rhodamine analysis.

The main result of the meteorological analysis was deposition of the material in an area and at a position downwind where it was not expected to arrive. As seen in Figure 1, based on meteorological wind analysis, the deposition pattern assuming a 1.5 m/sec fall velocity should have been considerably to the east. In fact, the area where the rhodamine was found was analyzed because it appeared that a background could be attained from this region. Once positive values were found, emphasis of the analysis was shifted to this area, leaving some samples further to the east yet to be analyzed.

CONCLUSIONS

Future tracer releases into frontal storms will be coordinated more closely with radar in order to position the aircraft into precipitating cells. The importance of this requirement was borne out by the negative results of the March 21 release in conjunction with our results from previous experiments. There is strong indication that transport of tracers with respect to cell movement within the storm system may be of primary importance in determining overall scavenging behavior.

Secondly, the March 31 test employing rhodamine as a tracer indicated the feasibility of using it,

although the method of release leaves much to be desired. Further studies are necessary to establish the concentrations of rhodamine observed in the March 31 samples since the observed values were close to background.

Thirdly, a recheck of the wind information is required as well as radar information in order to attempt to explain the deposition pattern observed on March 31, 1972.

A MODEL FOR CUMULUS WASHOUT OF COSMOGENIC RADIONUCLIDES

W. E. Davis

A model is presented in an attempt to explain observed ^{24}Na measurements in rainwater from cumulus clouds. Results indicate that values measured on June 9, 1972 can be explained only when evaporation is included. Also values for rising with no mixing require ∿97% evaporation of rainwater during fall to the ground as compared to ∿70% evaporation for a 50% linear mixing rate with environmental air during rise.

BACKGROUND

Cosmogenic radionuclides have been measured in rainwater over the past years (see Perkins et al., 1970 and Perkins et al., 1970).[8,9] Attempts have been made to explain these values by a model for frontal rain (Davis, 1972).[10]

In the past, thunderstorms have been associated with the removal of radioactivity from heights above the base of the storm (Davis et al., 1968)[11] and Reiter and Mahlman, 1965.[12] One should also suspect that the thunderstorms in the National Hail Research Experiment (NHRE) in Colorado could also remove cosmogenic radionuclides from the environmental air. Measurements are now available of cosmogenic radionuclides in rain from cumulus storms (Young 1973).[13] The following is a report on a model intended to attempt to explain the observed values.

THE MODEL

A model was developed to study cosmogenic radionuclides in ascending air parcels and their changes in concentration due to the balancing of production and decay. Also an assumed linear mixing was included to permit study of estimated changes of concentration in parcels due to mixing with free air values of the cosmogenics.

The time change of concentration is given by

$$\frac{dn}{dt} = -an + \beta + Kn^* - Kn \qquad (1)$$

where a = decay (sec^{-1}) and β is production rate dpm/scm sec, n is concentration dpm/scm, and t = time. K is the mixing constant (sec^{-1}) and n* is the environmental free air concentration. If we look at a free air equilibrium, we arrive at

$$an^* = B.$$

Using the measurements of ^{24}Na from Young et al.,[14] we can approximate the curve by

$$\beta = cz^j \text{ or } n^* = \frac{\beta}{\alpha} = \frac{c}{\alpha}z^j$$

where z is height in km and c is a proportionate constant. Thus as a parcel moves vertically with velocity w (m/sec^{-1}), the production rate can be represented

$$\beta = c\ (wt + z_o)^j.$$

We can rewrite Equation (1) with $\alpha^1 = \alpha + K$ and $\beta^1 = \beta + Kn^*$ as

$$\frac{dn}{dt} = -\alpha^1 n + c(wt + z_o)^j \qquad (2)$$

and, integrating over time from an initial height z_o and concentration n_o at time t = 0,

$$n = n_o e^{-\alpha^1 t} + c\int_o^t (z_o + wt)^j\ e^{\alpha^1 t}\ dt. \qquad (3)$$

This equation was solved numerically with varying w, z_o, t and K. Thus we have the model giving concentrations at some height $z_o + wt$ in cloud. The next step was to assume that the concentrations were in the precipitation phase and that after a given time t* the rain reached the ground.

The ratios as well as concentrations arrived at were compared with measurements made in the NHRE in Colorado in 1972. The following is the result of comparing the model's results to measurements of ^{24}Na on June 9, 1972 at NHRE.

RESULTS

The model was run for vertical velocities ranging from 1 m/sec to 10 m/sec. For the study a mean vertical velocity of 2 m/sec was applied over 3000 sec from a z_o = 1.5 km. The concentration of ^{24}Na (15-hr half-life) at the end of 3000 sec would have risen from 9.4 x 10^{-5} dpm/kg to 1.5 x 10^{-4} dpm/kg with no mixing to 8.3 x 10^{-4} dpm/kg for 50% entrainment during rise. A value of 8 g/kg, calculated from surface observations, was used for the mixing ratio of the air at 1.5 km for the June 9, 1972 study. The air parcel was allowed the same vertical rise and the assumption made that all cloud water was carried along with the parcel. At the top of the rise $\sim$3 g/m^3 of cloud water was calculated as being produced. Assuming the ^{24}Na was all in the cloud water, resulting concentration ranged from $\sim$0.03 dpm/liter for no entrainment during rise to $\sim$0.20 dpm/liter with 50% entrainment during rise. The latter concentration value was additionally increased by allowing entrainment of air with a lower water

vapor content, which in turn reduced the liquid water produced.

Next a 4 m/sec average vertical velocity was used with the result of moving the air parcel from 1.5 km to 13.5 km. The same mixing ratio was used at 8 g/kg at the ground, again carrying the water in the parcel and assuming that all the ^{24}Na was in the water.

The resulting concentration would be 4.3 x 10^{-4} dpm/kg with no mixing, and 3.4 x 10^{-3} dpm/kg with 50% mixing. Again raising the parcel and keeping the liquid water with the parcel resulted in a concentration of 0.06 dpm/liter with no mixing and 0.60 dpm/liter with 50% mixing.

If we assume 70% evaporation of the original cloud water before it reaches the ground and, further, that all of the ^{24}Na remains in the water that reaches the ground, the concentration range for no mixing would run from 0.10 dpm/liter to 0.20 dpm/liter for 2 m/sec and 4 m/sec mean vertical velocity. This is still below the observed range in the June 9 case (see Figure 2).

Even using a mean vertical velocity of 6 m/sec for 3000 sec would increase the concentrations only by a factor of 2, thus still leaving the concentrations unexplained. However, 50% entrainment with 70% evaporation would yield values of ∿0.66 dpm/liter to ∿2.0 dpm/liter. Thus one could infer that the concentrations of ^{24}Na cannot be explained by the no mixing case without higher evaporation rates of ∿97%. At present the only measurements available are rain gage and radar reports that may provide some estimation of expected rainfall. However, since radar data for the storm has not been reduced, attempts have not yet been made to correlate the data more closely with observations.

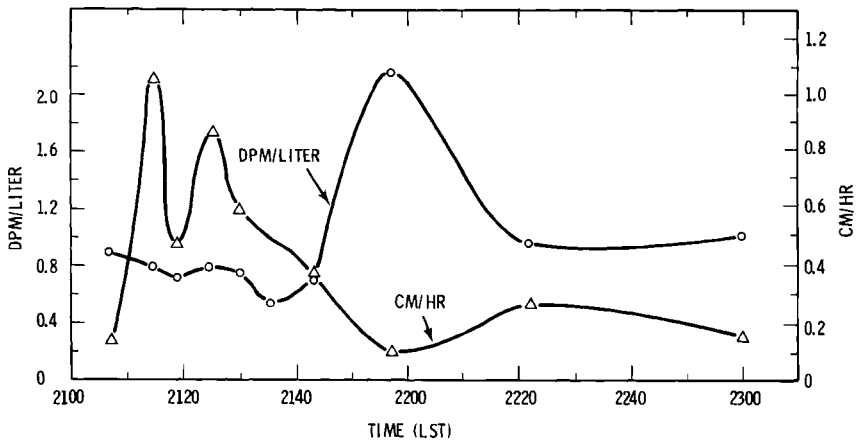

Neg 740788-2

FIGURE 2. Concentration of ^{24}Na (dpm/liter) Versus Rainfall Rate (cm/hr) for June 9, 1972

CONCLUSIONS

The study indicates that except for evaporation of ∿97% of the water associated with ^{24}Na the surface free air concentration cannot explain the ^{24}Na concentrations in the precipitation. When side entrainment was tested, it was found that by using a vertical velocity 4 m/sec for 3000 sec, a mixing ratio of 50% during rise, and also ≥70% evaporation we could explain the observed concentrations. At the same or higher speed up to 6 m/sec for 4000 sec, the values of ^{24}Na in rainwater are of higher concentrations, but the concentrations are still too low to explain without evaporation and/or scavenging during fall.

RECOMMENDATIONS

As Young et al., 1973[15] suggests, work considering side entrainment throughout the vertical extent of an existing growing cloud would yield significant results. One other study is the process of tapping as the cell is growing up through layers of air and entraining material from the environment. This study would also be useful in attempting to estimate scavenging effects.

Finally, work will continue in the study of storms measured during NHRE, from which more data on rain-producing clouds is available in conjunction with cosmogenic radionuclide measurements.

COMPARISON OF THE WASHOUT COEFFICIENT FOR A POLYDISPERSE AEROSOL TO THAT FOR AN AEROSOL OF FIXED PARTICLE SIZE

M. Terry Dana and J. M. Hales

When a polydisperse aerosol is involved in a calculation of washout coefficient, considerable error can result from an attempt to characterize the distribution by a single "representative" particle size. If the differential washout coefficient is expressed as $A = cr^{\alpha}$ and aerosol removal is expressed in terms of mass, the error is not eliminated unless the chosen representative size is the $(\frac{\alpha}{2} + 3)$th geometric mean particle radius.

Most attempts to determine washout coefficients and efficiencies experimentally have involved the use of polydisperse aerosols. The measured parameters are expected to depend strongly on particle size, and the usual procedure has been to determine an "integral" washout coefficient or efficiency (that is, one that pertains to the total distributed aerosol of study) by observing the total mass of aerosol collected

by the precipitation. Often some representative particle size is chosen which is assumed to characterize the aerosol appropriately, and the results are then reported in terms of true "differential" values which correspond specifically to that particle size. To our knowledge there has been no serious attempt to examine the errors associated with this practice. It is the purpose of this paper to address this problem theoretically in an attempt to provide information useful for improving the design of future experiments of this type.

To accomplish this objective we shall focus primarily upon the definition of the washout coefficient. A parallel derivation can be presented in terms of collection efficiencies; in the present context it will suffice to consider washout coefficients only. The relationship between the integral washout coefficient (based upon mass measurement) and the differential washout coefficient is given by the form

$$\Lambda_m = \int_0^\infty \Lambda(r)\ m(r)\ dr, \qquad (1)$$

where Λ_m and $\Lambda(r)$, respectively, represent the integral and differential washout coefficients, and $m(r)$ is the probability density function characterizing the mass associated with particle radius r of the distributed aerosol.

We next assume that the relationship between the differential washout coefficient and particle size, over the size range of interest, can be approximated by a power-law equation as

$$\Lambda(r) = cr^{\alpha}. \qquad (2)$$

This amounts to a "linearization" of the true relationship expressed in logarithmic form, as indicated by the straight-line fits to the hypothetical curve shown in Figure 3. If we proceed to choose some "representative" value of r ($r = r'$) to characterize the system as described above, then the associated differential washout coefficient is

$$\Lambda(r') = cr'^{\alpha}. \qquad (3)$$

Since Λ_m and $\Lambda(r')$, respectively, correspond to the integral value and the differential value based on an assumed r', the objective of this

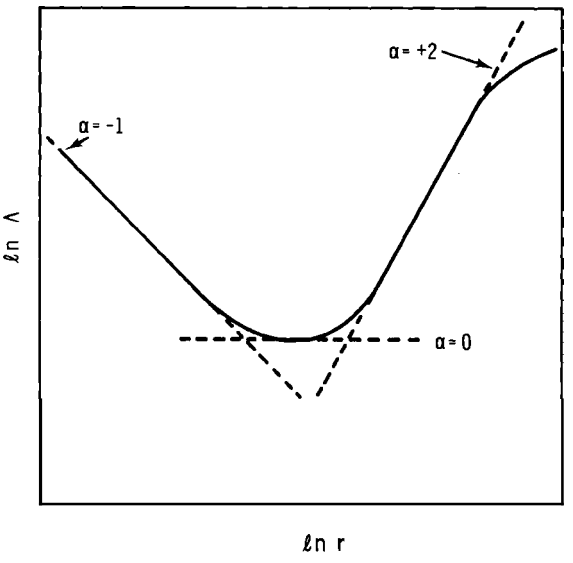

Neg 740789-8

FIGURE 3. Schematic Showing Linearized Fits to Hypothetical Washout Curve

paper can be fulfilled simply by comparing these values as they are affected by changes in pertinent parameters of the system.

Making the additional assumption that the aerosol count can be characterized in terms of a log-normal distribution,

$$f(r)dr = \frac{1}{\sqrt{2\pi}\ \ln \sigma_g} \exp\left[-\frac{(\ln r - \ln r_g)^2}{2(\ln \sigma_g)^2}\right] d \ln r, \quad (4)$$

where σ_g is the geometric standard deviation and r_g is the number median particle radius, one can write the mass density function as

$$m(r)\ dr = \frac{r^3\ f(r)\ dr}{\int_0^\infty r^3\ f(r)\ dr} \quad (5)$$

Combining the above equations, the ratio of the integral and differential washout coefficients can be expressed as

$$\frac{\Lambda_m}{\Lambda(r')} = \frac{1}{r'^\alpha} \frac{\int_0^\infty r^{\alpha+3}\ f(r)\ dr}{\int_0^\infty r^3\ f(r)\ dr}. \quad (6)$$

Equation (6) consists essentially of the ratio of moments of the log-normal distribution. The general expression for these moments is given[16,17] by

$$\int_0^\infty r^n\ f(r)\ dr = r_g^n \exp\left[\frac{n^2}{2}(\ln \sigma_g)^2\right], \quad (7)$$

so that Equation (6) becomes

$$\frac{\Lambda_m}{\Lambda(r')} = \left(\frac{r_g}{r'}\right)^\alpha \exp\left[\alpha\left(\frac{\alpha}{2} + 3\right)(\ln \sigma_g)^2\right]. \quad (8)$$

Figure 4 shows values of $\Lambda_m/\Lambda(r_g)$ for several values of a, as a function of a_g. It is clear that a choice of r_g as representative particle size can lead to considerable error, especially as σ_g becomes large. If we choose $r' = r_{ng}$, i.e., choose to characterize the size spectrum by a geometric mean value, Equation (8) becomes

$$\frac{\Lambda_m}{\Lambda(r')} = \exp\left[\alpha\left(\frac{\alpha}{2} + 3 - n\right)(\ln \sigma_g)^2\right], \quad (9)$$

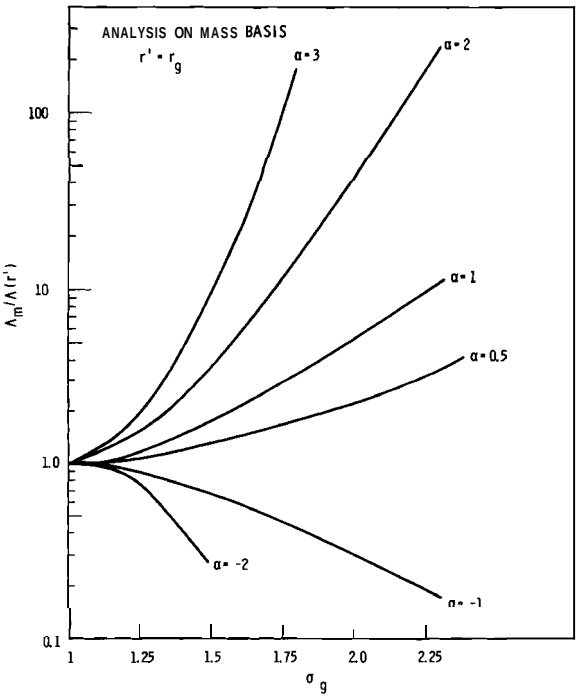

Neg 740789-3

FIGURE 4. Ratio of Mass-Integral Washout Coefficient to Differential "Representative" Washout Coefficient: Various Slopes of Differential Washout Curve

which is independent of r_g (as in Equation (8) when $r' = r_g$). Figure 5 shows the values of $\Lambda_m/\Lambda(r_{ng})$ for $a = 2$--which is the approximate value predicted by inertial washout theory[18]--for various values of n and σ_g. The error is not eliminated unless the chosen representative size is such that $n = \frac{\alpha}{2} + 3$.

This approach can be generalized to cases where the integral washout coefficient is generated in terms of particle size, area, or some other power of r. This is done simply by replacing the 3 in Equations (8) and (9) by x, where: $x = 0$ for washout in terms of number of particles; $x = 1$ for washout in terms of particle length; $x = 2$ for washout in terms of particle area; etc.

These results are significant in showing that the method of sampling (e.g., by mass: $x = 3$) as well as the differential form of the washout coefficient can influence the results of washout experiments when the tracer aerosol is polydisperse. Of course, these results apply to the washout of any polydisperse aerosol--natural or artificial--and show that some knowledge of the differential form is required to properly evaluate the integral washout coefficient.

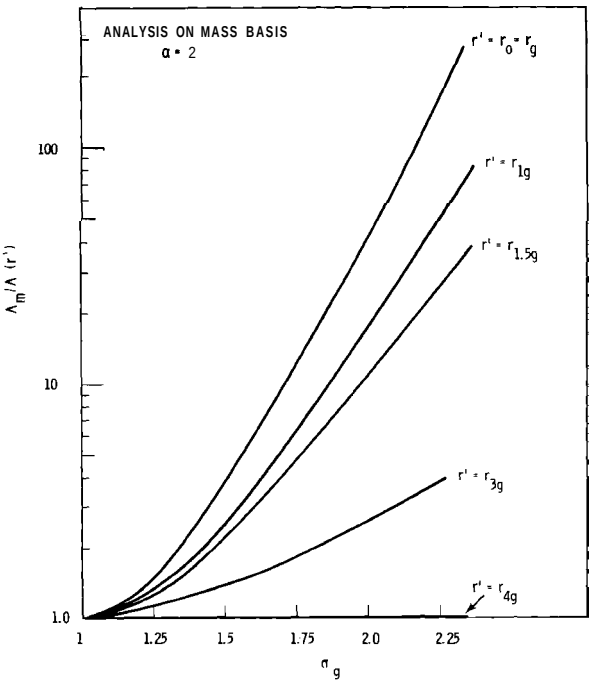

Neg 740789-2

FIGURE 5. Ratio of Mass-Integral Washout Coefficient to Differential "Representative" Washout Coefficient: Various r' for a = 2

A POSTULATED ESTIMATE OF WET VERSUS DRY DEPOSITION DOWNWIND OF A POINT SOURCE OF POLLUTION

W. G. N. Slinn

A simple postulate is advanced which permits an estimate of the relative magnitudes of wet and dry deposition downwind of a point source of pollution. The postulate is an extension of Chamberlain's estimate of the dry deposition velocity. It is assumed that the deposition velocity for aerosol particles is the product of $u_*^2/\bar{u}$ by a particle-size-dependent collection efficiency. With this assumption and approximations for the washout coefficient, the ratio of wet to dry deposition is found to be independent of the characteristics of the pollution. Comparisons of the theoretical results are made with available experimental data, and although the theory permits a reasonable interpretation of the data, it is seen that more data is needed before unequivocal conclusions can be drawn.

INTRODUCTION

Studies of natural atmospheric cleansing processes have been plagued for some time by the unanswered question of whether wet or dry removal processes are more significant. Facy's oft-quoted estimate that "between 95 and 80% of the total amount of radioactivity received on the ground surface is included in rain or snow" (Facy)[19] should not be generalized to provide a comparison of wet versus dry scavenging for all pollutants, because obviously the relative magnitudes of these two fluxes depend on the source height and the dispersive capabilities of the atmosphere. In the case of bomb-debris fallout, the major tropospheric source is the stratosphere, and therefore even a cursory estimate would conclude that precipitation scavenging would be more significant than dry deposition in the removal of fallout. In comparison, here we propose to estimate the relative importance of dry deposition and below-cloud rain scavenging, downwind of a stack of effective height h, under conditions of specified atmospheric diffusivity.

WET DEPOSITION

To estimate the flux of pollutants to the ground caused by below-cloud rain scavenging (viz., "washout") we first introduce some preliminaries. For particles and for gases which are scavenged irreversibly (compare Hales and Slinn),[20,21] the washout coefficient, A, is defined via

$$n(a,t) = n(a,o) \exp [-\Lambda(a)t] \qquad (1)$$

where $n(a,t)da$ is the number of aerosol particles (or gas molecules) per unit volume at time t whose radii are

between a and a + da. The washout coefficient can be obtained from the collection efficiency, E(a,R) via (Engelmann).[22]

$$A(a) = \int_o^\infty dR\ N(R)\ v_t(R)\ \pi R^2\ E(a,R) \quad (2)$$

where N(R)dR is the number of raindrops (similarly for snowflakes) whose radii are between R to R + dR, and v_t is the terminal speed of the drops.

To estimate the washout coefficient we notice the similarity of (2) with the expression for the rainfall rate J_o:

$$J_o = \int_o^\infty dR\ N\ v_t\ \frac{4}{3}\ \pi R^3. \quad (3)$$

In view of this similarity and accepting that this entire analysis is crude, we approximate (2) by

$$\Lambda(a) \simeq E_w(a) \int_o^\infty dR\ N\ v_s\ \pi R^2$$
$$\simeq \frac{3}{4}\ \frac{E_w(a)}{Rm}\ J_o \quad (4)$$

where $E_w(a)$ is an average collection efficiency and R_m is a characteristic raindrop radius.

There are two other results which provide some justification for (4). In his experimental studies of scavenging, Dana[23] has found that if he uses $A = \alpha E$ where E is the mean collection efficiency (of the entire raindrop size spectrum for a given particle size distribution) then α/J_o is essentially a constant for prefrontal rain on the Olympic Peninsula of Washington. An average value for α/J_o was found to be 1.4 mm^{-1}. Further, elsewhere we have used the semi-empirical fit to the collection efficiency (Slinn)[18]

$$E(a,R) = \left[1-\exp\left(\frac{-St}{k}\right)\right]$$
$$+ \frac{4}{Pe}\left(1 + 0.4\ Re^{1/2}Sc^{1/3}\right) \quad (5)$$

where St, Pe, Re and Sc are the Stokes, Péclét, Reynolds and Schmidt numbers (with lengths based on the drop radius) and k is a numerical constant near 2. Upon substituting (5) into (2) and integrating over a Khrigian-Mazin raindrop size distribution (e.g., see Zimin)[24] and using $v_t = 8000\ sec^{-1}\ R$, one obtains

$$\Lambda(a) = 2R_m \left\{\left[1 - \exp\left(\frac{-St}{k}\right)\right]\right.$$
$$\left. + \frac{0.8}{Pe}\left(1 + 0.8\ Re^{1/2}Sc^{1/3}\right)\right\} \quad (6)$$

where R_m is the mean raindrop radius and the dimensionless groups are evaluated using R_m. Notice the similarity between (4) and (6). Thus these two results and the realization that the entire theory presented here is approximate provide us with enough rationalization to proceed.

If the number of aerosol particles of radius a to a + da released during dt from a stack of height h is $\dot{n}(a)$ dt, then the number density downwind can be approximated by (Engelmann)[22]

$$n(x,y,z;a) = \frac{\dot{n}}{\bar{u}}\ \frac{1}{2\pi\sigma_y\sigma_z}$$
$$\exp\left[\frac{-y^2}{2\sigma_y^2} - \frac{(z-h)^2}{2\sigma_z^2}\right]\ \exp\left(\frac{-\Lambda_t x}{\bar{u}}\right) \quad (7)$$

where Λ_t is the total (wet and dry) removal rates, $\bar{u}$ is the mean wind speed and σ_Y and σ_z are the crosswind and vertical diffusivities. The wet deposition flux is obtained from (7) by integrating over all z [or all $z > 0$ if reflection were included in (7)]:

$$W(x,y;a) = \frac{\Lambda(a)\dot{n}}{\bar{u}(2\pi\sigma_y^2)^{1/2}} \exp\left(\frac{-y^2}{2\sigma_y^2} - \frac{\Lambda_t x}{\bar{u}}\right) \quad (8)$$

Thus our approximation for the wet deposition flux is obtained by sub stituting our expression (4) for A into (8).

DRY DEPOSITION

Estimating dry deposition involves considerable uncertainty. For the wet deposition problem the removal rate was to be found by integrating the collection efficiency over a reasonably well known raindrop size distribution. On the other hand, for the case of dry deposition, the integrals would be over all twigs, blades of grass, rocks, etc.! Further, in the wet deposition problem the relative velocity between the collector and the collected particles was the terminal velocity of the drops; for the dry deposition case we would need to know the intricate details of the wind around every element in the canopy cover of the ground.

To circumvent these difficulties we follow Chamberlain's use of Reynolds' analogy (e.g., see Chamberlain or Pasquill)[25,26] and assume that these unbelievably complicated integrals have essentially been done for us, if we know the flux of momentum to the ground, or equivalently, the friction velocity

$$u_* = (\tau_o/\rho)^{1/2} \quad (9)$$

where τ_o is the surface stress and ρ is the density of air. Thus it is reasoned that the physical processes governing the transports and the surface boundary conditions are similar (but not identical) for both momentum and pollution and therefore if we know the flux of momentum we should be able to deduce the flux of a pollutant.

There are at least two major problems with this approach. In the first, we must recognize that, especially near a stack, momentum will be "mixed" much more uniformly in the atmosphere than will be the pollutant. Therefore the flux of momentum to the surface will be much larger than the flux of pollution. To overcome this problem, Chamberlain first defines a deposition velocity for momentum, which is the momentum flux to the surface, τ_o, divided by the "concentration of momentum," $\rho\bar{u}$, at some convenient reference height, typically 1 m. Thus the deposition velocity for momentum is taken to be

$$v_{dm} = \frac{\tau_o}{\rho\bar{u}_{1m}} = \frac{u_*^2}{\bar{u}_{1m}} . \quad (10)$$

Then it is assumed that the deposition velocities (rather than the fluxes) of momentum and pollutant are equivalent.

The second major problem is to account for the differences in deposition velocities for different pollutants. The above may be acceptable for gases (e.g., I_2) which diffuse to each collector (blade of grass, etc.) as rapidly as do the air molecules carrying the momentum, but it would not be expected to be accurate for some aerosol particles. Sehmel[27] has recently investigated the dry deposition of particles to various surfaces in a wind tunnel and shown the significant variation of the dry deposition flux as a function of particle size. In the same spirit as the other approximations made herein, what we propose is just to adjust the deposition velocity as given by (10) with a multiplying factor $E_d(a)$ to account for the difference in the collection efficiency between particles and perfectly retained gases. Then the magnitude of the dry deposition flux for perfectly retained particles (or gas molecules) to the surface is taken to be the product of the deposition velocity by the air concentration at the reference height:

$$D(x,y;a) = E_d(a) \frac{u^{*2}}{u_{1m}} n(x,y,z = 1\ m). \quad (11)$$

We now need the air concentration at the reference height, $n(x,y,z = 1\ m)$. By arguments similar to those used to obtain (8), we propose to use semi-empirical Gaussian distribution, modified because of previous removal by a factor $\exp(-\Lambda_t x/\bar{u})$, where Λ_t is a total removal coefficient. Further, though, we note that in our expression for the concentration we have not taken into account partial plume reflection at the ground. We consider this neglect, as well as the neglect of the spatial variation of Λ_t, to be well within the general level of accuracy of this crude theory. If we now substitute n as given by (7) into (11), then we have for the dry deposition flux

$$D(x,y;a) = E_d(a) \frac{u_*^2}{\bar{u}^2} \frac{\dot{n}}{2\pi\sigma_y\sigma_z} \exp\left[-\left(\frac{y^2}{2\sigma_y^2} + \frac{h^2}{2\sigma_z^2}\right)\right] \exp\left(\frac{-\Lambda_t x}{\bar{u}}\right). \quad (12)$$

WET VERSUS DRY DEPOSITION

Dividing (8) by (12), we obtain an estimate of the relative importance of wet versus dry deposition downwind of a stack of effective height h:

$$\frac{W}{D} = C \frac{E_w}{E_d} \frac{J_o}{R_m} \frac{\bar{u}h}{u_*^2} \left(\frac{\sigma_z}{h}\right) \exp\left(\frac{h^2}{2\sigma_z^2}\right), \quad (13)$$

where C is a constant which is hoped will be near unity. As might have been expected (13) predicts that the ratio is independent of source strength and of crosswind location. It depends (strongly) on downwind distance because of the variation of σ_z with x.

There is one further major approximation we propose to make. We propose to equate the particle size dependencies of the two collection efficiencies and thereby cancel E_w and E_d from (13), leaving only a numerical factor, independent of particle size.

There are a number of reasons why we believe that this procedure is acceptably consistent with the other approximations we have made. First, looking at the collection processes in broad outline, we see that on the one hand, the collection is by objects of characteristic length in the range 0.05 to 5 mm and for relative velocities between the air and the collectors of typically 1 cm sec^{-1} to 10 m sec^{-1}, and on the other hand, the lengths and relative velocities for the other process are similar. Second, looking at the microphysics of the processes, we see that in both cases the large particles are collected by similar means (inertial and phoretic effects) and similarly for small particles (diffusional and electrical effects).

Finally, though, we are faced with the realism of our present very incomplete knowledge of either collection efficiency, even for controlled laboratory conditions and idealized theories. Further, even if rapid progress is made in these areas, the results may have little applicability to collection efficiencies in the real atmosphere, under conditions of microturbulence, coagulation among aerosols, chemical conversion of trace gases, condensation of water vapor, degree of particle wettability, electrical interactions, and the like. However, both wet and dry deposition processes will probably be affected similarly by this host of possibilities and therefore we conclude that even under these real conditions (and perhaps, especially because of them) we can proceed to take $E_w = kE_d$, with k not dependent on particle size.

In Figure 6 the ratio of wet to dry fluxes (with $E_w \equiv E_d$) is plotted as a function of σ_z for various effective stack heights and rainfall rates. We notice from (13) that as $a_1 \to o$, $W/D \to \infty$ (which follows since the air concentration at the ground is then vanishingly small); as $\sigma_z \to \infty$, $W/D \to \infty$ (which follows since dry deposition is literally a surface phenomenon whereas raindrops "integrate" through the entire volume); and W/D has a minimum at $\sigma_z = h$. For $\sigma_z = 0.1\,x$, this minimum occurs at 10 stack heights downwind of the source. For Figure 6 we have used $C = 1$, $R_m = 0.3$ mm, and $\bar{u} = 5$ m sec^{-1} and have shown two cases for the product hJ_o. Notice in (13) that the ratio of the fluxes depends directly on the product hJ_o. Thus the upper curve is appropriate for $hJ_o = 250$ mm hr^{-1} (e.g., $h = 50$ m, $J_o = 5$ mm hr^{-1} or $h = 100$ m, and $J_o = 2.5$ mm hr^{-1}), whereas the bottom curve is for $hJ_o = 50$ m mm hr^{-1}. Other cases can be found easily. In doing this we are ignoring the (weak) dependence of R_m on J_o (typically $R_m \sim J_o^{1/5}$).

With these results available it might be thought that we are in a position to evaluate the relative importance of wet versus dry deposition downwind of a particular pollution source. However, there is more information needed besides the obvious need for the specification of the receptor's location and for climatological data on total rainfall and σ_z. Namely, it is necessary to know the variation of the

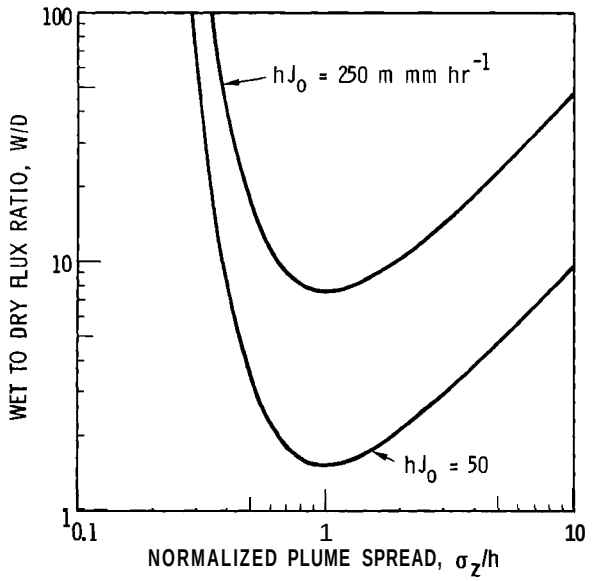

Neg 734803-1

FIGURE 6. The Ratio of Wet to Dry Flux Downwind of a Stack of Height h when the Rainfall Rate is J_o. To obtain these results it was assumed that the wet and dry collection efficiencies are equal and that R_m = 0.3 mm and $\bar{u}$ = 5 m sec^{-1}.

removal rates (or of the collection efficiencies) with other meteorological conditions. The seriousness of this need is well illustrated by the wet deposition data obtained by Engelmann et al.[28] for inorganic iodine, who found that process-plant iodine was removed three orders of magnitude more rapidly than iodine released from a tower during a controlled field experiment. The speculated cause of this difference was chat there was sufficient water vapor in the plant stack gases to cause condensational growth of water drops, these drops collected the iodine, and in turn it was these drops which were washed out so efficiently. If this is indeed the case, then we would need to take E_w and perhaps E_d near unity on rainy days, but perhaps a three orders of magnitude smaller E_d on days with low humidity. One might expect similar major variations, for example, for SO_2 which on humid days may be rapidly converted to sulphate particles and be removed rapidly if they grew to large ($\sim$10 μm) dilute, sulphuric acid droplets, but removed much more slowly if they remained as, say, 0.1 μm particles.

In spite of the crudeness of the entire approach taken here, it would seem prudent, in view of the above remarks, to not yet attempt to predict the relative importance of wet and dry deposition on a climatological basis. However, for specific meteorological conditions and for a specific downwind location, then the ratio would be given as in (13) or as shown in Figure 6. Further, we could attempt to assess the ratio of the two integrated depositions during a particular rainstorm. In this case, from (13), the total wet deposition (excluding in-cloud scavenging) is just

$$TWD = \frac{3}{4}\frac{E_w(a)}{R_m}\frac{\dot{n}}{\bar{u}}\int_o^T J_o dt \int_o^\infty \exp\left(\frac{-\Lambda_t x}{\bar{u}}\right)dx. \qquad (14)$$

If we continue to ignore the variation of Λ_t with distance and take $\bar{J}_o$ to be the average rainfall rate during the rain storm, then (14) yields

$$TWD = \frac{3}{4}\frac{E_w(a)\dot{n}J_o T}{R_m \Lambda_t} \qquad (15)$$

Evaluating the total dry deposition is more difficult. Similarly to the above, we would obtain from (12):

$$TDD = E_d(a)\,\frac{u_*^2}{\bar{u}^2}\,\dot{n}T\int_0^\infty \frac{1}{\sqrt{2\pi}}\,\frac{1}{\sigma_z}\,\exp\left(\frac{-h^2}{2\sigma_z^2}\right)\exp\left(\frac{-\Lambda_t x}{\bar{u}}\right)dx. \qquad (16)$$

A reasonable specification for a_z might be

$$\sigma_z = \begin{cases} 0.1\,x, & \sigma_z \le H/2 \\ H/2, & \frac{H}{2} < x < \infty \end{cases}, \qquad (17)$$

where H is the height of the mixed layer. Another alternative is

$$\sigma_z = k_z H\left[1 - \exp\left(\frac{-\alpha x}{H}\right)\right], \qquad (18)$$

where a depends on the stability and k_z is an appropriately chosen constant. However, both these choices leave us with an intractable integral to perform. What we propose to do for the present is just assume that upon leaving the stack, the pollutant is instantaneously mixed throughout the mixed layer of height H. This will result in an overestimate of the dry deposition adjacent to the stack, an underestimate at x = h, and then a fairly accurate estimate at larger x. Since we are comparing the total dry and wet depositions, it is suspected that the error caused by this approximation will be tolerable. Then (16) simplifies to

$$TDD = E_d(a)\frac{u_*^2}{\bar{u}}\,\frac{\dot{n}T}{H\Lambda_t}. \qquad (19)$$

The ratio of total wet to total dry during the rainstorm is then

$$\frac{TWD}{TDD} = \frac{3}{4}\,k\,\frac{J_o}{R_m}\,\frac{\bar{u}H}{u_*^2}, \qquad (20)$$

where $E_w(a) = kE_d(a)$. The result (20) is essentially the ratio of the two characteristic rate constants J_o/R_m and $u_*^2/\bar{u}H$. For J_o = 5 mm hr^{-1}, R_m = 0.3 mm, $\bar{u}$ = 5 m sec^{-1}, u_* = 50 cm sec^{-1} and H = 1 km, the ratio (20) has the value 70 k. From the data to be discussed in the next section, a value for k of about 0.2 may be appropriate. This would suggest that during the rainstorm wet deposition is about 10 times more important than dry deposition (for the above stated conditions). To obtain a climatological assessment of the relative importance, one must first decrease the ratio by the ratio of dry to wet days (which might thereby decrease the above result to unity) and then (probably) increase the ratio again, to account for lower E_d on dry days than on wet days.

COMPARISON WITH EXPERIMENTS

Recently Dana and Wolf[29] and Wolf and Dana[7] conducted a number of deposition experiments at Quillayute on the Olympic Peninsula, Washington. They measured total deposition of an aerosol tracer in samplers on arcs located 15.2, 30.5 and in some cases 45.7 m downwind of an 8-m tower. These will be referred to as Arcs A, B and C, respectively. The tracer used was a dry generated, water soluble

fluorescein aerosol dye of particle mass median diameter of about 10 μm. Pertinent data from their reports for four successful tests is shown in Table 1. Many other experiments were performed, but only for these is information on σ_z given. In particular, σ_z was inferred from measurements of σ_u via the relation

$$\sigma_z = 0.81\ \sigma_\phi x = 0.81\left(0.67\ \frac{\sigma_u}{\bar{u}}\right)x, \quad (21)$$

which they obtained from studies by Islitzer[30] and Elderkin and Hinds.[31] Since it will be seen how sensitive are the predicted results to an accurate specification of σ_z, we shall later investigate the consequences of the relation

$$\sigma_z = k_z \sigma_\phi x, \quad (22)$$

with k_z a free parameter, near the value used by Wolf and Dana.(7)

In Table 1, Λ_x is the experimentally observed, crosswind integrated, fractional removal rate, to which both wet and dry processes contribute. To obtain the corresponding fractional removal rates predicted by theory, we return to the expressions given for either flux, say F. If either flux is integrated over y from $-\infty$ to $+\infty$, then the crosswind integrated amount of material deposited on a strip of width dx during time dt is

$$dxdt\int_{-\infty}^{+\infty} dyF(x,y).$$

During dt, the amount of material released is $\dot{n}dt$. Therefore, using $dx/dt = u$, we have that the fractional removal rate attributable to the flux F is

$$\frac{\bar{u}}{\dot{n}}\int_{-\infty}^{+\infty} dyF(x,y).$$

For the experiments under consideration, Λ_x is typically 10^{-3} sec^{-1}, and therefore the effect of previous removal (i.e., the $\exp(-\Lambda_t x/\bar{u})$ term), can be ignored. Consequently we take as theoretical predictions the expressions

$$\Lambda_w(a) = \frac{3}{4}\ E_w(a)\ \frac{J_o}{R_m}\ w(x) \quad (23)$$

and

$$\Lambda_d(a) = \frac{1}{\sqrt{2\pi}}\ E_d(a)\frac{u_*^2}{\bar{u}}\ \frac{1}{\sigma_z}\ \exp\left(\frac{-h^2}{2\sigma_z^2}\right). \quad (24)$$

In (23) we have included a function w(x) to account for the fact that raindrops do not fall vertically unless $\bar{u} = 0$. Thus some of the small drops that land in a sampler may not have passed through the plume. To

TABLE 1. Experimental Data for Experiments UIL 1, 2, 4, and 6 from Dana and Wolf (1968)

Test	Arc	x (m)	u ($m\ sec^{-1}$)	σ_ϕ	J_o ($mm\ hr^{-1}$)	Λ_x ($\times 10^4$ sec)
UIL-1	A	15.2	4.92	0.306	7.5	11.0
	B	30.5				19.8
UIL-2	A	15.2	5.81	0.463	6.0	13.2
	B	30.5				26.2
UIL-4	A	15.2	3.80	0.162	1.5	1.8
	B	30.5				7.4
UIL-6	A	15.2	1.79	0.206	1.9	3.1
	B	30.5				5.0
	C	45.7				9.5

estimate this "plume undercutting effect" we notice that to evaluate the wet deposition flux, we should not integrate over all drop sizes, but only those whose settling velocity, v_s, satisfies $v_s \geq h\bar{u}/x$. If we use the Khrigian-Mazin drop size function and assume as a first approximation that $v_s = (8000\ sec^{-1})R$, then from (2) it is easy to determine that an approximate correction for this effect is

$$w(s) = \frac{1}{3!} \exp(-\xi)$$

$$(\xi^3 + 3\xi^2 + 6\xi + 6), \qquad (25)$$

where $5 = h\bar{u}/x\bar{v}_s$, in which $\bar{v}_s$ is the settling speed of the mean size drop.*

In Figure 7 we have plotted Λ_w, Λ_d and their sum, for $J_o = 2.5$ mm hr^{-1}, $R_m = 0.3$ mm, $\bar{u} = 5$ m sec^{-1}, $h = 8$ m, $u_* = 50$ cm sec^{-1}, and $\sigma_z = 0.1$ x for the case that $E_w = E_d = 1$. Also shown are the locations of Arcs A, B, and C for these hypothetical experimental conditions. It is obvious that this hypothetical case foretells that we will have difficulty extricating the separate contributions from wet and dry deposition in the experimental results.

Table 2 shows a comparison of the theoretical predictions with the experimental results. For this prediction we have tried to take some account of the change in mean drop size with rainfall rate through use of Dana's result[32] for Olympic Peninsula rain, that

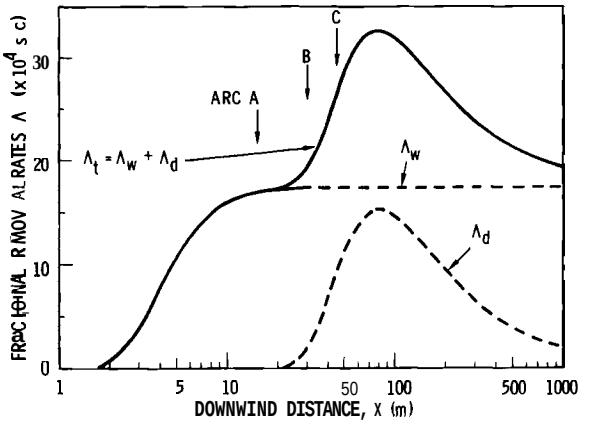

Neg 734803-3

FIGURE 7. The Fractional Removal Rates (Λ_w - wet, Λ_d - dry and Λ_t - total) as a Function of Distance Downwind from an 8-m Source for $J_o = 2.5$ mm hr^{-1}, $R_m = 0.3$ mm, $u = 5$ m sec^{-1}, $u_* = 50$ cm sec^{-1}, $\sigma_z = 0.1$ x and assuming $E_w = E_d = 1$. The locations of Arcs A, B and C for Wolf and Dana's Quillayute test series are indicated by arrows.

TABLE 2. Comparison of Theoretical Predictions with Experimental Results; All Λ's Are To Be Multiplied by 10^{-4} Sec^{-1}

Test	Arc	Λ_w/E_w	Λ_w (a)	Λ_d/E_d	Λ_d (b)	Λ_t (c)	Λ_x
UIL-1	A	45.2	9.0	2.1	2.1	11.1	11.0
	B	46	9.2	5.8	5.8	15.0	19.8
UIL-2	A	37	7.4	9.6	9.6	17.0	13.2
	B	37.7	7.5	10.1	10.1	17.6	26.2
UIL-4	A	11.4	2.3	0.004	0.004	2.3	1.8
	B	11.5	2.3	0.80	0.8	3.1	7.4
UIL-6	A	14.1	2.8	0.26	0.26	3.1	3.1
	B	14.1	2.8	5.3	5.3	8.1	5.0
	C	14.1	2.8	7.1	7.1	9.9	9.5

a. Assuming $E_w = 0.2$
b. Assuming $E_d = 1.0$
c. $\Lambda_t = \Lambda_d + \Lambda_w$

* For (25) we integrated $R^2 v_s N(R) dR$ rather than R^3, etc., for simplicity. The difference is relatively insignificant.

$R_m(mm) \simeq 0.25\ J_o^{0.15}$,

(J_o in mm hr^{-1}).

In addition, we have used Dana and Wolf's expression for a_z given earlier, Equation (21), and also have used $u_* = \sigma_\phi(m\ sec^{-1})$ in an attempt to account in some manner for the dependence of u_* on the level of turbulence.

A first impression from Table 2 should be some surprise that the theory is as close as it is! If judicious choices of E_w and E_d are made, then the fit can be made even closer: for example, the results from taking $E_w = 0.2$ and $E_d = 1.0$ ($k = E_w/E_d = 0.2$) are shown.* Nevertheless, the fit between theory and experiment is not sufficiently accurate to resolve which of the processes, wet or dry removal, is of major importance during these experiments. There is a suggestion that dry deposition was more important; almost certainly both processes contributed to the total removal. Apparently the plume undercutting effect was of negligible significance.

The reason the question cannot be resolved using this data is that with such a low release elevation σ_z must be known with considerable accuracy. To see this more clearly, we have plotted Λ_d/E_d in Figure 8 for each

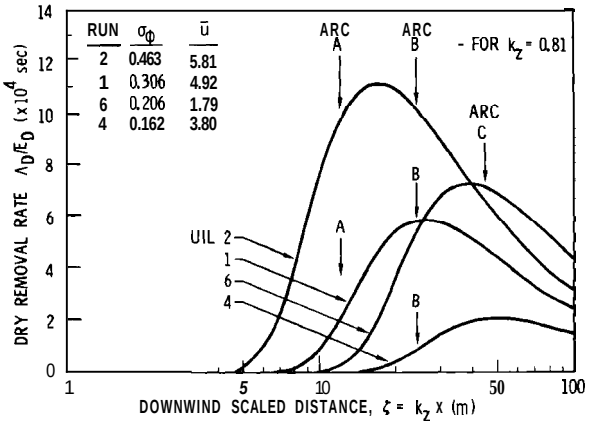

Neg 734803-2

FIGURE 8. The Predicted Dry Removal Rate as a Function of Downwind Distance for the Conditions of UIL Tests 1, 2, 4 and 6, Using $k_z = 0.81$. Notice how significant a slight change in k_z would be on the relative locations of the arcs and therefore on the predicted dry deposition.

of the four experiments. The abscissa is $\zeta = k_z x$, where $\sigma_z = k_z \sigma_\psi x$, and the locations of the three arcs for the case $k_z = 0.81$ are shown. If, as an example, the locations of Arcs A and B with respect to UIL-2 are noted, then it is seen how significant would be a slight change in k_z. Arc B would be at the peak of the dry deposition curve if $k_z \simeq 0.57$ and then Arc A would be at $\zeta = 8.66$. This would yield $\Lambda_d(x_B) = 11.1 \times 10^{-4}\ sec^{-1}$ and $\Lambda_d(x_A) = 4.8 \times 10^{-4}\ sec^{-1}$, which is a substantial change from the values given in Table 2.

A further point that should be mentioned is as follows. In earlier versions of this report, the author was often plagued by the thought that the predominant result demonstrating wet deposition to be the more significant removal process during these

* No significant effort was expended to find "best" choices of E_w and E_d for reasons mentioned later. Note that the range $E_d > 1$ could be considered since it would mean only that the particles are removed more efficiently than momentum.

experiments was that Λ_t was very nearly proportional to J_o, the rainfall rate. However, if we look again at the data, see Table 3, it is seen that not only did Λ_t increase with J_o, but so did σ_ϕ (which might have been expected). In fact the increase in A_t is even more closely correlated with the increase in σ_z rather than with J_o. It is hoped that further experiments will be performed to investigate this matter thoroughly.

TABLE 3. Observed Variations of J_o, σ_ϕ, and Λ_t

Test	J_o (mm hr^{-1})	a_ϕ	Λ_t(A) ($\times 10^4$ sec)	Λ_t(B)
UIL-2	6.0	0.463	13.2	26.2
UIL-1	7.5	0.306	11.0	19.8
UIL-6	1.9	0.206	3.1	5.0
UIL-4	1.5	0.162	1.8	7.4

CONCLUSIONS

As might be expected, the first summary statement the author desires to make is that he does not expect this theory to be very accurate. Some of the major assumptions that were made are the following. To obtain the wet deposition flux, the dependence of the collection efficiency, $E_w(a)$, on drop radius, R, was ignored and an extra R was placed inside the integral of Equation (4). To obtain the dry deposition flux, Chamberlain's use of Reynolds' analogy was extended by multiplying the deposition velocity by a particle-size-dependent collection efficiency $E_d(a)$. Then, to obtain the ratio of wet to dry fluxes, it was assumed that the particle size dependencies of the wet and dry collection efficiencies were the same: $E_w = kE_d$.

Throughout, extensive use has also been made of Gaussian distribution for the air concentration. Normally one would think that this assumption is acceptable--certainly stronger than the other assumptions which were made. But there are certain dissatisfying aspects of its use which should be mentioned. It is well recognized that the Gaussian distribution is a time-smoothed approximation to real concentrations, which one hopes would sufficiently accurately describe long-term-average concentrations. In a sense, then, the Gaussian distribution should be a rather insensitive, coarse description when used in the form for example, $\exp[-(z - h)^2/2\sigma_z^2]$ as a function of z. But here, in the dry deposition theory, it appears in the form $(1/\sigma_z)\exp(-h^2/2\sigma_z^2)$, as a function of σ_z. This is an extremely sensitive function of σ_z. In the limit, if one had $\sigma_z \sim x^n$, n large, then what was originally chosen as an insensitive function of z becomes similar to a Heaviside step function in σ_z. Thus the use of the Gaussian distribution cannot be considered a trivial approximation.

Although the results obtained here are expected to be only order-of-magnitude estimates, it is noted that they may substantially simplify evaluating deposition downwind of a point

pollution source. Thus if wet and dry collection efficiencies satisfy $E_w(a) = kE_d(a)$, with k independent of a, this will eliminate essentially half the problem, at least on wet days. However, this is based somewhat on an unfortunate aspect of atmospheric cleansing studies that has persisted for some time, ever since the earliest wet deposition studies by McCully et al.[33] and May.[34] It is that atmospheric cleansing studies have tended to focus on one or the other of wet or dry deposition, separately. But the problem of concern is the total deposition downwind of a point source of pollution, and the relative contributions of wet versus dry deposition is a rather academic distraction, at least for the stated problem. Thus, unless the study of the separate parts of total deposition is needed to evaluate this total deposition, we recommend that more emphasis be placed on the total problem, and less on its separate parts.

ACKNOWLEDGMENTS

I have had the good fortune to be associated with a strong group of scientists at Battelle who have been engaged in atmospheric cleansing processes for the past decade. Most of the ideas presented here have been gained through association with them, and their contributions to this report are therefore substantial. Early work was done by J. J. Fuquay and C. L. Simpson. R. J. Engelmann called the author's attention to the possibility of dry deposition and plume undercutting (e.g., Engelmann et al., 1966). Plume undercutting was subsequently accounted for by J. M. Hales in some of his modeling studies. The dry deposition problem was studied extensively both experimentally and theoretically by M. A. Wolf. M. T. Dana earlier calculated the relative contributions from wet and dry depositions, based on my approximate expression for Λ_w [see Equation (5)] and G. A. Sehmel's expressions for the deposition velocity. In summary, then, the only contribution I have made is to assume $E_w = kE_d$, which may yet prove to be wrong.

WET AND DRY ATMOSPHERIC REMOVAL PROCESSES FOR RADIOIODINE

L. C. Schwendiman, J. M. Hales and R. Mahalingam*

A study is under way to evaluate the relative importance of all processes which remove radioiodine in all its forms from the atmosphere. The washout of gaseous iodine is shown to be dependent on the gas phase and liquid phase mass transfer resistance and on the changing partition coefficient as the concentration in the droplet changes. Application of the models developed to the very limited data available show qualitative agreement. Washout rates are lower with realistic evaluation of the influence of liquid phase resistance. The more recently developed EPAEC model was applied to an initial case for various iodine release rates. Continued study is planned.

A study was initiated to clarify the relative importance of precipitation scavenging and dry deposition processes for radioiodine removal. The release of radioiodine from nuclear facilities, although being greatly limited by AEC regulations to "as low as practicable," nevertheless continues to account for a large fraction of the dose commitment to persons in the environment. For routine release, those calculating dose assume that dry deposition is the dominant mode of removal from the air. Yet in regions of persistent, high rainfall the point of maximum concentration and its consequences could be altered by precipitation scavenging in the assessment of dose. Furthermore, the possible impact of accidental releases from nuclear power plants and fuel reprocessing facilities could be significantly affected by assumptions concerning the importance of rain washout. Should a reactor accident occur in a heavy rain the location and concentration of iodine on the ground would be different than for dry deposition.

Another aspect which is to receive attention is the significance of the physical form and chemical nature of the iodine for the atmospheric process of interest. Most frequently the assumption is made that iodine exists as a true vapor, yet at ordinary temperatures the vapor pressure of iodine is very low, suggesting that iodine vapor would tend to condense and readily form particles. Experience has shown that the frequent seeming anomalous behavior of iodine might be explained by the strong tendency to "plate out" on solids. Whether iodine exists as elemental molecular iodine or in organic forms such as methyl iodide must also be investigated.

The initial effort in this work has been directed toward atmospheric

* Professor of Chemical Engineering, Washington State University, Pullman, Washington.

rain washout of gaseous iodine. Until quite recently models have been employed in which it is assumed that the only resistance to mass transfer is in the gas phase. Our effort has been to investigate these and more recently developed washout models in which the resistance in the liquid droplet is accounted for.

Unfortunately, little experimental data is available on the washout of iodine in the atmosphere. By contrast many experiments have been performed in vessels in which heavy sprays were employed.[35] We have attempted to account for the low washout coefficients obtained by R. J. Engelmann[36] by accounting for resistance to mass transfer within the rain droplets. The fractional removal rate was calculated by using estimates of the liquid mass transfer coefficient along the lines suggested by Griffiths[37] and partition coefficients as a function of iodine concentration from Diffey et al.[38] Since no information regarding iodine air concentrations was available from Engelmann's experiments, two base concentrations for the low rainfall point (0.18 mm/hr) were assumed. These concentrations have been prorated for the other rainfall points. The first concentration, 1.06×10^{-6} g mol of iodine/liter of water, was obtained by iteration from partition coefficient data with an assumed ground-level atmospheric concentration of 0.15 mg/m^3. The latter concentration is that estimated to occur when 100 g of I_2 is released from a 10-m tower in 5 min, wind speed 2 m/sec., stability category D. The second concentration assumed was 10^{-5} g mol iodine/liter of water, chosen arbitrarily to demonstrate the change in washout for the two assumptions.

Overall mass transfer coefficients to the droplets were calculated using the liquid and gas mass transfer resistances and the equation:

$$\frac{1}{K_y} = \frac{1}{k_y} + \frac{1}{H'' k_x}$$

in which K_Y is the overall mass transfer coefficient (or V_d), H'' is the partition coefficient, k_Y is the gas phase mass transfer coefficient, and k_x is the liquid phase mass transfer coefficient.

The fraction removed/second, allowing for resistance in both phases, was determined by adjusting the coefficients calculated by Engelmann, who assumed gas phase only resistance (perfect sink case). This adjustment was made under the assumption that the perfect sink washout coefficient was linear with the gas phase only mass transfer coefficient and that the overall washout coefficient was linear with the overall mass transfer coefficient. Results are as shown in Figure 9. This exercise showed that accounting for resistance in the liquid to mass transfer and the selection of a more appropriate partition coefficient can account for the considerably lower washout than that predicted for the gas-phase resistance limiting case. It is also apparent that at low rainfall

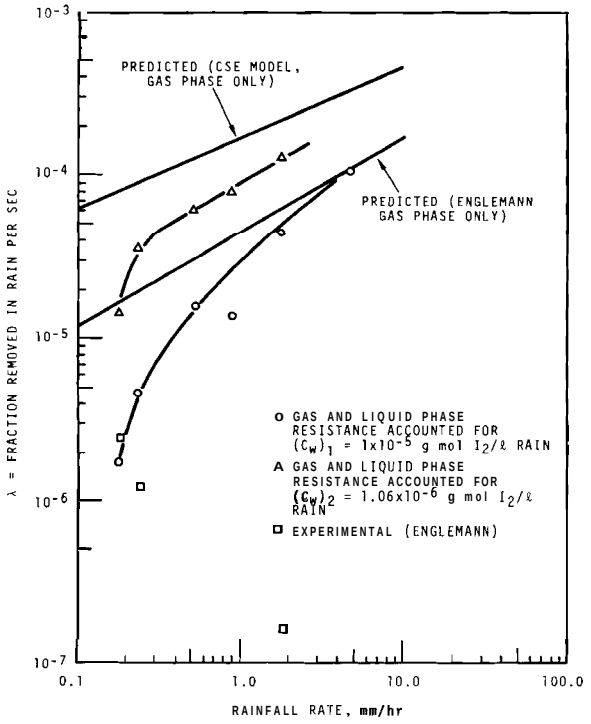

Neg 740436-2

FIGURE 9. λ Based on CSE Model

rates liquid-phase resistance has even greater significance in lowering the washout coefficient. The limitations in the available data make critical evaluation impossible.

Progress was made toward applying the EPAEC model to iodine washout. A computer subroutine for incorporating the partition coefficient data was developed. Figure 10 shows an initial application of the EPAEC model for various iodine release rates. Cases will be calculated to help evaluate the relative importance of the several atmospheric processes for removing iodine.

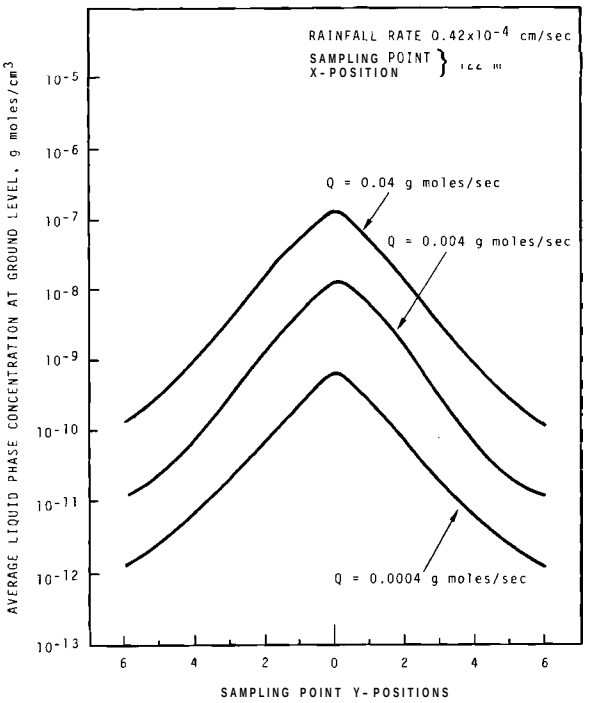

Neg 740436-1

FIGURE 10. Ground-Level Concentration in the Liquid Phase (EPAEC Model)

DEVELOPMENT OF AN "IDEAL" SAMPLER FOR BELOW-CLOUD SCAVENGING STUDIES

D. W. Glover and J. M. Hales

Findings during the past year have indicated rather strongly that a majority of field measurements of below-cloud washout may have been contaminated significantly by dry deposition and, in the case of gases, by resuspension. Because of these findings, an attempt to design and fabricate an "ideal" rain sampler (i.e., one that allows zero dry deposition or suspension) is in progress.

Many different designs have been conceived and prototypes of some of these built during this investigation (Figure 11). Several types would be satisfactory theoretically, and a few have been found to work to a limited degree in the laboratory; however, in actual outdoor field test conditions disadvantages appear in almost all designs used or tested thus far. The primary disadvantage to all samplers in Figure 11 is the inability to quantitatively recover the sample.

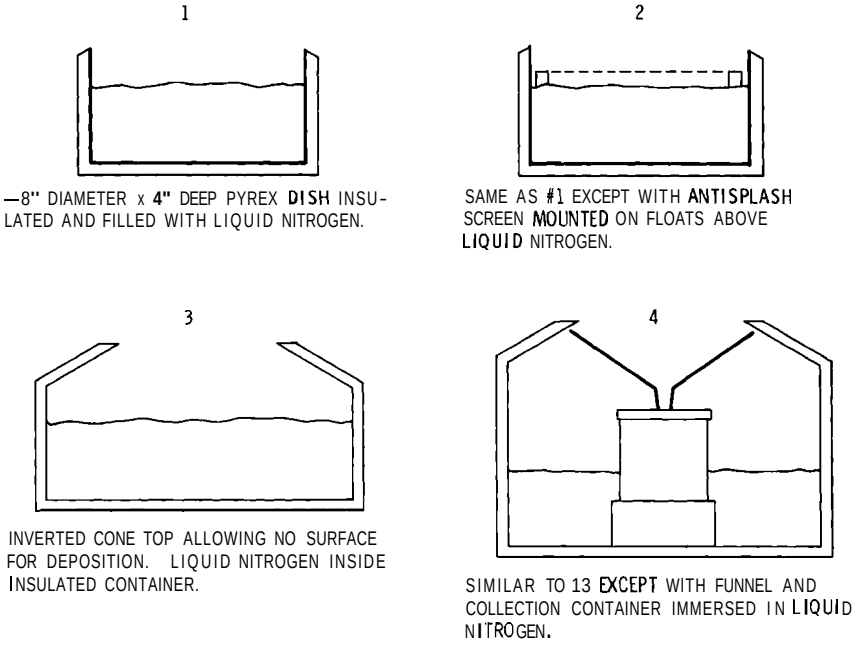

Neg 740789-5

FIGURE 11. Sampler Designs Investigated

One type (Figure 12) shows the most promise for a clean sampling allowing no deposition. However, its operation is complicated enough to make it impractical to implement a complete grid network. At this point it appears that much more must be done to perfect the sampler and to simplify its operation. But a few of this type sampler will be integrated into future sampling grid networks for comparison samples to provide correction factors for discriminating between washout and dry deposition in the primary network samples.

At present no actual field tests have been performed with the sampler. Future tests of this type will indicate its potential for extensive use.

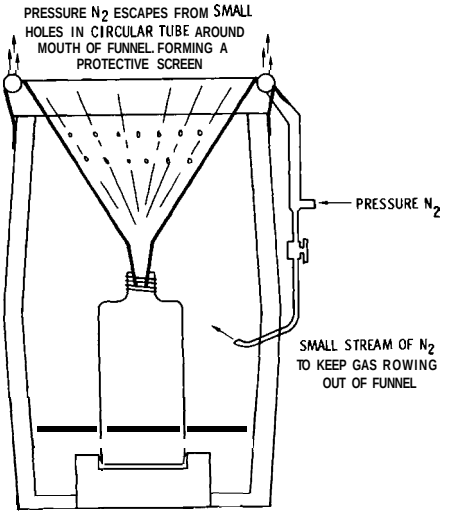

Neg 740789-6

FIGURE 12. Two-Gallon Picnic Jug with 8 Inch Poly Funnel Inserted into 1-Liter Poly Bottle. Holes in funnel permit gas to escape but no water to penetrate. Liquid N_2 in bottom freezes sample, and out-gassing forms a protective barrier in funnel.

AN EXTENSION OF THE ANALYSIS OF PLUME WASHDOWN TO INCLUDE DIFFUSION

W. G. N. Slinn

An extension is presented of the author's analysis of plume washdown caused by reversible washout of gases. The extension is to include diffusion. The results show that in the mean the plume falls at the washdown velocity $H'J_o$ where J_o is the rainfall rate and H' is the dimensionless Henry's law constant for the gas, and that diffusion is slightly enhanced.

INTRODUCTION

In the 1972 Annual Report the author presented an analysis of plume washdown caused by reversible washout. The steady-state convective diffusion equation describing the gas concentration χ is

$$\bar{u}\frac{\partial\chi}{\partial x} = D_y\frac{\partial^2\chi}{\partial y^2} + D_z\frac{\partial^2\chi}{\partial z^2} + \int_0^\infty dr\, f(r)\left[\beta(r)\, C_r - \alpha(r)\,\chi\right] \qquad (1)$$

where $\bar{u}$ is the mean wind speed, the diffusivities, D_Y and D_z are treated as constants, $f(r)dr$ is the number of raindrops per unit volume with radius r to $r + dr$, and the integrand reflects the reversible washout process. In particular a is essentially the familiar washout coefficient. C_r is the concentration of the gas in the drops and βC_r reflects the desorption of gas from the drops. Hales (1972) [20] has related a and β to appropriate physical parameters and, in particular, has shown

$$a = H'\beta \qquad (2)$$

where H' is the dimensionless Henry's law constant (both liquid phase concentration, C_r and gas phase concentration, χ expressed, for example, in moles cm^{-3}).

The companion equation to (1) which describes the concentration of the gas in drops of radius r is

$$-\gamma\frac{\partial C_r}{\partial z} = \alpha\chi - \beta C_r \qquad (3)$$

where, if the entire raindrop size distribution were characterized by a single drop size, then $\gamma = J_o$, the rainfall rate. If we make this assumption that $f(r)$ is a delta function, then (1) simplifies to

$$\bar{u}\frac{\partial\chi}{\partial x} = D_y\frac{\partial^2\chi}{\partial y^2} + D_z\frac{\partial^2\chi}{\partial z^2} + \beta C - \alpha\chi. \qquad (4)$$

In the previous report (3) and (4) were solved ignoring diffusion. The purpose of this report is to demonstrate the solution when diffusion is not negligible but can still be

described using constant diffusivities in (4).

SOLUTION

To solve (3) and (4) we eliminate the liquid-phase concentration and obtain the single equation

$$\frac{\partial \chi}{\partial t} = w \frac{\partial \chi}{\partial z} + \delta \frac{\partial^2 \chi}{\partial t \partial z} + D_y \frac{\partial^2 \chi}{\partial y z}$$

$$+ D_z \frac{\partial^2 \chi}{\partial z^2} - \delta D_y \frac{\partial^3 \chi}{\partial z \partial y^2} - \delta D_z \frac{\partial^3 \chi}{\partial z^3} \quad (5)$$

where $t = \frac{x}{u}$, $w = \frac{\alpha\gamma}{\beta} = J_o H'$ is the washdown speed (>o) and $\delta = \gamma/\beta$ is a characteristic length which for the example illustrated in the last report was about 5.5 m. Equation (5) is to be solved subject to the normalized boundary and initial conditions: $\chi(t \to o, y, z) = \delta(y)\,\delta(z-h)$; $\chi(t, y \to \pm\infty, z) = 0$; and $\chi(t, y, z \to \pm\infty) = 0$. These conditions correspond to the case downwind ($t = x/\bar{u}$) of a stack of height h for those situations when the influence of the ground can be ignored.

To solve (5) the method of multiple transforms will be used (Slinn, 1966).[39] Taking first a Laplace transform in time (parameter s), then infinite Fourier transforms in y (parameter η) and z (parameter ζ), leads to the algebraic equation which contains the boundary conditions:

$$\hat{\tilde{\chi}}(s,\eta,\zeta) = \frac{(1 - i\delta\zeta)\exp(-i\zeta h)}{s(1 - i\delta\zeta) + \eta^2 D_Y + \zeta^2 D_z - i\zeta(w + \delta D_Y \eta^2 + \delta D_z \zeta^2)} \quad (6)$$

Inverting the Laplace transform is trivial since there is only one simple-pole in the complex s-plane. Next the simple η-Fourier transform is inverted. Finally, the ostensible inversion of the 6-transform leads to

$$\chi(t,y,z) = \frac{1}{(4\pi t D_y)^{1/2}} \exp\left(\frac{-y^2}{4t D_y}\right) \cdot \frac{1}{2\pi}\int_{-m}^{+\infty} d\zeta \exp\left[-t D_z \zeta^2 - i\zeta(h - z) - \frac{wt}{\delta}\frac{\zeta}{(\zeta + i/\delta)}\right]. \quad (7)$$

The integral in (7) is rather difficult to evaluate. It converges only in the region $|\mathrm{Im}\zeta| < |R_e\zeta|$; there is an essential singularity at $\zeta = -i/\delta$; in order to find paths of steepest descent it is necessary to find the roots of the obvious cubic in ζ. Rather than pursue the interesting mathematics involved in evaluating (7), we attempt to simplify the last term in the exponential for cases of practical interest.

We first consider the case for $56 \ll 1$. From the previous report we notice that for the washdown of SO_2, $\delta \doteq 5.5$ m. On the other hand, the largest ζ value that will contribute significantly to the integral is seen from the first term in the exponential to be $\simeq (t\,Dz)^{-1/2}$. Thus ζ is small compared with δ^{-1} provided

$(t\ D_z)^{-1/2} << \delta^{-1}$ or $t >> 6^2/Dz_2$. This condition is satisfied for the case with D_z as small as 1 $m^2\ sec^{-1}$ and for the SO_2 plume, provided only that $t >> 1$ min. This is not at all a serious restriction. Then expanding the last term in the exponential according to

$$-4\frac{\zeta}{(\zeta + 1/\delta} \simeq iwt\ \zeta - wt\ \delta\zeta^2. \quad (8)$$

performing the simple integral, and returning to unnormalized quantities, we obtain

$$\chi(x,y,z) \sim \frac{\overset{\circ}{Q}}{\bar{u}} \frac{\exp\left(\frac{-y^2}{4t\ D_y}\right) \exp\left\{-\frac{[z - (h - wt)]^2}{4t\ (D_z + w\delta)}\right\}}{(4\pi t\ D_y)^{1/2}\ [4\pi t\ (D_z + w\delta)]^{1/2}} \quad (9)$$

where $t = x/u$. Thus for large time and for the approximations stated, the influence on the plume of reversible rain scavenging is that the plume diffuses about the effective plume height $(h - wt)$, where $w = J_o H'$ is the washdown speed, and the diffusivity is slightly enhanced by the factor $w\delta$.

For the case $\zeta\delta >> 1$ (e.g., small t) then it is easy to see from (7) that using only the leading term in the expansion of the same term as approximated above, yields

$$\chi(x,y,z) \sim \frac{\overset{\circ}{Q}}{\bar{w}} \exp\left(-\frac{wt}{\delta}\right) \frac{\exp\left(\frac{-y^2}{4t\ D_y}\right)\exp\left(\frac{-(z-h)^2}{4t\ D_z}\right)}{(4\pi t\ D_y)^{1/2}\ (4\pi t\ D_z)^{1/2}} \quad (10)$$

which describes only the diffusion and removal of the part of plume whose centerline is at h.

In the interim, until a complete inversion of (7) is obtained, it is suggestive that we take as an approximation for all x (and we expect that this approximation will yield results as realistic as those derived from the many other approximations made in this analysis) the sum of the result (10) and $\left[1 - \exp\left(-\frac{wt}{\delta}\right)\right]$ times the result (9). This proposed expression would describe both the removal and diffusion of the plume whose centerline is at h and the "washdown" and diffusion of the remainder of the plume. This proposed expression neglects the decrease of the air concentration caused by previous washout, but this is a customary practice in washout theory since it leads to conservative estimates in dose calculations.

PRECIPITATION SCAVENGING OF INORGANIC POLLUTANTS FROM METROPOLITAN SOURCES: ST. LOUIS, JULY, 1973

M. Terry Dana, Jeremy M. Hales, C. E. Hane and John M. Thorp

An additional series of rain scavenging experiments in St. Louis was conducted, this time using a large array of collectors. Some nine convective storms were sampled, and over 400 individual rain samples have been analyzed for SO_2, SO_4^{--}, NO_2^-, NO_3^-, NH_4^+, and H^+.

In last year's report[40] we summarized initial results of the first series of convective storm scavenging experiments in the St. Louis area. The final results of that study are available in an Environmental Protection Agency report.[41] The second series, in July, 1973, consisted similarly of precipitation and aircraft air sampling and meteorological observations, but on a much larger scale. In the new array, shown in Figure 13, the two downstorm lines of 1972 were replaced with a grid of collectors which extended from 2 to 52 km downstorm or east of the St. Louis Arch. This extension allowed for closer-in sampling of the city's pollution plume, as well as the capability for capturing a larger portion of the plume during spatially extensive rainfall.

The greater effort was made possible through cooperation with two current AEC-sponsored efforts, Atmospheric Aerosols and Trace Gases, and Tracer Studies in METROMEX; sufficient personnel were available so that all 120 sampling locations--plus one roving sequential sampling facility--could be outfitted with precipitation collectors on all storm days. The increase in manpower allowed essentially continuous deployment of collectors and thus led to some overnight rainfall being effectively sampled.

During the about three week field period some nine storms were sampled. Table 4 is a list of general information on precipitation sampling and times of release of radiosondes from Lambert - St. Louis Airport.

Chemical analyses of the precipitation samples have been completed for the species SO_2, SO_4^{--}, NO_2, NO_3^-, NH_4^+, and H^+. Currently, the concentration data exist in raw form; further analysis of quality of samples in terms of potential contamination, post-collection chemical reactions, effects of ambient temperature on some overnight samples, etc., is under way.

The data from these storms, plus that collected from four storms in

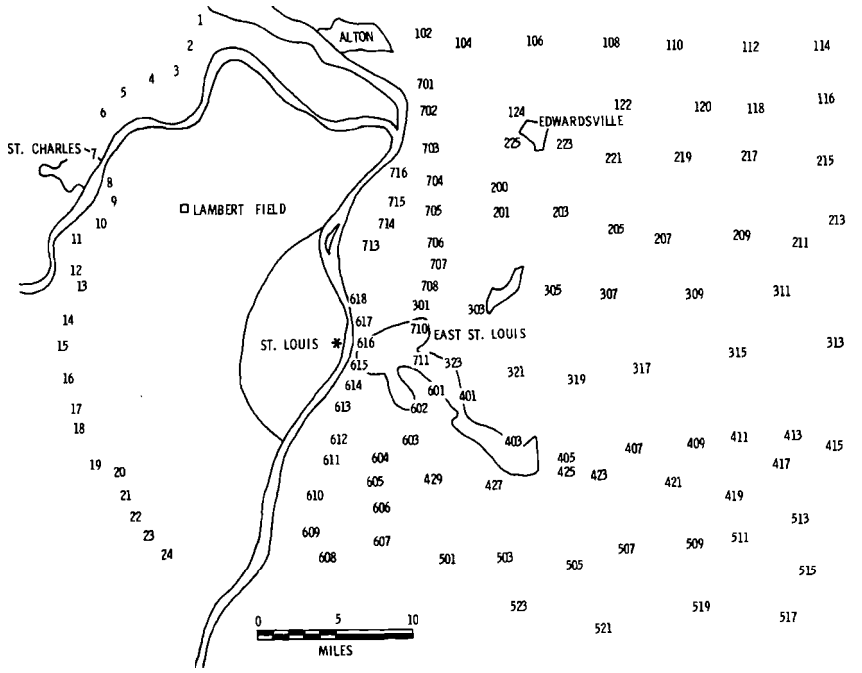

Neg 740789-1

FIGURE 13. July, 1973, **Precipitation Collection Array**

TABLE 4. General Data: Inorganic Pollution Scavenging Operations

Date	Run No.	Sampling Coverage[a]	Total No. of Samples	Approx. Time of Rainfall (CST)	Radisonde Release Time (CST)	Remarks
7-14-73	6	0,4-7	24	1600-1800		Most samples frozen - immediate recovery.
7-18/19-73	7	0-7, S301[b]	90	0800-1000	1329 (7-19)	Overnight collection - most unfrozen.
7-20/21-73	8	0	10	Early AM 7/21	1241 (7-20) 0928 (7-21)	No useable samples saved.
7-23-73	9	0-7	89	Early AM		Overnight - all unfrozen, immediate collection.
7-23-73	10	0-7, S301[b]	79	1500-1900	1323	Same day collection - most frozen
7-24-73	11	0-7	4	1300		Isolated shower all frozen.
7-25-73	12	3-6	14	Early PM	1308	Same day collection - most frozen.
7-25-73	13	S200	8	2100-2200		Sequential - all frozen.
7-25/26-73	14	0-3, 6-7	59	Late PM 7/25		Overnight - most unfrozen.

a. Sampler groups are identified by the first digit of the sample position number. See Figure 13.
b. Sequential samples taken at position indicated.

1972, will form an important data base for development and testing of convective storm models. The modeling effort has just begun; the eventual aim is a precipitation scavenging input to an overall model of urban pollution effects being developed within the Regional Air Pollution Study (RAPS) sponsored by the Environmental Protection Agency.

CONVECTIVE STORM MODELING AND ITS POSSIBLE APPLICATION TO PRECIPITATION SCAVENGING PROBLEMS

Carl E. Hane

The use of numerical convective cloud modeling in precipitation scavenging research is discussed. A particular two-dimensional time-dependent squall line model is described which includes a parameterization scheme for the microphysics of cloud and rain. Possible initial steps for the use of this model in scavenging research are discussed.

There is an increasing awareness of the consequences of the production of particulates and gases which remain for varying lengths of time in the atmosphere. One noteworthy consequence of concern is the high concentration of such materials in water clouds and rain. Convective clouds, in particular, are capable of producing large amounts of rain in short time intervals over limited areas and can both (1) deposit unusually high concentrations of these man-produced materials on the ground and (2) redistribute these materials in the atmosphere or else at other locations rid the atmosphere of their effects.

Research in this area of scavenging by convective clouds should therefore be concerned with the interactions occurring among these materials, cloud droplets, and rainwater both within and beneath the cloud. Among other things, these interactions depend heavily upon both the air motions within the cloud and in the near environment of the cloud since the two together determine the amounts of air incorporated into the cloud at various levels. The processes are thus complicated by the nature of the convective cloud, which may grow to great heights and exist in an environment possessing strong vertical wind shear.

A research tool developed over the last 10 to 15 years is the numerical modeling of convective clouds. These models are designed to calculate (1) air motion, (2) temperature and (3) various types of water distributions in and around convective

clouds in one, two or three space dimensions. Though the three-dimensional models should of course be the most realistic, they have not been exploited fully because of limitations in computer size and time. One and two-dimensional modeling efforts have become increasingly realistic as more refinement is introduced in the dynamics and the microphysical processes. A corresponding need for greater computer size and speed has developed, however, in conjunction with this refinement. The modeling efforts therefore must involve a compromise between (1) available computer size and speed and (2) the degree of realism gained by taking into account more space dimensions and more detailed dynamics and precipitation microphysics.

Use of such a tool in study of scavenging processes now appears possible and may contribute to significant progress in the solution of practical problems. Since scavenging is inseparably related to microphysical processes, a complete attack on the problem by numerical means should include a detailed accounting for cloud microphysics. This may be impossible at this time in the multi-dimensional models, but the possibility presently exists for parameterization of scavenging processes by means analogous to the parameterization of cloud microphysics now widely employed.

A description will now be given of one particular numerical model which is two-dimensional in space and perhaps most applicable to the type of thunderstorm prevalent in the Great Plains squall line. The model calculates as a function of time and space (1) air motion, (2) temperature, and (3) mixing ratios of water vapor, cloudwater, and rainwater. Condensation and evaporation plus associated heating and cooling are taken into account along with the sub-grid scale turbulent mixing between cloud and environment.

The Marshall-Palmer[42] distribution of drop sizes is assumed so that the fall speed of rainwater is a weighted mean for that distribution and depends upon rainwater mixing ratio only. Cloudwater is differentiated from rainwater in that cloudwater moves with the air and evaporates instantaneously when subsaturation occurs, whereas rainwater has an additional component of motion due to its terminal fall speed and evaporates only partially (at a rate depending upon the amount of rain present and the degree of subsaturation of the air at that point). Cloudwater is converted to rainwater by auto-conversion (coalescence of cloud droplets only) and by accretion (coalescence of raindrops with cloud droplets and other raindrops).

The above processes are parameterized assuming the Marshall-Palmer distribution of drop sizes rather than taking into account discrete drop sizes and calculating distributions in the model. This kind of parameterization was referred to above regarding incorporation of scavenging processes in numerical cloud models.

A complete description of the model may be found elsewhere,[43,44]

but Figure 14 is included as an example of the model output. Significant features include:

(1) updraft containing intense condensational warming and tilting from the vertical in an upshear direction,

(2) rain produced in updraft falling from updraft into dryer air,

(3) dry adiabatic warming in sinking air occurring outside the cloud and evaporative cooling occurring to the left of and below cloud,

(4) cold dome of air produced near the ground, and

(5) strong horizontal wind speeds near ground in outflow from updraft.

As a starting point in introducing scavenging into such a model, the following steps might be taken:

1. Introduce a plume at various locations within the two-dimensional domain and allow it to travel with the air motions and diffuse, allowing no interaction with cloud or raindrops.
2. Same as 1, except allow rainwater distribution to incorporate particles in the plume in a parameterized fashion (below-cloud scavenging).
3. Same as 1 and 2, except allow incorporation of particles within cloud droplets in a parameterized fashion (in-cloud scavenging or particles used as nuclei for condensation).

The type or types of particles in the plume would strongly influence the scavenging processes, and this influence would have to be accounted for

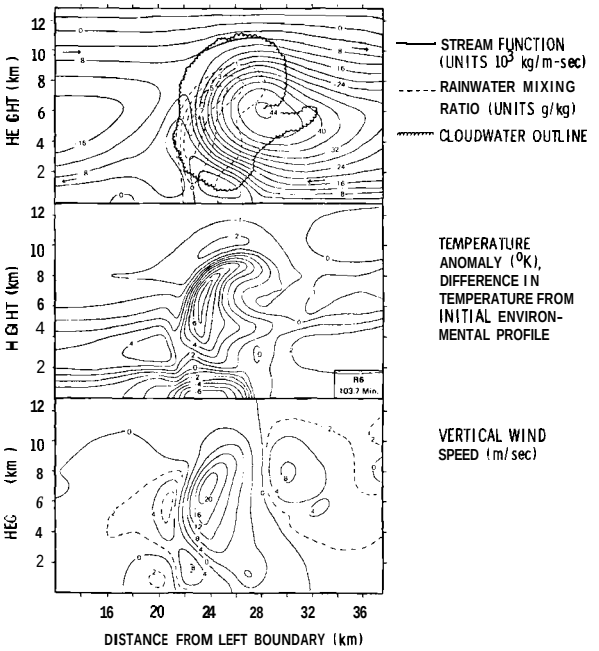

Neg 740789-4

FIGURE 14. Example of Model Output

through constants involved in the parameterization. Evaluation of these constants could perhaps best be done in simpler controlled laboratory or field experiments rather than by modeling a real storm situation in the atmosphere and then comparing results of model and observed scavenged materials in order to define constants.

One-dimensional modeling might be employed to allow for inclusion of discrete drop sizes and particle sizes and to better study processes of interaction. Results of one-dimensional modeling might be used to define better parametric techniques to be used in multi-dimensional models until the time that computer size and speed allows for the incorporation of discrete processes into these more general models.

Modeling efforts are worth little unless coupled with observational programs used for initiating calculations and verifying results. On the other hand, observational programs are often worth little without some conceptual model (qualitative, analytic, numerical, etc.) to provide ideas on needed accuracy and scale of observations, location of observational sites in relation to physical phenomena, and overall goals of observation. This sort of cooperative interdependence should be firmly established in any effort to incorporate convective cloud modeling into scavenging research.

THE ENTRAINMENT OF TRACERS NEAR THE SIDES OF CONVECTIVE CLOUDS

J. A. Young, T. M. Tanner, C. W. Thomas and N. A. Wogman

Tracers released sequentially at 10 to 13.5 thousand ft near the upwind sides of two convective towers near St. Louis spread between the towers and were almost completely scavenged by the precipitation.

The METROMEX experiment is a study of convective storms being conducted for five summers by several organizations beginning in 1971 in a 2000 $mile^2$ area centered around St. Louis, Missouri. Special attention is given to determining the effects of heat and contaminating material added to the atmosphere on precipitation processes and on aerosol scavenging in convective storms.

Lack of knowledge concerning the amount of air entrained into convective towers at altitudes above cloud base has severely hampered the understanding and modeling of convective storm dynamics. The air at higher altitudes is colder and drier than air entering the cloud through the updraft, so entrainment tends to decrease the vigor of the convective cloud. To measure the amount of air entrained into convective towers which later reaches regions of precipitation scavenging, tracers were released sequentially at 10 to 13.5 thousand ft near the edges of convective towers in the St. Louis area. The concentrations of the tracers were measured later in precipitation samples.

On August 3, 1972 europium, ruthenium, and tantalum were released near the upwind (western) edge of one eastward moving convective cell located near the center of the Battelle precipitation collection network. Iridium, rhenium, and gold were released near the western side of a second cell located near the

southwest corner of the network. The tracers were released by burning acetone solutions of the tracers in six aerosol generators mounted beneath the wings of the Battelle Cessna 411. The particles produced by the generators are less than 0.1 μm diam. Each tracer was released in 2 min, but with a short time allowed between releases of the individual tracers the release of the six tracers took 65 min. The tracers indium and lithium were also released into the updraft of the second cell at cloud base by the Illinois State Water Survey.

Following the tracer release, samples of precipitation were collected on a 25 x 36-mile network of 122 rain collectors. The main samples were quickly frozen and returned to the laboratory for neutron activation analysis. Most of these samples have been analyzed, and the remainder are now being analyzed.

Significant quantities of tantalum, iridium, rhenium, gold and indium were measured in precipitation samples collected downwind of the tracer releases. Ruthenium was not detected because of analysis difficulties. The europium concentrations in the precipitation were not significantly above background levels because of the relatively high background concentrations of europium and because only 6 g of europium were released due to difficulties in dissolving europium in acetone. Europium and several of the other tracers have since been obtained as acetonyl acetonate compounds, which are much more soluble in acetone; thus they now can be released in quantities of a few hundred grams.

High concentrations of each tracer were measured not only in the precipitation from the cell into which it was released, but also in the precipitation of the neighboring cell. Measurable concentrations of the tracers were present in the precipitation samples collected at the eastern and southern edges of the precipitation network, indicating that the tracers were probably present in precipitation falling outside the precipitation network. The calculated precipitation scavenging efficiencies for tantalum, iridium, rhenium, and gold were greater than 100%, indicating that the tracers released near the upwind edges of the convective towers were entrained and reached regions of nearly complete precipitation scavenging. The calculated scavenging efficiency for indium released at cloud base was only about 30%, however. Possibly some of the indium released was not carried up into the cloud by the updraft or else it was carried up through the cloud and out the top before being completely scavenged.

The results from 1972 indicated that the precipitation network used was not large enough to determine the distance the tracers would spread in a storm system. Therefore, in the summer of 1973 a much larger network was set up. However, as no suitable convective storms appeared over the network while the Battelle aircraft was available, no tracers were released.

THE EFFECTS OF RADIOACTIVITY ON ICE NUCLEATION

J. Rosinski,* G. Langer,* C. T. Nagamoto,*, C. W. Thomas, N. A. Wogrnan and J. A. Young

Supercooled drops containing dissolved radionuclides froze at warmer temperatures than drops containing no radionuclides.

In natural clouds aerosol and hydrosol particles act as ice-forming nuclei, causing supercooled water droplets to freeze. However, concentrations of ice crystals in clouds have been reported as much as several orders of magnitude greater than the concentrations of ice-forming nuclei. One possible explanation for at least part of this discrepancy could be that the ionization produced by the decay of radionuclides present in the supercooled droplets might cause the drops to freeze.

To determine whether radionuclides could in fact cause supercooled drops to freeze, experiments were performed in which the freezing temperature of 2 mm diam (4.2×10^{-3} g) supercooled drops containing ^{24}Na, ^{32}P, ^{38}Cl, ^{90}Sr, ^{137}Cs, ^{147}Pm, ^{241}Am or $^{253}Es + ^{247}Bk$ were compared with those of drops containing identical concentrations of dissolved salts, but not radioactivity. The drops were frozen on vaseline as the substrate in a closed chamber cooled at a rate of 0.6°C/min. Radionuclide activities used in the tests were between 40 and 10^8 dpm per ml.

It was found that drops made of pure water and those of dilute salt solutions froze over a very narrow range of temperature, but drops containing radionuclides froze over a wide range of temperatures and always started freezing at a warmer temperature. There appeared to be little correlation between the activity and the type and energy of the radiation and the increase in the freezing temperature. The freezing temperatures of droplets made from saturated solutions of $NaNO_3$, $(NH_4)_2HPO_4$ or NH_4Cl were not affected by radionuclide activities of 10^3 to 10^4 dpm/ml.

It should be pointed out that the radionuclide concentrations used in these experiments were generally higher than those found in cloud droplets. Total radionuclide activities in cloud droplets should be about 40 dpm/ml, with cosmogenic radionuclides contributing about 10 dpm/ml, radon daughters contributing about 30 dpm/ml and nuclear weapons-produced radionuclides contributing 1 dpm/ml. If gaseous cosmogenic radionuclides such as ^{41}Ar, ^{14}O, ^{15}O, and ^{13}N become attached to cloud droplets, however, the total activity could be as great as 10^3 dpm/ml.

* From the National Center for Atmospheric Research, Boulder, Colorado.

These results indicate that radioactive silver iodide should be a more active ice-forming nucleus than normal silver iodide. Morachevsky,[45] however, has claimed on the basis of laboratory experiments that radioactive silver iodide has no ice-nucleating ability even at -19°C. In view of the above discrepancy., the ice-nucleating abilities of normal silver iodide, gamma irradiated silver iodide, and radioactive silver iodide were compared in experiments in which ice nucleation by contact and by condensation followed by freezing were studied concurrently in a cloud chamber, and ice nucleation by freezing drop technique. The results showed clearly that radioactive silver iodide did not lose its ice-nucleating ability. On the contrary, $Ag^{131}I$ seemed to nucleate ice more effectively.

Bryant and Mason,[46] and Rowland et al.[47] have found that the density of oriented ice crystals increased on freshly formed surfaces of silver iodide when exposed to UV radiation for a short period of time. Fukuta and Paik[48] said the increase results when the UV radiation liberates iodine atoms from the surface of the silver iodide, leaving silver atoms behind. Water molecules absorbed on the exposed Ag^{+} enjoy a greater freedom of rotation which appears to be responsible for the initiation of the ice embryo. This process could be responsible for the increased ice-nucleation ability of $Ag^{131}I$. For an extremely radioactive $Ag^{131}I$ the Ag^{+} concentration should increase with time as the iodine decays until the surface eventually becomes nearly completely covered with silver atoms. At this time it should lose its ice-nucleation ability.

RADIONUCLIDE CONCENTRATION MINIMUMS FROM 6 TO 9 km

J. A. Young, W. E. Davis and N. A. Wogman

Radionuclide concentrations measured 1.5 km above a cirrus deck were an order of magnitude lower, and concentrations within the cirrus were an order of magnitude higher than would be expected on the basis of the measured concentrations in the rest of the vertical profile, indicating that cirrus scavenging could be responsible for the downward transport of radioactivity.

Vertical profiles of radionuclide concentrations have been measured from 1.5 to 3 km to over 18 km in air filter samples collected by RB-57 aircraft since 1967 as part of a program to determine the rates of atmospheric mixing and deposition on the

earth's surface. Most of these profiles were measured either near Albuquerque, NM at 35°N, 107°W; south of Spokane, WA at 46°N, 117°W; or near Barbados, British West Indies from 12 to 18°N and 54 to 59°W. The profiles collected near Barbados were taken during the summer of 1969 for the BOMEX project. The most surprising feature of these profiles has been the regular occurrence of concentration minimums between 6 and 9 km. These minimums occurred in about 40% of the samples collected near Albuquerque and Spokane and 50% of those collected near Barbados. The radionuclide concentrations in some of these 3- or 6-km samples were only a few percent of the concentrations at lower or higher altitudes.

Some of the less striking minimums could have been due to the predominantly horizontal advection of air from locations of lower radionuclide concentrations. However, it is unlikely that the horizontal advection of unscavenged air could have caused the concentrations which were more than an order of magnitude lower than the concentrations at higher or lower altitudes, since the horizontal concentration gradients are generally not great enough. It is also unlikely that the transport of high concentration stratospheric air to altitudes below 6 km could have caused apparent minimums at 6 and 9 km, since the concentrations below 6 km were generally normal, and the concentrations at 6 or 9 km were below normal on days that minimums occurred. The back trajectories which have been calculated by W. E. Davis have failed to identify a cause for the minimums.

It appears that precipitation scavenging is the only mechanism that could have caused the very low concentrations measured at 6 and 9 km. The objection to this mechanism, of course, is that the minimums occur at altitudes above normal for non-convective precipitation formation. The northward transport of scavenged air from the towering cumuli of the intertropical convergence zone could possibly have caused the minimums near Barbados, but no such mechanism is available at 35° or 46°N. Deep convective activity is very rare near or west of Spokane.

At present it appears that the most plausible mechanism for the production of the large minimums is the scavenging of the radionuclide-bearing aerosol by cirrus followed by the settling of the ice particles. Cirrus layers are rather extensive and form at altitudes where minimums occur. The ice particles in cirrus clouds are large enough to have appreciable settling velocities. Because IPC filters used for sample collection disintegrate when exposed to liquid water, RB-57 pilots are instructed to fly just above any clouds encountered at planned sample collection altitudes. These flight parameters place the aircraft in the regions scavenged by cirrus.

If cirrus is responsible for the minimums, then cirrus scavenging could be responsible for considerable downward transport of radioactivity. However, it is difficult to estimate the volume of air which

might be scavenged by cirrus, or the distance radioactivity might be transported downward by the ice particles. Samples collected near Barbados at altitudes differing by 600 m at around 9 km often showed the same very low concentrations, while samples collected 3 km above or below sometimes showed some evidence of depressed concentrations. Thus the scavenged layer could be reasonably thick. Samples collected at each of the corners of a 5° latitude and longitude square east of Barbados often showed the same very low concentrations at 9 km, suggesting that scavenged layers could have a very large horizontal extent.

To test the hypothesis that cirrus scavenging is responsible for the minimums and to determine the thickness of the scavenged layer, an RB-57 aircraft was used to collect air samples 3 km, 1.5 km, and 150 m above and below and then at the center of a cirrus deck located at 10 km near Albuquerque, NM on November 30, 1973. The concentrations of the nuclear weapons-produced radionuclides ^{95}Zr-^{95}Nb, ^{103}Ru, ^{106}Ru, ^{137}Cs, ^{140}Ba, and ^{144}Ce 1.5 km above the cirrus were an order of magnitude lower than would be expected on the basis of the concentrations measured in the other samples, and the concentrations at the center of the cirrus were an order of magnitude higher than would be expected. The concentrations 150 m above the center of the cirrus were near normal, probably because the sample was collected partly in and partly out of the cirrus. The radionuclide concentrations in the sample collected 3 km above the cirrus appeared to be about normal. These results strongly indicate that the cirrus was responsible for the scavenging of around 90% of the radionuclides from a layer of air at least 1.2 km thick and possibly less than 2.8 km thick. It is possible that a thicker layer was scavenged but that wind shear resulted in the transport of the scavenged air in this thicker layer to another location.

The concentration of the 15-hr half-life cosmic ray-produced radionuclide ^{24}Na measured 1.5 km above the cirrus was about one-half of the average measured value at that altitude on previous flights. Because of its short half-life, the atmospheric concentrations of ^{24}Na should remain relatively constant in the absence of precipitation scavenging. Therefore, the concentration measured 1.5 km above the cirrus indicates that the air at that altitude had been scavenged around 15 hr earlier, and that the ^{24}Na therefore had had time to reach about 50% of equilibrium. Since the measured concentrations have varied from flight to flight, this calculated time should not be taken as absolute. The ^{24}Na concentration measured at the center of the cirrus was also below normal. This may suggest that the collection efficiency for the aerosol and ice particles was significantly less than 100% within the cirrus. The IPC filters are normally not used on flights within clouds because the filters tend to disintegrate. However, on this flight the filters did not appear to have disintegrated appreciably.

FEASIBILITY STUDY OF THE USE OF INERT TRACERS IN THE NATIONAL HAIL RESEARCH EXPERIMENT

J. A. Young, N. A. Wogman, C. W. Thomas and T. M. Tanner

Six tracers released sequentially into the updrafts of convective storms in northeast Colorado spread extensively through the storm system and were nearly completely scavenged.

Six inert tracers were released sequentially into the updrafts of two convective storms in Northeast Colorado to obtain basic information on processes occurring in the convective storms. The tracers were released into storms being seeded with silver iodide. The concentrations of silver and of the tracers gold, rhenium, and indium have been measured in rain and hail samples collected from these storms.

These measurements indicate that silver and the tracers were almost completely scavenged by the precipitation. These and similar measurements carried out in a separate program in St. Louis also indicate that a tracer added to one location in a squall line will spread throughout the squall line and will spread from cell to cell. The comparison of the concentrations of the tracers with those of silver in the hail indicates that the silver was not scavenged preferentially by the hail, suggesting that the scavenging was primarily by contact or by droplet nucleation. The measurements of the short-lived cosmogenic radionuclides ^{38}Cl and ^{39}Cl in rain samples indicate that the elapsed time between the beginning of droplet or ice crystal nucleation and the arrival of the precipitation at ground level generally averaged 70 min but that there were short periods when elapsed time was much shorter, varying between 6 and 29 min.

This work was previously supported by the National Science Foundation.

REFERENCES

1. W. G. N. Slinn, "In-Cloud Scavenging Studies," Pacific Northwest Laboratory Annual Report for 1972 to the USAEC Division of Biomedical and Environmental Research, Vol. II, Physical Sciences, Part 1, Atmospheric Sciences, BNWL-1751 PT 1, Battelle-Northwest, Richland, WA, April 1973.

2. A. N. Dingle, Rain Scavenging Studies, Progress Report No. 6, Dept. of Meteorology, University of Michigan, Ann Arbor, MI, 1969.

3. R. G. Semonin, Presentation at METROMEX Scientific Workshop, Pierre-Marquette State Park, Garfton, IL, November 5-9, 1973.

4. R. J. Engelmann and W. G. N. Slinn, Precipitation Scavenging (1970), available from NTIS as CONF-700601, p. 409, 1970.

5. F. O. Gladfelder, Field notes, 1972.

6. M. T. Dana, Battelle-Northwest, personal communication to W. E. Davis, Battelle-Northwest, 1973.

7. M. A. Wolf and M. T. Dana, "Experimental Studies in Precipitation Scavenging," Pacific Northwest Laboratory Annual Report for 1968 to the USAEC Division of Biology and Medicine, Vol. II: Physical Sciences, Part 1, Atmospheric Sciences, BNWL-1051, PT 1, Battelle-Northwest, Richland, WA, 1969.

8. R. W. Perkins, C. W. Thomas and J. A. Young, "Application of Short-Lived Cosmogenic Radionuclides as Tracers of In-Cloud Scavenging Processes," J. Geophy. Res., vol. 75, p. 3076, 1970.

9. R. W. Perkins, C. W. Thomas, J. A. Young and B. C. Scott, "In-Cloud Scavenging Analysis from Cosmogenic Radionuclide Measurements," in Precipitation Scavenging (1970), available from NTIS as CONF-700601, pp. 69-95, 1970.

10. W. E. Davis, "A Model for In-Cloud Scavenging of Cosmogenic Radionuclides," J. Geophy. Res., vol. 77, no. 12, pp. 2159-2165, April 1972.

11. W. E. Davis, C. A. Oster, B. C. Scott and J. M. Thorp, "Additional Meteorological Analysis of Shot Smoky, Plumbbob Test Series," Pacific Northwest Laboratory Annual Report for 1967 to the USAEC Division of Biology and Medicine, Volume II: Physical Sciences, Part 3, Atmospheric Sciences, BNWL-715 3, Battelle-Northwest, Richland, WA, October 1968.

12. E. R. Reiter and J. D. Mahlman, "Heavy Iodine-131 Fallout Over the Midwestern United States, May 1962." Progress Report No. 2, September 1965, to USAEC, Further Studies on Radioactive Fallout, Colorado State University, Dept. of Atmospheric Sciences, Tech. Paper No. 70.

13. J. A. Young, Unpublished data, July 1973.

14. J. A. Young, C. W. Thomas, N. A. Wogman and R. W. Perkins, "Cosmogenic Radionuclide Production Rates in the Atmosphere," J. Geophy. Res., vbl. 75, p. 2385, 1970.

15. J. A. Young, N. A. Wogman. C. W. Thomas and T. M. Tanner, Final Report: Feasibility Study of the Use of Inert Tracers in the National Hail Research Experiment to the National Science Foundation, Battelle, Pacific Northwest Laboratory, BNWL-1763, Richland, WA, June 1973.

16. T. F. Hatch, J. Franklin Inst., vol. 215, p. 27, 1933.

17. T. F. Hatch and S. P. Choate, J. Franklin Inst., vol. 207, p. 307, 1929.

18. W. G. N. Slinn, "Numerical Exploration of Washout of Aerosol Particles," Pacific Northwest Laboratory Annual Report for 1970, Volume II: Physical Sciences, Part 1, Atmospheric Sciences, BNWL-1551-1. Battelle-Northwest, Richland, WA, pp. 75-81, June 1971.

19. L. Facy, "Radioactive Precipitation and Fallout," Nuclear Radiations in Geophysics, H. Israel and A. Krebs, eds., Springer-Verlag, Berlin, pp. 202-240, 1962.

20. J. M. Hales, "Fundamentals of the Theory of Gas Scavenging by Rain," Atmos. Environment, vol. 6, pp. 635-659, 1972.

21. W. G. N. Slinn, "The Redistribution of a Gas Plume Caused by Reversible Washout," Atmos. Environment, in press.

22. R. J. Engelmann, "The Calculation of Precipitation Scavenging," Meteorology and Atomic Energy 1968, D. H. Slade, ed., available as TID-24190 from NTIS, Springfield, VA, 1968.

23. M. T. Dana, "Scavenging of Soluble Dye Particles by Rain," Precipitation Scavenging, R. J. Engelmann and W. G. N. Slinn, coords., Proceedings of a Symposium held at Richland, WA, available as CONF-700601 from NTIS, Springfield, VA, 1970.

24. A. G. Zimin, "Mechanisms of Capture and Precipitation of Atmospheric Contaminants by Clouds and Precipitation," Problems of Nuclear Meteorology, I. L. Karol and S. G. Malakhov, eds., available as AEC-tr-6128 from NTIS, Springfield, VA, 1964.

25. A. C. Chamberlain, "Aspects of the Deposition of Radioactive and Other Gases and Particles," Aerodynamic Capture of Particles. E. G. Richardson, ed., Pergamon Press, New York and London, pp. 63-88, 1960.

26. F. Pasquill, Atmospheric Diffusion, D. Van Nostrand, London, 1962.

27. G. A. Sehmel, "Particle Eddy Diffusivities and Deposition Velocities for Isothermal Flow and Smooth Surfaces," Aerosol Science, vol. 4, pp. 125-138, 1973.

28. R. J. Engelmann, R. W. Perkins, D. I. Hagen and W. A. Haller, "Washout Coefficients for Selected Gases and Particulates," Proc. 59th Annual Meeting Air Poll. Control Assoc.: also BNWL-SA-657, Battelle-Northwest, Richland, WA, available from NTIS, Springfield, VA, 1966.

29. M. T. Dana and M. A. Wolf, "Experimental Studies in Precipitation Scavenging," Pacific Northwest Laboratory Annual Report for 1967 to thk USAEC Division of Biology and Medicine. Volume II: Physical Sciences. Part 3, Atmospheric Sciences, BNWL-715 3, available from NTIS. Springfield, VA, 1968.

30. N. F. Islitzer, "Short-range Atmospheric Dispersion Measurements from an Elevated Source," J. Meteor, vol. 18, pp. 443-450, 1961.

31. C. E. Elderkin and W. T. Hinds, "Predictions of Exposures from an Elevated Source," Pacific Northwest Laboratory Annual Report for 1965 to the USAEC Division of Biology and Medicine, Volume I, BNWL-235, Battelle-Northwest, Richland, WA, available from NTIS, Springfield, VA, 1966.

32. M. T. Dana, "Olympic Peninsula Rain: Characterization of Size and Electrical Charge," Pacific Northwest Laboratory Annual Report for 1969 to the USAEC Division of Biology and Medicine, Volume II: Physical Sciences, Part 1, Atmospheric Sciences, BNWL-1307, Battelle-Northwest, Richland, WA, available from NTIS, Springfield, VA, 1970.

33. C. R. McCully, M. Fisher, G. Langer, J. Rosinski, H. Glaess and D. Werle, "Scavenging Action of Rain on Air-borne Particulate Matter," Ind. Eng. Chem., vol. 48, pp. 1512-1516, 1956.

34. F. G. May, "The Washout of Lycopodium Spores by Rain," Q. J. Roy. Met. Soc., vol. 84, pp. 451-458, 1958.

35. A. K. Postma, L. F. Coleman and R. K. Hilliard, Iodine Removal from Containment Atmospheres by Boric Acid Sprays, BNP-100, Battelle-Northwest, Richland, WA, 1970.

36. R. J. Engelmann, "Precipitation Scavenging Studies," Hanford Radiological Sciences Research and Development Annual Report for 1964, BNWL-36, Battelle-Northwest, Richland, WA, 1963.

37. V. Griffiths, "Use of Sprays as a Safeguard in Reactor Containment structures," Nuclear Safety, vol. 6 (2) Sec. IV, p. 186, 1964-1965.

38. H. R. Diffey, C. H. Rumary, M. J. S. Smith and R. A. Stinchcombe, Iodine Clean-up in a Stream Suppression System, AERE-R-4882, 1965.

39. W. G. N. Slinn, "Multiple Transforms for Mathematical Physics Courses," Amer. J. Physics, vol. 24, pp. 93-97, 1966.

40. M. T. Dana, J. M. Hales and J. M. Thorp, "Precipitation Scavenging of Inorganic Pollutants from Metropolitan Sources," Pacific Northwest Annual Report for 1972 to the USAEC Division of Biomedical and Environmental Research, Volume II: Physical Sciences, Part 1, Atmospheric Sciences, BNWL-1751-1, Battelle Pacific Northwest Laboratory, Richland, WA, pp. 93-97, April 1973.

41. M. T. Dana, J. M. Hales, C. E. Hane and J. M. Thorp, Precipitation Scavenging of Inorganic Pollutants from Metropolitan Sources, Final Report to Division of Meteorology, Environmental Protection Agency, BNW-389, Battelle Pacific Northwest Laboratory, Richland, WA, 1974.

42. J. S. Marshall and W. McK. Palmer, "The Distribution of Raindrops with Size," J. Meteor., vol. 5, pp. 165-166, 1948.

43. C. E. Hane, "Squall Line Structure and Maintenance," Florida State University, Dept. of Meteorology Report No. 72-5, p. 190, 1972.

44. C. E. Hane, "The Squall Line Thunderstorm: Numerical Experimentation," J. Atmos. Sci., vol. 30, pp. 1672-1690, 1973.

45. V. G. Morachevsky, "Activity of AgI Particles as Ice-forming Nuclei," Iz. Atmos. Oceanic Phy., vol. 3, pp. 105-107, 1967.

46. G. W. Bryant and B. J. Mason, "Photolytic De-activation of Silver Iodide as an Ice-Forming Nucleus," Q. J. Rog. Meteor. Soc., vol. 86, pp. 354-357, 1960.

47. S. C. Rowland, R. G. Layton and D. R. Smith, "Photolytic Activation of Silver Iodides in the Nucleation of Ice," J. Atmos. Science, vol. 21, pp. 698-710.

48. N. Fukuta and Y. Paik, "Water Adsorption and Ice Nucleation on Silver Iodide Surfaces." J. Appl. Physics, vol. 44, pp. 1092-1100, 1973.

REMOVAL AND RESUSPENSION PROCESSES

DRY DEPOSITION OF PARTICLES

An important mechanism by which an atmosphere is depleted of particulate material is by gravity settling and by turbulent eddy diffusion processes. Historically research at Battelle-Northwest has been directed to deposition studies with monodisperse particles, first in tubes transporting particles, then in wind tunnel studies. Some field studies were undertaken much earlier to determine by mass balance the depletion of particles from a plume.

Our recent work in the wind tunnel has shown the relationship of deposition velocity to particle size, average velocity, friction velocity, and the unique characteristics of surfaces. Models have been developed which take into account these variables, and a large body of data has been made available. Wind tunnel studies are to be implemented with field studies using well characterized aerosols. The studies in 1973 were concerned with deposition to crushed rock surfaces, shallow water, and vegetation canopies. Ongoing field studies have utilized comparisons of depositing with nondepositing tracers for evaluating deposition. This technique, as well as direct turbulent flux measurements of pollutants, should provide expanded capability for future investigation of deposition over larger regions and onto varied surfaces of wider range of interest.

- RADIOISOTOPES AS PARTICLES AND VOLATILES
- RADIOACTIVE FALLOUT RATES AND MECHANISMS
- ATMOSPHERIC DIFFUSION, DEPOSITION AND TRANSPORT PHENOMENA
- COOLING TOWER AND COOLING POND ATMOSPHERIC IMPACT
- AEC DIVISION OF LICENSING
- BATTELLE MEMORIAL INSTITUTE PHYSICAL SCIENCES PROGRAM

DRY DEPOSITION OF PARTICLES

G. A. Sehmel, W. H. Hodgson and S. L. Sutter

Deposition velocities for monodispersed particles were measured for deposition onto surfaces of both ~1.6 and ~3.8 cm diam crushed gravel. Deposition velocities are greater for the larger gravel. For the larger gravel about 20% of the deposited particles were found below the top layer of gravel, suggesting that particle deposition may be enhanced in thick, coarse beds.

INTRODUCTION

Dry deposition of airborne pollutant particles is one means by which pollutants are removed from the atmosphere. Removal fluxes are dependent upon airborne concentration, particle diameter, deposition surface, and meteorological conditions. Airborne concentrations and surface removal rates must be known to determine if airborne pollutants will exceed ecologically acceptable limits

Dry deposition rates in the environment were characterized initially by Chamberlain[1,2] in terms of a deposition velocity, v_d, equal to

$$v_d = \frac{N}{\chi} = \frac{\text{amount deposited/cm}^2\text{ of surface sec}}{\text{airborne particle concentration above the surface/cm}^3}. \quad (1)$$

The units of v_d are length/time, usually reported as cm/sec. In environmental field experiments, the concentration, χ, has been measured at various heights above the deposition surface. Usually heights are on the order of 1 m. The term, v_d, is an overall mass transfer coefficient which includes effects of both surface resistance in the lower 1 cm adjacent to the deposition surface as well as transport resistance from the concentration measurement height to 1 cm. In these field experiments, deposition velocities, v_d, were evaluated using particles with wide size distributions. Since deposition velocities are known to depend upon

particle diameter, quantities v_d describe deposition rates only for particle size distributions used in the determination of v_d.

Deposition velocities, K, evaluated by Sehmel,[3-6] describe transfer rates of single size particles and include only surface resistance to mass transfer. The deposition velocity, K, is defined as

$$K = \frac{N}{C} = \frac{\text{amount deposited/cm}^2\text{ of surface/sec}}{\text{airborne particle concentration above the surface/cm}^3}. \quad (2)$$

In this case, the concentration, C, for the monodispersed particles is measured 1 cm above the deposition surface.

THEORY

Deposition velocities, K_z, for any desired reference height, z, can be calculated from K for establishment of the airborne concentration to use in conjunction with standard meteorological diffusion equations. The calculation will be specifically illustrated by using the three-box conceptual model[6] describing the overall deposition process. In each box particle transport is described by:

Box 1--The atmospheric turbulent layer in which the transfer processes are best described by micrometeorological eddy diffusivity.

Box 2--A layer just above and just within the vegetative canopy or surface elements in which the transfer processes are modified by the presence or structure of the canopy or surface.

Box 3--A layer (occupied by the canopy or surface elements) in which the final transfer process is best expressed by surface mass transfer coefficients, where the interaction between the surface material and the pollutant is important

Our research has been mainly directed toward determining the mass transfer resistance at the deposition surface in Box 3. Indeed, we have reported our measured deposition velocities as K_1 in which the subscript one refers to the particle concentration at 1 cm from the deposition surface.

The general equations will be set up for calculating the relative mass transfer resistance in each box and for calculating K_z from K_1. Particle deposition will be described by a one-dimensional, steady-state continuity equation for the deposition flux. Basic assumptions in this model are that particles are diffusing at a constant flux from a uniform concentration of particles, that a relationship for eddy diffusivity can be determined, that the effect of gravity can be described by the

terminal settling velocity, that particle agglomeration does not occur, and that particles are completely retained by the surface. Based upon these assumptions, the deposition flux to a surface can be described by[5]

$$N = -(\varepsilon + D)\frac{dC}{dz} - v_t C, \quad (3)$$

in which v_t is the absolute value of the terminal settling velocity.

The deposition velocity is predicted from a dimensionless integral form of Equation (3),

$$-\int_{C_z}^{\circ} \frac{u_* \, dC}{N + v_t C} = \int_{z^+}^{r^+} \frac{dz^+}{\varepsilon/\nu + D/\nu \text{ at } C_z} \quad (4)$$

in which ε is the particle diffusivity, D is the Brownian diffusivity, ν is the kinematic viscosity of air, u_* is the friction velocity, $z^+ = zu_*/\nu$ is the dimensionless distance above the surface, and v_t is the terminal settling velocity. Integration limits are that particle concentration is a constant C_z at a reference height of z cm and above and that particle concentration is zero at a dimensionless particle radius, r^+, from the deposition surface. The right-hand side of this equation contains the dimensionless eddy diffusivity, ε/ν, and hence quantifies mass transfer resistance as a function of elevation. This resistance integral will be abbreviated by Int. After integration, Equation (4) reduces to the flux

$$N = \frac{v_t \, C_1 \, \alpha}{1 - \alpha} \quad (5)$$

in which

$$\alpha = \exp(-v_t \, \text{Int}/u_*). \quad (6)$$

Now the deposition velocity is defined in terms of the reference concentration, C_z, at z cm height,

$$K_z = \frac{(-N)}{C_z}. \quad (7)$$

Thus, the deposition velocity at height z is

$$K_z = \frac{v_t}{1 - (1/\alpha)}. \quad (8)$$

As shown by this equation, the lower limit of predicted deposition velocities is v_t. The reason for this limit is that if the diffusional resistance were large (Int is a negative number), a would approach infinity and l/a would approach zero. However, as diffusional resistance became relatively less, the deposition velocity would become increasingly greater than the gravitational settling velocity.

The deposition velocity, K, is defined in Equation (2) as the deposition flux, N, divided by the particle concentration, C, at a reference height. Thus, K_z at any height can be calculated[7] from K_1 by the relationship

$$\frac{K_z}{K_1} = \frac{N/C_z}{N/C_1} = \frac{C_1}{C_z}, \quad (9)$$

where N is constant. Substituting Equation (8) in Equation (9) and rearranging yields

$$\frac{C_1}{C_z} = \left(\frac{\alpha_z}{\alpha_1}\right)\left(\frac{1 - \alpha_1}{1 - \alpha_z}\right) \quad (10)$$

where subscript α_1 refers to a 1-cm reference height. Values of the

turbulent diffusivity to be used in calculating[5] α's from Equation (6) can be obtained (assuming equality of particle and momentum turbulent diffusivity) from a generalized correlation(*) for momentum transport as a function of thermal stability.

MASS TRANSFER RESISTANCE

The relative resistance to particle mass transfer in each box of the three-box model can be calculated if K_1 is known and the flux N is constant. The surface resistance, Int_3, in box three is from Equation (6),

$$Int_3 = - \frac{u_* \ln \alpha_1}{v_t} \qquad (11)$$

where from Equation (8)

$$\alpha_1 = \frac{K_1}{K_1 - v_t} . \qquad (12)$$

Integral resistances Int_2 in Box 2 and Int_1 in Box 1 are calculated directly from Equation (4). Thus,

$$Int_2 = \int_{z^+_{2-3}}^{z^+ \text{ at } 1 \text{ cm}} \frac{d_{z^+}}{\varepsilon/\nu + D/\nu} \qquad (13)$$

where the distance z^+_{2-3} is the height selected for interfacing between Box 2 and Box 3. Similarly,

$$Int_1 = \int_{z^+ \text{ at } z}^{z^+_{2-3}} \frac{d_{z^+}}{\varepsilon/\nu + D/\nu} \qquad (14)$$

where z is the height at which concentration boundary conditions are to be matched with airborne concentrations predicted from meteorological diffusion and transport equations.

This three-box model can be used to predict particle removal rates by combining the three integral resistances Int from Equation (11), (13), and (14). A relatively large data base exists in the meteorological literature for calculating the diffusional resistances in Box 1 and Box 2. The real unknown is the surface resistance in Box 3. Surface resistance is being experimentally evaluated in a wind tunnel in terms of the deposition velocity, K_1.

EXPERIMENT

Experimental techniques used for measuring particle deposition in a wind tunnel, shown schematically in Figure 1, consist essentially of measuring both the particle deposition flux and the airborne particle concentration at the test section. The particles are introduced into the wind tunnel in a manner to have a nearly constant airborne particle concentration from about 1 to several cm adjacent to the deposition test surface. In this manner, the model assumption was satisfied that diffusion occurred from a uniform source of particles.

The wind tunnel is a single-pass system contained in a large air-conditioned room. Air enters the wind tunnel through a 1.8 × 1.8-m bank of high-efficiency filters. Downstream of these filters is a 1.8-m long chamber within which the particles are introduced near the floor surface. Next the tunnel dimensions are reduced to a 60 × 60-cm cross-section in a 61-cm long converging section. The working section

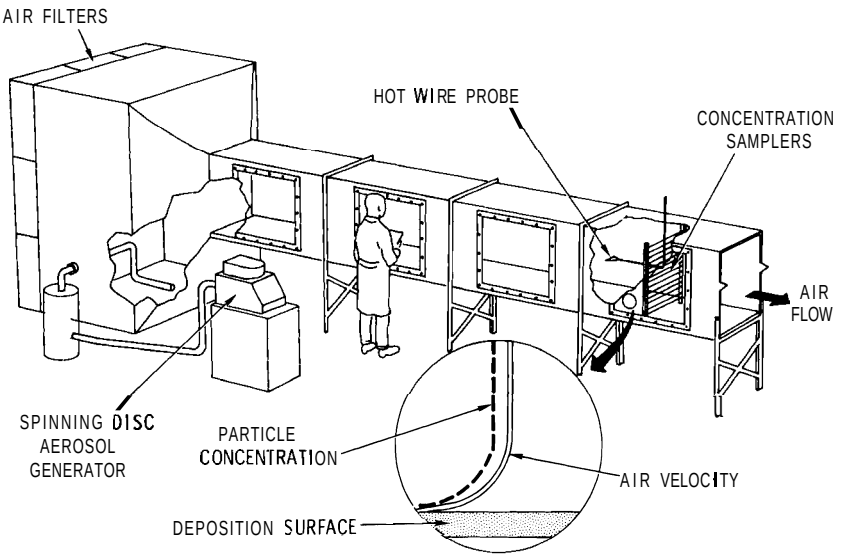

Neg 734648-2

FIGURE 1. Wind Tunnel for Particle Deposition Studies

is a 9.1-m length of the 60 × 60-cm cross-section with the test section at the 6.1-m length. Air is pulled through the wind tunnel, and air leaving the blower is passed through high-efficiency filters and exhausted into the room. The air and wind tunnel are essentially isothermal.

RESULTS AND DISCUSSION

Particle deposition velocities are being determined as a function of surface roughness, particle diameter, and air friction velocity. Different crushed gravels are currently used in the wind tunnel to simulate surface roughness changes in anticipation that generalized deposition velocity correlations can be determined.

Deposition velocities were extended[6] for a large particle size range of monodispersed particles onto clear chip gravel placed in a uniform layer on the wind tunnel floor. The gravel was minus 1.6 cm (5/8 inch) in diameter as received, and in subsequent sieving all gravel less than 0.47 cm was removed. The deposition velocities are shown in Figure 2 as open symbols for friction velocities of 22 and 133 cm/sec. Flagged symbols show deposition when gravel was wet and water was evaporating.

Air flow over gravel was described by the equation

$$u = \frac{u_*}{k} \ln \left[\frac{(z + S) + z_o}{z_o} \right] \qquad (15)$$

where k is von Kármán's constant equal to 0.4, z is the height above a flat surface laid across the gravel surface, z_o is the roughness height, and S is a sub-layer distance. Since the air flows through the gravel, S was required to establish a log profile.

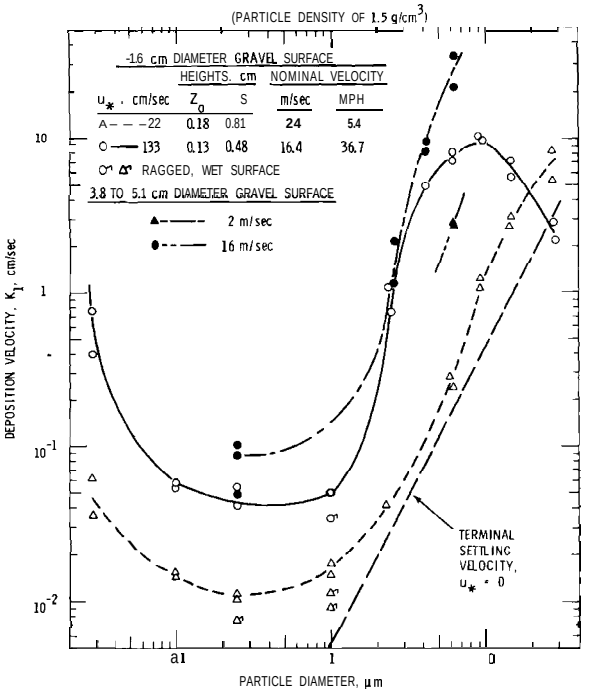

Neg 740044-5

FIGURE 2. Deposition Velocities to Crushed Gravel Surfaces

Deposition velocities are being similarly determined for a 3.8 to 5.1-cm sieved railroad rock or crushed gravel, which is the most geometrically nonuniform surface studied to date. Friction velocities are yet to be determined for this surface. Data for this surface are shown as the solid symbols.

From an inspection of these deposition velocity curves we reached the following conclusions:

1. Minimum deposition velocities occur at a particle diameter from 0.1 to 0.5 µm even when surface roughness is increased.
2. When surface roughness is increased, deposition velocities significantly increase. This increase is especially apparent for 6-µm particles.
3. For the 0.47 to 1.6-cm gravel and a 22 cm/sec friction velocity, particle re-entrainment occurs for particles greater than 9 µm. Net deposition velocities for 28-µm particles are less than for 9-µm particles.
4. Water evaporation decreases the deposition velocity for the three combinations of particle diameter and friction velocity investigated. These results are confirmed by water deposition experiments.(9)

The location of particle deposition in the gravel is being determined for the 3.8 to 5.1-cm gravel of 5-cm average depth. Approximately 20% of the particles penetrate the 5-cm depth and deposit on the surface upon which the gravel is placed.

FIELD TEST

Experiments in the wind tunnel are determining if electrical charges on particles will significantly alter deposition velocities in the minimum deposition velocity diameter range. Based on the results of these wind tunnel measurements, we will conduct field deposition experiments using particles produced in an array of nebulizers. Particles produced in nebulizers should have nonequilibrium electrical charges. Effects on deposition of these charges are being determined in the wind tunnel. Deposition velocities are being determined, both with normal operation and without the Krypton-85 source in the Collison particle generator which brings particles to charge equilibrium.

DRY DEPOSITION PROCESSES ON VEGETATION CANOPIES

J. G. Droppo

A brief review of forestry and agricultural literature relating to processes of dry deposition on plant canopies is presented. The results are summarized in terms of development of a model for dry deposition processes in a vegetation canopy. Various aspects of the processes in both high and low vegetation are discussed.

INTRODUCTION

The objective of this research is to develop a model for dry deposition processes within vegetation canopies. A large percentage of the United States is covered by some vegetation cover such as grass, crops, bushes or forests. Nuclear facilities, including electricity generating stations, are often located at sites surrounded by vegetation. Assessment of routine or accidental release dosage requires an estimate of the deposition rate onto the natural surfaces surrounding any nuclear facility. Though deposition processes deplete the air concentrations, they may lead into additional biological pathways at the earth's surface. This is particularly true if the deposition occurs on a plant which is a significant part of a food chain.

The current phase of this research was to obtain an understanding of how plant variables influence the rate of deposition for particular substances. Emphasis has been placed on processes in higher plant canopies such as forests. Dry deposition data are available for a number of lower vegetation surfaces such as grasses, but little is known about processes in higher canopies such as forests.

The term "plant surface" has been adopted for use in place of "leaf surface" when referring to deposition. The leaf surface in a plant canopy does in fact compose a large percentage of the total surface available for deposition under full foliation. However, plants do have other surfaces which can have quite different properties than do leaf surfaces. In addition, a large portion of the United States is covered by deciduous forests and other vegetation which lose their foliage once a year. In deciduous forests the plant and atmospheric processes are so different between winter and summer that they must be considered separately in terms of plant effects on deposition processes. A deposition velocity which refers to fully foliaged forests cannot be used for the winter months in a deciduous forest. Similarly, deposition on other plant canopies can be expected to be a function of their stage of growing as the plant surfaces increase and the roughness of the canopy changes.

Literature is currently being surveyed to give more insight into these processes. The present results are not to be considered definitive, but rather only a current summary. The following describes our model in its present qualitative stage.

MODEL

The overall process of dry deposition over a canopy has been divided into three regimes: (1) air layer over the canopy, (2) air-vegetation layer within the canopy, and (3) the surface layers over the individual plant elements.[6,10] A fourth regime may be considered as occurring inside the plant elements. The latter are internal processes limiting the assimilation rate of certain materials into the plant such as suggested by Bennett et al.[11]

This division was adopted as a useful concept for separating the processes by the location in which they occur. The travel of any material from the atmosphere above the canopy, into the canopy and onto a plant surface is a continuous path. The steps only represent regimes of processes that a material will pass through during deposition. Within each regime there may well be multiple processes that may be variously limiting. The characteristics of the depositing material can be expected to strongly determine what processes in each regime are important, but they are not in the scope of this report.

The concept of each regime having a resistance to flow of material is useful. A total resistance of the entire atmosphere and canopy may be defined as the sum of the resistances of the individual regimes. The functional relationship for a given site would be:

$$r(z,t) = r_1(z,t) + r_2(z,t) + r_3(z,t) \quad (1)$$

where r is the total resistance, r_1 resistance in the first regime, r_2 resistance in the second regime, r_3 resistance in the third regime, z height, and t time. The assumption is made that atmospheric and canopy characteristics can be expressed as functions of height and time.

A number of plant characteristics and processes have been identified that are tentatively considered as model input variables.

1. Physical Characteristics
   - canopy height
   - density of foliage
   - canopy roughness
   - leaf area index
2. Physiological Characteristics
   - stomata openings
   - surface characteristics
3. Concurrent Fluxes
   - momentum
   - latent heat
   - sensible heat

There are two facets to the input of physical characteristics. First, the canopy will have an effect on the wind profile and the turbulence in the wind. This will affect processes in the first two regimes. The wind profile under near neutral conditions over a vegetative canopy

may be fitted to a log-wind profile of the form:

$$\bar{u}(z) = \frac{u_*}{K} \ln \frac{z-d}{z_o} \qquad (2)$$

where $\bar{u}$ is the mean wind speed, u_* the friction velocity, z height, d zero plane displacement thickness, z_o roughness length, and K the Kármán constant. The top of zero plane displacement thickness is the height at which the mean wind speed would approach zero in the canopy, based on wind measurements just over the canopy. The zero displacement height and roughness length of a canopy as determined by log-wind profiles extending into the upper canopy are logical input variables. These may be expected to vary with actual canopy height and density both between different stands and in the same stand under differing prevailing conditions and stages of foliation. The displacement height is currently being used as the definition of the boundary between the first two regimes. Most of the foliage above this layer will experience very little if any resistance of regime 2. Deposition processes will go directly into regime 3, i.e., the second term on the right of Equation (1) would be zero. This would be equivalent to the two-regime model assumed by Elderkin et al. in this volume.[12] The second resistance term can be expected to progressively increase going down into the canopy. A large increase in this resistance is expected in the lower canopy of a forest during full foliation with strong insolation occurring. The last term in Equation (1) can be expected to vary as a function of height both as the total plant surface changes with height and also as the characteristics of plant surface change. Second, the plant surface available for deposition will affect the deposition rate. This relates to the third regime. For grass it has been found that as the leaf surface area per unit horizontal area increases, the deposition rate increases.[13] This process may be expected to reach an upper limit where increases in leaf area and canopy height will not significantly increase the deposition rate. The grass surfaces studied by Markee apparently had not reached this limit.

In a well developed forest canopy the wind profile drops off to a fairly low value within the canopy and then is more or less constant down to the forest floor, where it drops to zero. The transport by the wind can be expected to roughly follow the wind profile. The profile of leaves is determined mainly by the availability of solar radiation and has little direct relationship to the wind profile. Total resistance for deposition can be expected to vary with the exposure of plant surfaces in the wind profile.

Papers and reports on turbulence characteristics of forests have been reviewed. The available literature has included both dynamic and physical models. These have pointed out that turbulence characteristics of a canopy are dependent on the height and density of the canopy. The deposition process will change as a function of these turbulence changes.

For example, if the profiles of mass flux to surfaces are assumed to follow profiles of momentum flux, considerable information may be obtained from available literature. The process of mass transport downward in regimes 1 and 2 can be expected to have similar processes as momentum transport. The eddy diffusivities defined in Fickian diffusion equations for water vapor and sensible heat transport have been reported to be nearly equal with the eddy diffusivities for momentum transport although there seems to be a dependence on stability. The basis for the divergence is felt to be the bias in convective energies at plant surfaces where the sources of sensible heat and water vapor (latent heat) occur. Hence the relationship may be closer for transport of other materials onto the surfaces since the source of the mass is in the atmosphere, not the plant surfaces.

Profiles of momentum flux suggest that penetration may be relatively deeper into low, dense vegetation covers such as grass than in high, less dense covers such as crops and forests. The implication is that the deposition profile would be uniform on low vegetation covers as compared to high covers. On high covers most of the implied deposition would be on the upper layers of plants. However, the total flux should be considerably greater for the higher covers. For example, momentum fluxes over short grass and a tall crop with 3 m/sec wind speed at 4 m, has been reported to be an order of magnitude greater over the tall crop.[14] The implication is that the deposition rate is an order of magnitude greater, although surface properties may modify this increase.

Studies of pollen deposition on the leading edge of a forest stand have shown that the initial deposition on the edge is quite great and that additional deposition occurs at a slower rate inside the stand.[15]

If a material does penetrate beneath a forest canopy, the direction of transport can be expected to be highly variable. Hanna[16] has estimated that for distances of greater than 100 m from the source shear diffusion dominates lateral turbulent diffusion under a forest canopy.

Electrostatic effects would be important only in regime 3. However, according to wind tunnel results of Langer,[17] electrostatic effects were of no significance in the deposition of dust particles of between 1.9 and 2.4 μm surface diameter on individual leaves of coniferous trees. Inertial deposition was found to be the controlling parameter. The collection efficiency of a cedar leaf for 2.4-μm surface diameter dust was found to be 6 and 0.5% for the edge and broadside positions. Wake capture in the turbulence on the back of the leaves was not observed. The shadowing effect of leaves on other leaves was also demonstrated. Aylor[18] has observed that the trapping efficiencies of regional pollen by corn foliage was between 3 and 7%. As more such results become available they will be

incorporated into the model under development.

The physiological characteristics relate to the third and fourth regimes. Numerous studies have been performed on stomata1 resistances, and these are being considered in the deposition model.

The concurrent fluxes can be expected to affect the deposition rate. The deposition rate is often assumed to occur at the same rate as allowed by the momentum flux to the surface. This assumption is likely best in the first regime. Latent heat fluxes and sensible heat fluxes may be related to diffusiophoresis and thermophoresis effects. Although these processes have generally been considered of secondary importance, according to our estimates the greater adsorption of solar energy (lower albedo) resulting in increased latent and sensible heat fluxes can lead to fluxes which can significantly affect deposition rates. In the daytime in foliated forest canopies, the latent heat flux is often considerably larger than the sensible heat flux and represents a counter mass flux to deposition processes. Despite high resistances per unit surface plant area, the total deposition in a plant canopy can be greater than on other surfaces because of greater total area. Such an effect was noted in a field study, where the collection efficiency of grass was less per unit plant surface area than a ground surface, but the overall deposition rate was greater.[13]

The assumption may be made that the resistances determined for water vapor transport in vegetation canopies will also apply to the flux of materials being deposited on the vegetation. This can be expected to be best for regimes 1 and 2 and not necessarily valid for regime 3. Interaction between the surface and the particle depends on the chemical and physical nature of both, and physiological processes within the plant may differ for different substances.

The bulk aerodynamic resistance to water vapor transport from a pine forest has been reported to be between 0.05 and 0.10 sec/cm, which corresponds to velocities of deposition of between 10 and 20 cm/sec.[19] The bulk physiological resistance of the forest exhibited a diurnal trend, from 1.2 sec/cm in the morning to 4 sec/cm by late afternoon. These results may be applied to the deposition on forests only with certain reservations.

1. The depositing substance may not have the same physical or chemical characteristics as water vapor.
2. The source and sink profile relationship will not be identical between water vapor and the depositing substance as a result of the opposite directions of the fluxes. In addition these relationships may be modified by interactions between the fluxes.

These resistances are in general agreement with other estimates of resistances in forests.[20]

SUMMARY

The processes of deposition on high canopies cannot be expected to be the same as on low canopies. The deposition in a canopy will be dependent on the physical characteristics of the canopy. The amount of penetration of material, and hence deposition, into the lower regions of the low canopies can be expected greater than for higher, less dense canopies. The significant portion of material is expected to be deposited onto the upper portions of higher vegetation canopies. A model is being developed that includes results of diffusion, wind profiles, energy budget, and physiological research relating to vegetation canopies.

SUGGESTED FUTURE RESEARCH

Studies of the turbulence within various canopies would provide a better estimate of the resistance in regime 2. A number of recent researchers have provided this information for several canopies. These results should be organized in terms of prevailing canopy and atmospheric conditions.

A predictive model for dry deposition should be developed. Current canopy turbulence information should be used in this model. A deposition model for canopies should take into account the physical characteristics of the canopy. The model should be used to learn how and where dry deposition occurs in various canopies and to ascertain the sensitivity to various input variables.

The above research would identify needed field research. The present recommendations for a field research project are that the profile of deposition be studied as well as the total deposition and that a careful record be kept of a number of canopy and atmospheric conditions.

ELEMENTAL CONTENT OF TRACE ELEMENTS IN VEGETATION COLLECTED AT CENTRALIA, WASHINGTON

L. A. Rancitelli, K. H. Abel and W. C. Weimer

Samples of vegetation collected around the Centralia coal-fired electric plant contained concentrations of As, Hg, Sb, and Se that were up to an order of magnitude higher than the concentrations measured in Alaskan vegetation samples.

Large quantities of trace elements are known to emanate as a result of the fossil fuel consumption by power plants. Although the effects of these trace elements on atmospheric quality have been characterized to some degree, their impact on the biosphere is still unknown. The impact of fossil fuel power plants on the local environment can be assessed by measuring daily air concentrations of the noxious trace elements along with SO_2 and NO_2.

However, the long-term effects on the environment are not readily extrapolated from air concentrations. It is necessary to measure the deposition rates on local vegetation. In an attempt to assess the impact of the 1400-MW Centralia power plant on the local biosphere, a sampling network of vegetation has been established around the power plant. Vegetation samples which include annuals such as grasses, leaves from deciduous trees, conifer needles, lichens and mosses have been collected for trace element analysis. The grasses were selected since they should reflect recent deposition and uptake, while mosses and lichens, with their unique dependence on atmospheric deposition of nutrients, should supply information on long-term effects of the power plant to local environs.

Twenty-eight major, minor and trace elements were measured in these vegetation samples by instrumental neutron activation analysis. The results of the analyses of vegetation samples are presented in Table 1 with a comparison of lichen samples collected from a remote region in Alaska. A comparison of the concentrations for the volatile elements As, Hg, Sb, and Se in lichens shows that concentrations in samples taken near Centralia, Washington are elevated up to an order of magnitude relative to the Alaskan samples. The highest increment occurred for As, which reached 7 parts per million in the Centralia lichen and moss. The concentrations of the other 24 elements do not appear to reflect increased values around Centralia. While it is not possible at present to ascribe the elevated concentrations of As, Hg, Sb and Se to the operations at Centralia only, implications are that monitoring of plant materials should provide an excellent indicator of the impact of power plants on local vegetation once a proper local baseline of elemental concentrations has been established.

TABLE 1. Elemental Content in Plants from Centralia, Washington (μg/g Dry Basis)

Elements	Pasture Grass	Tree Leaves	Moss	Lichen	Alaskan Lichen
Ag	<0.03	0.011	0.032	0.046	0.13
As	0.14	0.93	7.0	7.2	0.82
Au	<0.04	<0.01	<0.02	<0.03	<0.02
Ba	25	81	20	60	66
Br	32	4.5	14	30	4.2
Cd	<3	<1	<1	<2	<1
Co	0.062	0.23	0.45	1.3	0.75
Cr	1.8	2.2	1.7	5.1	5.3
Cs	0.12	0.15	0.089	0.30	0.24
Eu	0.0061	0.030	0.049	0.13	0.05
Fe	120	340	1,100	3,000	2,100
Hf	0.011	0.061	0.22	0.53	0.19
Hg	<0.02	0.055	0.17	0.12	0.049
K	15,000	10,400	2,400	3,800	2,400
La	<0.1	0.72	1.1	2.5	1.3
Na	3,600	220	720	1,400	812
Ni	3.2	3.3	<2	7.9	<2
Rb	75	27	9.2	19	9.0
Sb	0.025	0.11	0.78	0.99	0.060
Sc	0.039	0.13	0.49	1.2	0.79
Se	<0.06	0.077	0.49	0.60	0.16
Sm	0.025	0.086	0.18	0.47	0.25
Sn	<3	<4	<4	<6	<3
Sr	56	230	33	78	28
Ta	<0.005	0.028	0.084	0.20	0.085
Tb	<0.004	0.020	0.032	0.084	0.039
Th	<0.01	0.074	0.20	0.53	0.38
Zn	33	31	37	70	36

PARTICLE DEPOSITION RATES ON A WATER SURFACE AS A FUNCTION OF PARTICLE DIAMETER AND AIR VELOCITY

G. A. Sehmel and S. L. Sutter

Deposition rates of airborne monodispersed particles onto a water surface were determined in a wind tunnel. Average air velocities over water were 2.2, 7.2, 13.8 m/sec, and particle diameters were from 0.3 to 28 μm. For particles greater than 1 μm, deposition rates increased with both particle diameter and wind speed. For particles less than 1 μm diam, phoretic forces are comparable to transport forces from eddy diffusion and Brownian diffusion. Minimum deposition velocities are approximately 1 × 10^{-2} cm/sec. Maximum deposition velocity was 37 cm/sec, the largest ever reported for any surface.

INTRODUCTION

Dry deposition of airborne pollutant particles onto water surfaces is one means by which pollutants are removed from the atmosphere. Since approximately two-thirds of the earth's surface is covered with water, the dry deposition rates of particles onto water should be known if the true pollutant removal capacity from air to water is ever to be established. In discussing pollutant removal rates at the air-sea interface, dry deposition rates include all mechanisms for particle removal not attributed to precipitation. These mechanisms include eddy diffusion, gravitational settling, inertial effects attributable to air eddy size and particle relaxation time, impaction, interception, electrostatic effects, wave spray collection, diffusiophoresis and thermophoresis.

The deposition velocity, K, describes transfer rates of single sized particles and includes only surface resistance to mass transfer. The deposition velocity; K, is defined as

$$K = \frac{N}{C} = \frac{\text{amount deposited/cm}^2 \text{ of surface/sec}}{\text{airborne particle concentration above the surface/cm}^3} \qquad (1)$$

The concentration, C, for the monodispersed particles is measured about 1 cm above the deposition surface.

One would expect for water surfaces a deposition velocity dependence on particle diameter and wind velocity. Some particle size dependency was observed in a wind tunnel by Moller and Schumann,[21] but no wind velocity dependence was observed. They showed that deposition velocities, K, were from 0.01 to

0.04 cm/sec for particle diameters ranging from 0.03 to 1 μm. No data were reported for larger sized particles.

Particle deposition mechanisms onto an ocean surface are complex since the water surface is usually covered with a monolayer film or multilayer film composed of fatty acids or glycoproteins. These films could alter mass transfer rates at the surface. Baier and Goupil[22] report films are usually 100 to 200 Å thick, and are up to 4000 Å in more polluted regions. Films (Szekielda)[23] may consist of about 80% inorganic material and 20% organic. Deposited particles may preferentially collect in sea foam. Film resistance can be altered by microorganisms since Twitchell[24] reports surface films are mechanically agitated with flagella (dunaliella tertioleda), which increase evaporation rates.

The purpose of this study is to determine from water wind tunnel studies the deposition velocities, K, as a function of monodispersed particle diameters from 0.3 to 28 μm and wind speeds from 2 to 14 m/sec. In the determination surface films have been ignored since distilled water was used as the deposition surface. Nevertheless, these data are the first reported for deposition of monodispersed 1 to 28-pm diam particles onto a water surface.

EXPERIMENT

Particle deposition velocities, K, for water surfaces were determined(**) using monodispersed uranine particles and distilled water on the floor of a wind tunnel. Water was contained within the wind tunnel by placing a plastic sheet (leak proof surface) across the wind tunnel floor and up the sides and over two dams placed at the inlet and outlet of the test section. The test section was 9.1 m long by 60 cm wide. The initial water depth for each run was held constant at approximately 2.2 cm. For deposition determinations, particles were generated, airborne concentrations measured and deposition fluxes measured for each experiment. Air velocity, friction velocity, wave length, wave height, and wet and dry bulb temperatures were measured in selected runs.

RESULTS AND DISCUSSION

Particle size as reported is the size of particles entering the wind tunnel. However, because uranine particles are hygroscopic, the possibility exists that particle sizes may have been enhanced by sorbed moisture just before final deposition into the water. This sorption was not believed a serious problem. Nevertheless, future research should consider using the ammonium salt of fluorescein rather than uranine (the sodium salt). The ammonium salt has a very low water solubility (Stöber).[26]

Wave Description

Water wave characteristics for the three wind speeds used were a function of wind speed. These wave

lengths and heights are summarized in Table 2. For the lowest wind speed of 2.2 m/sec, neither wave length nor wave height could be characterized by the still photographic technique used. For higher wind speeds of 7.2 and 13.8 m/sec, both wave height and wave length increased with increased wind speed. The maxima observed were 2.5 and 24 cm respectively.

Table 2. Wave Description

Air Velocity m/sec	Wave Length cm	Wave Height cm
2.2	Small	Small
7.2	10 to 15	1.0 to 1.6
13.8	10 to 24	1.3 to 2.5

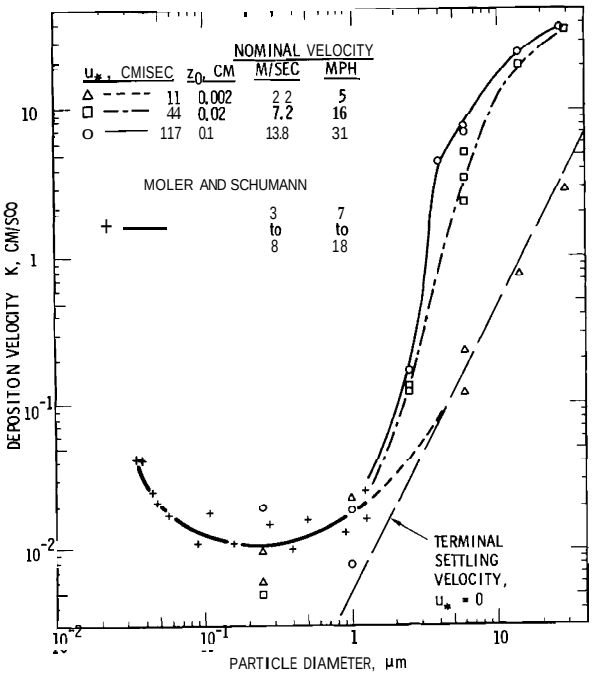

Neg 736356-1

FIGURE 3. Deposition Velocities to a Water Surface (Particle Density of 1.5 g/cm^3)

Deposition Velocities

Experimental deposition velocities are shown as a function of particle diameter in Figure 3 for wind speeds of 2.2, 7.2 and 13.8 m/sec (corresponding to friction velocities of 11, 44, 117 cm/sec, respectively). Also shown is a broken line representing particle deposition velocities corresponding to the terminal settling velocity.

Deposition velocities for particle diameters greater than 2 µm show consistency as a function of wind speed. At the lowest wind speed of 2.2 m/sec, experimental data points are considered to be indistinguishable from the terminal settling velocity broken line. At this low air speed neither increased air turbulence nor small wave motion enhanced particle deposition. At higher wind speeds, enhanced deposition was significant. Deposition velocities increased with both an increase in particle diameter and wind speed. Similar increases have been shown for dry surfaces by Sehmel.[3-6]

For the largest particles a significant difference occurs between dry surfaces and a water surface. For dry surfaces, net deposition velocities decrease with an increase in particle diameter above about 15 µm. This decreased net apparent deposition is caused by particles depositing but not sticking to a dry surface and being re-entrained into the airstream. For a water surface, re-entrainment does not occur since particles dissolve in the water.

Deposition velocity dependency upon wind speed could not be established for particle diameters below about 1 μm. Although a consistent wind speed depencency was not shown, deposition velocities are similar to those reported by Möller and Schumann,[21] who did not discuss any effect of wind speed. As indicated by temperature gradients, phoretic effects[25] are considered important in this particle diameter range. Phoretic effects were not controlled by either group of investigators. Nevertheless, data consistency suggests that the heavy solid curve reasonably represents deposition velocity data in this size range and that the minimum expected deposition velocity over a water surface is 1×10^{-2} cm/sec.

CONCLUSIONS

Particle deposition velocities now provide an experimental basis with which particle removal rates at the air-sea interface can be predicted. The rates are as expected in that: (1) a minimum deposition velocity was determined in the particle size range where eddy and Brownian diffusion are comparable and (2) deposition velocities for particles greater than 2 μm increased with both an increase in particle diameter and wind speed. Although the nonbreaking water waves developed with the small water depth in the wind tunnel were smaller than most ocean waves, deposition velocities as high as 37 cm/sec were measured for 28-μm diam particles. This is the largest experimental deposition velocity ever reported for any surface. When spray occurs the deposition velocity may be even greater. Experimental data are needed when breaking waves are simulated. This wave surface should include surface films.

DETERMINATION OF AEROSOL DEPOSITION RATES ON A LAKE SURFACE USING RADON DAUGHTERS

J. A. Young

A deposition velocity of 1.5 cm sec^{-1} and a vertical eddy diffusion coefficient of 43 cm^2 sec^{-1} at a depth of 6 ft were calculated from the measured concentrations of the short-lived radon daughters ^{214}Pb and ^{214}Bi in Lake Crescent water.

INTRODUCTION

Average rates of atmospheric mixing and particulate deposition on the earth's surface have been fairly well established from measurements of radionuclide concentrations in the atmosphere and the oceans. Extensive measurements of radionuclide concentrations in precipitation have also been made to obtain wet deposition rates.

PROBLEM

The average rates and the meteorological parameters affecting the deposition rates of atmospheric aerosols on the earth's surface by turbulent transport are considerably less well known. The problem is that the nature of the surface and the characteristics of the air flow near the surface determine the deposition rate, at least for submicron particles which do not settle at appreciable rates. Therefore, at least from a theoretical standpoint, fallout trays which interfere with the air flow do not provide valid data on turbulent deposition rates. Deposition rates must be measured either on natural surfaces under conditions in which the normal air flow is not disturbed or else in wind tunnels where the characteristics of the air flow are known.

MEASUREMENTS

The deposition rates of atmospheric aerosol particles on a water surface were determined by measuring the concentrations of the radon daughters, ^{214}Pb (26.8 min) and ^{214}Bi (19.7 min) in Lake Crescent, a very clear lake on the Olympic Peninsula of Washington State. These radionuclides are produced by the decay of ^{222}Rn (3.8 d) gas emanating from the earth's surface. They rapidly become attached to the atmospheric aerosol particles and therefore serve as tracers of the subsequent behavior of these particles. They are ideal for the determination of the variation in the rate of deposition on a lake surface because of their high atmospheric concentrations and short half-lives. The concentrations were determined by pumping lake water through a filter and then through anion and cation exchange resins. The filters and the resins were then counted using

Ge(Li) diodes and NaI(Tl) multidimensional gamma-ray spectrometers.

RESULTS

The measured concentrations of ^{214}Pb and ^{214}Bi decreased by a factor of about five between the surface and a depth of 20 ft and then remained constant. Presumably the concentrations below 20 ft represent background concentrations produced by the decay of radon dissolved in the water. The deposition velocities of ^{214}Pb and ^{214}Bi on March 28, 1973 were calculated to be about 1.5 cm sec^{-1}. The wind was relatively light on this day. On March 25, 1973 the wind speed was somewhat higher and the surface concentration of ^{214}Pb and ^{214}Bi were 60% higher, indicating a higher deposition velocity. The vertical eddy diffusion coefficient in the lake was calculated to be 43 cm^2 sec^{-1} at a depth of 6 ft. When these measurements were made, the lake was isothermal within about 0.1°C down to 70 ft.

FUTURE WORK

In the spring of 1974 it is planned to measure the concentrations of ^{214}Pb and ^{214}Bi in the lake and in the atmosphere at the same time as wind speed measurements are being made to determine deposition velocities and vertical eddy diffusion coefficients in the lake as functions of wind speed.

A FLUX METER FOR DIRECT FIELD MEASUREMENT OF DEPOSITION AND RESUSPENSION RATES

J. M. Hales and T. W. Horst

A conceptual design for a dry-deposition flux meter is described. A prototype of this design will be constructed and tested during the coming year.

In recent years a variety of field methods have been employed to measure the deposition and/or resuspension of gaseous and particulate material to and from the earth's surface. These have all met with rather limited success owing to experimental complexities, which have forced the measurements to be either indirect or else largely inappropriate for extensive use for calculating behavior in the real atmosphere. As indicated by the summary in Table 3, the technique of direct flux measurement--if possible--would overcome most of the difficulties encountered

TABLE 3. Summary of Characteristics of Experimental Methods for Dry Deposition Measurement

Experiment Class	Major Advantages	Major Disadvantages	Dispersion Regime(s) Required for Study
Wind tunnels	Direct measurement, good control on most conditions	Limited choice of deposition surfaces, assumes deposition is rate limited near surface, difficult to simulate typical mixed pollutant conditions.	Not applicable--artificial atmospheres employed
Static chambers	Direct measurement	Limited choice of deposition surfaces, assumes deposition is rate limited near surface, difficult to simulate typical mixed pollutant conditions.	Not applicable--artificial atmospheres employed
Deposition-surface measurements	Direct measurement	Almost impossible to accomplish except for highly specialized tracers. Possible interferences from chemical reaction subsequent to deposition.	Any regime
Plume decay measurements	Direct measurement	Difficult to account for hetrogeneous terrain, high probability of obscuration by in-plume reaction. Requires highly difficult cross-sectioning of plume or reliance on unreliable plume models.	Transition and deposition controlled
Simultaneous depositing-nondepositing measurements	Direct measurement	Difficult to account for heterogeneous terrain, high probability of obscuration by in-plume reaction. Requires highly difficult cross-sectioning of plume or reliance on unreliable plume models.	Transition and deposition controlled
Profile measurement methods	Independent of Chem. rxn. measures total deposition effect. Single-point sampling sufficient for analysis	Indirect measurement, depends on measurement of diffusivity, must be conducted under deposition-controlled conditions unless dispersion model is employed.	Deposition controlled
Flux-measurement methods	Independent of Chem. rxn. measures total deposition effect. Single-point sampling sufficient for analysis	Extremely sensitive and fast-response instrumentation required. Such equipment not presently available for most substances of interest	Any regime

by these other methods and provide a convenient tool for deposition/resuspension analysis. This technique has been limited, however, by its requirements for fast-response (on the order of 0.5 sec) monitoring instrumentation, which does not presently exist for a majority of the pollutants of primary interest.

During the past year we have discovered a method for overcoming the requirement for fast-response monitoring instrumentation, thus enabling the conceptual design of a practical flux meter. The design of this meter is based on the assumption that at the measurement sites the deposition flux occurs primarily by eddy diffusion. Thus the flux is characterized totally in terms of the time-smoothed cross term

$$\text{flux} = \overline{v_z'(z)\chi'(z)}, \qquad (1)$$

which is the vertical component of pollutant movement taken from the overall continuity equation

$$\frac{\partial \chi}{\partial t} = - \nabla \cdot (\bar{v}_A \chi) - \nabla \cdot (\bar{v}_A' \chi') + D_{AB} \nabla^2 \chi + r_A. \quad (2)$$

Here v_z' is the fluctuating component of vertical velocity and χ' is the fluctuating component of concentration; the bar indicates averaging of the product of these values over a suitably long time period.

The most obvious method of measuring the flux in Equation l directly is simply to obtain simultaneous measurements of v_z' and χ' and average their product. As discussed previously, this is not possible because of difficulties in measuring χ' with sufficient response. The alternative procedure we suggest is shown schematically in Figure 4. Here the time-smoothed product in Equation (1) is measured intact by means of drawing air samples into two reservoirs (one for updrafts and one for downdrafts) at rates exactly proportional to the vertical velocities experienced in the vicinity of the inlets. Rates of air withdrawal are controlled by two fast-response, proportional control valves, actuated by a signal from an anemometer. Appropriate linearization circuitry is provided to compensate for nonlinearities in valve response.

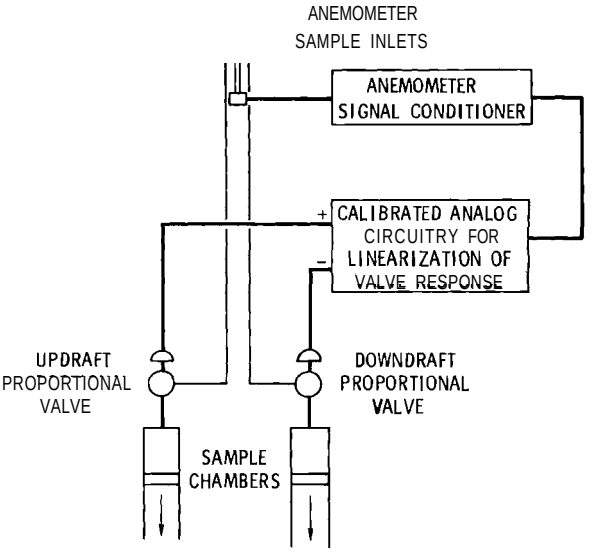

Neg 740789-7

FIGURE 4. Schematic of Flux Meter

Starting with empty sample chambers, a measurement of gaseous pollutant flux can be initiated by actuation of the meter for an appropriate period. Subsequent analysis of the contents of each chamber and subtraction of the values determine the flux defined in Equation (1) . Aerosol deposition rates are measured simply by placement of filters at the sample inlets with subsequent analysis and subtraction of the values.

A frequency response analysis for this method has been conducted and a prototype design initiated. Current plans call for construction and testing of at least one of these units during the coming year.

ANALYTICAL INVESTIGATIONS OF INERTIAL DEPOSITION OF SMALL AEROSOL PARTICLES FROM LAMINAR FLOWS ONTO LARGE OBSTACLES PART A - GENERAL FORMULATION

W. G. N. Slinn

Rather than follow the usual formulation of the inertial deposition problem, a continuum model is presented which replaces Newton's second Zaw by a continuity equation and a pseudo-momentum equation. Some features of the general solution are discerned and it is seen that regular perturbation methods fail both at Zarge and small Stokes numbers.

INTRODUCTION

The importance in many practical problems of evaluating inertial deposition of aerosol particles onto various obstacles is well known. An application that has recently interested the author is the precipitation scavenging of particles from the atmosphere. Elsewhere we have reported on estimates of particle collection by raindrops caused by electrical forces, molecular diffusion, and diffusio- and thermophoresis (slinn, 1968; Slinn and Shen, 1970; Slinn and Hales, 1972). (27,28,29) Here a search is made for an analytical solution for the collision efficiency when the inertia of the aerosol particles is significant.

From the wording of the previous sentence and from the title, the reader can (correctly) infer that the attempt to find an exact solution has met with only partial success. Presumably this is not surprising to those familiar with the problem, since it is known to be quite difficult. We do not propose to review other investigations here, but instead refer the reader to recent reviews by Fuchs,(30) Davies,(31) Hidy and Brock(32) or Marble.(33) However, we note as illustration that a recent article (Michael and Norey)(34) makes reference to early work by Sell,(35) and note that current applications still rely heavily on contributions made by Langmuir and Blodgett(36) and Taylor.(37)

The purpose of the present report is to demonstrate a different approach to the problem and a first few steps towards its solution. Because of our interest in the rain scavenging problem (i.e., in the inertial deposition of particles onto approximately spherically shaped obstacles moving at large Reynolds numbers) there is a tendency in what follows to concentrate on the case of potential flow about a sphere. However, there is no apparent restriction of the method of this case, and results are also displayed for the case of potential flow about a cylinder. In Part C of this paper, which in the main concentrates on the small Stokes number case, some results are also presented for viscous flow about a sphere.

PROBLEM FORMULATION

The usual way to approach the problem is to start from Newton's second law of motion for a single aerosol particle and use an inertial frame fixed with respect to the obstacle. It is assumed that the difference between the velocity of the particle, $\vec{u}$, and the velocity of the fluid, $\vec{v}$, is small enough so that a linear relationship exists between the drag force on the particle and the relative (or slip) velocity $(\vec{u} - \vec{v})$. Then in the absence of other forces, Newton's law becomes

$$\frac{d\vec{u}}{dt} = -\frac{1}{\tau}(\vec{u} - \vec{v}) \qquad (1)$$

where the (particle velocity) relaxation time constant, τ, can be found, for example, using Stokes' or Epstein's[37] drag law (or some interpolation between these two) depending on the Knudsen number. For example, for a spherical particle of radius p and density ρ_p, then if the fluid is air and if we ignore the buoyancy of the particle, Stokes' drag law gives

$$\tau = \frac{2}{9}\frac{\rho_p}{\rho_a}\frac{p^2}{\nu} \qquad (2)$$

where ρ_a is the density and v is the kinematic viscosity of air.

In addition to ignoring nonlinear terms in the drag law, we shall also ignore the influence of the particles on the flow field and thereby take $\vec{v}$ in (1) to be the single-phase velocity field about the obstacle. The added mathematical complexity caused by these interaction terms is significant (for example, see Fuchs, p. 70 et seq or Hocking)[30,39] whereas physical intuition suggests that their consequences will be small provided the total aerosol mass loading of the fluid is small compared with the density of the fluid and provided that the particle size is an order of magnitude or less, smaller than the size of the obstacle.*

Rather than proceed from (1) which describes the motion of a single particle, consider the case of usual interest in aerosol physics in which there is a population of particles described, say, by a number density $n(\vec{r},t)$. Typically, far upstream from the obstacle, the number density is uniform, say n_o. Now let us use $\vec{u}(\vec{r},t)$ of (1) to describe not just the velocity of a single particle at position $\vec{r}$ and time t, but instead, the velocity of the particle field at $\vec{r}$ and t. Then the equations which describe this particle continuum are a continuity equation

$$\frac{\partial n}{\partial t} + \nabla \cdot (n\vec{u}) = 0 \qquad (3)$$

and a (pseudo) momentum equation

$$\frac{D\vec{u}}{Dt} \equiv \frac{\partial \vec{u}}{\partial t} + \vec{u} \cdot \nabla\vec{u} = \frac{1}{\tau}(\vec{v} - \vec{u}). \qquad (4)$$

* For example, in the case of precipitation scavenging of aerosol particles, the aerosol mass loading of the atmosphere may be as high as 10^3 μg m^{-3} versus the density of air, $\rho_a \sim 10^9$ μg m^{-3}, and the largest particle of interest may have radius $\sim 10^1$ μm whereas the smallest raindrop size of interest would be more than 10^2 μm = 0.1 mm. Thus the influence of the particles on the air flow about a raindrop would be expected to be negligible.

In particular, we shall be concerned in the sequel almost exclusively with the steady state versions of (3) and (4), i.e.,

$$\nabla \cdot n\vec{u} = o \tag{5}$$

$$\vec{u} \cdot \nabla\vec{u} = \frac{1}{\tau}(\vec{v} - \vec{u}). \tag{6}$$

EXPLORATIONS FOR AN EXACT SOLUTION

1. Limiting τ Values

Equations (5) and (6) appear deceptively simple, but we have been unable to find exact solutions in spite of the availability of considerable theory on quasi-linear first order partial differential equations. Nevertheless it may be of interest to display some features of the exact solution which are immediately available.

For example, for the case $\tau \to o$ (small particles) we have from (6) that $\vec{u} = \vec{v}$, $\tau \to o$ and from (5) and the continuity equation for the fluid, then $n = p$, the density of the fluid. Thus, as expected, the small-particle limiting form of the equations predicts that the particle field is indistinguishable from the fluid, or the "particle lines" become identical with the streamlines.*

* Actually this result is somewhat of an enigma because it seems to imply that when the inertia of the particles is negligible, then the inertia of the fluid must also be negligible. The author expects that the reason for this result is the neglect of other terms in Newton's equation, mentioned earlier, particularly the buoyancy term. Therefore the limiting case $\tau \to o$ should be treated as the case, not when the particles become inertialess but instead, when the particles acquire the properties of an infinitesimal element of the fluid.

At the other extreme, for large particles, $\tau \to \infty$ and the exact solution to $\vec{u} \cdot \nabla\vec{u} = o$ is $\vec{u} =$ constant, which is obviously the free-stream fluid velocity, far from the obstacle. This limit also conforms to expectations. The particle density is then $n =$ constant which we see must be N_o, the uniform free-stream density, everywhere except in a "shadow" cast by the obstacle (much as in geometric optics) where $n = o$. This will be discussed further in Part C.

That we can find exact solutions at these two extremes of the velocity relaxation time, τ, suggests that τ be treated as a perturbation parameter and that perturbation solutions to the equations be sought. This endeavor is in fact the main concern of this report, but, as will be seen, it is not a trivial undertaking.

What we seek is the collision efficiency, E, for the obstacle as a function of τ. For the cases above: $\tau \to o\,(\vec{u} \to \vec{v})$, $E \to o$ and for $\tau \to \infty$ $(\vec{u} \to \vec{u}_o)$, $E \to 1$. Thus the collision efficiency is defined as the flux of particles to the obstacle normalized by the flux for the case $\tau \to \infty$. It can also be interpreted as the normalized collision cross section.

2. Arbitrary τ Values

Before pursuing perturbation solutions, it is worthwhile to investigate other features of the exact solution, especially for intermediate values of τ. For example, if (4) is written as

$$\frac{\partial \vec{u}}{\partial t} + \frac{1}{2}\nabla u^2 - \vec{u} \times \text{curl}\ \vec{u} = \frac{1}{\tau}(\vec{v} - \vec{u}) \quad (7)$$

and if we let $\vec{\Omega} = \text{curl}\ \vec{v}$ and $\vec{\omega} = \text{curl}\ \vec{u}$ be the vorticity of the two velocity fields, then upon taking the curl of (7) we obtain for the vorticity of the particle field

$$\frac{\partial \vec{w}}{\partial t} + \vec{u} \cdot \nabla\vec{\omega} - \vec{\omega} \cdot \nabla\vec{u} + \vec{\omega}\nabla \cdot \vec{u}$$

$$= \frac{1}{\tau}(\vec{\Omega} - \vec{\omega}). \quad (8)$$

Now consider the case of two-dimensional or axi-symmetric flow, for which $\vec{\omega} \cdot V\vec{u} = o$, and suppose that the fluid velocity is derivable from a potential (i.e., $\vec{\Omega} = o = V \cdot \vec{v}$). Then (8) simplifies to

$$\frac{D\vec{\omega}}{Dt} = -\left(\frac{1}{\tau} + \nabla \cdot \vec{u}\right)\vec{\omega} \quad (9)$$

This result states that under the conditions specified there is no source of vorticity within the particle field. In particular, at large distances upstream we would expect $V \cdot \vec{u}$ to be negligibly small and then (9) yields

$$\vec{\omega} \simeq \vec{\omega}_o \exp(-t/\tau) \quad (10)$$

where $\vec{\omega}_o$ is any initial vorticity at infinity and τ is a parameter along the particle lines. For a uniform particle field at infinity we then have the result that the particle velocity field is irrotational everywhere, except perhaps on particle lines downstream of the obstacle.

The above is interesting but does not appear to be very useful in an endeavor to find the solution to the original equations. Thus if we now put $\vec{u} = \nabla\chi$ into the steady-state equations (5) and (6), we obtain

$$\nabla^2\chi = -\vec{u} \cdot \nabla\ \ell n\ n \quad (11)$$

and

$$\frac{1}{2}\nabla(\nabla\chi)^2 = \frac{1}{\tau}(\nabla\phi - \nabla\chi) \quad (12)$$

where ϕ is the velocity potential for the fluid. Now (12) can be integrated to give us a Bernoulli-type first integral (also see Marble). (33)

$$\frac{1}{2}(\nabla\chi)^2 = \frac{1}{\tau}(\phi - \chi) \quad (13)$$

but our tradeoff for reducing the number of variables from 2 to 1 ($\vec{u}$ to χ) has been to change from a quasi-linear to a nonlinear first-order equation, neither of which the author has been able to solve.

However, in spite of this rather negative result, this formalism does allow some insight into the exact solution. From (10), i.e.,

$$\vec{\omega} = \vec{\omega}_o \exp(-t/\tau) \quad (14)$$

there is a suggestion that $\tau = o$ may be an essential sigularity of the solution. This can also be seen from the original equation (6) whose components in intrinsic coordinates s,n (along and normal to particle lines, respectively) are $\kappa = v_n/\tau u^2$, where κ is the curvature of the particle lines, and

$$u\frac{\partial u}{\partial s} = \frac{1}{\tau}(v_s - u). \quad (15)$$

If in (15) we use the parameter (time) $t = s/u$, then the implicit solution to (15) is

$$u(t) = \frac{1}{\tau} \int_{\Theta}^{\infty} v_s (t - \xi) \exp(-\xi/\tau)\, d\xi. \quad (16)$$

This result, for $\tau \to o$, again forewarns possibly significant difficulties. For example, if $\tau = o$ is an essential singularity, then an asymptotic expansion of the form

$$\vec{u}(\vec{r},\tau) \sim \vec{u}_o(\vec{r}) + \tau \vec{u}_1(\vec{r}) + \tau^2 \vec{u}_2(\vec{r}) + \ldots, \tau \to o \quad (17)$$

which would normally be assumed in a perturbation analysis for small τ, will <u>not</u> be valid.

FAILURE OF REGULAR PERTURBATION TECHNIQUES

1. Small Stokes Numbers

In spite of the above mentioned possibility of failure, it is of interest to examine the consequences of assuming a perturbation solution of the form given above in (17). First, we nondimensionalize the momentum equation using as characteristic velocity the free-stream speed U_o and as characteristic length some dimension of the body, say a (e.g., the radius of a spherical obstacle). Then using the same symbols for nondimensional quantities as were used when they possessed dimensions, we obtain the momentum equation

$$s \vec{u} \cdot \nabla \vec{u} = \vec{v} - \vec{u} \quad (18)$$

where

$$s = \frac{U_o \tau}{a} \quad (19)$$

is the Stokes number. For small particles, the Stokes number is small. An order of magnitude reminder of the size of the Stokes number for particles in a flow field about a raindrop falling at its terminal velocity is

$$s = O\left(\frac{1}{10} p^2\right) \quad (20)$$

where p is the particle radius in microns.

We now seek a solution to (18) of the form

$$\vec{u}(\vec{r},s) \sim \vec{u}_o(\vec{r}) + s \vec{u}_1(\vec{r}) + s^2 \vec{u}_2(\vec{r}) + \ldots, s \to o. \quad (21)$$

This results in the series of equations

$$s^o : \vec{u}_o = \vec{v} \quad (22)$$

$$s^1 : \vec{u}_1 = -\vec{u}_o \cdot \nabla \vec{u}_o = -\vec{v} \cdot \nabla \vec{v} \quad (23)$$

$$s^2 : \vec{u}_2 = -\vec{u}_1 \cdot \nabla \vec{u}_1, \text{ etc.} \quad (24)$$

In fact it is easy to obtain in this manner the solution to any order, for example,

$$\vec{u} = \vec{v} - \frac{1}{2} s \nabla \vec{v} \cdot \vec{v} + \frac{s^2}{2} \nabla \vec{v} \cdot \nabla \vec{v} \cdot \vec{v} - \frac{3}{4} s^3 \nabla \vec{v} \cdot \nabla \vec{v} \cdot \nabla \vec{v} \cdot \vec{v} + \frac{5}{4} s^4 \nabla \vec{v} \cdot \nabla \vec{v} \cdot \nabla \vec{v} \cdot \nabla \vec{v} \cdot \vec{v} + O(s^5) \quad (25)$$

or write the solution in operator form, which follows directly from (18)

$$\vec{u} = \left(\frac{1}{1 + s\,\vec{u}\cdot\nabla}\right)\vec{v}, \qquad (26)$$

which quickly leads by iteration to a continued fraction representation for $\vec{u}$.

But it soon becomes apparent that $\vec{u}$ does not have a solution of the form (21) or if it does, then the solution is not physically meaningful. For example, consider the case of potential flow about an obstacle. Then

$$\vec{u}_1 = -\vec{v}\cdot\nabla\vec{v} = \frac{1}{\rho}\nabla p. \qquad (27)$$

In particular, for potential flow about a sphere, (27) yields

$$u_1 = \frac{3}{r^4}\left\{\left[\left(\frac{1}{r^3} - 1\right)\cos^2\theta + \left(\frac{1}{4r^3} + \frac{1}{2}\right)\sin^2\theta\right]\hat{e}_r + \left(\frac{1}{4r^3} - 1\right)\sin\theta\cos\theta\,\hat{e}_\theta\right\} \qquad (28)$$

where the positive z direction is chosen in the direction of the free-stream velocity and θ is the polar angle from z. On the sphere, $r = 1$, (22) and (28) in (21) gives

$$\vec{u}(r = 1, \theta) = v_\theta\,\hat{e}_\theta + s\,\frac{9}{4}\sin\theta\left(\sin\theta\,\hat{e}_r - \cos\theta\,\hat{e}_\theta\right) + \Theta(s^L) \qquad (29)$$

which states that $v_r \geq 0$ for all θ except on $\theta = 0, \pi$, where it is zero. Thus not only does this formalism predict that no particles collide with the sphere, it is as if there was a flow of particles from the sphere. Meanwhile, if one seeks a perturbation solution to the continuity equation, it yields

$$n = n_\infty\left[1 - \frac{3}{2}s\cos\theta + \Theta(s^2)\right], \qquad (30)$$

which in itself does not herald any failure of the method.

If flow fields other than potential flow are used then, of course, different results are obtained. For example, in the case of Stokes flow about a sphere, it is assumed that $\vec{v}\cdot\nabla\vec{v} \equiv 0$ (i.e., negligible fluid inertia) and therefore we obtain

$$\vec{u} = \vec{v},\ \vec{u}_1 = -\vec{v}\cdot\nabla\vec{v} = 0 = \vec{u}_2 = \vec{u}_3 = \ldots. \qquad (31)$$

Thus this formalism predicts that, regardless of the Stokes numbers for the particles, there would be no collection of the particles since they move exactly with the fluid for the case of Stokes flow. On the other hand, as will be seen later in Part C, one does obtain particle collection if Oseen flow is used but certainly one must question this method of solution if other flows, particularly potential flow, yield such unreasonable results.

A qualitative illustration of the behavior of these solutions for different flow fields is shown in Figure 5.

Actually there are other reasons why we should not have expected the above regular perturbation analysis to succeed, besides the possibility

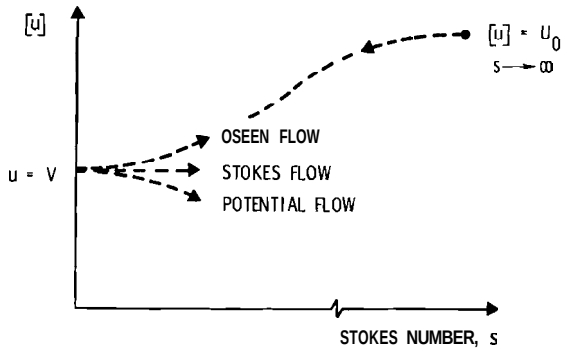

Neg 740722-7

FIGURE 5. A Qualitative Indication of the Behavior of the Small Stokes Number, Regular-Perturbation Solutions for Various Flow Fields.

of an essential singularity at Stokes number equal zero. Namely, for $s \to o$, the order of the governing differential equation is reduced. In particular, to lowest order in s, the differential equation becomes an algebraic equation. The loss of the highest order derivative in the lowest order equation is a classic warning that regular perturbation techniques will fail (e.g., Van Dyke, Cole, Nayfeh). (40,41,42)

2. Large Stokes Numbers

In spite of the above problems as $s \to o$, we might hope for more success with regular perturbation methods at large Stokes numbers since there is no hint of an essential singularity as $s \to \infty$ nor do we lose the highest derivative in the lowest order equation. In fact, though, as we shall see, regular perturbation methods also fail at large Stokes numbers, although the failure is not nearly so obvious as was seen above. We take the time to demonstrate this both because of its intrinsic interest in perturbation theory and because most of the results will be useful later.

For convenience we label the reciprocal of the Stokes number as $a \equiv 1/s$ and in this subsection we are considering the limit $s \to \infty$ or $\sigma \to o$. Also, certain of the integrals to appear later are somewhat simplified (i.e., fewer negative signs appear) if we reverse the coordinate system from that used in the previous section. See Figure 6.

We now seek a perturbation solution to

$$\vec{u} \cdot \nabla \vec{u} = \sigma \, (\vec{v} - \vec{u}) \qquad (32)$$

of the form

$$\vec{u}\,(r,\sigma) \sim \vec{u}_o\,(\vec{r}) + \sigma\, \vec{u}_1\,(\vec{r}) + \sigma^2\, \vec{u}_2\,(\vec{r}) + \ldots, \quad \sigma \to o. \qquad (33)$$

Substituting (33) into (32) gives the series of equations

$$\sigma^o : \vec{u}_o \cdot \nabla \vec{u}_o = o \qquad (34)$$

$$\sigma^1 : \vec{u}_1 \cdot \nabla \vec{u}_o + \vec{u}_o \cdot \nabla \vec{u}_1 = \vec{v} - \vec{u}_o \qquad (35)$$

$$\sigma^2 : \vec{u}_2 \cdot \nabla \vec{u}_o + \vec{u}_1 \cdot \nabla \vec{u}_1 + \vec{u}_o \cdot \nabla \vec{u}_2 = -\vec{u}_1, \text{ etc.} \qquad (36)$$

The solution to (34) subject to the boundary condition $\vec{u}_o = -\hat{k}$, $z \to \infty$ is simply

$$\vec{u}_o = -\hat{k}. \qquad (37)$$

Notice that there is only one boundary condition on the equations,

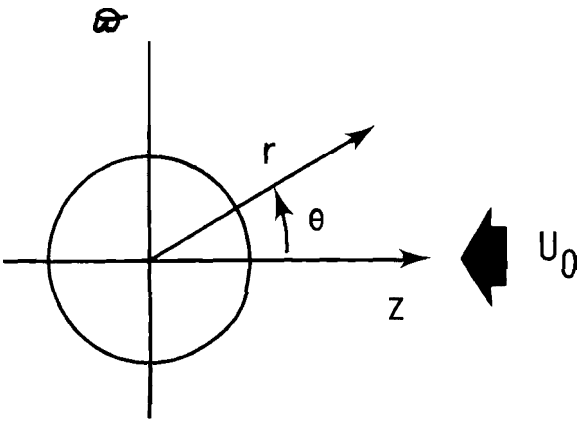

Neg 740722-9

FIGURE 6. Notation Used in Section IV-2 and V (Part B), Only. Otherwise U_o is chosen in the positive z-direction.

i.e., at infinity, which is all that can be forced on a first order equation. In a sense it is as if the obstacle were not present as far as the particle velocity field is concerned. On the other hand we can distinguish two disjoint boundary conditions on the particle density field: for those particle lines which emerge from infinity, $n = N_o$, a constant, and for those particle lines which "emerge" from the obstacle (e.g., on the downstream side of the obstacle) $n = o$.

Substituting the solution (37) into (35) yields for the first order perturbation

$$-\hat{k} \cdot \nabla \vec{u}_1 = \vec{v} + \hat{k}. \qquad (38)$$

For example, for potential flow about a sphere, the solution to (38) which vanishes at infinity is

$$\vec{u}_1 = \vec{f}_1 (\varpi) + \frac{\hat{e}_r}{2r^2} \qquad (39)$$

where $\vec{f}_1 (\varpi)$ is an arbitrary function of the radial distance ϖ (read "pi") from the axis of symmetry. $\vec{f}_1 (\varpi)$ must vanish as $\varpi \to \infty$ but otherwise no information is available to specify it.

For the moment, if we ignore this difficulty caused by $\vec{f}_1$ and substitute (39) and (37) into (36), then to find $\vec{u}_2$ we must solve

$$\frac{\partial \vec{u}_2}{\partial z} - \vec{f}_1 (\varpi) + \frac{\hat{e}_\varpi}{2r^2} + \vec{u}_1 \cdot \nabla u_1. \qquad (40)$$

From (40), to avoid an obvious infinity in $\vec{u}_2$ as $z \to \infty$, we must take $\vec{f}_1 (\varpi) = o$. Then the solution to (40) which vanishes at infinity is found to be

$$\vec{u}_2 = \vec{f}_2 (\varpi) + \left(-\frac{1}{2r} + \frac{1}{8r^4}\right) \hat{k} + \left[\frac{-\varpi}{2r(z+r)} + \frac{1}{2\varpi^4} \left(\frac{3}{8}\theta - \frac{1}{4}\sin 2\theta + \frac{1}{32}\sin 4\theta\right)\right] \hat{e}_\varpi \qquad (41)$$

where $\vec{f}_2 (\varpi)$ is another arbitrary function of ϖ.

This result needs closer scrutiny. It can be seen by expanding the term in parenthesis ( ) in (41) that in fact there is not a singularity as $\varpi \to o$, $z > o$. However as $\varpi \to o$, $z < o$, the first term in the $\hat{e}_\varpi$-component of $\vec{u}_2$ tends to infinity as ϖ^{-1}. This singularity can be removed through an appropriate choice of $\vec{f}_2$. But if any value for $\vec{f}_2$ is chosen other than zero, then just as above, there would be a singularity of the form $z\vec{f}_2$ in $\vec{u}_3$ as $z \to \infty$ which cannot be eliminated by an appropriate choice of $\vec{f}_3$. On the other hand, though, we might rationalize that this singularity on

the downstream axis can be tolerated since the particle density vanishes there. Thus perhaps we can justify taking $\vec{f}_3 = o$.

But major problems remain. Obviously this procedure, whereby higher order terms in the expansion for the velocity field are obtained by integrating lower order terms, will soon lead to expressions containing Rn r, r, r Rn r, etc. (see the z-component of $\vec{u}_2$). These singularities at infinity can neither be tolerated nor eliminated by the procedure. Thus we must conclude that even in the case of large Stokes numbers, either $\vec{u}$ does not have a uniformly valid asymptotic expansion of the form assumed in (33)* and/or this method of obtaining a solution is inappropriate.

* Recently Michael and Norey(34) sought a solution to the same problem of the form (33) and proceeded to obtain a solution to terms $O(s^2)$. However, they approximated the term $\vec{u} \cdot \nabla\vec{u}$ by $u_z \partial\vec{u}/\partial z$ [see their equations (3) and (4)]. Possibly it is this approximation which removes the difficulties encountered above.

CONCLUDING REMARKS FOR PART A

In the above we have attempted to solve the pseudo-momentum equation for the particle field: $\tau \vec{u} \cdot \nabla\vec{u} = \vec{v} - \vec{u}$. For $\tau \to o$ (small particles) this equation yields the obviously correct solution $\vec{u} = \vec{v}$, and for $\tau \to \infty$ (large particles) we obtained $\vec{u} = \vec{U}_\Theta$ which also is obviously correct. Given the exact solution of a nonlinear equation at limiting values of a parameter, it is customary to use this parameter as a device to obtain a perturbation solution. Upon proceeding in the usual manner, though, we have found that regular perturbation techniques fail at both limits of the perturbation parameter. In Parts B and C we shall explore the two obvious possible reasons for failure, i.e., that the correct solution does not admit an expansion of the proposed form or that the method of solution is inappropriate.

ANALYTICAL INVESTIGATIONS OF INERTIAL DEPOSITION OF SMALL AEROSOL PARTICLES FROM LAMINAR FLOWS ONTO LARGE OBSTACLES
PART B - LARGE STOKES NUMBER SOLUTION BY THE METHOD OF MATCHED ASYMPTOTIC EXPANSION

W. G. N. Slinn

The reason for the failure of the regular perturbation techniques used in Part A is identified. The method of matched asymptotic expansions is applied to obtain the first order correction to the collection efficiency at large Stokes numbers. Analytical continuation of the solution to a result valid for all Stokes numbers is discussed, and it is concluded that the most productive procedure would be to gain information about the small Stokes number limit. This will be described in Part C.

INTRODUCTION

That it is the method of solution used in Part A which is inappropriate is strongly suggested if we re-examine the original momentum equation (A-5) :

$$\tau \vec{u} \cdot \nabla\vec{u} = \vec{v} - \vec{u}. \qquad (1)$$

This equation possesses what has become an even more reliable indicator of singular behavior than loss of the highest derivative in the lowest order equation; namely it possesses two characteristic length scales, (the length $U_o\tau$ and the characteristic dimension of the body, a), and, further, the perturbation parameter $s = U_o\tau/a$ is the ratio of these two characteristic length scales. This is the same as arises in the problem of viscous flow about a sphere, where the two length scales are the viscous length ν/U_o and the body dimension, a, and the Reynolds number is their ratio. To solve this problem Proudman and Pearson[43] and Kaplum and Lagerstrom[44] invented the method of matched asymptotic expansions (see Van Dyke, Cole, or Nayfeh)[40,41,42] and evidently its application here is highly appropriate.

The source of the problem with regular perturbation analysis, even in the limit $s \to \infty$, is that for large distances from the obstacle, the gradient becomes so small that in

$$\vec{u} \cdot \nabla\vec{u} = \sigma (\vec{v} - u) \qquad (2)$$

the term $\vec{u} \cdot \nabla\vec{u}$ becomes of the same order in o as the lowest order term on the rhs. Clearly this occurs at distances from the body of the order of r/σ. Alternatively one can see this by taking the ratio of u_2 to u_1 found in the previous section. For the asymptotic series to be useful we must have higher order terms smaller

than those of lower order, yet we have that the ratio of the second order to first order terms is (returning to dimensional quantities)

$$\frac{u_2}{u_1} \doteq \sigma\left(\frac{a}{r}\right)\left(\frac{r^2}{a^2}\right) = \frac{\sigma r}{a} \qquad (3)$$

which is larger than unity if $r > a/\sigma$.

To overcome this failure, we follow the now-standard analysis procedure and consider the two different regions separately. In the "inner region," near the obstacle the characteristic length scale is a (or the fastest time scale of interest is measured by the characteristic time for changes in the fluid properties: a/U_o). In this region the nondimensional equation is as above:

$$\vec{u} \cdot \nabla\vec{u} = a\,(\vec{v} - \vec{u}). \qquad (4)$$

On the other hand, far from the obstacle, the fastest time scale of interest is the particle stopping time τ (or the characteristic length is $U_o\tau$). In this region we nondimensionalize distances with $U_o\tau$ and then the appropriate nondimensional equation is

$$\vec{U} \cdot \bar{\nabla}\vec{U} = \vec{V} - \vec{U} \qquad (5)$$

where capital letters are used just to distinguish the variables in the two regions. In both regions the characteristic velocity is U_o and in (5) the overbar on V reflects that the coordinates are, for example,

$$R = \frac{r}{U_o\tau} = \frac{a}{U_o\tau}\,\frac{r}{a} = \sigma r \qquad (6)$$

where r is the dimensional length.

The next step in the procedure is to solve the relevant equations in the two separate regions and then match their asymptotic expansions into the adjacent regions, to all orders in the perturbation parameter. In our case, since we have only one boundary condition and this is at infinity in the outer region, then this matching process provides us with the boundary conditions for the inner solution.

FIRST ORDER SOLUTION FOR THE VELOCITY FIELD BY THE METHOD OF MATCHED ASYMPTOTIC EXPANSIONS

We now tackle the outer equation. We seek a solution to (5) of the form

$$\vec{U}(\vec{R},\sigma) \sim \vec{U}_o(\vec{R}) + \sigma\vec{U}_1(\vec{R}) + \sigma^2\vec{U}_2(\vec{R}) + \ldots, \qquad (7)$$

which may seem somewhat strange since σ does not appear explicitly in (5). However it is present in the nondimensionalization of $\vec{V}$. For example, for potential flow about a sphere,

$$\vec{V} = -\left(1 - \frac{\sigma^3}{R^3}\right)\cos\theta\ \hat{e}_R + \left(1 + \frac{\sigma^3}{2R^3}\right)\sin\theta\ e_\theta. \qquad (8)$$

Substituting (7) with (8) into (5) we obtain the σ° equation

$$\vec{U}_o \cdot \bar{\nabla}\vec{U}_o = -\hat{k} - \vec{U}_o. \qquad (9)$$

The solution which satisfies the boundary condition at infinity is

$$\vec{U}_o = - \hat{k} . \qquad (10)$$

If this result is used in the a[1] equation, there results

$$-\frac{\partial}{\partial Z} \vec{U}_1 = - \vec{U}_1 . \qquad (11)$$

The solution is

$$\vec{U}_1 = \vec{F}_1 (\Pi) \, e^Z \qquad (12)$$

where $\vec{F}_1 (\Pi)$ is an arbitrary function of the off-axis distance Π. To satisfy the boundary condition $\vec{U}_1 \to o$, $Z \to \infty$, we must set $\vec{F}_1 \equiv o$ which leaves us in this method with no arbitrary function (compare this with the trouble which appeared in Part A).

Continuing in this manner it is easy to see that $\vec{U}_2 = o$ and the first nontrivial equation is for $\vec{U}_3$:

$$-\frac{\partial}{\partial Z} \vec{U}_3 + \vec{U}_3 = \frac{3}{2} \frac{\Pi Z}{R^5} \hat{i} + \left(\frac{Z^2}{R^5} - \frac{\Pi^2}{2R^5} \right) \hat{k} . \qquad (13)$$

The formal solution for the $\hat{i}$ component is

$$U_{3\Pi} = e^Z \left[F_{3\Pi} (\Pi) - \frac{3}{2} \Pi \int_\infty^Z \frac{Z' e^{-Z'}}{(R')^5} \, dZ' \right] \qquad (14)$$

in which $F_{3\Pi} \equiv o$ and the integral is over Z' at fixed off-axis distance, Π.

As it stands the result (14) does not appear to be of much value since the integral can not be evaluated in closed form. However it is gratifying that this form of solution suggests that the logarithmic singularities seen earlier have been successfully removed. Further we are most interested in the solution near the sphere, and, as was mentioned above, to obtain the inner solution all we need is the asymptotic expansion of the outer solution into the inner region. To obtain this asymptotic expansion we first integrate (14) by--parts:*

$$U_{3\Pi} = \frac{\Pi}{2} \left\{ \frac{1}{R^3} - \frac{1}{R(R+Z)} + \frac{1}{R+Z} - \frac{\Pi^2}{4(Z+R)^2} + \frac{1}{2} \ln (Z+R) + e^Z \int_\infty^Z \left[\frac{1}{2} \ln (Z'+R') - \frac{\Pi^2}{4(Z'+R')^2} \right] e^{-Z'} \, dZ' \right\} \qquad (15)$$

and then rewrite this result in inner variables (R = or etc.)

$$\sigma^3 U_{3\Pi} = \sigma \frac{\sin\theta}{2r^2} - \sigma^2 \frac{\sin e}{2r(1+\cos\theta)} + \sigma^3 \frac{\sin\theta}{2(1+\cos\theta)} - \sigma^4 \frac{r \sin 3\theta}{8(1+\cos\theta)^2} + \sigma^4 \frac{r \sin\theta}{4} \ln r \, (1 + \cos\theta) + (\sigma^4 \ln\sigma) \frac{r \sin\theta}{4} + O(\sigma^5) . \qquad (16)$$

This result is now used to match with the outer expansion of the inner solution.

* Some of these integrals caused the author significant difficulty since all the tabulated integrals the author was able to find were not finite as $\Pi \to o$. It is hoped that the integrals used will be checked independently by others interested in this-problem.

In a similar manner one can obtain

$$U_{3Z} = \frac{1}{2}\frac{Z}{R^3} - \frac{1}{2R} - \frac{1}{2}\ln(Z+R) + \frac{R}{2} - \frac{1}{2}Z\ln(Z+R) - \frac{1}{2}e^{Z}\int_{\infty}^{Z}[Z'\ln(Z'+R') - R']\,e^{-Z'}\,dZ' \quad (17)$$

which leads to

$$\sigma^3 U_{3Z} = \frac{\sigma\cos\theta}{2r^2} - \frac{\sigma^2}{2r} - \frac{\sigma^3}{2}\ln r\,(1+\cos\theta) - \frac{1}{2}(\sigma^3\ln\sigma) + \frac{\sigma^4 r}{2} - \frac{1}{2}\sigma^4 r\cos\theta\ln r\,(1+\cos\theta) - \frac{1}{2}(\sigma^4\ln\sigma)\,r\cos\theta + O(\sigma^5). \quad (18)$$

The appearance of $\ln\sigma$ terms in such expansions is no longer a surprise in perturbation analysis (cf. Van Dyke).[40] Here they arise naturally from repeated integrals of reciprocals of the outer coordinates.

Actually it is illusionary to think that (15) and (17) will provide matching to the inner solution to terms $O(\sigma^5)$ since $\vec{U}_4$, $\vec{U}_5$, etc., can be expected to provide additional terms to these orders. This will be examined immediately. The reason so many terms were displayed above is partly to make them available for other researchers and partly so that the $\ln\sigma$ terms could be displayed.

If we now pursue higher order terms in the outer solution, we soon see that $\vec{U}_4 \equiv 0 \equiv \vec{U}_5$ and the next nontrivial equation is for $\vec{U}_6$

$$\vec{U}_0\cdot\nabla\vec{U}_6 + \vec{U}_3\cdot\nabla\vec{U}_3 = -\vec{U}_6. \quad (19)$$

(After this equation, we would obtain equations for $\vec{U}_9$, $\vec{U}_{12}$ etc., which tells us that the original expansion should "obviously" have been in powers of σ^3.) Since the algebra involved in solving (19) is rather lengthy, there is significant opportunity for error and we will not quote our complete result. However, when $\vec{U}_6$ is expanded into the inner region it contributes terms $O(a^2)$ and the leading terms are

$$\sigma^6 U_{6\Pi} = \frac{\sigma^4}{8}\frac{1}{\varpi^4}\left(\frac{3}{2}\theta - \sin 2\theta + \frac{1}{8}\sin 4\theta\right) + O(\sigma^3) \quad (20)$$

$$\sigma^6 U_{6Z} = \frac{\sigma^2}{8r^4} + O(\sigma^3). \quad (21)$$

We now turn to the inner region. We assume a solution of the form

$$\vec{u}(\vec{r},\sigma) \sim \vec{u}_0(\vec{r}) + \sigma\,\vec{u}_1(\vec{r}) + \sigma^2\,\vec{u}_2(\vec{r}) + \ldots,\ \sigma\to 0. \quad (22)$$

Based on the results from the outer solution, terms of the form $\sigma^n\ln\sigma$ must be included in (22), for $n \geq 3$. The σ^0 term of (4) is then

$$\vec{u}_0\cdot\nabla\vec{u}_0 = 0 \quad (23)$$

which gives

$$\vec{u}_0 = \vec{c}. \quad (24)$$

Matching (the asymptotic expansion into the outer region of) this result with the outer solution gives $\vec{c} = -\hat{k}$. The first order equation is then

$$-\frac{\partial}{\partial Z}\vec{u}_1 = \vec{v} - \vec{u}_0 \quad (25)$$

whose solution we have found earlier [Equation (A-39)] to be

$$\vec{u}_1 = \vec{f}_1(\varpi) + \frac{\hat{e}_r}{2r^2}. \quad (26)$$

If this is matched with the outer solution we must have $\vec{f}_1(\varpi) = 0$. Similarly $\vec{u}_2$ becomes

$$\vec{u}_2 = \left(-\frac{1}{2r} + \frac{1}{8r4}\right)\hat{k} + \left[-\frac{\sin\theta}{2r(1+\cos\theta)} + \frac{1}{8\varpi^4}\left(\frac{3}{2}\theta - \sin2\theta + \frac{1}{8}\sin4\theta\right)\right]\hat{e}_\varpi \quad (27)$$

where, for example, the first term in the &component matches with a corresponding term in $U_{3\Pi}$ and the second, with a corresponding term in $U_{6\Pi}$ [see Equations (16) and (20)].

The conclusion reached from the above is that apparently the method of matched asymptotic expansion does provide a satisfactory solution to the problem, at least for large σ. We can create a uniformly valid composite expansion via the usual procedure

$$\vec{u}_c = \vec{u}_o + \vec{u}_i - (\vec{u}_o)_i \quad (28)$$

(where the subscripts read: composite, outer, inner, and outer expanded into the inner region), but it is unnecessary to do this since this problem is one of the rare (trivial!) cases where $(\vec{u}_o)_i \equiv \vec{u}_i$ and the outer expansion is already a uniformly valid solution.* Thus in summary we have the uniformly valid solution

$$\vec{u} = \vec{U}_o + \int_Z^\infty dZ' (\vec{v}-\vec{U}_o) \exp\left[-(Z'-Z)\right] + O\left(\frac{1}{\tau^2}\right), \quad (29)$$

where $Z = z/U_o\tau$, and, near the sphere (29) has the asymptotic expansion

$$\vec{u} = \hat{k}\left[-1 + \sigma\frac{\cos\theta}{2r^2} - \sigma^2\left(\frac{1}{2r} - \frac{1}{8r^4}\right) + O(\sigma^3)\right] + \hat{e}_\varpi\left\{\sigma\frac{\sin\theta}{2r^2} - \sigma^2\left[\frac{\sin\theta}{2r(1+\cos\theta)} - \frac{1}{8\varpi^2}\left(\frac{3}{2}\theta - \sin2\theta + \frac{1}{8}\sin4\theta\right)\right] + \Theta(\sigma^3)\right\}. \quad (30)$$

In the case of two-dimensional flow about a right circular cylinder we can obtain in an analogous manner the uniformly valid solution given by (29) and the expansion near the cylinder

$$\frac{\vec{u}}{U_o} = -\hat{k} + \frac{\sigma}{r}\hat{e}_r - \sigma^2\theta\hat{e}_\varpi + O(\sigma^2 \ln u) \quad (31)$$

where r is nondimensionalized with the radius of the cylinder. It is interesting that here, as in the problem of viscous flow about a cylinder, the log terms arise sooner for the two-dimensional than for the three-dimensional case.

PARTICLE CONCENTRATION, THE COLLISION EFFICIENCY AND COMPARISONS WITH OTHER RESULTS

To obtain the particle concentration and ultimately the collision efficiency, we must first solve the continuity equation

$$\vec{u} \cdot \nabla n = -n \nabla \cdot \vec{u}. \quad (32)$$

* Van Dyke (personal communication) points out this problem could therefore be called not a singular perturbation problem but a regular one, if the right nondimensionalization (i.e., $U_o\tau$ instead of a) is used! Perhaps this is caused because there are boundary conditions only in one region.

Since this equation is homogeneous in n, $\vec{u}$, and the length scale, choice of nondimensionalization is immaterial. For convenience, though, outer variables are used and we seek a perturbation solution to (32) of the form

$$N(\vec{r},\sigma) \sim N_o(\vec{R}) + \sigma^3 N_1(\vec{R}) + \ldots, \quad \sigma \to o \qquad (33)$$

and use the uniformly valid result for $\vec{u}$:

$$\vec{U}(\vec{r},\sigma) \sim \vec{U}_o(\vec{R}) + \sigma^3 \vec{U}_3(\vec{R}) + \ldots, \quad \sigma \to o \qquad (34)$$

where $\vec{U}_o$, $\vec{U}_1$ etc. are as found above.

The lowest order equation is

$$\vec{U}_o \cdot \nabla N_o = 0 \qquad (35)$$

which yields N_o = constant which we take to be unity (for n nondimensionalized with the uniform upstream particle density).*

The equation for N_3 is then

$$\hat{k} \cdot \nabla N_3 = \nabla \cdot \vec{U}_3 \qquad (36)$$

or

$$\frac{\partial N_3}{\partial Z} = \frac{\partial U_{3\Pi}}{\partial \Pi} + \frac{\partial U_{3Z}}{\partial Z} + \frac{U_{3\Pi}}{\Pi}. \qquad (37)$$

Using the results of the previous section and the properties of asymptotic series that allow us to integrate term by term (e.g., see Morse and Feshbach),[45] we arrive at the result that the leading term in the density is $O(\sigma^2)$ in the inner region. Thus on the sphere,* r = 1,

$$nu_r = [1-O(\sigma^2)]\ [-\cos\theta + \tfrac{\sigma}{2}]. \qquad (38)$$

Similarly for the cylinder problem we obtain in the inner region**

$$n = 1 + \sigma \ln \frac{z + r}{2} + O(\sigma^2). \qquad (39)$$

The singularity along the negative z-axis in this result is of no consequence because the above result is valid only outside the shadow region.

To obtain an expression for the collision efficiency, we first note that if the particle stream was undeflected by the obstacle then the flux of particles to a sphere, i.e.,

---

* The shadow effect will be examined in Part C. It can be discussed here but it has no effect on the collision efficiency.

* As might be expected, there is significant opportunity for an algebraic slip in these extensive calculations. Because of this, we shall work here only with first order terms. However we record our second order results for comparison with possible future calculations made by others

$$\sigma^2 \left\{ -\frac{1}{4} + \frac{3}{16\sin^5\theta} [38 - 2\theta\sin^2\theta - 3\cos\theta\sin\theta] \right\}.$$

The author would be glad to provide more detailed results to those who are interested.

** The author would appreciate it if others would independently study this case and come to their own conclusions about the presence or absence of the numerical factor in the log term. The question arises because of the unavailability of tabulations of suitable integrals.

$$F = -\int_0^{\pi/2} \left(nu_r/_{r=a}\right) \; 2\pi a \text{ sine ade} \quad (40)$$

would be $\pi a^2 n_o U_o$. If we now use (38) for nu_r in (40) and normalize the result by $\pi a^2 n_o U_o$, we obtain for the collision efficiency for the sphere, the simple result*

$$E_s = 1 - \sigma + O(\sigma^2). \quad (41)$$

For potential flow about a right circular cylinder the similar result is

$$E_c = 1 - \sigma(1 + \ln 2) + O(\sigma^2). \quad (42)$$

As with all results obtained via perturbation analyses, the above leave much to be desired. The results should not be used for Stokes numbers ($s = 1/\sigma$) smaller than about 10, but one is anxious to apply them to smaller values. To do this a number of methods are currently being developed using Euler transformations (e. g., see Shanks or Van Dyke)[46,40] or the Pade approximant method (e.g., see Baker and Gammel, eds., 1970).[47] In the following we shall explore methods for extending our results so that they are applicable to a large range of Stokes numbers; in fact, most of Part C is directed toward this goal.

* Using the expression presented in an earlier footnote and integrating only up to the angle θ_m beyond which $u_r > o$, we obtain the σ^2 coefficient:

(1/16) [11 + 3π/2].

Hopefully others will check to see if this result is correct.

First we note that a series for the collision efficiency of the form say,

$$E = 1 - \sigma^2 + \sigma^4 - + \cdots$$

may not converge beyond some finite small value for σ, solely because of simple singularities in the complex a plane, in this case at $\sigma = \pm i$, and a simple analytic continuation, e.g., here, to

$$E = \frac{1}{1 + a^2}$$

may allow us to correctly move past this physically artificial bound. Thus in the case for the collision efficiency for a sphere we might make the (Euler) transformation of (42) to

$$E = \frac{1}{1 + \sigma} \quad (43)$$

and for the cylinder,

$$E = \frac{1}{1 + (1 + \ln 2)\,\sigma}.$$

Now one hopes that these expressions will be useful for all a values. In particular we note that for small Stokes numbers, (43) gives

$$E = s - s^2 + s^3 - + \ldots. \quad (44)$$

But in our case we should be skeptical of the value of (43) for two main reasons. First we have had hints that the exact solution may have an essential singularity as $s \to o$, whereas we see that (43) is regular as $s \to o$. Second, we have tried to find a small solution of the form of a power series in s similar to (44) but found that the series and/or the

method failed. Therefore we propose to reject (43) and for similar reasons reject a form for E that was introduced earlier (Slinn) [48] to simplify some numerical calculation. The specific functional form chosen was

$$E = 1 - \exp(-s/k)$$

where k is a numerical constant.

Instead we look for an analytic continuation of our perturbation series which has an essential singularity as $s \to o$. Perhaps the simplest such function, for potential flow about a sphere, is

$$E_s = \exp(-1/s) \qquad (45)$$

which, incidentally, is the same form as was suggested by Berg [49] on the basis of semi-empirical fit to data. Similarly, for potential flow about a cylinder we try

$$E_c = \exp[-(1 + \ln 2)/s]. \qquad (46)$$

These expressions are compared with numerical and experimental results in Figure 7.

CONCLUDING REMARKS FOR PART B

As is seen in Figure 7, our assumed results (45) and (46) are close to both the numerical and experimental results. Of course we could search

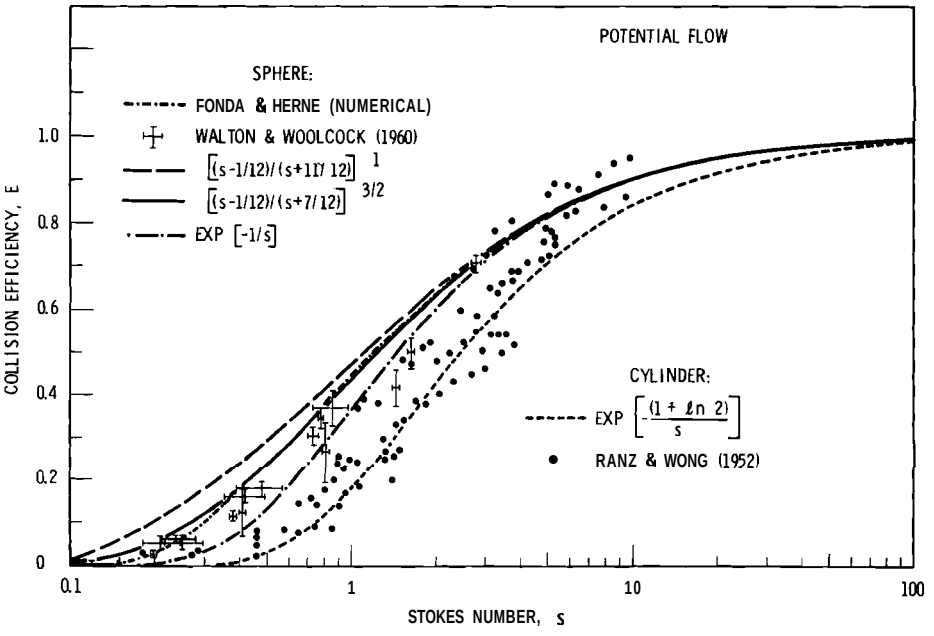

Neg 740753-1

FIGURE 7. Comparisons of Equations (45) -(48) with Numerical and Experimental Results for the Collection Efficiency for a Sphere and Cylinder. The results of Fonda and Herne's calculations were obtained from Herne.[50] The therory is for the case of infinite Reynolds number but, of course, not the data (Walton and Woolcock, Ranz and Wong).[51,52]

for other functions which are even closer to either. For example, we also show in Figure 7 the expressions for the collection efficiency for a sphere

$$E = [1 - (s + 11/12)^{-1}] \qquad (47)$$

which is regular as $s \to o$ and

$$E = \left[1 - \frac{2}{3}\left(\frac{7}{12} + s\right)^{-1}\right]^{3/2}, \qquad (48)$$

both of which vary as $(1 - 1/s)$ for large s. But one soon becomes discouraged with this essentially curve-fitting procedure. On the one hand there is very significant scatter of the data, and on the other hand there are questions about the accuracy of the numerical calculations [arising from starting the particle with the full upstream velocity at a finite distance from the sphere or from approximating $\vec{u} \cdot \nabla\vec{u}$ by $u_Z \partial\vec{u}/\partial z$ or simply from numerical limitations, for example, if the true solution is of the form $\exp(-1/s)$].

It is clear that to proceed rigorously, then considerably more analysis must be performed. To improve upon the solutions we can either seek more terms in the large Stokes number perturbation solution or attempt to gain some information about the solution's small Stokes number behavior. However, it appears that there would be far too little return on the significant investment of effort needed to obtain higher order terms in the large Stokes number solution. Even if multiple terms were obtained, it probably would be extremely difficult to recognize the analytic continuation. Instead we have searched for some indication of the small Stokes number hehavior of the solution, and in fact (48) contains one such feature, namely: it is zero at the Taylor critical Stokes number of 1/12. Our progress in this very difficult search is described in Part C. In addition, in Part C we will partially remedy a substantial deficiency in the above analysis by seeking solutions at other than infinite Reynolds numbers.

ACKNOWLEDGMENTS

I wish to thank Professor Milton Van Dyke of Stanford Univeristy for his hospitality and helpful comments.

REFERENCES

1. A. C. Chamberlain, "Transport of Gases to and from Grass and Grass-like Surfaces," Proc. Roy. Soc. (A) London, vol. 290, pp. 236-265, 1966.

2. A. C. Chamberlain, "Transport of Lycopodium Spores and Other Small Particles to Rough Surfaces," Proc. Roy. Soc. (A) London, vol. 296, pp. 45-70, 1967.

3. G. A. Sehmel, "Particle Deposition from Turbulent Air Flow," J. Geo. Phys. Res., vol. 75, no. 9, pp. 1766-1781, 1970.

4. G. A. Sehmel, "Turbulent Deposition of Monodispersed Particles on Simulated Grass," II, Assessment of Airborne Particles, ed. T. T. Mercer, P. E. Morrow and W. Stober, C. Thomas Publishing Co., Springfield, IL, pp. 18-42, 1972.

5. G. A. Sehmel, "Particle Eddy Diffusivities and Deposition Velocities for Isothermal Flow and Smooth Surfaces," J. Aerosol Sci., vol. 4, pp. 125-138, 1973.

6. G. A. Sehmel, S. L. Sutter and M. T. Dana, "Dry Deposition Processes," Pacific Northwest Laboratory Annual Report for 1972, to the USAEC, Division of Biomedical and Environmental Research, Volume II: Physical Sciences, Part 1, Atmospheric Sciences, BNWL-1751, PT1, Battelle, Pacific Northwest Laboratories, Richland, WA, pp. 43-49, 1973.

7. G. A. Sehmel and T. W. Horst, "Deposition Velocities as a Function of Particle Concentration Reference Height and Atmospheric Stability," Pacific Northwest Laboratory Annual Report for 1971, to the USAEC, Division of Biomedical and Environmental Research, Volume II: Physical Sciences, Part 1, Atmospheric Sciences, BNWL-1651, PT1, Battelle, Pacific Northwest Laboratories, Richland, WA, pp. 150-153, 1972.

8. J. A. Businger, J. C. Wyngaard, Y. Izumi and E. F. Bradley, "Flux-profile Relationships in the Atmospheric Surface Layer," J. Atmos. Sci., vol. 28, pp. 181-189, 1971.

9. G. A. Sehmel and S. L. Sutter, "Particle Deposition Rates on a Water Surface as a Function of Particle Diameter and Air Velocity," in this report.

10. G. A. Sehmel, W. H. Hodgson and S. L. Sutter, "Dry Deposition of Particles," in this report.

11. J. H. Bennett, A. C. Hill and D. M. Gates, "A Model for Gaseous Pollutant Sorption by Leaves," J. of the Air Pollution Control Assoc., vol. 23, no. 11, pp. 957-962, November 1973.

12. C. E. Elderkin, D. C. Powell, G. H. Clark and P. W. Nickola, "Comparison of Diffusion-Deposition Model Components with Experimental Results," in this report.

13. E. H. Markee, Jr., "Studies of the Transfer of Radioiodine Gas to and from Natural Surfaces," NOAA Technical Memorandum, ERL-ARL-29, Department of Commerce, NOAA, Environmental Research Laboratories, Air Resources Laboratories, Silver Spring, MD, April 1971.

14. J. L. Monteith, Principles of Environmental Physics, American Elsevier Publishing Co.. New York, p. 92, 1973. .

15. G. S. Raynor, Janet V. Hayes and E. C. Ogden, "Particulate Dispersion into a Forest Edge," presented at the 11th Conference on Agricultural and Forest Meteorology of the American Meteorology Society, January 1973, Durham, NC.

16. S. R. Hanna, "Lateral Turbulence Intensity in a Pine Plantation." presented at the Third Eastern Forest Meteorology Conference, Syracuse, New York, September 13-14, 1971.

17. G. Langer, "Particle Deposition and Reentrainment from Coniferous Trees -- Part II: Experiments with Individual Leaves," Kolloid-Zeitschrift und Zeitschrift fur Polymere, Band 204, Heft 1/2, pp. 119-124, 1956.

18. D. Aylor, "Trapping of Airborne Particles by Vegetation," presented at the 11th conference on Agricultural and Forest Meteorology, American Meterorological Society, Durham, NC, January 1973.

19. J. B. Stewart and A. S. Thom, "Energy Budgets in a Pine Forest," Quart. J. R. Met. Soc., vol. 99, pp. 154-170, 1973.

20. R. P. Hosker, Jr., "Estimates of Dry Deposition and Plume Depletion over Forest and Grassland," presented at IAEA Symposium on the Physical Behavior of Radioactive Contaminants in the Atmosphere, Vienna, Austria, November 12-16, 1973.

21. U. Möller and G. Schumann, "Mechanisms of Transport from the Atmosphere to the Earth's Surface," J. Geophys. Res., vol. 75, no. 15, pp. 3013-3019, 1970.

22. R. E. Baier and D. W. Goupil, "Collection and Identification of Sea Surface Films with Special Attention to Natural Slicks and Foams," presented at International Symposium on the Chemistry of Sea/Air Particulate Exchange Processes, October 4-10, 1973, abstracts, Bulletin de L'union des Oceanographes de France, p. A-1, 1973.

23. K. H. Szekielda, "Accumulation of Minerals at the Air-sea Interface," presented at International Symposium on the Chemistry of Sea-Air Particulate Exchange Processes, October 4-10, 1973, abstracts, Bulletin de L'union des Oceanographes de France, p. A-14, 1973.

24. P. F. Twitchell, "The Effect of Organisms in the Surface Microlayer," presented at International Symposium on the Chemistry of Sea/Air Particulate Exchange Processes, October 4-10, 1973, abstracts, Bulletin de L'union des Oceanographes de France, p. A-15, 1973.

25. G. A. Sehmel and S. L. Sutter, "Particle Deposition Rates on a Water Surface as a Function of Particle Diameter and Air Velocity," BNWL-SA-4755, presented at the International Symposium on the Chemistry of Sea-Air Particulate Exchange Processes, October 4-10, 1973, and submitted for publication in J. de Recherches Atmosphériques, 1973.

26. W. Stöber and H. Flachsbart, "An Evaluation of Nebulized Ammonium Fluorescein as a Laboratory Aerosol," Atmos. Environment, vol. 7, pp. 737-748, 1973.

27. W. G. N. Slinn, "Precipitation Scavenging of Submicron Particles, Part A - Theory," Proceedings of the USAEC Meteorological Information Meeting, September 11-14, 1967 at the Chalk River Nuclear Laboratories, Ontario, Canada, C. A. Mawson, ed., AECL-2787, 1968.

28. W. G. N. Slinn and S. F. Shen, "Anisotropic Brownian Diffusion and Precipitation Scavenging of Submicron Particles," J. Geophys Res., vol. 75, pp. 2267-2270, 1970.

29. W. G. N. Slinn and J. M. Hales, "A Re-evaluation of the Role of Thermophoresis as a Mechanism of In- and Below-cloud Scavenging," J. Atmos. Sciences, vol. 28, pp. 1465-1471, 1972.

30. N. A. Fuchs, The Mechanics of Aerosols, Pergamon Press, New York, 1964

31. C. N. Davies, ed., Aerosol Science, Academic Press, New York, 1966.

32. G. M. Hidy and J. R. Brock, The Dynamics of Aerocolloidal Systems, Pergamon Press, New York, 1970.

33. F. E. Marble, "Dynamics of Dusty Gases," Annual Review of Fluid Mechanics, vol. 2, M. Van Dyke et al., eds., Annual Reviews, Inc., Palo Alto, CA, 1970.

34. D. H. Michael and P. W. Norey, "Particle Collection Efficiencies for a Sphere," J. Fluid Mech., vol. 37, pp. 565-575, 1969.

35. W. Sell, Forschungsh. Ver Dtsch. Ing., vol. 347, pp. 1-22, 1931.

36. I. Langmuir and K. B. Blodgett, A Mathematical Investigation of Water Droplet Trajectories, U.S. Army-Air Forces Technical Report No. 5418, 1948.

37. G. I. Taylor, Rept. Memo., No. 2024 (A.R.C.), 1940.

38. P. S. Epstein, "On the Resistance Experienced by Spheres in Their Motion Through Gases," Phys. Rev. vol. 23, pp. 710-733, 1924.

39. L. M. Hocking, "The Theoretical Collision Efficiency of Small Drops," Q.J. Roy. Met. Soc., vol. 85, pp. 44-50, 1959.

40. M. Van Dyke, Perturbation Methods in Fluid Mechanics, Academic Press, New York, 1964.

41. J. D. Cole, Perturbation Methods in Applied Mathematics, Blaisdell Pub. Co., Waltham, MA, 1968.

42. A. H. Nayfeh, Perturbation Methods, John Wiley and Sons, New York, 1973.

43. I. Proudman and J. R. A. Pearson, "Expansions at Small Reynolds Numbers for the Flow Past a Sphere and a Circular Cylinder," J. Fluid Mech., vol. 2, pp. 237-263, 1957.

44. S. Kaplun and P. A. Lagerstrom, "Asymptotic Expansions of Navier-Stokes Solutions for Small Reynolds Numbers," J. Math. Mech., vol. 6, pp. 585-593, 1957.

45. P. M. Morse and H. Feshbach, Methods of Theoretical Physics, Part 1, McGraw-Hill, New York, 1953.

46. D. Shanks, "Non-linear Transformations of Divergent and Slowly Convergent Sequences," J. Math. and Physics, vol. 34, pp. 1-42, 1955.

47. G. A. Baker and J. L. Gammel, eds., The Pade Approximant in Theoretical Physics, Academic Press, New York, 1970.

48. W. G. N. Slinn, "Numerical Explorations of Washout of Aerosol Particles," Pacific Northwest Laboratory Annual Report for 1970 to the USAEC Division of Biology and Medicine, Volume II, Physical Sciences Part 1, Atmospheric Sciences BNWL-1551, Battelle-Northwest, Richland, WA, 1971. Available from NTIS, Springfield, VA.

49. T. G. O. Berg, "Collection Efficiency in Washout by Rain," Precipitation Scavenging (1970), R. J. Engelmann and W. G. N. Slinn, coords, Proceedings of a symposium held at Richland, WA. Available as CONF-700601 from NTIS, Springfield, VA.

50. H. Herne, "The Classical Computations of the Aerodynamic Capture of Particles by Spheres," Aerodynamic Capture of Particles, E. G. Richardson, ed., proceedings of a conference held at B.C.U.R.A., Leatherhead, Surrey, 1960, Pergamon Press, New York.

51. W. H. Walton and A. Woolcock, "The Suppression of Airborne Dust by Spray," Aerodynamic Capture of Particles, E. G. Richardson, ed., Pergamon Press, New York.

52. W. Ranz and J. Wong, "Impaction of Dust and Smoke Particles on Surface and Body Collectors," Ind. Eng. Chem., vol. 44, p. 1371, 1952.

REMOVAL AND RESUSPENSION PROCESSES

RESUSPENSION OF PARTICLES

Particles, once airborne and deposited, can again become airborne when wind stresses are sufficiently high. Research in this area is undertaken to help establish the important variables and their interrelationships. The ultimate use for data of this kind is to determine the exposure to man from such secondary sources and to set permissible limits on ground contamination. An important variable is the wind speed, but the interaction between the primary particle of interest and the bulk soil particles is also very important. We are primarily using areas contaminated inadvertently with radioisotopes from various processes, but have also performed initial studies using a tracer placed on an instrumented plot of prairie-like terrain. An important part of this work is to develop models which account for particles resuspended and deposited. Diffusion and dispersion in the atmosphere, once particles are resuspended, are important in diluting the airborne material; hence, this work interfaces directly with diffusion studies. The physics of wind blown sand and fine particles is also studied to determine the mechanisms of resuspension and transport. Studies on the nature and release of radioactive particles in local Hanford project areas during fires are also closely related to DBER supported programs.

- **PARTICLE RESUSPENSION AND TRANSLOCATION**
- **ATLANTIC RICHFIELD HANFORD COMPANY**

RESUSPENSION OF TRACER PARTICLES BY WIND

G. A. Sehmel and F. D. Lloyd

A particle resuspension rate of 1.2 × 10^{-10} fraction/sec removed by wind stresses was determined for a submicrometer inert molybdenum tracer deposited on a sandy soil surface.

INTRODUCTION

Wind-caused particle resuspension rates from environmental surfaces are being determined using inert tracer particles as a substitute for radioactive particles such as plutonium. Obviously the inert tracer is used because placing plutonium in the environment could develop into a potential hazard comparable to that being simulated. Several advantages derive from using inert tracers: deposited tracers can be a known source in terms of particle diameter, quantity of tracers per unit area, and time lapse from initial deposition. Nevertheless, in using inert tracers, the tracer distribution must simulate both expected plutonium'particle sizes and attachment of plutonium to host soil particles.

EXPERIMENT

The initial molybdenum tracer resuspension experiment was designed to (1) determine whether the molybdenum would be resuspended in a measurable amount and (2) ascertain the tracer distribution on the airborne soils. These objectives were found satisfied in an experiment schematically shown in Figure 1. The tracer used was submicrometer calcium molybdate particles. Calcium molybdate particles were initially prepared as a precipitate in a water suspension by mixing solutions of calcium chloride and sodium molybdate. The precipitate was washed several times to remove soluble salts. The final precipitate was stabilized with Dowfax 2A1® anionic surfactant. Tracer suspension was initially sprayed on the ground in a circle of 75-ft radius around a sampling tower. The tracer particle size, droplet size, and suspension concentration were such that each droplet contained many particles. The average surface concentration of tracer as elemental molybdenum was 58 mg/ft^2.

High-volume, 20-cfm cascade* impactor-cowl air sampling systems[1,2]

® Dowfax 2A1 solution; Dow Chemical Co. (active ingredient: disodium 4-dodecylated oxydibenzenesulfonate).

* Andersen 2000, Inc., Model 65-100 High-Volume Sampler Head, P.O. Box 20769, Atlanta, Georgia 30320

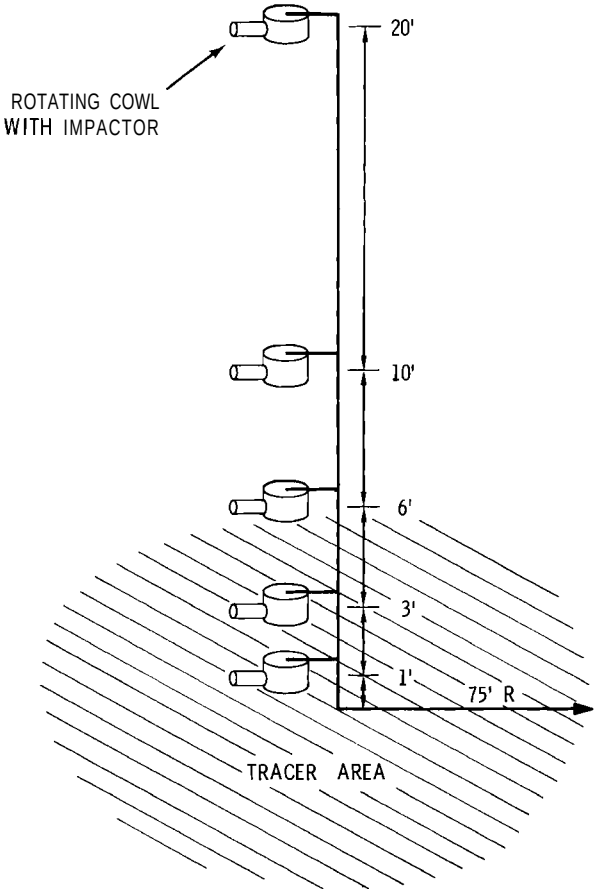

Neg 740044-8

FIGURE 1. Tracer Source and Resuspension Sampling Tower

were mounted at 1, 3, 6, 10, and 20-ft tower heights to determine the resuspended tracers as a function of respirable particle diameters. Sampling was started on the same day the tracer was deposited and was continued periodically for 566 hr from October 2 to November 4. Samplers were deactivated during precipitation conditions. Wind speed charts at the resuspension site have not yet been read. At the 50-ft level of the meteorological tower during resuspension the average hourly wind speed was 6.4 mph; maximum hourly average was 16.5 mph; and the maximum peak gust was 45 mph. At the end of the experiment filters were weighed to determine the mass of collected material at each stage. Afterwards the filters were leached to remove the molybdenum tracer and the leach solutions analyzed by X-ray fluorescence for molybdenum.

CALCULATION

A tracer resuspension rate was calculated from a mass balance extending to the top sampler. Although the tracer plume concentration decreased from the lowest sampler to the highest sampler, the plume did extend above the top sampler. The effects of plume noncontainment were disregarded in the mass balance.

Several assumptions were required in the mass balance. Isokinetic sampling was assumed even though the sampling flow rate of 20 cfm corresponds to a wind speed of only 1.2 mph at the cowl inlet. To calculate the airborne molybdenum flux at each sampler height, fluxes were integrated as a function of height to obtain the total airborne tracer. This total tracer was calculated for a vertical area 6 in. wide (corresponding to the cowl inlet diameter) and 20 ft high. Similarly the tracer ground source for calculating the resuspension rate was a 6-in. wide by 75-ft long tracer area.

RESULTS

The resuspension rate was 1.2×10^{-10} fraction removed/sec, which is less than the 5×10^{-9} to 6×10^{-7}

fraction removed/sec reported for the resuspension of ZnS from an asphalt surface.(3)

In comparison, the decreased resuspension rate of calcium molybdate on soils is reasonable due to differences in surface properties between soils and asphalt. The actual resuspension rate for calcium molybdate should not be above an order of magnitude greater than that reported if wind speed corrections were made rather than assuming isokinetic flow.

The molybdenum tracer distribution on airborne soil is similar to fissile particle distribution on airborne soils at Rocky Flats.(4) In Table 1 are shown the g Mo/g airborne soil as a function of impactor stage 50% cut-off diameter and sampling elevation. Even though the original tracer was submicrometer in diameter, the tracer has attached to all airborne host soil particles of all diameters. As expected, the largest tracer concentration on the airborne soil was at the lowest sampling height. At higher elevation an increasingly greater portion of the airborne soil comes from outside the tracer source area.

This experiment demonstrated that the calcium molybdate produces a reasonable simulant for the plutonium airborne from contaminated soil at Rocky Flats. This conclusion derives from the similarity between the distribution of the tracer among soil particles of various sizes and that of fissile material among like airborne particles. Tracer resuspension rates are being measured to determine the resuspension decrease with weathering time and the resuspension rate dependency upon wind speed.

TABLE 1. Molybdenum Airborne Distribution on Soil (g Mo/g Soil) × 10^5

Sampling Elevation, ft	Impactor State 50% Cutoff Diameter, μm				
	7	3.3	2.0	1.1	Backup Filter
1	8.25	11.3	11.9	9.33	4.41
3	2.39	2.20	2.17	2.42	2.12
6	1.95	1.20	*	0.518	0.860
10	1.64	*	0.211	4.75	3.08
20	0.598	0.753	2.32	0.272	0.170

* Missing Data

RESUSPENSION BY WIND AT ROCKY FLATS

G. A. Sehmel and F. D. Lloyd

A field experiment at Rocky Flats was conducted to initially determine plutonium air concentration dependency upon wind speed and sampling height and to determine the respirable particle size distribution and subsequently to determine plutonium resuspension rates from ground source samples concurrently collected by HASL. Radiochemical plutonium analyses for filter samples are awaited from DOW at Rocky Flats. Airborne soil size distributions indicate that airborne concentrations of respirable soil particles increase proportionately with the wind speed to the 4th to 6th power.

INTRODUCTION

This particle resuspension research program is directed towards developing a general model or models for predicting particle resuspension from all environments such as arid regions, forests, urban areas, etc., which might in the future become resuspension sites of concern. Much of this research is conducted using controlled inert tracers to simulate radioactive contaminants.[5] Nevertheless, it has been useful in model development to use data from Rocky Flats where actual contamination is measurable above fallout levels.

In our model development we have been analyzing the reported airborne plutonium concentrations and meteorology at Rocky Flats. Initial resuspension modeling efforts[6] based upon the Health and Safety Laboratory's weekly data at sampling station S8 have demonstrated dependence of airborne plutonium concentrations on wind speed and direction. Model predictions indicate that during the weekly sampling period from July 1970 to January 1971 the average airborne plutonium concentration during each hour increased with wind speed to the 2.1 power. Since that time[7] mechanical activities such as ditch digging have apparently altered source characteristics, making existing data unsuitable for extending that model development. For model development additional direct measurement of airborne plutonium concentration was needed under conditions of controlled mechanical activities together with wind data and observations of surface conditions. It was also important to determine the airborne plutonium as a function of airborne particle diameter and as a function of sampling height.

The objectives of this Rocky Flats resuspension experiment were to determine the vertical airborne plutonium and soil concentrations and particle size distributions of plutonium and the associated soil at three sampling sites and to relate these measurements to meteorological conditions and surface contamination.

EXPERIMENTS

In a July 1973 field experiment at Rocky Flats, vertical airborne plutonium concentrations and particle size distributions were determined at three sampling sites. These sites are schematically shown in Figure 2. Particulate air samplers mounted on towers were either high-volume air samplers[8] (8 in. by 10-in. filters) sampling at 1.4 m^3/min or were cascade impactor-cowl[9] systems.[1,2] The cascade systems had the sampler inlet continuously directed into the wind. Site A, along the eastern security fence, employed several high-volume cascade impactor-cowl systems mounted vertically on a utility pole. Site AB was between the eastern security fence and the cattle fence. At this site, a 100-ft meteorological tower was erected and was instrumented at several heights with wind speed and wind direction sensors and high-volume cascade impactor-cowl systems. Wind speed instrumentation activated selected impactor-cowl systems as a function of wind speed. Plutonium concentration and particle size distribution were measured as a function of both height and wind speed. Site B, near the cattle fence, used several high-volume cascade impactor-cowl systems mounted on a 45-ft pole.

Samplers at Site A were designed to operate continuously during the experiment and consisted of three sub-sites. Sub-site A2 and A3 were located on utility poles at indicated spacings of 61 m and 30 m. Since our earlier analysis[6] suggested that the maximum airborne plutonium concentration might be S to SW of any routine sampling station, Stations A2

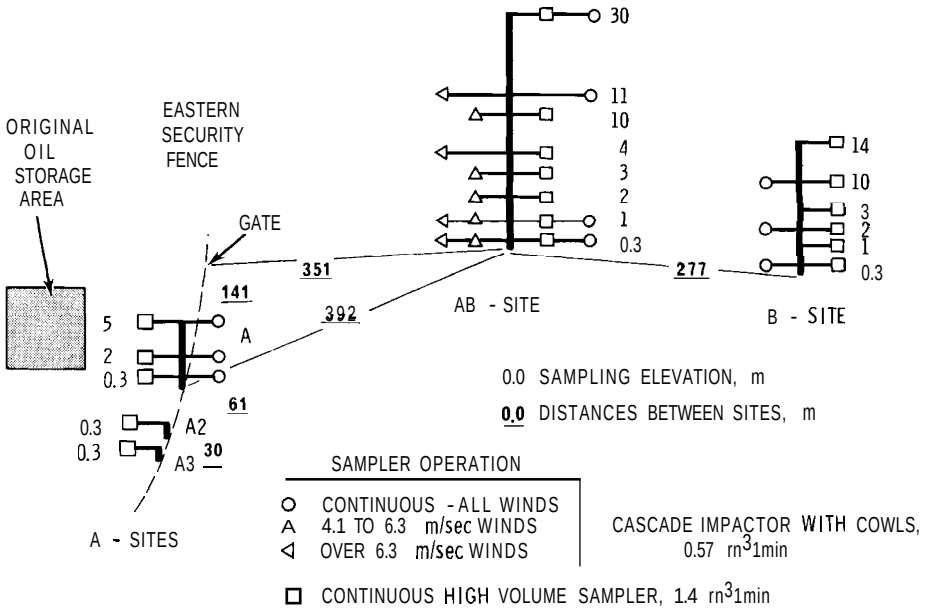

Neg 740044-9

FIGURE 2. Schematic of Rocky Flats Resuspension Tower Locations

and especially A3 were located so as to determine a maximum concentration at a constant elevation above ground.

Air samples were located as a function of height at Sites A, AB, and B, to grossly estimate the total airborne plutonium flux at each site and to determine the change in total flux with distance. At Sites A and B these fluxes were to be determined from impactor systems operating continuously for all wind speeds. In contrast the impactor systems at Site AB were activated as a function of wind speed in an attempt to determine the increased airborne plutonium activity with an increase in wind speed. One impactor system sampled continuously, the second for wind speeds between 4.1 and 6.3 m/sec at the 1-m height, and the third for wind speeds greater than 6.3 m/sec. These final selections of wind speed set points were selected based upon wind experienced while setting up equipment and also based upon the July wind speeds recorded for previous years. The 4.1 m/sec corresponded (1) to the initiation of surface creep for the open ground at Site AB and (2) to a wind speed of about 8 to 9 m/sec at 6.8 m elevation.

For comparison to airborne activity at the three plant sites, a background sampling site was also operated continuously from 1540 on July 18 to 0600 on August 2. The site was 8 miles into the mountains in the Cold Creek Valley at an elevation of 8100 ft. Elevations at Sites A, AB, and B were about 5900 to 5950 ft. The background sampler was a cascade impactor mounted on the roof of a house in a forest. The sampler was about 20 ft above ground in a forest about 30 ft tall.

RESULTS AND DISCUSSION

Rain Damaged Filters

There were two purposes in having both 8 × 10-in. continuous high-volume (1.4 m^3/min) sampler and impactor-cowl systems at each sampling height. Primarily the 8 × 10-in. samplers were to be analyzed to ascertain the presence of sufficient airborne plutonium on each impactor stage for radiochemical analytical results above background. The second purpose was to determine the decreased apparent airborne plutonium concentration or anisokinetic sampling error caused by the 8 × 10-in. samplers being rigidly fixed and not continuously facing into the wind.

After the first few days of the experiment heavy rains precluded the completely successful accomplishment of these purposes. A rainstorm on Sunday July 15 severely abraded the 8 × 10-in. glass fiber filters in the continuous high-volume samplers. In some cases only partial filters were left while in all cases rain appeared to have partially washed collected material from the filters. This rain damage precluded a comparison between collection in the 8 × 10-in. samplers and undamaged impactor-cowl systems. Subsequently adequate rain protectors and new 8 × 10-in. filters were installed.

However, rain damage turned out to be beneficial by forcing reassessment of the chemistry and improved recovery.

When filters were analyzed for plutonium by Rocky Flats personnel, the recovery of ^{236}Pu tracer used in the radiochemical analyses was less than 10%. The improved radiochemical technique will be used by Rocky Flats personnel for analyzing all other filter samples. Radiochemical analyses of these filters is only now beginning.

Analytical results and airborne concentrations from these rain damaged filters are shown in Table 2. Counting statistics show a wide range of uncertainty. Nevertheless, average airborne ^{239}Pu concentrations range from no detectable activity up to 8.5 fCi/m^3. In general, airborne activity decreases with both distance and sampling height. Since sampling times at Sites A, AB, and B were only 10.5, 96, and 52.3 hr, these data are interpreted to suggest that all succeeding filters can be satisfactorily analyzed with the improved radiochemical technique. The technique to be used is total dissolution, followed by chemical separation steps, electrodeposition, and alpha spectroscopy.

Wind Speed Dependency

Some fissile particle data and airborne particle size distributions have been obtained from filters collected by automatic sampling as a function of wind speed at Site AB. During the total time period from 1900 July 7 to 1315 July 31, the continuous impactor-cowl systems were activated for 15.2 days; 13.5 hr for 4.1 to 6.3 m/sec winds; and 38.3 min for winds greater than 6.3 m/sec. During the total time period, samplers were deactivated between 1900

TABLE 2. Airborne Plutonium Concentrations from Rain Damaged 8 × 10-in. Air Sampling Filters at Rocky Flats Ending July 15, 1973

Sampling Elevation, m	^{239}Pu DPM on Filter*			Airborne ^{239}Pu Concentration, fCi/m^3		
	Site A	Site AB	Site B	Site A	Site AB	Site B
30		NDA			NDA	
14			0.17 ± 140%			0.017
10		0.99 ± 36%	0.27 ± 200%		0.054	0.027
5	0.1 ± 88%			0.05		
4	NDA	NDA		NDA	NDA	
2		0.27 ± 140%			0.015	
1		NDA	0.3 ± 200%		NDA	0.03
0.3	17 ± 24%	2.1 ± 54%	0.65 ± 14%	8.5	0.11	0.065

NDA - No Detectable Activity
* ^{236}Pu Recovery was <10%

July 15 and 0830 the next morning due to a power outage and between July 21 and 24 because of predicted poor weather. Rain fell on 12 days during the experiment for a total precipitation of 1.5 in.

Fissile Particles

A 1 × 3-in. section of each filter was removed for sizing individual particles of fissile material. The fissile material could be either ^{239}Pu or ^{235}U. For analysis[10] a polycarbonate film was placed in contact with a filter section and the composite irradiated with neutrons. After irradiation, the film was etched to develop tracks from the fissions. The tracks were converted to equivalent PuO_2 particles with a minimum detectable particle diameter of 0.06 μm. The maximum observed particle diameter was 0.25 μm.

This sizing technique measures particles only on the top surface of the filter and particles which are not covered by dirt. Since some fissile particles probably do not satisfy these criteria, the reported total fissile particles concentration may be too low.

Airborne concentrations of fissile material are shown in Table 3 as a function of sampling elevation and sampling collection by either total high-volume filter collection or by particle sizing with cascade impactors. The impactor data are shown (1) as a function of particle diameter corresponding to the 50% cut-off diameter for unit density spheres; (2) as a function of total impactor collection; and (3) as a function of

TABLE 3. Particles of Fissile Material/m^3 Air at Rocky Flats During July 1973 (all individual fissile particles were <0.25 μm diam if PuO_2)

Sampling Elevation, m	Fissile Particles/m^3 Concentration as Function of Impactor Collection Stage (50% Cutoff Diameter, Unit Density)																				
	Total Sample				7 μm			3.3 μm			2.0 μm			1.1 μm			Backup Filter			
	Hi-Vol	Impactor Totals All	4-6	6+	All	4-6	6+	All	4-6	6+	All	4-6	6+	All	4-6	6+	All	4-6	6+	
30	1.76	3.34			1.589			0.885			0.402			0.329			0.137			
11		1.3+			0.771			0.624												
10	2.17																			
4	2.63																			
3		4.47			1.43			0.831			0.818			0.623			0.761			
2	2.06																			
	1.84		5+		1.72			1.64			1.01			1.40					5.36	
0.3	1.92		59.5	1601		20.3	288		13.8	192		9.26	150		8.90	771		7.28		200
House in Mountains																	1.28			

\+ Incomplete Data

All - Continuous Sampling with Impactor-Cowl System
4-6 - Air Sampling Between 4.1 to 6.3 m/sec Wind with Impactor-Cowl System
6+ - Air Sampling Over 6.3 m/sec Wind with Impactor-Cowl System
Hi-Vol - Continuous Sampling with a High-Volume Air Sampler Pointed into Winds Coming Across the Original Oil Storage Area

wind speed during collection. The term ALL refers to continuous sampling; 4-6 for sampling wind speeds from 4.1 to 6.3 m/sec; and 6+ for sampling wind speeds greater than 6.3 m/sec.

Fissile particles were collected on each impactor stage and all observed particles were less than 0.25 μm diam. The analytical technique used did not determine if these submicrometer fissile particles were attached to larger host particles.

Airborne concentrations ranged from 1 to 1601 particles/m^3. The lower values from 1.0 to 4.47 particles/m^3 correspond to time averaged concentrations for all wind speeds. As wind speed is increased, the concentration increases to 5 to 59.5 particles/m^3 for wind speeds from 4.1 to 6.3 m/sec and to 1601 particles/m^3 for wind speeds greater than 6.3 m/sec. Based upon data received, the concentrations appear to show only minor changes with sampling elevation. The most significant result is that airborne concentration increases rapidly with increases in wind speed.

The concentration of 1.28 particles/m^3 determined from the back-up filter of the impactor at the house in the mountains is similar in magnitude to the concentrations shown for the total samples at Site AB. Since only fallout plutonium concentrations should be in the mountains, this similarity in fissile particles/m^3 must indicate that most of the fissile material observed by the fission track technique is crustal uranium rather than plutonium. Radiochemical analysis of the filters for plutonium should identify the fissile material. These analyses are still in progress.

Fissile particles on each filter have been normalized to increased filter weight during sampling. In Table 4, fissile particles/g airborne

TABLE 4. Particles of Fissile Material/g Airborne Material at Rocky Flats During July 1973 (all individual fissile particles were <0.25 μm diam if PuO_2)

	(Fissile Particles/g Airborne Material) × 10^{-5}																			
	Total Sample				Airborne Material Contamination as a Function of Impactor Collection State (50% Cutoff Diameter, Unit Density)															
		Impactor Totals			7 μm			3.3 μm			2.0 μm			1.1 μm			Backup Filter			
Sampling Elevation, m	Hi-Vol	All	4-6	6+	All	6-6	6+	All	4-6	6+	All	4-6	6+	All	4-6	6+	All	4-6	6+
30	1.61	1.16			2.10			2.06			1.14			1.45			0.124		
11					0.871			1.41											
10	1.25																		
4	1.41																		
3					1.70			1.88			2.98			1.85			0.726		
2	1.06																		
1	0.922				1.62			3.77			2.32			3.38				1.93	
0.3	0.722		1.65	3.20		2.78	3.11		2.12	1.94		1.28	1.54		1.17	8.54		0.976	2.12
House in Mountains																	1.99		

+ Incomplete Data

All - Continuous Sampling With Impactor-Cowl System
4-6 - Air Sampling Between 4.1 to 6.3 m/sec Wind With Impactor-Cowl System
6+ - Air Sampling Over 6.3 m/sec Wind With Impactor-Cowl System
Hi-Vol - Continuous Sampling With a High-Volume Air Sampler Pointed Into Winds Coming Across the Original Oil Storage Area

materials are shown as a function of wind speed, particle size, and sampling elevation in a manner similar to Table 3 for fissile particles/m^3. In this case the range is from 0.7 to 3.2 × 10^5 particles/g at site AB. In comparison, the concentration of 1.99 × 10^5 particles/g at the mountain house is similar and tends to confirm that the fission track technique is counting principally crustal uranium rather than plutonium.

Airborne Particle Size Distribution

Changes in airborne size distributions as a function of wind speed were determined from filter weight gains from site AB impactor-cowl systems. These size distributions are shown in Figure 3, based upon impactor 50% cut-off diameters of 0.78, 1.4, 2.3, and 5.0 μm, corresponding to a particle density of 2 g/cm^3. This density is used since larger particles collected in the cowls attached to the impactors were sized as a function of sieve size rather than aerodynamic size. Also shown are line A and line B which were determined[11] from tower sampling at Hanford. Size distributions from impactor systems are similar for continuous sampling at both Hanford and Rocky Flats since the data approximate line A. Changes in size distributions as a function of height are not readily apparent. In fact, a few data points overlapped and are indistinguishable in the graphical representation.

Particle size distribution dependency for low wind speeds was estimated by drawing lines with the same

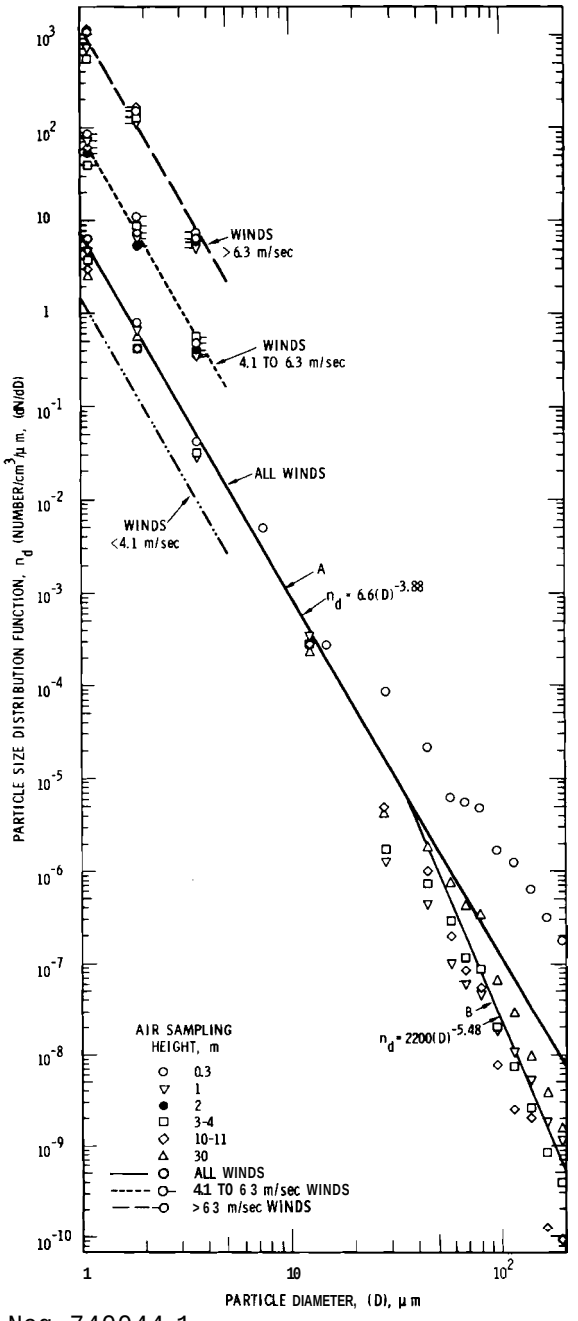

Neg 740044-1

FIGURE 3. Airborne Particle Size Distributions at Rocky Flats During July 1973

slope as line A through the data for 4.1 to 6.3 m/sec wind speed sampling and a second line for greater than 6.3 m/sec wind speed sampling. Since these data appear to exhibit

approximately the same slope dependency, these two lines were used to adjust line A to predict the size distribution for wind speeds less than 4.1 m/sec. Sampling times at each of the wind speed increments were used to make the adjustment. The calculated line for wind speeds less than 4.1 m/sec is significantly lower than the all-wind line.

The size distribution function increases rapidly with an increase in wind speed. However, assumptions must be made to determine the dependency. Arbitrary but realistic assumptions. are that the high winds were between 6.3 and 11 m/sec and that the calculated line is for wind speeds between 2 and 4.1 m/sec. Based upon these assumptions, the particle size distribution increases approximately as the 4 to 6 power of wind speed. Direct measurements with optical particle counters are planned to more adequately quantify this wind speed dependency.

Size distributions for particle diameters greater than respirable are also shown in Figure 3. These data were calculated using particles collected in self-orientating wind direction-sensitive cowls attached to the impactors. Particles were removed from the cowls and sized using sieves. Data are plotted at the sieve sizes. Concentrations were calculated assuming isokinetic sampling. For the 0.3-m height, the distribution is largest and may be partially attributed to dirt collected by rain splash. For higher elevations, the data approximate line B, which was determined for continuous sampling at Hanford.

Plutonium Concentration Prediction

Calculation of airborne plutonium concentrations as a function of wind speed and particle diameter will be completed when radiochemical analyses are received. Nevertheless, the size distribution data can be used as a basis of speculation. If the plutonium were uniformly distributed on all host soil particle diameters, plutonium resuspension rates would also increase as the 4 to 6th power of wind speed. However, if plutonium, while on the soil, is in the fine sand (>50 μm diam) and silt (2 to 50 μm diam) rather than the clay fraction (<2 μm diam), overall plutonium resuspension rates for all particle diameters would not increase so rapidly as do the respirable sized particles as a function of wind speed.

Results from this study will be used to determine resuspension rates from published data and HASL's concurrent experiment for determining ground concentrations and size distributions of plutonium.[12] Most of the analysis will depend upon the plutonium radiochemical analyses which are in process.

ACKNOWLEDGMENTS

The authors wish to acknowledge the the inter-laboratory cooperation for the experiment. Dow Chemical, Rocky Flats Division, through Don Nickels, supplied required field support, determined soil moisture, and is doing the radiochemical analysis and through John Hayden is doing the fission track sizing.

RESUSPENSION SOURCE CHANGE AT ROCKY FLATS

G. A. Sehrnel and M. M. Orgill

The plutonium resuspension model developed for sampling station S-8 was used to predict resuspension for the time period following the model data base time period. Observed airborne plutonium concentrations being greater than predicted is attributed to changes in source characteristics caused by soil disturbance.

INTRODUCTION

Wind stresses are resuspending plutonium at Rocky Flats and are producing local airborne plutonium concentrations which are above fallout levels but below MPC_{air} concentrations. Despite low activity levels and smoothing of variability in airborne concentrations caused by sampling over relatively long time periods, the reported weekly data at sampling station S-8 were useful in defining some dependency of plutonium resuspension on meteorological parameters.

Previously in developing the model,[13] the total plutonium collected on a filter was determined to be a function of time duration at each wind speed during the sampling period. The model was developed so that the airborne plutonium concentration caused by each hour of wind could be predicted and the effect of all hours summed in order to predict the total filter collection during the filter sampling time.

The model predicts that at station S-8 near the original oil storage area during July 1970 to January 1971 the total activity in each hourly time period was

$$fCi/m^3 = FO + 0.3 + 0.45\ (mph)^{2.1},$$

in which FO is the plutonium fallout activity in fCi/m^3 during the time period and the constant 0.3 fCi/m^3 is the plutonium activity which cannot be attributed to W and SW winds. Fallout and local activity concentrations were usually insignificant compared to contributions from high wind speeds. The model predicts that hourly average concentrations can be much higher than weekly average concentrations.

SOURCE CHANGE

The model was used to predict plutonium collection on station S-8 filters for the succeeding time period from February 1971 to November 1972. In this time period filter samples were analyzed on a monthly rather than weekly basis. Predicted and measured total plutonium collections on each filter are shown in Figure 4 along with concentrations, temperature, and precipitation. Reasonable

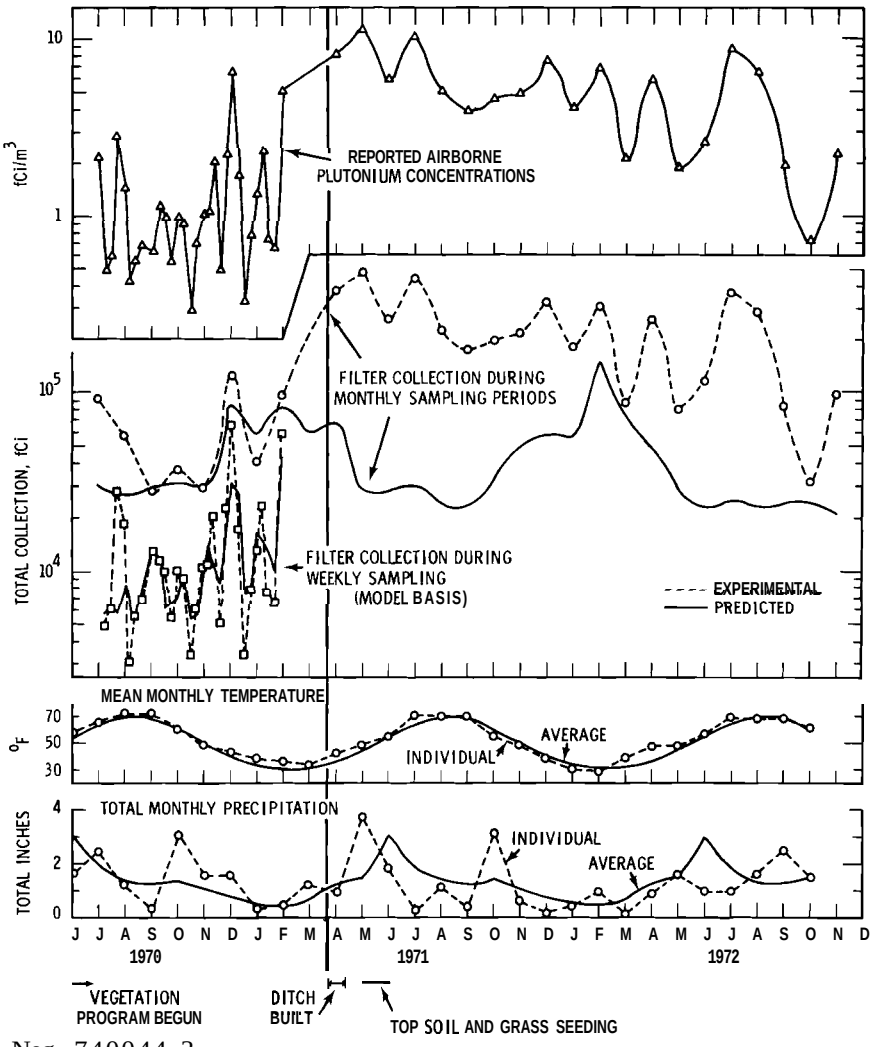

Neg 740044-3

FIGURE 4. Airborne Plutonium at Sampling Station S-8

agreement in total collection is shown for the July 1970 to January 1971 weekly data, but agreement is not shown for the March 1971 to November 1972 monthly collection. The data are plotted at the end of each sampling period.

Measured plutonium collection is much greater than the model predicted. This increased airborne activity is explained on the basis of vehicular and construction activity disturbing the weathered plutonium source. In mid-March 1971 a ditch was dug east of the original oil storage area and west of sampling station S-8. This time period corresponds to the time period within which airborne activity increased significantly. Unfortunately there is no data for March 1, 1971. Nevertheless, we conclude that digging the ditch and disturbing the soil surface resulted in a more readily resuspended source of plutonium. A similar increased resuspension appears to have occurred during June 1970 when a vegetation program was begun to limit resuspension. The monthly total plutonium collection was relatively high compared to

the decreased collection in the succeeding weeks. Based upon these two instances, the conclusion is that any soil surface disturbance will increase the subsequent plutonium resuspension rates.

Resuspension rates after soil disturbance appear to be a function of the type of soil disturbance. Subsequent to the June 1970 vegetation program, the increased vegetation cover appears to have rapidly decreased the availability for plutonium resuspension. In contrast, ditch digging significantly increased the availability of plutonium for resuspension. In this latter case the average weathering half-life for decreasing airborne concentration from April 1971 to October 1972 is about 9 months (based upon concentration decrease and disregarding wind variations).

REGIONAL WIND RESUSPENSION OF DUST

M. M. Orgill, G. A. Sehmel and T. J. Bander

Particle wind resuspension is important in planning and operation in the nuclear power industry. To obtain a better understanding of the frequency, duration and occurrence of wind resuspension (dusty) periods on a regional scale, we are determining, from hourly meteorological observations, the frequency of dusty periods throughout the country. Dust storm criteria are being initially defined and tested for this study using the hourly weather observations from the Hanford Area.

INTRODUCTION

Future nuclear power reactors, chemical separation and fuel enrichment plants may be located in a number of different climatic regions where wind resuspension of radioactive materials may be possible. These could be urban, forested, agricultural, desert and range-land sites. For planning and operation, it is important to know the frequency, duration and intensity of wind resuspension periods for these new sites, as well as for existing operational sites. In addition, we are now examining wind resuspension information valuable for designing experiments and studying the physical mechanisms for resuspension in nonarid regions. Consequently the purpose of this study is to determine from literature and meteorological data the natural wind-caused airborne dust loadings over the country.

There are two principal methods for examining existing data which can be used to determine regional wind

resuspension. The first requires examination of actual airborne particulate-concentration data from national and local air pollution sampling stations during wind resuspension periods. The second utilizes the National Weather Service reporting observations of dust and visibility to infer the approximate frequency and dust loadings for resuspension periods.

METHOD

Hagen and Woodruff[14] have used the second method for studying the frequency and particulate concentrations of dust storms for the Great Plains region. Particulate concentrations were estimated by using the hourly visibility observations and an experimental relationship between observed dust concentration at 6 ft above the surface and observed visibility. The relationship is

$$C_6 = \frac{56}{V^{1.25}} \ [mg/m^3], \qquad (1)$$

where V is horizontal visibility in km. A nearly identical theoretical visibility-concentration relationship can be derived by assuming (1) airborne particles of uniform size, (2) constant scattering-area coefficient, and (3) visibility extinction is caused only by scattering. In this case,

$$C = \frac{57.2}{V} \ [mg/m^3]. \qquad (2)$$

Hagen and Woodruff estimated particulate concentrations by using hourly visibility observations and equation (1). One serious limitation of this method is that visibility restrictions such as dust are not reported on hourly observations when the visibility is 7 miles or greater. In this case Hagen and Woodruff assumed that dust was the visibility restriction on days when the visibility ranged from 7 to 9 miles and the wind speed exceeded 5.4 ms^{-1} (12 mph).

The visibility method was selected for initial regional examination of dusty periods for two reasons: (1) the Kansas agricultural research group had shown that the visibility method could be used to define dusty periods, and (2) examination of particulate sampling data from several stations throughout the country would be a very large task to complete in a relatively short time. Therefore hourly weather observations for each day that dust or blowing dust was reported will be obtained from the National Climatic Center for 24-hr weather stations in the country and will be analyzed. Generally, a 10 to 15-year period will be used in this study.

HANFORD ANALYSIS

To establish initial criteria for defining a wind resuspension period or duststorm, the 24-hr weather data for Hanford are being analyzed on a test basis for 17 years (1953-1970). Different combinations of visibility, wind speed and relative humidity have been investigated to define the optimum criteria for a dust storm. Unfortunately the range of criteria available for study is limited because of

the inherent limitations of the hourly weather observations. Nevertheless, the following criteria appear to give the best definition of a wind resuspension or dust storm period based on the Hanford data. These are:

1. Visibility less than 7 miles and dust, blowing dust or sand reported.
2. Visibility 7 to 14 miles, wind speed greater than 5.8 ms^{-1} (13 mph) and relative humidity less than 70%. Dust is assumed.

To assure that all relevant observations associated with a dusty period were not missed, certain additional criteria were established to include beginnings and endings of storms. These other limiting criteria were also necessary to exclude unwanted observations associated with smoke, fog and precipitation. A preliminary error analysis of the Hanford data showed that the calculated frequency of dusty periods based on these criteria may be 2 to 3% too high because of a few non-dusty time periods meeting the above criteria.

During the Hanford data analysis it was apparent that a significant number of hours would meet the wind speed and relative humidity criteria but that the visibility would be 15 miles or greater. In such situations dust could be present (as indicated in the Remarks column of the hourly weather observations) or not present, depending upon other factors such as state of ground and precipitation.

Since the potential for wind resuspension is still present under such conditions, these events should be taken into account. We are presently analyzing these data for Hanford to ascertain the best way to incorporate this type of observation into the regional study. In addition, analysis of these data will also assist in obtaining a better understanding of the physical mechanisms and meteorological history of local wind resuspension.

RESULTS

Results of this study to date are based on the Hanford data. Table 5 presents a summary of some of the dust parameters for the total period of 1953-1970.

TABLE 5. Frequency of Wind Resuspension Periods by Hanford (1953-1970)

Total Dust Hours	476
Total Dust Days	142
Number of Dust Storms	150
Average Dust Hr/Yr	26.4
Average Dust Days/Yr	7.9
Average Dust Storms per Year	8.3
Range in Duration of Dust Storms (hr)	1-16
Average Duration of Dust Storms (hr)	3.2

Hours of dust occurrence, average visibility, and estimated average dust concentration (Eq. 1) as a function of wind direction and speed are presented in Tables 6, 7 and 8.

Tentative conclusions based on these results are:

1. The distribution of hours of occurrence of dust was bimodal with the highest number of hours

TABLE 6. Hours Satisfying Dust Storm Criteria at Hanford 1953-1970

HOURS WITH (1) VISIBILITY <7 MILE AND DUST REPORTED OR (2) VISIBILITY 7 TO 14 MILES. WINDSPEED >5.8 MISEC; RH< 70%; DUST ASSUMED

WIND DIRECTION	WIND SPEED CLASS (MPH) 1-3	4-7	8-12	13-18	19-24	25-31	32-38	39-46	47-54	55-63	64-UP	TOTAL HOURS
SE	0	0	0	0	0	0	0	0	0	0	0	0
SSE	0	0	0	1	1	1	0	0	0	0	0	3
S	0	0	1	3	1	3	3	0	0	0	0	11
SSW	0	0	0	4	3	11	13	2	0	0	0	33
SW	0	0	1	3	13	24	26	6	0	1	0	74
WSW	0	0	1	7	17	39	13	4	0	0	0	81
W	0	1	1	3	5	7	1	0	0	0	0	18
WNW	0	0	5	5	11	6	1	1	0	0	0	29
NW	0	1	6	4	3	5	2	0	0	0	0	21
NNW	0	2	8	6	2	0	0	0	0	0	0	18
N	0	1	12	34	10	1	0	0	0	0	0	58
NNE	0	1	3	31	23	7	1	0	0	0	0	66
NE	0	2	3	19	15	5	0	0	0	0	0	44
ENE	0	0	0	3	6	0	0	0	0	0	0	9
E	0	0	1	6	2	1	0	0	0	0	0	10
ESE	0	1	0	0	0	0	0	0	0	0	0	1
TOTAL HOURS	0	9	42	129	112	110	60	13	0	1	0	476

Neg 740679-6

TABLE 7. Visibility Dependency on Wind Speed and Direction at Hanford, 1953-1970

WIND DIRECTION	AVERAGE VISIBILITY, MILES WIND SPEED CLASS (MPH) 1-3	4-7	8-12	13-18	19-24	25-31	32-38	39-46	47-54	55-63	64-UP	OVERALL AVERAGE
SE	.00	.00	.00	.00	.00	.00	.00	.00	.00	.00	.00	.00
SSE	.00	.00	.00	7.00	12.00	13.00	.00	.00	.00	.00	.00	10.67
S	.00	.00	3.00	10.67	12.00	7.00	6.92	.00	.00	.00	.00	8.07
SSW	.00	.00	.00	8.25	10.67	9.09	7.08	5.00	.00	.MI	.00	8.09
SW	.00	.00	7.00	7.25	9.40	8.88	5.79	4.50	.00	.06	.00	7.32
WSW	.00	.00	10.00	10.29	8.04	7.51	6.05	4.06		.00	.00	7.49
W	.00	10.00	10.00	10.33	8.20	5.64	7.00	.00	.00	.00	.00	7.69
WNW	.00	.00	6.60	8.40	10.27	10.17	6.00	5.00	.00	.00	.00	8.97
NW	.00	6.00	9.67	9.00	11.33	9.60	8.50	.00	.00	.00	.00	9.48
NNW	.MI	9.00	8.25	9.17	4.50	.00	.00	.00	.00	.00	.00	8.22
N	.00	6.00	7.58	7.94	5.10	2.00	.00	.00	.00	.00	.00	7.24
NNE	.00	10.00	6.00	7.95	6.91	5.73	3.00	.00	.00	.00	.00	7.22
NE	.00	5.00	6.83	9.17	7.27	7.60	.00	.00	.00	.00	.00	7.99
ENE	.00	.00	.00	8.00	8.83	.00	.00	.00	.00	.00	.00	8.56
E	.00	.00	6.00	9.33	7.00	7.00	.00	.MI	.00	.00	.00	8.30
ESE	.00	7.00	.00	.00	.00	.00	.00	.00	.00	.00	.00	7.00
OVERALL AVERAGE	.00	7.44	7.68	8.53	8.02	7.96	6.25	4.48	.00	.06	.00	7.77

.00 NO DATA

Neg 740679-5

TABLE 8. Dust Concentration Dependency on Wind Speed and Direction at Hanford, 1953-1970

WIND DIRECTION	PREDICTED CONCENTRATION FROM VISIBILITY, mg/m^3 WIND SPEED CLASS (MPH 1-3	4-7	18-12	13-18	19-24	25-31	32-38	39-46	47-54	55-63	64-UP	OVERALL AVERAGE
SE	.00	.OO	.00	.00	.00	.OO	.00	.00	.00	.00	.00	.00
SSE	.00	.00	.00	2.71	1.38	1.25	.00	.00	.00	.00	.00	1.78
S	.00	.OO	7.83	1.62	1.38	5.70	15.92	.00	.00	.00	.00	7.17
SSW	.00	.OO	.00	2.48	1.62	2.21	3.86	4.13	.00	.00	.00	2.95
SW	.00	.OO	2.71	6.34	3.54	2.75	8.83	13.87	.00	988.88*	.00	19.40
WSW	.00	.00	1.74	1.81	4.96	4.13	12.95	48.31	.00	.00	.00	7.67
W	.00	1.74	1.74	1 .	2.89	5.37	2.71	.00	.00	.00	.00	3.54
WNW	.00	.OO	3.49	2.64	1.77	1.99	3.29	4.13	.00	.00	.00	2.39
NW	.00	3.29	1.88	2.58	1.50	1.98	2.23	.00	.00	00	.00	2.08
NNW	.00	2.02	2M)	2.58	4.80	.00	.00	.00	.00	.00	.00	2.77
N	.00	3.29	2.92	3.50	5.06	12.99	.00	.00	.00	.00	.00	3.81
NNE	.00	1.74	3.38	3.41	6.08	7.M	7.83	.00	.00	.00	.00	4.77
NE	.00	4.38	4.60	3.38	4.54	2.81	.00	.00	.00	..00	.00	3.84
ENE	.00	.00	.00	3.05	2.19	.00	.00	.00	.00	.00	.00	2.48
E	.00	.00	3.29	2.44	3.60	2.71	.00	.00	.00	.00	.00	2.78
ESE	.00	2.71	.00	.00	.00	.00	.00	.00	.00	.00	.00	2.71
OVERALL AVERAGE	.00	2.84	3.00	3.15	4.15	3.71	8.57	22.22	.00	988.88	.00	6.77

.00 NO DATA
* VISIBILITY 0 TO 1116 MILE DUE TO ONE-HOUR DUSTSTORM

Neg. 740679-4

distributed between the southwest and north sectors. The dust source in the southwest sector evidently requires a higher wind speed threshold than the north sector (Table 6). Dust from the north sector originates, for the most part, offsite and occurs with lighter winds.

2. Average dust storm visibility was 8 miles but decreased to 7 miles with southwesterly and northerly winds. Generally, average visibility decreased with increasing wind speed (Table 7).
3. Average dust concentration during dusty periods was approximately 7 mg/m^3. Average dust concentration, during periods of southwest winds above 30 mph, exceeded the overall average from 2 to 100 times (Table 8).

These results appear to give a fairly accurate tabulation of significant wind resuspension periods for the Hanford area when compared with other local climatological records.[15] A separate report will consider the details of the Hanford analysis.

In the future we will obtain from the National Climatic Center hourly weather observations of wind resuspension periods for several weather stations in the State of Washington. This will provide an opportunity to analyze the frequency of dusty periods for more than one station in

our local area before proceeding to analyze observations from weather stations in other regions of the country. Once the overall analysis is completed, maps of wind resuspension frequency, duration, and dust concentration, etc., will be prepared for the whole country.

INTERSTAGE PARTICLE LOSSES IN A HIGH-VOLUME CASCADE IMPACTOR

G. A. Sehmel

Commercially available 20-cfm cascade impactors were evaluated under field sampling conditions for particle sampling bias caused by interstage losses. Particles larger than respirable are being deposited throughout the cascade impactor.

INTRODUCTION

Accurate sampling is vital in determining airborne particulate concentrations, airborne particulate size distributions, and particulate pollution composition by subsequent chemical analysis. An important application of sampling is in field studies of particle resuspension research. In this research, wind surface stresses cause soil particles to become airborne. These are subsequently sampled.

When the host soil particles are contaminated by tracers such as radioactive material, the overall removal processes or particle resuspension rates need to be determined. Resuspended particles can be in the respirable size range (less than about 3 μm diam) or can be much larger. This potential hazard can be determined through sampling airborne material without regard for particle size with the assumption that all of the contaminant is associated with the respirable size range. This sampling procedure does give a maximum airborne concentration and consequently the most conservative airborne concentration of radiological assessment. However, sampling is more realistic when airborne concentrations are determined as a function of particle diameter. In this case, the potential inhalation hazard is not only quantified, but information on the basic physics of resuspension is also obtained regarding larger particles. These physical concepts are needed to develop generalized models for predicting resuspension rates.

EXPERIMENT

A sampler system was designed[1] to separate particles into aerodynamic particle diameters in the respirable size range and to simultaneously collect larger airborne

particles. Each particle impactor system was assembled from a 20-cfm Andersen 2000 Inc.* high-volume cascade impactor and a rotating cowl attached to the impactor. These impactors separate particles into nominal diameter ranges of 1.1, 2.0, 3.3, and ≥7 μm which are stage 50% cutoff diameters for unit density spheres. For field resuspension experiments these systems were mounted on towers at heights up to 30 m at sites on the Hanford reservation and a site at the Rocky Flats plant near Boulder, Colorado.

Air and particles entering an impactor are shown schematically in Figure 5. Air flows through the multiple orifices in each support plate. Due to the particle inertia caused by each orifice air jet, successively smaller particles are impacted on the fiberglass filter collectors on each support plate. These collectors are perforated to match the orifice pattern of the succeeding stage. Particles are collected not only at each desired site on the four perforated collectors and back-up filter but also are deposited on the support plate, as is shown by the interstage loss.

For determining interstage losses, each stage collector support plate was brushed to remove most adhering dirt particles. This dirt was collected and weighed to determine the interstage loss for each stage.

Size distributions of the interstage loss particles were determined from twenty impactors used at the Rocky Flats site. Particles were brushed from the impactor surface and combined for each stage. Subsequently these combined particles were sieved through a series of 210, 177, 149, 125, 105, 86, 74, 63, 53, 37, 20, and 10-μm sieves and then weighed. Sieving was done with an Allen Bradley Co., Model L3P sonic sifter.**

* Andersen 2000, Inc., Model 65-100 Hi-Volume Sampling Head, P.O. Box 20769, AMF, Atlanta, Georgia 30320.

** Allen Bradley Co., Model L3P Sonic Sifter, Milwaukee, Wisconsin,

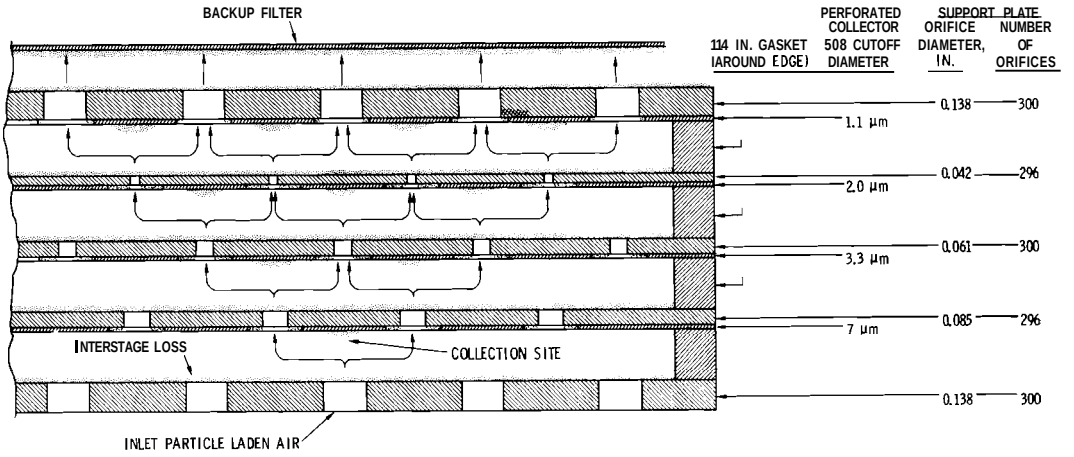

Neg 740044-2

FIGURE 5. Orifice Plate Cascade Impactor, Partial Section

DATA ANALYSIS AND CONCLUSIONS

Interstage loss on each support plate was normalized to the weight on the stage collector making up the downstream surface of the interstage cavity. That is, the loss between each two support plates was divided by the weight found on the perforated collector of that stage. Similarly loss is also reported for the support plate immediately upstream of the 8 × 10-inch back-up filter.

Normalized Interstage Losses

Interstage losses were determined at two Hanford sampling sites and one Rocky Flats sampling site. In Figure 6, losses are shown as a function of the mg of dirt collected on each stage. The different symbols indicate impactor 50% cut-off diameters for unit density spheres. These data confirm that there is no apparent relationship between interstage loss and stage loading. These data show that for other than dust storm conditions, soil particle interstage losses[1] can be expected to be from about 1 to 20%. These soil interstage losses are greater than the 10% or less interstage losses reported[16] for 1-μm diam particles. Interstage losses can be expected to depend on particle diameter.

Interstage Loss Particle Size Distributions

Interstage soil loss particle size distributions were determined for the combined weight loss for twenty impactors used at Rocky Flats. Each sample collected from between two adjacent stages was sized by sieving. Size distributions are shown in Figure 7 for each impactor stage. The average particle size in the interstage loss at each stage is much greater than the physical design should permit to appear at that

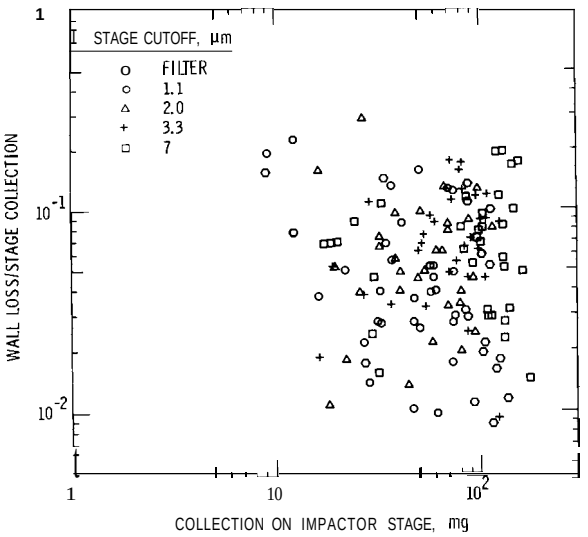

Neg 734648-5

FIGURE 6. Impactor Interstage Losses

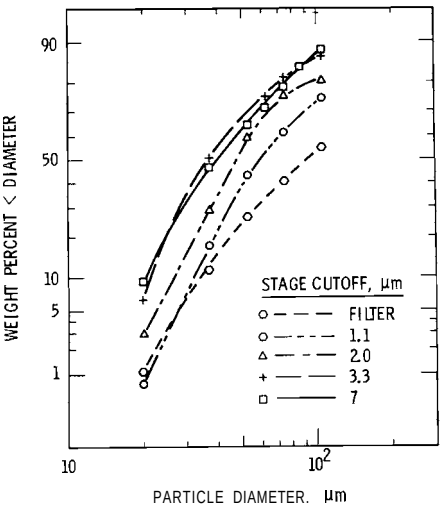

Neg 734648-8

FIGURE 7. Size Distributions for Interstage Loss Particles

stage. The average particle diameter for the first stage is about 40 μm while the average particle size for interstage losses adjacent to the back-up filter is about 90 μm. The brushing techniques used to remove interstage loss particles from support plates might have preferentially removed larger particles for subsequent size analysis. Nevertheless, large particles should not penetrate so deeply through the impactor. Apparently, if larger than respirable particles are not collected on the 7-pm perforated collector, some will bounce and be partially re-entrained all the way through to the back-up filter.

It should also be emphasized these interstage loss particles are much larger than the particle diameter which should deposit on each perforated collector. There is no apparent relationship between interstage particle diameter and stage cut-off diameters. Interstage loss has been normalized to the collector weight at that stage rather than to collector plus interstage loss.

Interstage losses for field experiments are greater than interstage losses for 1-μm particles under laboratory conditions. Nevertheless, realistic field measurments of resuspended radioactive particles can be made with this impactor system. Since laboratory experiments have shown that impactors operate satisfactorily for respirable sized particles, the important question then concerns the effect of larger airborne particles on airborne concentrations and size distributions. If resuspended radioactive particles are in the respirable size range, size distributions from field sampling with a large-volume impactor will probably be comparable to results from laboratory measurements.

However, in application to field sampling, should radioactive contamination on large particles represent an appreciable fraction of the total airborne radioactive material, interstage losses would be very significant. The attendant penetration and deposition of larger particles on stage collectors beyond the first make it appear that the air sampled had a larger number of particles in the respirable size range than actually present. This would always bias the sample conservatively toward assessing the potential respirable particle hazard as greater than actual. Those using or intending to use large-volume impactors are thus cautioned that results may be biased when the impactors are to be used where large particles (>20 μm) are in the stream sampled. This study did not address the important question of the degree to which the stage collector itself collects these larger larger airborne particles. Hence the quantitative significance of errors from this source are as yet unknown and will be a topic for study.

AN ASSESSMENT OF THE LONG-TERM EXPOSURE DUE TO RESUSPENSION

T. W. Horst, J. G. Droppo and C. E. Elderkin

A simple model of the interaction between an airborne pollutant and the underlying surface is postulated which includes the processes of deposition, fixation by the soil, resuspension and redeposition. This model is used to calculate the ratio between the exposure to the resuspended material and the exposure to the primary material. Utilizing current estimates of model parameters, this ratio could range from 5 to 5 × 10^{-4}. In the case where resuspension is locally balanced by redeposition, however, this range is narrowed to 0.5 - 0.05. Horizontal homogeneity is a sufficient condition for this balance to hold true.

At present a special need exists to evaluate potential environmental hazards of plutonium. Resuspension into the air of hazardous material previously deposited on a natural surface is one potentially important pathway for plutonium to enter the human lung. Attempts are currently being made to develop realistic physical models of the resuspension process through computer analysis, controlled experimentation, and careful monitoring of actual surface contamination. However, the measurements are only just beginning to produce the information necessary for model development. Therefore an attempt is made here to utilize the currently available empirical information on resuspension to develop a simple analytic model which fits the observations and which can be extended to the situation of a continuous, trace level release of plutonium to the environment.

OBSERVATIONS

A considerable number of measurements of airborne, resuspended material have been made. In the majority of cases, these have been normalized by the amount of material on the surface presumed to be the resuspension source. This produces the resuspension factor

$$K(m^{-1}) = \frac{\text{Airborne concentration (units/m}^3)}{\text{Surface concentration (units/m}^2)}. \qquad (1)$$

The resuspension factor has obvious shortcomings because it ignores many meteorological conditions, properties of the surface, and properties of the tracer material which play important roles in the resuspension process. However, K is not entirely without value since normalizing by the surface concentration does compensate

for one important source of variability in measured air concentrations. The bulk of the data appears to point to a K value of 10^{-5} to 10^{-6} m^{-1} for freshly deposited material resuspended by natural processes.[17,18] $10^{-4} m^{-1}$ would represent a conservative upper limit.

A first step in refining a description of the resuspension process would be to separate the actual resuspension from the atmospheric dilution and transport of the airborne material. The flux (units/m^2 sec) of material from the ground to the air would, in the first approximation, be proportional to the amount of material on the ground (units/m^2) through a resuspension rate Λ(sec^{-1}) This flux would represent a source of material for downwind diffusion and subsequent redeposition. A very limited number of measurements of resuspension rates have been made. Healy and Fuquay[19] obtained a rate of 10^{-7} sec^{-1} at a wind speed of 3 m/sec for resuspension from several different environmental surfaces. Sehmel,[3] using a similar tracer on an asphalt road, found resuspension rates of 5×10^{-9} to 6×10^{-8} sec^{-1} at wind speeds of 1-4 m/sec.

Measurements of airborne, resuspended material at the same site over an extended period of time have shed light on another facet of the resuspension process. The airborne concentration appears to decay exponentially with a half-life of 30 to 40 days.[20,21] Assuming that the factors governing the resuspension process do not vary greatly over the period of measurement, this can only mean that the source is being depleted at that same rate. However, concurrent measurements show that the soil inventory is not changing, i.e., less than 10% of the material is being lost by resuspension. Since the material is not being carried away by the wind, this can be interpreted to mean only that the material is becoming unavailable for resuspension. It is becoming more or less permanently attached or fixed to the soil by a process ambiguously called "weathering."

MODEL

The preceding observations can now be related to one another by equations describing the evolution with time of two quantities. These are defined as S, the total concentration (units/m^2) of material on the ground, and G, the surface concentration of material that is available for resuspension (some portion of S). G will be increased by deposition from some airborne concentration χ and will be depleted by resuspension and soil fixation (weathering). The deposition flux is assumed to be proportional to the airborne concentration through a deposition velocity V_d. As explained above, the resuspension and fixation processes are assumed to be proportional to the amount of available material through, respectively, a resuspension rate A and a fixation rate a. Thus, if the only airborne concentration is that due to upwind resuspension χ_r,

$$\frac{\partial G}{\partial t} = V_d \chi_r - \Lambda G - \alpha G. \qquad (2)$$

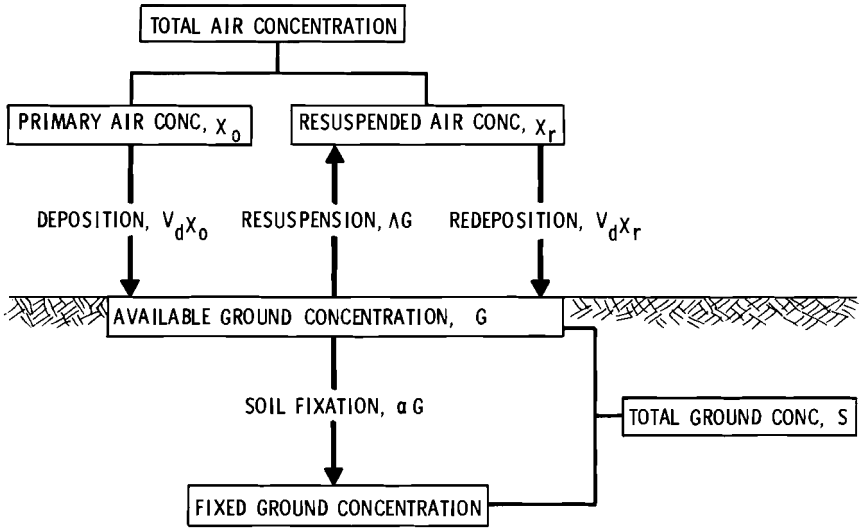

Neg 740260-4

FIGURE 8. Schematic Diagram of Resuspension Model Concepts

This equation can be simplified if we define an "initial" resuspension factor in terms of the available ground concentration,

$$K_o = \chi_r/G. \qquad (3)$$

If now K_o is independent of time,

$$G = G_0 \exp\left[(V_d K_o - A - \alpha)t\right] = G_o e^{-\beta t} \qquad (4)$$

where G_o is the available ground concentration at time t = o. We will return later to a discussion of the assumption on K_o.

The total surface concentration S will similarly be increased by deposition but will be depleted only by resuspension since soil fixation does not affect S. Hence

$$\frac{\partial S}{\partial t} = V_d\chi_r - \Lambda G = (V_d K_o - \Lambda)\, G_o e^{-\beta t}. \qquad (5)$$

If t = o at the time when the surface was originally contaminated, $G_o = S_o$ and

$$S = \frac{S_o}{\beta}\left[a + (A\text{-}V_d K_o) e^{-\beta t}\right]. \qquad (6)$$

Equations (4) and (6) can now be shown to be consistent with the observations discussed above and can provide some additional insight to the resuspension process. As observed, (4) shows that the available ground concentration decays exponentially at the rate $\beta = a + A - V_d K_o$. Equation (6) additionally tells us that for $t >> \beta^{-1}$, several half-lives, $S = a\, S_o/\beta$. But the observed total ground concentration remains at better than 90% of the original; hence $a \gtrsim 0.9\ \beta$ and

$$(\Lambda\text{-}V_d K_o) \lesssim 0.1\ \alpha. \qquad (7)$$

Equation (7) says that either the <u>difference</u> between resuspension and

redeposition is much smaller than fixation or these two are each smaller than fixation. The observations do not indicate a clear answer. A 40-day half-life for the fixation of material by the soil is identical to a fixation rate of 2×10^{-7} sec^{-1}. Measured resuspension rates are in the range of 10^{-8} to 10^{-7} sec^{-1} and would agree with either interpretation. Similarly, deposition velocities for these particles have minimum values from 10^{-4} to 10^{-2} m sec^{-1}, depending on the particle size, surface roughness, wind speed, etc.[22] Combined with K_o values from 10^{-6} to 10^{-4} m^{-1}, these give values of $V_d K_o$ from 10^{-10} to 10^{-6} sec^{-1}. Thus the observations are consistent with each other and the model but do not presently differentiate between the two possibilities expressed by Eq. (7). The observations may contain instances which exemplify both circumstances.

APPLICATION

With the conditions expressed by (7), the air concentration of resuspended material is

$$\chi_r \simeq S_o K_o e^{-\alpha t}, \tag{8}$$

and the resulting exposure will be

$$E_r = \int_o^t \chi_r d\tau = \frac{S_o K_o}{\alpha} (1 - e^{-\alpha t}). \tag{9}$$

If the ground contamination is due to deposition from an air concentration χ_o which passed in a time T,

$$S_o = \chi_o T V_d = E_o V_d. \tag{10}$$

After several half-lives the exponential term in (9) can be neglected, and the ratio between the exposure to resuspended material and the exposure to the original passage of material is

$$E_r/E_o = V_d K_o/\alpha. \tag{11}$$

As indicated in the discussion following (7), this could range from 5 to 5×10^{-4}.

The model presented here can also be extended to the situation where a continuous trace level release of material to the atmosphere produces a uniform air concentration χ_o. Then we must add the term $V_d \chi_o$ to Eq. (2) and (5). Letting $G_o = S_o = 0$,

$$G = \frac{V_d \chi_o}{\beta} (1 - e^{-\beta t}). \tag{12}$$

Applying (7) to this situation, we find that after several half-lives the ratio between the resuspended air concentration χ_r and the primary air concentration χ_o is the same as found in (11):

$$\chi_r/\chi_o = V_d K_o/\alpha. \tag{13}$$

Recall now that to obtain the solutions (4), (6) and (12) to the differential equations (2) and (5) we assumed that K_o was independent of time. [The conclusions based on (4) and (12) with $\beta \simeq a$, however, are valid in any case satisfying simply condition (7), since it states that the net sum of resuspension and redeposition plays a minor role in (2).] This assumption depends on

many things. Environmental factors such as wind speed and soil moisture change from hour to hour, day to day and month to month, but it is assumed here that a time average of these conditions can be made such that there will be no long-term trends in the ratio χ_r/G which will seriously affect the solution of (2) and (5). If, however, the distribution of available upwind material changes significantly with time (e.g., the area contaminated with available material increases in size by an order of magnitude), K_o will change with time since the airborne concentration depends, through atmospheric diffusion, on the upwind source configuration while it is defined here in terms of the local ground concentration.

One condition which would negate this latter possibility is horizontal homogeneity of the surface distribution. An appropriate approximation of this condition would exist if the distribution were uniform over a distance greater than the "communication" distance implied by the resuspension-redeposition process For $V_d/U = 10^{-2}$, U being the mean horizontal wind speed, this distance ranges from 100 m to several kilometers, depending on the mixing capabilities of the atmosphere. Under these conditions resuspension must be balanced by redeposition,

$$\Lambda - V_d K_o = 0 \qquad (14)$$

or

$$K_o \equiv \frac{\chi_r}{G} = \frac{\Lambda}{V_d} . \qquad (15)$$

Note that in this situation K_o is a function only of the competing processes of resuspension and redeposition and does not depend on the source configuration. Rather than being, as is usually the case, merely a description of a particular resuspension event, K_o reduces to a parameter characteristic of the micrometeorological processes taking place and can much more readily be applied to situations differing from that in which it was measured. Eq. (13) then becomes

$$\chi_r/\chi_o = \Lambda/\alpha, \qquad (16)$$

and this ratio is also seen to be determined only by the relative efficiency of the two processes of resuspension and soil fixation. The available measurements are much less ambiguous for this ratio, assigning a value between 0.05 and 0.5.

AIRBORNE RELEASE OF ^{137}Cs FROM A CONTAMINATED AREA DURING A RANGE FIRE

J. Mishima and L. C. Schwendiman

To aid in evaluation of the potential airborne hazard during a range fire, the distribution and fractional airborne release of ^{137}Cs involved with various contaminated materials on-the surface of prairie land were measured. The distribution was determined by collecting and measuring the ^{137}Cs content of all surface materials including soil to a depth of 1 cm in ten random 1-m^2 plots. Approximately 90% of the ^{137}Cs activity measured was found in the soil. Little of the ^{137}Cs involved in the soil was airborne during fires promoted by gasoline under static or flowing air conditions. Fractional airborne releases of 4×10^{-4} and 10^{-3} were obtained during fires where a combination of organic litter and animal droppings was involved at wind speeds of 2.5 and 20 mph respectively. Radioactive particles in the ashes were entrained to the extent of 6×10^{-3} at 2.5 mph and 4×10^{-2} at 20 mph, in a 24-hr period immediately after the fire.

Surficial contamination in areas exposed to the elements poses a continual potential for atmospheric release by alteration of local physical conditions. To evaluate the potential consequences, data is required on the quantity and distribution of the radioisotope and its fractional airborne release as a result of the action of wind and possible fires. A study is presently in progress to evaluate the potential airborne release of ^{137}Cs and ^{90}Sr-contaminated prairie land during a range fire. To date information on ^{137}Cs has been obtained.

DISTRIBUTION OF ^{137}Cs IN VARIOUS SURFACE MATERIALS

All surface materials including the top cm of soil from ten random 1-m^2 plots were collected, segregated into four types and the ^{137}Cs contents measured by gamma spectrometry. Approximately 90% of the ^{137}Cs was found in the soil itself. Animal droppings contained 8.5% while 1.5% was found in the organic debris (decayed vegetation and animal droppings). Very little (approximately 0.5% of the ^{137}Cs measured was associated with various kinds of plants found in the area. The ^{137}Cs radioactivity per unit weight of soil tended to increase with decreasing size of the soil particles. The measured ^{137}Cs activity/m^2 of 13.3 μCi agrees with a maximum value of 10 μCi $^{137}Cs/m^2$ obtained in an aerial survey of the same area. Summaries are shown in Table 9.

TABLE 9. Distribution of ^{137}Cs in Surface Materials

Mass collected from 1 m^2 (average of 10 plots)	22,360 g
^{137}Cs found in 1 m^2 (avg.)	13.3 μCi
Surface Component Mass Distribution (to depth of approx. 1 cm)	
Soil	93.4%
Vegetation	4.0%
Organic debris	2.3%
Animal droppings	0.2%
Component Radioactivity (^{137}Cs) Distribution	
Soil	89.5%
Vegetation	0.4%
Organic debris	1.5%
Animal droppings	8.5%

FRACTIONAL AIRBORNE RELEASE OF ^{137}Cs DURING A FIRE

Eleven bench-scale and five engineering-scale experiments were performed to measure the fractional airborne release of ^{137}Cs involved with various surface materials during fires fed by gasoline. Only the three surface materials (soil, animal droppings and organic debris) which contained approximately 99.5% of the ^{137}Cs were used as sources in these experiments.

Bench-Scale Experiments

Specimens of the surface materials were burned on gasoline-soaked sand held in a 100-ml glass beaker. The materials generated were entrained in air drawn up and around the burning specimens and collected on a glass fiber filter followed by a caustic scrubber (for cesium vapors, if any). The apparatus is shown in Figure 9. A measured quantity of activity was airborne in only one experiment where contaminated organic debris was burned -- 2.7×10^{-6} of the ^{137}Cs in the source. There was no measurable release during fires involving contaminated soil or animal droppings.

Engineering-Scale Experiments

Specimens of the three contaminated materials were involved in fires on gasoline-soaked soil at two wind speeds in the 242-B Building wind tunnel (see Figure 10). No measurable release was found during a 1-hr fire at 2.5 mph when the ^{137}Cs present was predominantly involved with soil. When the source was a mixture of organic debris and animal droppings, fractional releases of 4×10^{-4} and 10^{-3} were measured at 2.5 and 20 mph respectively. Entrainment of an additional 6×10^{-3} and 4×10^{-2} of the ^{137}Cs was measured during the 24-hr period immediately following the fire at the respective wind speeds. The information obtained is summarized in Table 10.

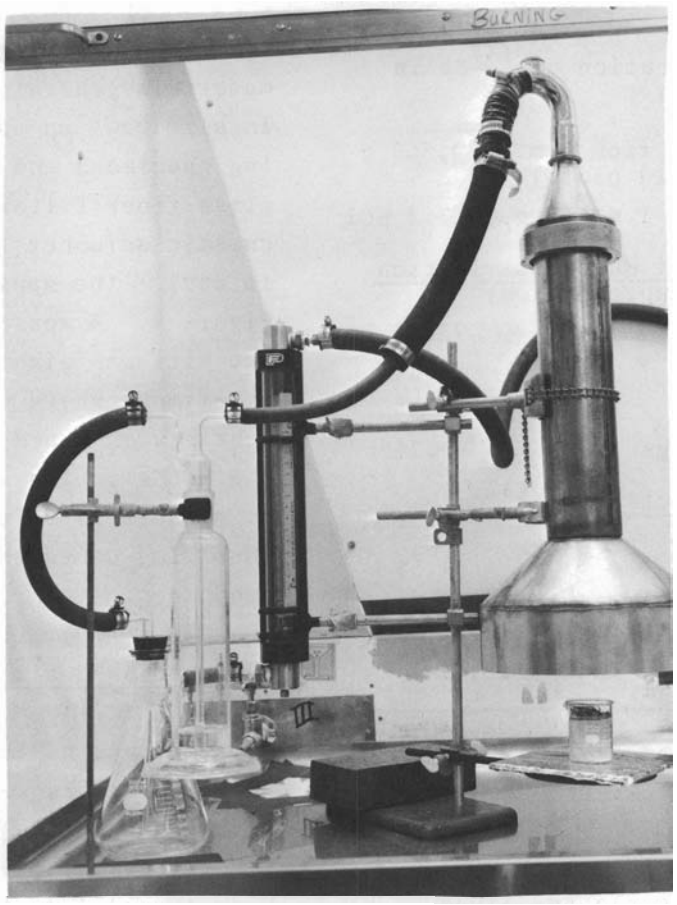

Neg 732382-2

FIGURE 9. Apparatus Used in Bench-Scale Experiments of Fractional Airborne Release of ^{137}Cs

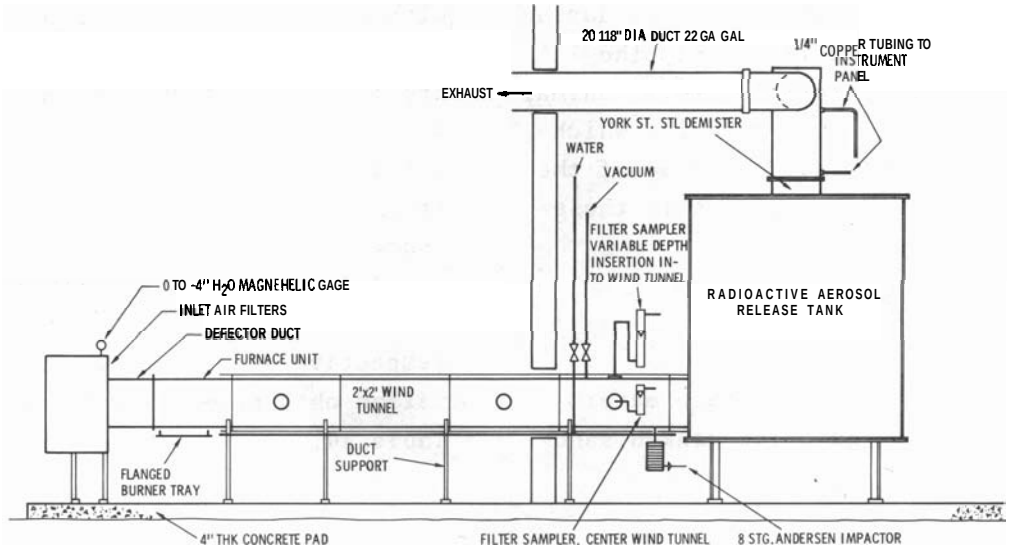

Neg 731439-5

FIGURE 10. 242-B Building Wind Tunnel

TABLE 10. Fractional Airborne Release of ^{137}Cs During a Gasoline Fire Involving Contaminated Materials Engineering Scale Experiments -- Summary Sheet

Date	5/9/73	5/14/73	6/4/73	6/19/73	6/27/73
Experiment Number	2	3	4	5	6
• SOURCE					
Wt. Contaminated Soil, g	302.5	286.5	--	--	--
µCi ^{137}Cs in Soil	1.34	1.60	--	--	--
Wt. contaminated animal droppings, g	25.7	25.4	0.674	1.564	0.674
µCi ^{137}Cs in animal droppings	0.081	0.067	4.22	12.2	9.83
Total µCi ^{137}Cs in Source	1.42	1.68	4.22	12.2	9.83
• BURNING CYCLE -- One gal gasoline					
Air speed, mph	2.5	2.5	2.5	2.5	20
Duration of cycle, minutes	52	54	52	65	18
Percent source airborne	<0.4	<0.27	0.11	0.041(-0.52)	0.091-0.13
Activity median diameter, µm	n.d.	n.d.	n.d.	n.d.	2.8
• ENTRAINMENT FROM RESIDUE					
Air speed, mph	2.5	2.5	20	2.5	20
Duration, hours	1	1	24	24	24
Percent source airborne	<0.4	<0.27	0.6-1.0	0.151(-0.63)	1.4-4.9
Activity median diameter, µm	n.d.	n.d.	n.d.	2	2
• RECOVERY OF ACTIVITY USED IN SOURCE					
Airborne during burning cycle, %	<0.4	<0.27	<0.11	0.04	0.1
Entrained from residue, %	<0.4	<0.27	1.0	0.63	3.7
On floor, %	<0.01	<0.01	0.0042	0.0026	0.04
On walls, %	<0.01	<0.01	0.0018	<0.00015	0.0044
In residue burner tray, %	101	82.1	81.4	84.5	52.8
In residue, duct, %	--	--	0.44	--	1.3
In residue, R.A.R.T., %	--	--	6.9	--	2.4
Percent activity used in source recovered	101	82.1	90.0	87.4	61.5

n.d. -- not detectable

REFERENCES

G. S. Sehmel, "An Evaluation of a High-Volume Cascade Particle Impactor System," presented at the 2nd Joint Conference on the Sensing of Environmental Pollutants, Washington, D.C., Dec. 10-12, 1973, BNWL-SA-4677, Battelle, Pacific Northwest Laboratories, Richland, WA.

2. G. A. Sehmel, "Interstage Particle Losses in High-Volume Cascade Impactors," see this report.

3. G. A. Sehmel. "Tracer Particle Resuspension Caused by Wind Forces Upon an Asphalt Surface," Pacific Northwest Laboratory Annual Report for 1971 to the USAEC Division of Biology and Medicine. Volume II: Physical Sciences. Part 1, Atmospheric sciences; BNWL-1651, Pt. 1, pp. 136-138, 1972.

4. G. A. Sehmel and F. D. Lloyd, "Resuspension by Wind at Rocky Flats," see this report.

5. G. A. Sehmel and F. D. Lloyd, "Resuspension of Tracer Particles by Wind," see this report.

6. G. A. Sehmel and M. M. Orgill, "Resuspension by Wind at Rocky Flats," Pacific Northwest Laboratory Annual Report for 1972, to the USAEC Division of Biomedical and Environmental Research, Volume II: Physical Sciences, Part 1, Atmospheric Sciences, BNWL-1751, Pt. 1, pp. 15-22, 1973.

7. G. A. Sehmel and M. M. Orgill, "Resuspension Source Change at Rocky Flats," see this report.

8. General Metal Works, Inc., Model GMWL-2000-hi-vol. air sampler with filter holder, 8368 Bridgetown Road, Cleves, Ohio 45002.

   Andersen 2000, Inc., Model 65-100 High-Volume Sampler Head, P.O. Box 20769, AMF, Atlanta, Georgia 30320.

10. J. A. Hayden, Dow Chemical Corp., Rocky Flats Division, personal communication, Dec. 1973.

11. G. A. Sehmel and F. D. Lloyd, "Influence of Soil Resuspension on the Airborne Particle Size Distribution," Pacific Northwest Laboratory Annual Report for 1972 to the USAEC Division of Biomedical & Environmental Research, Volume II, Physical Sciences, Part I, Atmospheric Sciences, BNWL-1751. Pt. 1, pp. 1-5, 1973.

12. P. A. Krey, Health and Safety Laboratory, personal communications, 1973.

13. G. A. Sehmel and M. M. Orgill, "Resuspension by Wind at Rocky Flats," Pacific Northwest Laboratory Annual Report for 1972, to the USAEC Division of Biomedical & Environmental Research, Volume II: Physical Sciences. Part 1, Atmospheric Sciences, BNWL-1751, Pt. 1, pp. 15-22, 1973.

14. L. J. Hagen and N. P. Woodruff, "Air Pollution from Duststorms in the Great Plains," Atmos. Environ., vol. 7, pp. 323-332, 1973.

15. W. A. Stone, D. E. Jenne and J. M. Thorp, Climatography of the Hanford Area, BNWL-1605, Battelle, Pacific Northwest Laboratories, Richland, WA, 1972.

16. C. Erickson. Andersen 2000 Inc., P.O. Box 20769 AMF, Atlanta, GA, 30320, unpublished data, 1973.

17. J. Mishima, A Review of Research on Plutonium Release During Overheating and Fires, HW-83668, Hanford Laboratories, General Electric Co., Richland, WA, August 1964.

18. K. Stewart, "The Resuspension of Particulate Material from Surfaces," Surface Contamination, B. R. Fish, ed., Pergamon Press, Oxford, pp. 63-74, 1967.

19. J. W. Healy and J. J. Fuquay, "Wind Pickup of Radioactive Particles from the Ground," Progress in Nuclear Energy Series XII, Health Physics, Pergamon Press, London, pp. 291-295, 1958.

20. R. H. Wilson, R. G. Thomas and J. N. Stannard, Biomedical and Aerosol Studies Associated with a Field Release of Plutonium, WT-1511, Sandia Corporation, Albuquerque, NM, 1961.

21. L. R. Anspaugh, P. L. Phelps, N. C. Kennedy and H. G. Booth, "Wind-Driven Resuspension of Surface-Deposited Radioactivity," Proc. Symposium on Environmental Behavior of Radionuclides Released in the Nuclear Industry, IAEA, Vienna (in press).

22. G. A. Sehmel, S. L. Sutter and M. T. Dana, "Dry Deposition Processes," Pacific Northwest Laboratory Annual Report for 1972 to the USAEC Division of Biology and Medicine, Volume II: Physical Sciences, Part 1, Atmospheric Sciences, BNWL-1751-1, Battelle, Pacific Northwest Laboratories, Richland, WA, April 1973.

SPECIAL STUDIES

This section reports the results of research not appropriate to the first four sections.

COOLING TOWER RESEARCH

The number of cooling towers being constructed in the U.S. is rapidly increasing due to the expansion of electrical generating capacity demand, water quality thermal limits, and competition for fresh water resources. In addition, the localization of electrical demand in coastal areas is encouraging wide utilization of salt water cooling towers. With this trend and the trend for progressively larger power plants on the same site, it has become obvious that immediate attention must be given to establishing the basic information necessary to assess the impact of such actions. The data base available for predicting salt water cooling drift amounts and the potential for inadvertent weather modification is indeed meager and far behind plans for future development.

It was with this background that cooling tower studies were initiated at Battelle. In the first year, emphasis has been placed upon both theoretical and experimental studies of drift modeling and scoping the effects of waste heat releases to the atmosphere. The results to date and the trends in utility developments have not only confirmed and reinforced the initial motivation for these investigations, but have injected a sense of urgency to such research if the scientific community is to keep pace with the requirements for its product. Cooling tower studies at Battelle will continue to address the need for drift models, and increased emphasis will be placed on obtaining cooling tower plume data and evaluating potential effects on weather from multi-unit reactor sites.

BIOMETEOROLOGY

Elucidating the relationships between animal population dynamics, radiation sensitivity, and physiological adaptions to environmental parameters requires a knowledge of microclimatology because of its relationship to plant distribution, growth, reproduction, and yields. The microclimatology of the Arid Lands Ecology Reserves is continuing to be studied as part of the terrestrial ecosystem studies. Program activity for 1973 is reported.

- **COOLING TOWER AND COOLING POND ATMOSPHERIC IMPACT**
- **AEC DIVISION OF LICENSING**

  ECOLOGICAL MICROMETEOROLOGY AND CLIMATOLOGY

  OF THE ALE RESERVE
- **BATTELLE MEMORIAL INSTITUTE PHYSICAL SCIENCES PROGRAM**

MEASUREMENTS OF DRIFT FROM A MECHANICAL DRAFT COOLING TOWER

A. J. Alkezweeny, D. W. Glover, R. N. Lee,
J. W. Sloot and M. A. Wolf

Measurements were made at the Oak Ridge Gaseous Diffusion Plant to determine the air concentrations and surface deposition rates of chromium in solution in drift droplets originating from a mechanical draft cooling tower. Observed deposition fluxes were about 1 mg $(m^2\ hr)^{-1}$ within 50 m of the tower and approximately two orders of magnitude lower at 1 km. Air concentrations over that same distance were observed to decrease by less than an order of magnitude with values of approximately 40 ng m^{-3} observed to distances of about 200 m. Air concentration and deposition flux appear unrelated, the former probably due to downwash of fine droplets at the tower. The chromium circulation rate during these measurements, based on a chromate concentration of 25 ppm in the circulating water, was 76 kg hr^{-1}. Work is continuing in the effort to utilize the experimental results for improvement of drift models.

PURPOSE

Chromium concentrations in the air and the rates of chromium deposition on the ground were measured at the Oak Ridge Gaseous Diffusion Plant (ORGDP) as a portion of a program by Union Carbide Nuclear Company to assess the environmental effects due to chromium emissions from the ORGDP cooling towers. Parallel investigations such as the one to determine the effect of chromate on the flora require a measurement of these parameters.

Chromium is contained in solution as chromate in the circulating, cooling tower water and is released to the atmosphere with the drift droplets carried in the tower exhaust. The chromate concentration is maintained near 20 ppm to inhibit corrosion within the ORGDP cooling system.

FIELD OPERATIONS

Selection of the cooling tower to be studied was based on the prevailing wind directions at ORGDP as determined from its climatology.(1) It was necessary that obstructions between the source and samples be minimal and that other sources of chromium be excluded from the sampling array insofar as possible. A sampling configuration which satisfies these criteria under the predominant northeast and southwest wind directions is shown in Figure 1 with the K-31 cooling tower as the source. The K-33 cooling tower and two others,

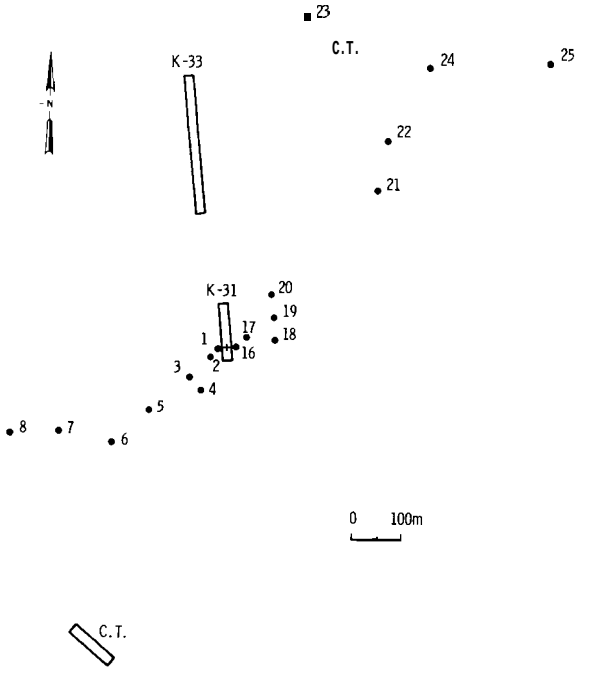

Neg 740260-2

FIGURE 1. Chromium Sampling Configuration

denoted C.T., are shown in this figure because they also are chromium sources. Several more-distant sampling locations did not receive significant amounts of chromium and are omitted from the figure.

Deposition samples were collected in petri dishes with an exposed area of approximately 79 cm^2. Air sampling was performed with gasoline-powered vacuum pumps which drew air through a 47-mm filter at 0.113 m^3 min^{-1}. High-volume samplers in standard shelters, at positions 1 and 16, were operated at a flow rate of 0.282 m^3 min^{-1} for comparison with the unsheltered filter results.

Wind speed and direction were recorded continuously from a sensor operated by the Air Resources Atmospheric Turbulence and Diffusion Laboratory at Oak Ridge. This sensor was mounted on top a 21.4-m mast about 100 m south of the K-31 tower. Additional meteorological data were obtained by tracking a rawinsonde from a location about 100 m south of the tower. The rawinsonde provided vertical profiles of wind velocity, temperature and humidity.

Weather during the field operation in mid-April 1973 was generally unsettled, with the result that complete measurements were obtained only on April 19. Samplers were deployed from 0930 until 1600, and limited success was achieved despite a major wind shift. Figure 2 indicates the wind direction variability during the measurements period. As a consequence, extensive data editing was necessary to assure that observed air concentration and deposition fluxes were related to a single source. Had a constant wind direction prevailed, more definitive results would have been possible.

An additional factor affects the degree of definition which can be expected. The K-31 cooling tower consists of 16 cells extending over a length of 117 m. Each cell, 6.8 m diam, contains a fan which draws air through the tower packing. At any time, the circulating water may flow through several or all of the cells. In addition, the flow of water through a cell does not necessarily indicate the operation of that cell's fan. Furthermore, the fans, packings and drift eliminators are not identical for all cells. The chromium source for April 19 was defined only by the total circulation rate and the chromate concentration, which were 11,300 m^3 hr^{-1} and 15 ppm, respectively.

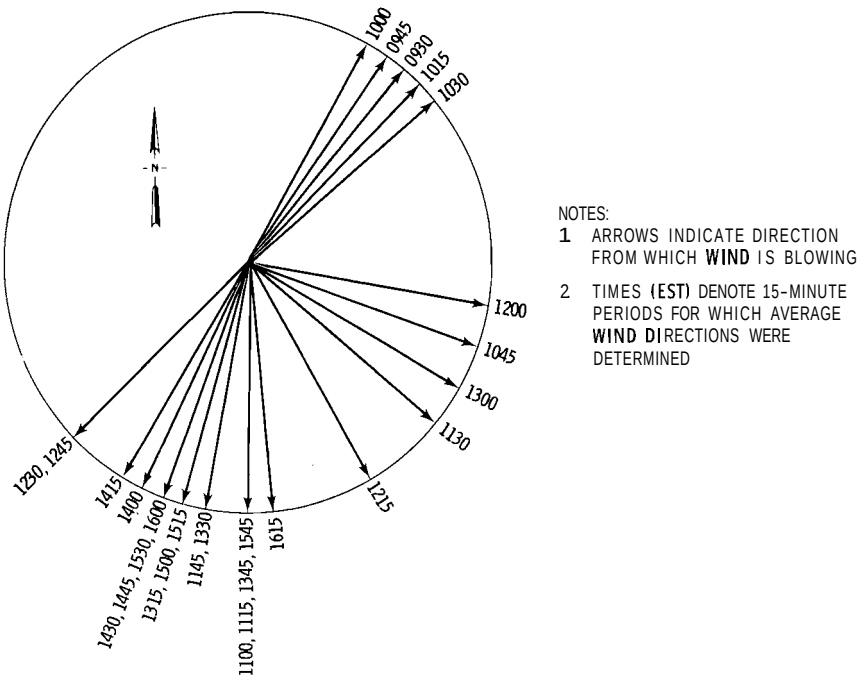

Neg 740260-1

FIGURE 2. Wind Direction Variability

SAMPLE ANALYSES

The chromium content of all samples was determined by flameless AA using a Perkin-Elmer Model 306 Atomic Absorption Spectrophotometer with the HGA-70 graphite furnace accessory. Atomization was accomplished by heating to 2400°C (9V), and sample homogeneity was confirmed by the analysis of at least two aliquots of a sample. Possible positive interference by an organic component of a sample was checked by noting the relative intensity of the absorbance signals observed following ashing at 1100°C for periods of 0.5 to 10 min. All acid solutions were prepared from distilled concentrated acid and distilled-deionized water. The chromium contribution of the acid, filters, and sample containers was determined by running blanks at the same time as the field samples.

The filters were placed in new 100-ml polyethylene beakers, 10.0 ml of 10^{-2} N HNO_3 were added and the beakers covered with polyfilm to prevent loss of solvent. After soaking at least 16 hr, aliquots were removed for analysis. This period of time was adequate for chromium removal as demonstrated by the agreement between the initial results and those obtained for that same sample 1 to 7 days later.

Five milliliters of 1:1 HF were added to the deposition sampler, taking care to expose the entire bottom surface to the acid. Following evaporation under a heat lamp, 20.0 ml of 10^{-2} N HNO_3 were added and the

cover fastened securely. The containers were kept under mild agitation overnight before removing 5 to 100 μ liters aliquots for analysis.

DISCUSSION OF RESULTS

The masses of chromium on the filters and in the petri dishes were converted to concentrations and deposition fluxes, respectively. The exposure times pertinent to these calculations were determined by the number of 15-min periods during which the mean wind direction was aligned between the cooling tower and each sampler location. These exposure times are presented in Table 1, together with the resulting concentrations and deposition fluxes from the ten sampling positions which received significant chromium from the K-31 tower. The distances between the tower and the samplers are also listed. The deposition velocities, which are the ratios of the fluxes to the air concentrations, are included for subsequent discussion.

Reference to Figures 1 and 2 shows that positions 1-9 and positions 16-25 received material before and after the wind shift, respectively. It is not surprising, therefore, that significant differences occur at samplers which are at comparable distances. However, the large difference observed

TABLE 1. Observed Chromium Air Concentration and Deposition Fluxes

Position No.	Distance (m)	Exposure (min)	Flux ($\mu g\ m^{-2} hr^{-1}$)	Concentration ($ng\ m^{-3}$)	Deposition Velocity ($cm\ sec^{-1}$)
1	36	120	1018	81 (77)*	349 (488)
2	57	**	929	41	--
4	126	30	306	41	207
5	219	30	38	12	88
6	318	30	13	--	--
9	645	15	9	--	--
16	36	30	993	883 (62)*	31 (657)
17	42	30	433	130	92
20	120	30	97	38	71
25	855	30	9	5	50

NOTE: *Concentrations in parenthesis were measured by the sheltered, high-volume samplers.
**Flux was received for 60 min, but air sampler operated only 30 min.

between the chromium concentrations in air at positions 1 and 16 for the unsheltered samplers is not apparent in the sheltered, high-volume sampler measurements. In addition, the values determined by the sheltered samplers extend to distances on the order of the cooling tower length although the flux values decrease by an order of magnitude over a comparable distance.

It is inferred from this that the measurements of flux and concentration represent independent processes. It appears that the air concentration of chromium is due primarily to the smallest drift droplets, which are continually fed into the tower wake from the edges of each cell by aerodynamic downwash. Little change in concentration with distance is apparently a consequence of the diminished effect of lateral diffusion for a crosswind line source. The high values of chromium concentration at samplers close to the tower, particularly at position 16, may be due to wind gusts which carry larger drops into the samplers.

The deposition velocities give further support to the independence of the air concentration and the flux. Where the two are related, deposition velocity is near-constant. The high values of deposition velocity are indicative of the large drift droplets falling through a fine-droplet aerosol. Insofar as drift droplets with appreciable fall velocity are present, it would be unwise to base flux determinations on airborne concentrations.

The chromium flux values are shown as a function of sampling distance in Figure 3. There is an apparent difference in flux distributions before and after the wind shift, but no explanation can be offered at this time.

A meaningful discussion of the observed distributions must include definition of the buoyant plume, of the drift droplet spectrum and of the adjacent atmosphere, and it must consider the interaction between them. Additional data are being analyzed in the continuing effort to compare these experimental results with existing drift models and to utilize these results for the development of more realistic drift models.

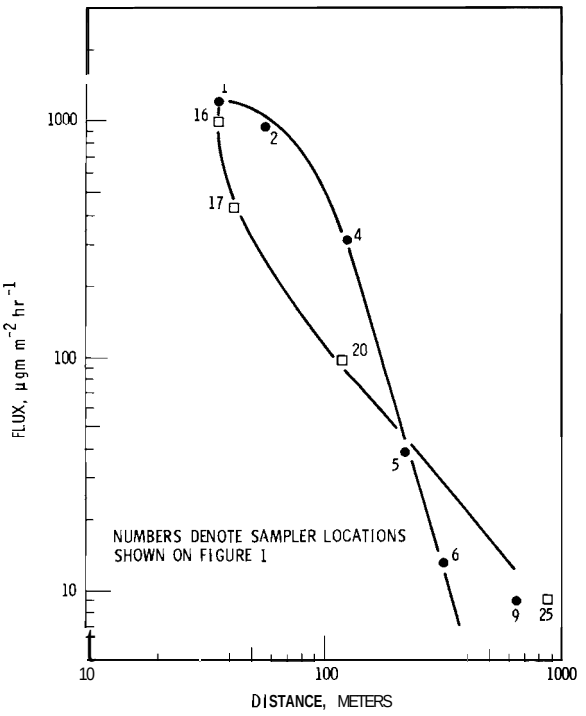

Neg 740260-3

FIGURE 3. Deposition Flux Distribution

ACKNOWLEDGMENTS

The authors sincerely appreciate the support of Dr. Steven Hanna of the Air Resources Atmospheric Turbulence and Diffusion Laboratory, who made available to us the wind data from the 21.4-m mast, and the efforts of Messrs. William Simon and Theodore Shapiro, who coordinated the logistical support provided by the Union Carbide Nuclear Company.

A SIMPLE MODEL FOR BUOYANT PLUMES BASED ON THE CONSERVATION LAWS

W. G. N. Slinn

Equations for the steady-state rise of a buoyant plume are derived directly from the conservation laws for mass, momentum and energy. Top-hat profiles are used and it is assumed that there is no horizontal pressure gradient across the plume's boundary. In the resulting equations there are four unspecified quantities: the drag and heat transfer coefficients, the entrainment velocity and heat production. Results are shown for the (isentropic) case when all these quantities are zero as well as for cases with various combinations of these quantities different from zero and using simple relaxation models. In this way some insight is gained into their separate effects on the plume's properties. Results of a simple model to account for a mean wind are also demonstrated. The need for more field data is obvious.

INTRODUCTION

On first encounter, plume rise modeling may seem to contain more art than science. Most of us can accept the limitations to "top-hat" profiles of plume properties and the poor account (if any) of turbulence. But then one seems able to choose a single entrainment expression (Morton et al.)[2] or two (Briggs),[3] or three (Slawson and Csanady),[4] or instead, specify the plume radius and let the entrainment be whatever it desires (Scorer).[5] And worse, after one becomes accustomed to equations for radius change (Hanna)[6] or buoyancy flux (Scorer)[5] or density defect (Slawson and Csanady),[4] he is assaulted by nonphysical "conservation laws" of volume, buoyancy, and separately for heat and kinetic energy (e. g., see Morton).[7] As a (hopefully) final insult, when one looks more closely at most results,

he finds that "the computer calculations show ...."

The purpose of this paper is to report on what we presume all others have done but have decided not to describe. That is, we will start from the faithful conservation laws for mass, momentum and energy, and see what type of plume they predict. Further, where appropriate, we will approximate the resulting equations in the hope of gaining some insight into the true solutions from analytical solutions to approximate equations. In this way, perhaps, one can see the consequences of some of the many assumptions involved in modeling buoyant plumes.

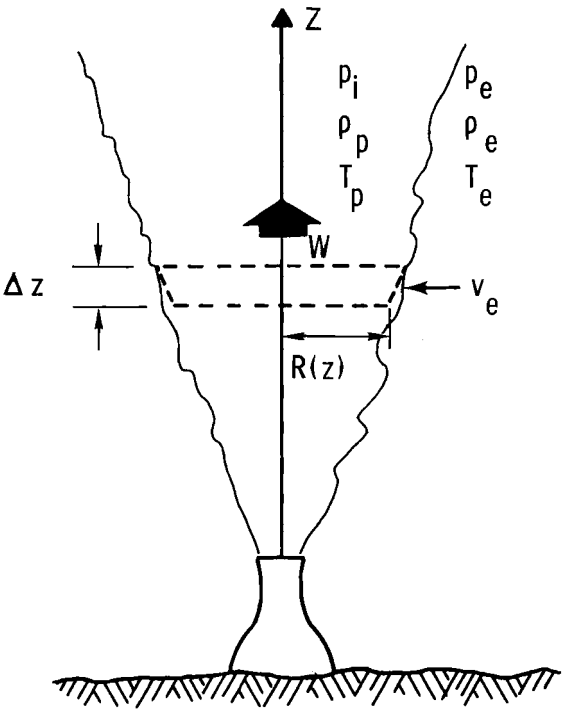

Neg 740722-8

FIGURE 4. Notation: p = pressure, ρ = density, T = temperature, w = updraft velocity, R = plume radius, v_e = entrainment velocity; subscripts i = internal, e = external or environment, p = plume

GOVERNING EQUATIONS

We look first at the conservation laws for a vertical plume. Notation to be used is illustrated in Figure 4. Because of the complexity of the problem, we introduce a number of simplifications at the outset. One is to work only with cross-sectional-area averages of plume properties or, equivalently, assume top-hat profiles for the plume's variables. Further, steady-state conditions are assumed throughout. Also for now we ignore the influence of a mean wind, but later we shall account for it in a simpleminded manner.

A major problem with the plume equations which does not appear to have been specifically addressed previously is that even if drag, heat transfer and entrainment were known, still the equations do not form a closed set. There are five unknown plume variables: p_i, ρ_p, T_P, w and R and only four equations: state and the conservation laws for mass, vertical momentum and energy. A fifth equation, for horizontal momentum, can be introduced but this introduces a sixth unknown: the horizontal velocity. The source of this lack of closure is probably the assumption that a plume can be separately identified from the rest of the fluid medium. In reality there are six unknowns: p, ρ, T and the single velocity field, say $\vec{v}$, and there are six equations (counting the vector momentum equation as three scalar equations). To extricate ourselves from

the problem, we postulate that the horizontal velocity is negligible and then deduce from the horizontal momentum equation that there is no horizontal pressure gradient. Thus we take the internal pressure to be the same as the external pressure, $p_i = p_e = p$ and further, we make the not unreasonable assumption that the vertical gradient of this single pressure field is given by the hydrostatic equation in the ambient environment:

$$\frac{dp}{dz} = -\rho_e \, g. \qquad (1)$$

We now turn to the conservation equations.

Conservation of mass requires that the amount of mass leaving the control volume at z + Az during At, i.e., $\rho_p \, w \, \Delta t \, \pi R^2|_{z+\Delta z}$, is the amount flowing in through the face at z plus the amount of environmental air entrained through the surface, i.e., $\rho_e \, v_e$ At $2\pi R$ Az. Then the steady state continuity equation is

$$\frac{d}{dz} (\rho_p \, w \, R^2) = 2\rho_e \, v_e \, R. \qquad (2)$$

The z-component of the momentum equation states the net rate of outflow of momentum from the control volume, viz.,

$$\frac{d}{dz} (\rho_p \, w^2 \, \pi R^2)\Delta z,$$

is equal to the sum of the vertical forces. These forces include the weight, $\rho_P \, g \, \pi R^{\prime} \, Az$, the resultant of the pressure forces,

$$p \, \pi R^2|_z - p \, \pi R^2|_{z+\Delta z} + 2\pi R \, \Delta R \, p =$$

$$- \pi R^2 \frac{dp}{dz} \, Az,$$

and the drag force, $- C_D \, \rho_p \, \frac{w^2}{2} \, 2\pi R \, \Delta z$, where C_D is an (unknown) drag coefficient. Thus, using (1), and assuming that the entrained air possesses no initial vertical velocity (which seems a fairly accurate assumption, see Slinn)[8] we obtain the momentum equation

$$\frac{d}{dz} \left(\rho_p \, w^2 \, R^2\right) = g \, R^2 \left(\rho_e - \rho_p\right) - 2 \frac{C_D}{R} R^2 \, \rho_p \, \frac{w^2}{2}. \qquad (3)$$

The energy equation is just a statement of the first law of thermodynamics and requires for steady-state conditions that the energy outflow from the control volume,

$$\rho_p \, \pi R^2 \, w \, \Delta t \left(\frac{w^2}{2} + c_v \, T_p\right)\Big|_{z+\Delta z}$$

where c_v is the specific heat at constant volume and per unit mass, is equal to the inflow plus the heat added within the control volume less the net work done by the fluid. The inflow of energy is

$$\rho_p \, \pi R^2 \, w \, \Delta t \left(\frac{w^2}{2} + c_v \, T_p\right)\Big|_z$$

$$+ \rho_e \, 2\pi R \, \Delta z \, v_e \, \Delta t \, E_e$$

where E_e is the energy of the entrained air. The heat addition is

$$\dot{Q} \, \text{At} \, \pi R^2 \, Az - \frac{C_H}{R} c_p \left(T_p - T_e\right)$$

$$\rho_p \, R^{\prime} \, w \, \Delta t \, \Delta z$$

where $\dot{Q}$ is the rate of heat addition per unit volume from processes such as water vapor condensation, and C_H is an (unknown) heat transfer coefficient. The additional variables in the heat transfer term are introduced solely for convenience and to nondimensionalize C_H. The net work done by the fluid in the control volume is against gravity, $\rho_p\ g\ \pi R^2\ \Delta z\ \Delta t$, against the pressure forces, $\frac{d}{dz}\ (p\ \pi R^2\ w\ \Delta t)\ \Delta z$ and against the drag force, $C_D\ \rho_p\ \frac{w^2}{2}\ 2\pi R\ \Delta z\ w\ \Delta t$. Thus the energy equation is

$$\frac{d}{dz}\left[\rho_p\ R^2\ w\left(\frac{w^2}{2} + gz + c_p\ T_p\right)\right]$$

$$= \dot{Q}\ R^2 + 2R\ \rho_e\ v_e\ E_e$$

$$- \frac{C_H}{R}\ c_p\left(T_p - T_e\right)\ \rho_p\ R^2\ w$$

$$- 2\frac{C_D}{R}\ \frac{w^2}{2}\ \rho_p\ R^2\ w, \qquad (4)$$

where we have included the work done against the pressure forces in the enthalpy term,

$$h = c_p\ T = u + \frac{p}{\rho}.$$

The final equation available to us is the equation of state

$$p = \rho\ RT \qquad (5)$$

where R is the gas constant for the plume air.

ISENTROPIC RISE, OF A DRY BUOYANT PLUME

In the above five equations, there are five unknowns (p, ρ_p, w, R, T_p) and four unspecified quantities (v_e, C_D, Q and C_H). The environmental conditions are presumed known. To proceed, obviously some specification of the entrainment, drag coefficient, heat generation and heat transfer coefficient are needed. The simplest case is to assume they are all zero, which would then correspond to the adiabatic, reversible (i.e., isentropic) rise of a dry, buoyant plume. We look at this case now not so much because we think the results will be realistic, but in order to gain some indication of the nature of the solution to the full equations.

For this case, the continuity and energy equations can be integrated to

$$\rho_p\ w\ R^2 = C_1 = \rho_{po}\ w_o\ R_o^2 \qquad (6)$$

$$\frac{w^2}{2} + gz + c_p\ T_p = c_2 = \frac{w_o^2}{2} + g\ z_o$$

$$+ c_p\ T_{po} \qquad (7)$$

The momentum equation can be converted to

$$\frac{1}{2}\ \frac{dw^2}{dz} = g\left(\frac{T_p}{T_e} - 1\right). \qquad (8)$$

If we now differentiate (7) and eliminate dw^2/dz between the result and (8) we obtain

$$-\frac{dT_p}{dz} \equiv \gamma_p = \gamma_d\ \frac{T_p}{T_e} \qquad (9)$$

which states that the lapse rate of the plume's temperature is slightly larger (by the factor T_p/T_e) than the dry adiabatic lapse rate, $\gamma_d = g/c_p$.

This result can be used in a graphical evaluation of (12) given an arbitrary (complicated) environmental temperature profile.

For simple environmental temperature profiles, an explicit expression for T_p can be found from the general solution to (12), viz.

$$T_p = c_3 \exp\left[-\gamma_d \int \frac{dz}{T_{e(z)}}\right]. \qquad (10)$$

For example, for an isothermal atmosphere, $T_e = T_{eo}$ then (10) yields

$$T_p = T_{po} \exp\left[\frac{\gamma_d (z - z_o)}{T_{eo}}\right]. \qquad (11)$$

If the environmental temperature profile can be fitted over restricted height intervals $z_i \le z \le z_{i+1}$ with a series of straight lines, i.e.

$$T_e = T_{ei} - \gamma_{ei} (z - z_1) \qquad (12)$$

where γ_{ei} is the environmental temperature's lapse rate in the i^{th} interval, then (10) yields

$$T_p = T_{pi} \left(\frac{T_e}{T_{ei}}\right)^{\delta_i} \qquad (13)$$

where $\delta_i = \gamma_d / \gamma_{ei}$.

The updraft velocity can now be found simply by substituting these solutions for T_p into the energy equation. Thus for an isothermal atmosphere the result is

$$\frac{w^2}{2} = \frac{w_o^2}{2} - g (z - z_o) + c_p T_{po} \left\{1 - \exp\left[\frac{-\gamma_d (z - z_o)}{T_o}\right]\right\}. \qquad (14)$$

For the case of nonzero but constant environmental lapse rates as in (12), the result is

$$\frac{w^2}{2} = \frac{w_i^2}{2} - g (z - z_i) + c_p T_{pi} \left[1 - \left(\frac{T_e}{T_{ei}}\right)^{\delta_i}\right]. \qquad (15)$$

These results yield that the updraft will continue to increase until $T_p = T_e$ which, of course, can also be seen from the original momentum equation.

To find the radius of the plume, we first need the plume's density or the pressure. From the hydrostatic equation and for an isothermal atmosphere, we get

$$p = p_o \exp\left[-\frac{\gamma}{\gamma - 1} \frac{g(z - z_o)}{c_p T_{eo}}\right] \qquad (16)$$

where $\gamma = c_p/c_v$ is the ratio of specific heats. For constant, nonzero, environmental lapse rates we obtain

$$p = p_i \left(\frac{T_e}{T_{ei}}\right)^{\gamma \delta_i / (\gamma - 1)}. \qquad (17)$$

Now ρ_p can be found from the equation of state, and when the result is substituted into the continuity equation, there results

$$\frac{R^2}{R_i^2} = \frac{w_i}{w} \left(\frac{T_{ei}}{T_e}\right)^{\delta_i / (\gamma - 1)} \qquad (18)$$

or, for an isothermal atmosphere

$$\frac{R^2}{R_o^2} = \frac{w_o}{w} \exp\left[\frac{\gamma_d (z - z_o)}{(\gamma - 1) T_{eo}}\right] \qquad (19)$$

where w is given in (14) and (15).

These results for the isentropic rise of a dry plume are illustrated in Figures 5 and 6. Figure 5 is for the case of an isothermal atmosphere, and in Figure 6 a comparison is made between the plume's behavior in an isothermal atmosphere with its behavior in a weak (but extensive) temperature inversion.

There are a number of interesting and informative features of these results. First it is interesting to see that the familiar "mushroom" shape is predicted. This follows even though entrainment has been neglected; it is required for mass conservation. The temperature of the plume falls steadily and even falls below the environmental temperature until finally the kinetic energy is exhausted. Actually, though, it is clear that our approximations fail as $w \to o$. In reality there is another term in the energy equation, namely $u^2/2$, where u is the radial velocity. Thus as $w \to o$, the details of the results are not reliable.

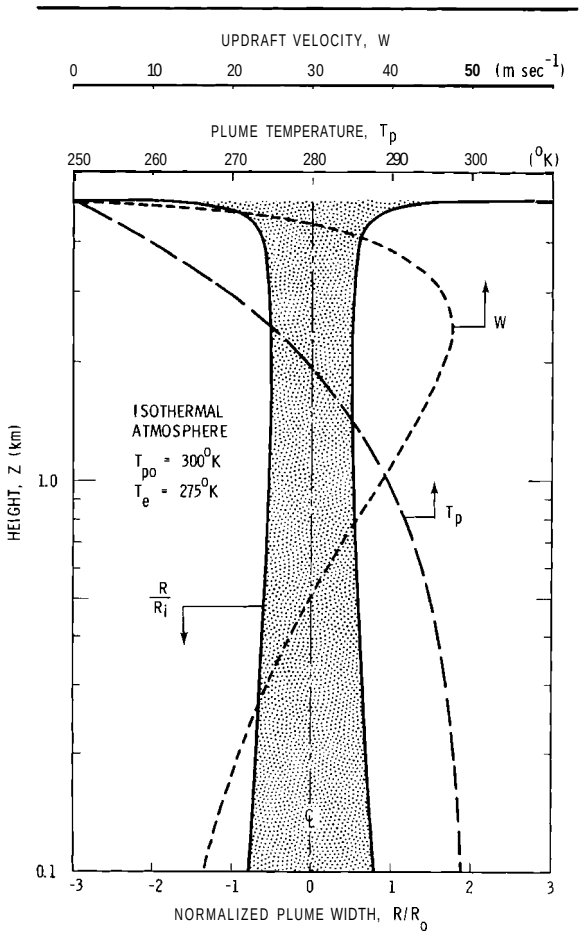

Neg 740722-3

FIGURE 5. Plots of Equations (11), (14) and (19) for the Isentropic Rise of a Buoyant Plume in an Isothermal Atmosphere. T_{eo} = 275°K, T_{po} = 300°K, w_o = 10 msec^{-1}.

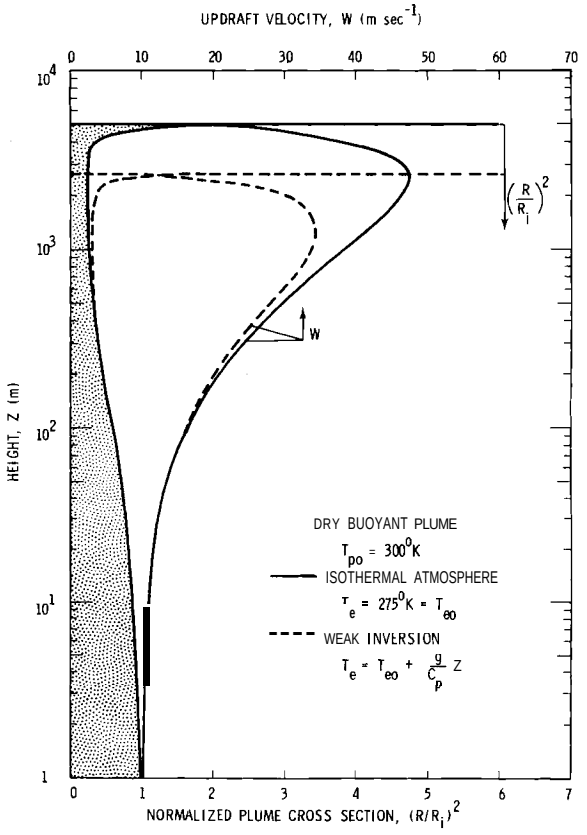

Neg 740722-2

FIGURE 6. A Comparison of the Isentropic Rise of a Buoyant Plume in an Isothermal Atmosphere (T_{eo} = 300°K) with its Rise Against the Temperature Inversion $T_e = T_{eo} + \gamma_d z$

Further, once $w \to o$, it is clear that the plume will begin to accelerate downward because $T_p < T_e$. It is expected that we can obtain a solution to our set of equations to describe the subsequent evolution of the plume (actually it is the same solution, just different boundary conditions), but we have not taken the time to explore this quantitatively. Qualitatively, the motion is one of damped oscillation, which can be seen by rewriting the momentum equation in the form

$$\ddot{z} + \frac{g}{2c_p T_e}\dot{z}^2 + \frac{g^2}{c_p T_e} z = g\left(\frac{c_2}{c_p T_e} - 1\right) \quad (20)$$

where $w = \dot{z} = dz/dt$ and t (time) appears in the parametric representation of the w(z) curve. The natural frequency of this oscillation in an isothermal atmosphere is $\omega^2 = g^2/c_p T_{eo}$, or the natural period

$$\tau = \frac{2\pi}{g}\sqrt{c_p T_{eo}} \quad (21)$$

which for $T_{eo} = 275°K$ is about 5.6 min. Vertical motion finally stops at the elevation where $T_p = T_e$, which for the case shown in Figure 5 is at about 2.44 km.

ESTIMATE OF THE INFLUENCE OF DRAG

At first encounter most of the results above seem physically reasonable except for the magnitude of the updraft velocity. It seems improbable that, even with an initial temperature excess as large as 25°K, updrafts in excess of 40 m sec^{-1} would be attained. Indeed if this were so, there would be even less justification for our ignoring drag. In this section we will attempt to estimate the consequences of accounting for drag but continue to ignore entrainment and heat generation and transfer.

In this case we can still integrate the continuity equation to

$$\rho_p w R^2 = c_1. \quad (22)$$

The momentum equation can be written as

$$\frac{d\chi}{dz} = g\left(\frac{T_p}{T_e} - 1\right) - \frac{2C_D}{R}\chi \quad (23)$$

where $\chi = w^2/2$. The energy equation becomes

$$\frac{d}{dz}(\chi + gz + c_p T_p) = -\frac{2C_D}{R}\chi. \quad (24)$$

If we now eliminate $d\chi/dz$ between (23; and (24), we obtain, as before,

$$-\frac{d T_p}{dz} \equiv \gamma_p = \gamma_d \frac{T_p}{T_e}. \quad (25)$$

Thus the plume's temperature profile does not change because of drag and the results found in the previous section for T_p can be used without modification.

The updraft velocity can now be found from (23) or (24) provided C_D is specified. We are not prepared to attempt to specify C_D at the present time and instead rationalize as follows. Since R was seen to change but little over most of the plume rise

(at least when drag was ignored) and since for large Reynolds numbers, C_D for bluff bodies becomes independent of the Reynolds number (and, therefore, of w), but especially since we only seek some indication of the influence of drag, we take $2C_D/R$ in (23) to be a constant inverse (momentum relaxation) length:

$$\ell_m = \frac{R}{2C_D} = \text{constant.} \qquad (26)$$

Then upon substituting (26) into (23) and using T_P for an isothermal atmosphere as found in the previous section we get

$$\chi = \chi_o \exp\left(\frac{-z}{\ell_m}\right) - g\,\ell_m\left[1 - \exp\left(-\frac{z}{\ell_m}\right)\right] + g\,\frac{T_{po}}{T_{eo}}\left(\frac{1}{\ell_m} - \frac{\gamma_d}{T_{eo}}\right)^{-1}\left[\exp\left(-\frac{\gamma_d z}{T_{eo}}\right) - \exp\left(-\frac{z}{\ell_m}\right)\right]. \qquad (27)$$

Reasonable estimates for ℓ_m and T_{eo}/γ_d suggest that $(1/\ell_m) >> (\gamma_d/T_{eo})$. Then for $z << T_{eo}/\gamma_d$, (27) can be approximated by

$$\chi = \chi_o \exp\left(-\frac{z}{\ell_m}\right) + g\,\ell_m\left(\frac{T_{po}}{T_{eo}} - 1\right)\left[1 - \exp\left(-\frac{z}{\ell_m}\right)\right]. \qquad (28)$$

A similar result can be obtained when the environmental lapse rate is a nonzero constant. However, recognizing the approximations in the formulation, we suggest that an approximate solution will be consistent. To obtain one we note that the momentum Equation (23) predicts a relatively rapid relaxation (the exp $(-z/\ell_m)$ term) from any initial velocity, to a "steady-state" velocity, which is obtained by putting the inertial term in the momentum equation (i.e., $d\chi/dz$) equal to zero. Taking $d\chi/dz = 0$ implies a balance between buoyancy and drag forces. Thus we propose that an acceptable approximate description of the updraft velocity is

$$\frac{w^2}{2} = \frac{w_o^2}{2}\exp\left(-\frac{z}{\ell_m}\right) + g\,\ell_m\left(\frac{T_p}{T_e} - 1\right)\left[1 - \exp\left(-\frac{z}{\ell_m}\right)\right] \qquad (29)$$

or in cases where the initial velocity is generated by buoyancy (for example, probably the exit velocity from a natural draft cooling tower) just

$$\frac{w^2}{2} = g\,\ell_m\left(\frac{T_p}{T_e} - 1\right). \qquad (30)$$

In Figure 7 a comparison is made among (14), (27), (29) and (30) for an isothermal atmosphere. We have chosen the order of magnitude "guesstimate" $C_D = O(10^{-1})$ and used ℓ_m = 300 m. In Figure 7 the substantial influence (our assumed) drag has on the updraft velocity is obvious. Further, given that we do not know the drag coefficient nor the initial velocity of the plume, there seems little point in using the "exact" solution (27) or even the approximate solution (29) unless a specific initial velocity must be fit. Instead, in what follows we will use the concept implicit in (30), that is, that the buoyancy and (unknown) drag forces are always in balance.

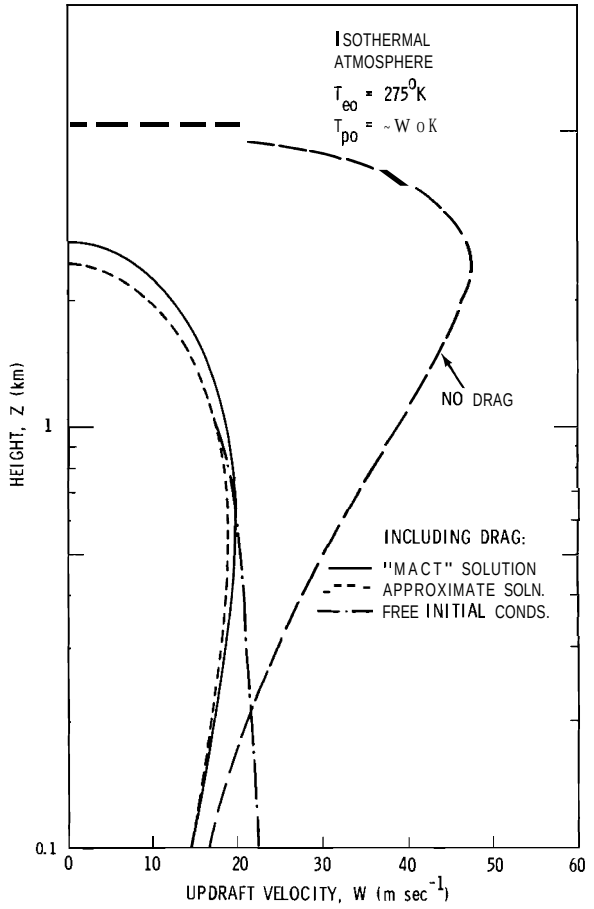

Neg 740722-5

FIGURE 7. A Comparison Among the Predictions of Equations (14), (27), (29) and (30) to Show the Influence of Drag on the Updraft Velocity of a Buovant Plume in an Isothermal Atmosphere. The "exact" solution is the result (27). For the approximate solution it is assumed that the inertial term in the momentum equation is negligible but the initial velocity w_o = 10 msec^{-1} is forced. This initial condition is removed for the third (dotted) curve.

ESTIMATE OF THE INFLUENCE OF HEAT TRANSFER

The original five equations contained five unknowns and four unspecified quantities (v_e, C_D, Q and C_H). We have now looked at the consequences of taking all the unspecified quantities to be zero (isentropic case) and the case with only $C_D \neq 0$. We now take both $C_D \neq 0$ and $C_H \neq 0$ to estimate the additional consequences of some heat transfer. In this case, the continuity equation can still be integrated to

$$\rho_p \, w \, R^2 = c_1. \tag{31}$$

The momentum equation does not contain any explicit dependence on heat transfer and is as before

$$\frac{d\chi}{dz} = g\left(\frac{T_p}{T_e} - 1\right) - \frac{\chi}{\ell_m}. \tag{32}$$

Finally, if (31) is used in the energy equation, it becomes

$$\frac{d}{dz}\left(\chi + gz + c_p T_p\right) = -\frac{\chi}{\ell_m} - \frac{C_H}{R} c_p \left(T_p - T_e\right) \tag{33}$$

where, again, $\ell_m = R/2C_D$.

Rigorously we cannot proceed any further since the heat transfer coefficient is unknown. However, we rationalize as before and take

$$R/C_H = \ell_t \tag{34}$$

where ℓ_t is another (unknown, temperature relaxation) constant, length. If $d\chi/dz$ is now eliminated between (32) and (33), we obtain

$$\frac{dT_p}{dz} + \left(\frac{\gamma_d}{T_e} + \frac{1}{\ell_t}\right) T_p = \frac{T_e}{\ell_t}. \tag{35}$$

The solution to (35), for example for an isothermal atmosphere, is

$$T_p = T_{po} \exp\left(-\frac{z}{\ell}\right) + T_{eo} \frac{\ell}{\ell_t} \left[1 - \exp\left(-\frac{z}{\ell}\right)\right] \quad (36)$$

$$\text{where } \frac{1}{\ell} = \frac{1}{\ell_t} + \frac{\gamma_d}{T_{eo}} \quad (37)$$

Solutions for other simple environmental temperature profiles can be found similarly.

To find the updraft velocity in this case, we return to the momentum equation and again assume that a balance has been established between drag and buoyancy:

$$\chi = \frac{w^2}{2} = g\,\ell_m \left(\frac{T_p}{T_e} - 1\right). \quad (38)$$

These results will be illustrated later where [compare (26) and (34)] we will take $\ell_t = 2\ell_m$ which follows if $C_D = C_H$.

ESTIMATE OF THE INFLUENCE OF ENTRAINMENT

If we take $v_e \neq 0$ (but, for the moment, we ignore heat transfer and drag), the continuity equation cannot be integrated. It is

$$\frac{d}{dz}(\rho_p\, w\, R^2) = 2\rho_e\, v_e\, R \quad (39)$$

If this is used in the momentum equation, it becomes

$$\frac{d\chi}{dz} = g\left(\frac{T_p}{T_e} - 1\right) - 2\,\frac{T_p}{T_e}\,\frac{v_e\, w}{R}. \quad (40)$$

Similarly for the energy equation, if we take the total energy of the entrained air to be $E_e = (v_e^2/2) + c_p T_e + gz$, we obtain

$$\frac{d}{dz}(\chi + gz + c_p T_p) = -\frac{2}{R}\frac{v_e}{w}\frac{T_p}{T_e}\left[c_p (T_p - T_e) + \frac{1}{2}(w^2 - v_e^2)\right]. \quad (41)$$

As yet v_e has not been specified. If we were to use the customary assumption that v_e is proportional to the updraft velocity, $v_e = aw$ the above momentum and energy equations become almost identical to the similar equations used earlier when heat transfer and drag were included. In particular, the momentum Equation (40) is identical if in (32) we take

$$C_D = 2\alpha\, T_p/T_e, \quad (42)$$

and the energy equation is essentially the same if in (33) we take

$$C_H = 2\alpha\, T_p/T_e = C_D. \quad (43)$$

Consequently, given the crudeness of the specifications of v_e, C_D and C_H, it seems inconsistent to modify the momentum and energy equations any further because of entrainment, and we propose to keep in them only the drag and heat transfer terms.

However, the continuity equation is significantly altered. If we use $v_e = a\,w$ and then (42) in (39) we obtain

$$\frac{d}{dz}(\rho_p\, w\, R^2) = \frac{1}{2\ell}\,\rho_p\, w\, R^2. \quad (44)$$

In (44) we might take $2\ell_m = \ell_t$ as was suggested earlier, but instead it seems more appropriate to call $2\ell_m$ a third characteristic (entrainment) length ℓ_e. Then (44) yields

$$\rho_p \, w \, R^2 = (\rho_p \, w \, R^2)_o \exp (z/\ell_e), \quad (45)$$

which means that the plume's radius increases at a more rapid rate because of entrainment.

In Figure 8 these results are illustrated for the case of an isothermal atmosphere. The specific equations used are (45) with ℓ_e = 900 m, (36) with ℓ_t = 600 m and (38) with ℓ_m = 300 m. Upon comparing Figures 7 and 8, the substantial difference caused by heat transfer is seen. In Figure 7 it is seen that drag reduced the final plume rise by a factor of about 2 from the case with no drag (for our essentially arbitrary choice of ℓ_m). Now in Figure 8 it is seen that heat transfer reduces the plume rise by about another factor of 2. Also, the plume's radius can be seen to be considerably larger than without entrainment and increases almost linearly with height for a good portion of the rise.

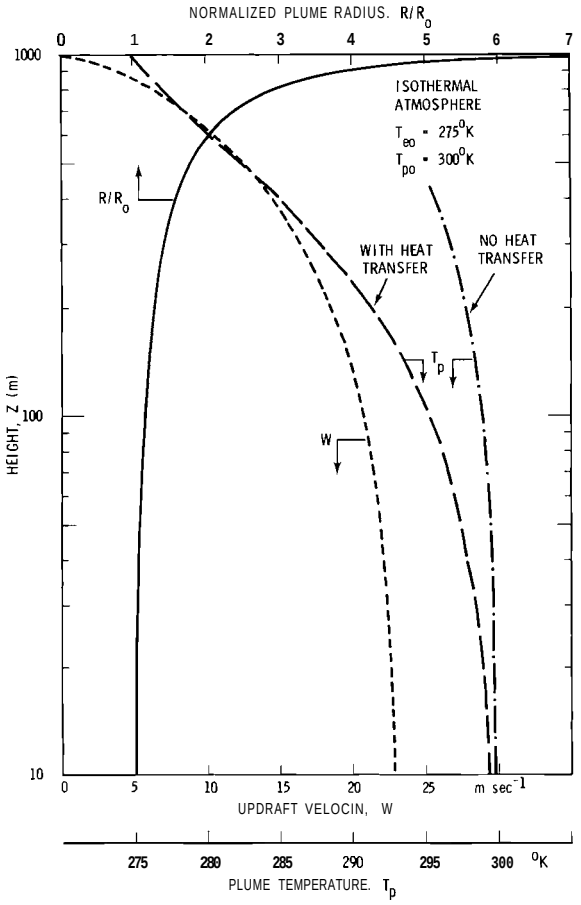

Neg 740722-1

FIGURE 8. An Illustration of the Influences of: Entrainment on the Continuity Equation, Heat Transfer on the Energy Equation, and Drag on the Momentum Equation for a Buoyant Plume in an Isothermal Atmosphere. The (arbitrary) choices of the relaxation lengths are ℓ_e = 900 m, ℓ_t = 600 m, ℓ_m = 300 m. To determine the updraft velocity, inertial acceleration was ignored and no initial velocity was forced. T_{eo} = 275°K, T_{po} = 300°K.

HEAT SOURCE IN A MOIST PLUME

So far in this report, we have cursorily examined the specification of three of the original four unspecified quantities (C_D, C_H, v_e and $\dot{Q}$). Now we wish to look at the consequences of some heat production Q and the case of a moist plume may seem ideal. However, it is not because besides $\dot{Q}$ a host of new unknowns enter: the mass concentration of dry air, ρ_d; water vapor, ρ_v; cloud water, ρ_{cw} as well as rainwater or even ice, and there are also the possibly different velocities for each constituent. Correspondingly there is a host of new equations, for example, continuity equations for each constituent.

Rather than delve into the full problem for a moist plume, we propose just to indicate the effect of $\dot{Q}$.

For example, suppose that the plume is saturated and that entrainment is negligible. Then the rate of heat production per unit volume $\dot{Q}$ is just $L\dot{P}_{cw}$, where L is the latent heat of condensation and $\dot{P}_{cw}$ is the rate of production of cloud water. Ignoring entrainment, conservation of water vapor requires

$$\frac{d}{dz}\left(\rho_d\, m_s\, w\, R^2\right) = -\dot{P}_{cw}\, R^2 \qquad (46)$$

where $m_s = \rho_v/\rho_d$ is the mixing ratio. Upon substituting $\dot{Q}$ from (46) into the energy equation and taking $\rho_p \doteq \rho_d$, we obtain

$$\frac{d}{dz}\left(\chi + gz + c_p\, T_p + Lm_s\right) = 0. \qquad (47)$$

If we now use the Clausius-Clapeyron equation (e.g., Haltiner and Martin, 1957)[9] to evaluate dm_s/dz and eliminate $d\chi/dz$ between (47) and the momentum equation, we obtain for the plume's lapse rate

$$\gamma_p = \gamma_m \frac{T_p}{\overline{T}_e} = \gamma_d \frac{T_p}{\overline{T}_e}\left(1 + \frac{Lm_s}{R_d\, T_p}\right)\left(1 + \frac{L^2\, m_s}{c_p\, R_v\, T_p^{\,2}}\right)^{-1} \qquad (48)$$

where R_d and R_v are the gas constants for dry air and water vapor, respectively, and γ_m is the moist adiabatic lapse rate. Thus one consequence of the presence of water vapor (and $\dot{Q}$) is to require that γ_d, used in our previous results, be replaced by γ_m. Other changes needed to describe a moist plume, though, include accounting for the weight of the cloud water in the momentum equation and including the cloud water evaporation necessary to saturate the entrained air. Such effects are contained in the cumulus cloud models of, for example, Simpson and Wiggert[10] and have recently been used in a buoyant plume model by Hanna.[11]

SIMPLEMINDED ACCOUNT FOR A MEAN WIND

Most experimental data for buoyant plumes are given in terms of plume rise. Briggs[12] has recently summarized essentially all the data and concludes that one of the best plume rise formulae is the "2/3 law," which gives for the trajectory of the plume's centerline

$$z = h + 1.6\, F^{1/3}\, x^{2/3}/\bar{u} \qquad (49)$$

where h is the stack height, $\bar{u}$ is the mean wind speed at the top of the stack and F is the initial buoyanty flux

$$F = \left[1 - (\rho_o/\overline{\rho}_e)\right] g\, w_o\, R_o^{\,2} \qquad (50)$$

in which $\overline{\rho}_e$ is the average density of the environmental air. In this section we present a simpleminded analysis of the effect of a mean wind on the plume's trajectory.

To properly account for a mean wind would be difficult. One way is to write the conservation equations using instead of z, the distance s along the plume's trajectory. This has been done by Hoult, Fay and Forney (1969),[13] but the resulting equations are essentially intractable

for all but numerical analyses. Instead, suppose we naively retain our previous equations, use them to predict the updraft velocity w(z), and then assume that in addition the plume possesses a horizontal velocity u(z) equal to the mean wind. Then the plume's trajectory would be given by the solution to

$$\frac{dz}{dx} = \frac{dz/dt}{dx/dt} = \frac{w(z)}{u(z)}. \quad (51)$$

Unfortunately, even the above simplified model leads to analytical difficulties if we choose any of the expressions for w(z) found earlier [e.g., (27), (29) or even (30)]. Instead, suppose we were to fit the resulting w(z) curves with simple "power laws"

$$w(z) = w_o\ (z_o/z)^{1/r} \quad (52)$$

where, for example, we might take the limiting case r = ∞ if w is constant with height or r = 3 for Scorer's model of a buoyant plume in which he assumes the buoyancy flux is a constant (Scorer, 1970). Also, suppose that the horizontal wind is fit by another "power law"

$$u(z) = u_1\ (z/z_1)^{1/s} \quad (53)$$

where Plate[14] gives (approximately) s = 10, 6, 4, 2 for underlying terrains described as open sea, flat open country, woodland forest and urban area, respectively. Upon substituting (53) and (52) into (51), we obtain

$$z = h + (\text{constant})\ (x)^{rs/(r+rs+s)} \quad (54)$$

Although (54) does not predict the "2/3 law," the exponent β = rs/(r + rs + s) is surprisingly insensitive to reasonable choices of r and s. Table 2 illustrates this statement. Further, the "2/3 law" is not omnipotent, as is illustrated in Figure 9 where we have replotted Briggs' Figure 5.2 (Briggs),[12] which shows various plume rise observations in near neutral conditions (see Briggs for details) and just added two lines of slope β = 1 and β = 1/3.

REVIEW AND CONCLUSION

In the above there may be little that is new or practical. However, it has been profitable for the author and hopefully it will be useful to

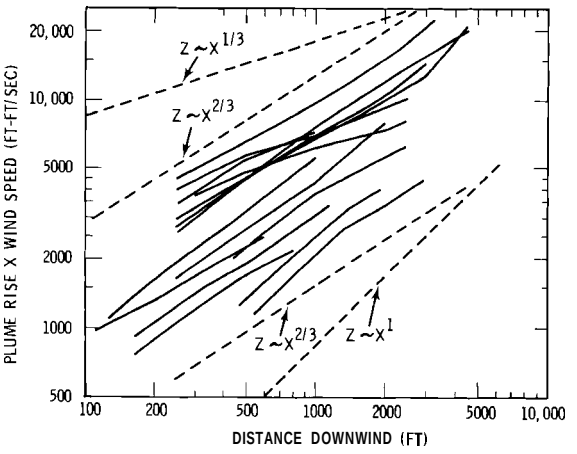

Neg 740722-6

FIGURE 9. A Replot of Briggs' Figure 5.2 (Briggs, 1969)[12] Which Illustrates that Plume Trajectories (at Least in Near-Neutral conditions) Satisfy $z \sim x^{\beta}$ with $1/3 \lesssim \beta \lesssim 1$. See Briggs for detail about the experimental data.

TABLE 2. The Variations of $\beta = rs/(r + rs + s)$ with r and s Where $w = w_o(z_o/z)^{1/r}$, $u = u_1(z/z_1)^{1/s}$

r	1				3				6				10			
s	2	4	6	10	2	4	6	10	2	4	6	10	2	4	6	10
β	0.40	0.44	0.46	0.48	0.55	0.63	0.66	0.70	0.60	0.70	0.75	0.79	0.625	0.74	0.79	0.83

others to see the derivation of plume equations from the three conservation laws of mass, momentum and energy without any approximations other than the simplifications of top-hat profiles, steady-state conditions and negligible horizontal wind. However, we did assume that the pressure was the same inside and outside the plume, but this appears to be a reasonable (and necessary) assumption.

In the resulting equations, there are four unspecified quantities: the drag coefficient, heat transfer coefficient, the entrainment velocity, and the heat production. If they all were zero, it was seen that the (isentropic) rise of buoyant plume was too fast, too hot, too narrow and too high. Using simple relaxation models, we looked at the consequences of adding drag, heat transfer and entrainment, and as expected the plume slows down, cools down, broadens out and the ultimate plume rise decreases. One effect of moisture condensation is that where the dry adiabatic lapse rate previously appeared in the formalism, it is replaced by the moist adiabatic lapse rate.

Though few conclusions can be derived from this report, the author would like to make the following observations. Viewed by a novice to the plume modeling field, the diagnosis of the state-of-the-art is depressing. First there appears to be a chronic need for more data, and not just of plume trajectories since that appears to be a quite insensitive test of the models. Even for the simpleminded model of the effect of a mean wind we could not seem to do worse than predict $z \sim x^{1/3}$ or $z \sim x^{1}$, and neither extreme is significantly different from the data. What is needed most and can be obtained most easily is data on the plume's temperature. With such data, perhaps, the unspecified quantities can be specified empirically.

But there are other items in a prescription for improvement. One is to abandon past usage of nonphysical conservation laws. A second, designed to ease the incorporation of fresh ideas from new researchers entering the field, is to do more than state equations of "density defect," or "radius change," etc. If these equations do not follow from the conservation laws, they should either be presented as postulates or discarded. Third, considerable effort should be placed on deriving the "unspecified" quantities from first principles. Finally, there is a somewhat personal plea to attempt to find more analytical solutions and rely less on numerical calculations.

Then more insight will probably be gained on the effect of the assumptions on the results. Besides, there is little point in having an exact (five or ten significant figure) numerical solution, rather than an analytical solution to an approximate equation, if the original equation may be wrong by more than an order of magnitude.

AN ANALYTICAL SEARCH FOR THE STOCHASTIC-DOMINATING PROCESS IN THE DRIFT-DEPOSITION PROBLEM

W. G. N. Slinn

The random processes in the drift-deposition problem are examined separately to see if any one of them dominates the statistical properties of the outcome. The three prime candidates are assumed to be the drop size distribution, the distribution of breakaway points, and turbulent diffusion. It is seen that the drop size distribution probably has dominant influence on the deposition of the large-size (drift or carry-over) drops. Turbulence has a comparable influence on the deposition of the small drops for downwind distances of the order of 10 tower heights and then dominates for large downwind distances, provided the atmosphere is not stable. Uncertainties in details of how the drops break free from the plume's updraft preclude an accurate evaluation of this effect and seriously limit the accuracy of any drift-deposition prediction. To remedy this, more field data is needed.

INTRODUCTION

When a final outcome is the consequence of a number of intermediate events, then the prediction of the outcome can be quite complicated. For example consider the generation of some chemical compound which is the product of a series of chemical reactions, or as another example, the in-cloud precipitation scavenging of some pollutant. For the in-cloud scavenging problem there are at least the two processes of first attachment of the pollutant to the cloud water and then removal of the cloud water to the ground. In such examples of multi-intermediate rate processes it is valuable to see if one of the intermediate processes is significantly slower than all the rest, for then it will be the rate-limiting stage of the overall process, and an estimate only of the rate of progression of this rate-limiting stage can be used as an estimate of the rate of progression of the overall process. Using this reasoning, we have suggested that

the (overall) "rainout-rate" for in-cloud scavenging can usually be approximated by the cloud-water removal rate (Slinn). (15)

In a similar way, imagine that a final outcome depends on more than one intermediate stochastic (or random) process. Such is the case when the final outcome is the deposition downwind of a cooling tower of, say, some chromium which is sometimes used as an anti-rust agent in the cooling system. A specific deposition of chromium could have been carried by any drop chosen from the distribution of drop sizes; the trajectory of the particular drop could have been any of a large number of possibilities depending on the level of atmospheric turbulence; the drop could have broken free from the influence of the plume's updraft at any of many locations, and so on. Similar to the multi-intermediate rate process described above, it is intuitively obvious that when there are multistochastic processes, it is to our advantage when attempting to describe the outcome, to inquire if one of the random intermediate processes has the greatest influence on the randomness of the outcome. If so, then to a first approximation the statistical distribution of the outcome can be related directly, solely to the statistical distribution of what we call the "stochastic-dominating" (contrast: "rate-limiting") process. Recently we have used this concept to conclude that in the problem of predicting the size distribution of resuspended soil particles, it is the size distribution of soil particles which is the stochastic-dominating process (Slinn). (16) A simpler example is if the outcome were the mathematical sum of a series of independent outcomes, then instead of equating the variance of the outcome to the sum of the individual variances, we would approximate the sum just by the largest variance.

The purpose of this report is to describe our attempt to find the stochastic-dominating process in the drift-deposition problem. This search was made in lieu of solving the complete problem because, as will be seen, the entire problem is quite difficult, and, further, it contains a number of processes whose mathematical description is obscure. Relying only on physical intuition of the entire process, we conclude that the three prime stochastic-dominating candidates are: the drift-drop size distribution; the randomness of the point where a drop breaks free from the turbulence in the plume; and the turbulent diffusion of the drop's trajectory from the "breakaway" point to the ground. Our analysis plan is to determine the statistical distribution of the ground-level deposition pattern resulting from each of these three stochastic processes acting separately and then compare their magnitudes in an attempt to see if one can be identified as having dominant influence. As will be seen, the attempt is only partially successful. Notation to be used is shown in Figure 10.

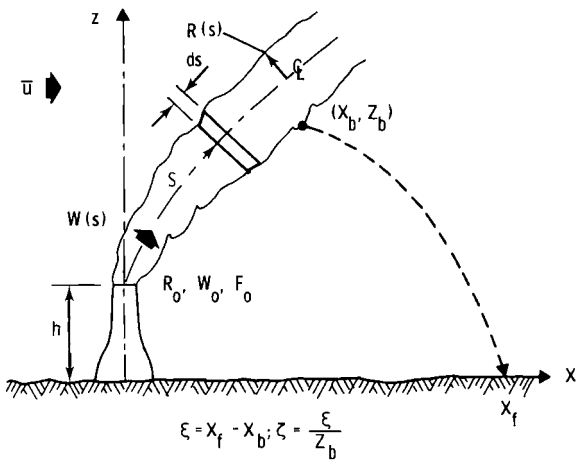

Neg 740753-7

FIGURE 10. Notation

INFLUENCE OF THE DISTRIBUTION OF DROP SIZES

If we ignore the acceleration of the drift drops, then quite generally we can state that their final location (where they hit the ground) is

$$\tilde{x}_f = \tilde{x}_b + \tilde{u}\,\tilde{t} \qquad (1)$$

where

$$\tilde{t} = \tilde{z}_b/\tilde{v}_s \qquad (2)$$

and where we have used the tilda (~) to identify random variables. In (1) and (2) $(\tilde{x}_b, \tilde{z}_b)$ are the coordinates of the breakaway point (in the main we will be concerned with the cross-wind integrated deposition and therefore $\tilde{y}_b$ is not significant), $\tilde{u}$ is the wind speed and $\tilde{v}_s$ is the settling (or terminal) velocity of a drop of a given size. In this section we ignore the randomness of the wind and of the breakaway points and seek to determine the distribution of $\tilde{x}_f$ caused by the distribution of drop sizes. Thus we desire the probability density function (pdf) for $\tilde{x}_f$ (or for $\tilde{\xi} = \tilde{x}_f - \tilde{x}_b$) where

$$\tilde{\xi} = \frac{\bar{u}\, z_b}{\tilde{v}_s}$$

given the pdf of $\tilde{v}_s$.

This would be a relatively straightforward problem to solve if we knew the distribution of drop sizes. Unfortunately there is very little data available. What there is [Wistrom and Ovard:[17] Hanna and Perry[18]] can be fit with reasonable accuracy (given the limited accuracy of the data, the variability in the data for different cooling towers, and the accuracy of other aspects of the theory presented here) by varying the parameters in the bimodal gamma distribution:

$$f(r) = N_1 \left(\frac{r}{a}\right)^2 \exp\left(-\frac{r}{a}\right) + N_2 \left(\frac{r}{b}\right)^2 \exp\left(-\frac{r}{b}\right) \qquad (4)$$

where $f(r)\,dr$ is the number of drops per unit volume whose radii are between r to r + dr, N_1 and N_2 are normalization constants and a and b are free parameters. For example in Figure 11 are shown the number and mass distributions resulting from (4) if we take a = 10 μm, b = 100 μm and d = $N_2/N_1 = 10^{-5}$ (we chose d = 10^{-4} for the number distribution since if d = 10^{-5}, the second peak would not have appeared on the graph).

To determine the pdf of $\tilde{\xi}$ from (3) we also need $v_s(r)$. Data is shown in Figure 12 and we propose to fit the data with the two analytic expressions shown. Further we propose to use

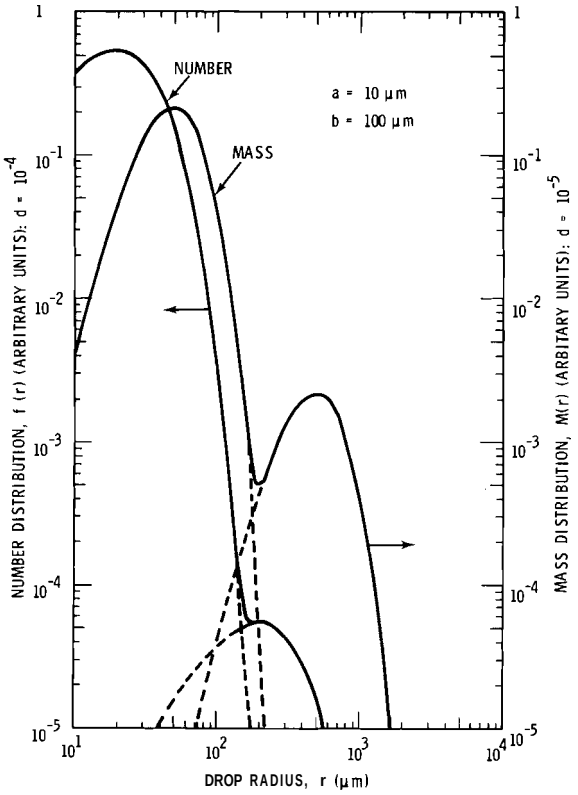

Neg 740753

FIGURE 11. Model Number and Mass Distributions as Given by Equation (4) with a = 10 μm, b = 100 μm and Two Cases for d = N_2/N_1: 10^{-4} for the Number Distribution and 10^{-5} for the Mass Distribution

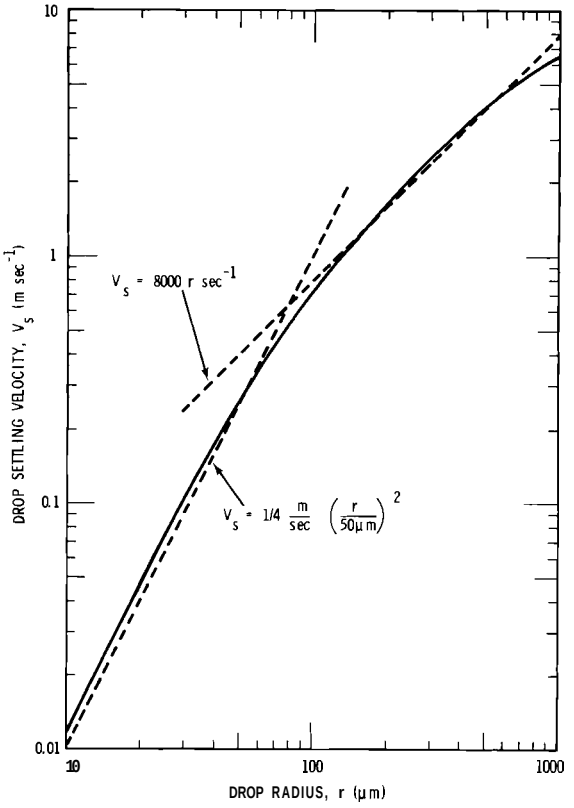

Neg 740753-2

FIGURE 12. Data and Proposed Analytical Expressions for the Drop Settling Speed as a Function of Drop Radius

$$v_s = 0.8 \times 10^{-2}\ r\ (\text{msec}^{-1}),\ r \text{ in pm}, \quad (5)$$

for the settling velocity of the drops in the large-drop mode of (4), and

$$v_s = 1/4\ \frac{\text{m}}{\text{sec}} \left(\frac{r}{50\ \mu\text{m}}\right)^2,\ r \text{ in } \mu\text{m}, \quad (6)$$

for the small-drop mode.

To determine the normalization constants in (4)-let the total amount of, say, chromium released from the tower per second be $\dot{Q}_o$. Then

$$\dot{Q}_o = \int_o^{r_{max}} 4/3\ \pi r^3\ \rho c\ (w_o - v_s)\ \pi R_o^2\ f(r)\ dr \quad (7)$$

where c is the concentration (e.g., in grams per gram of water) of chromium in the water (assumed to be the same for all drops), w_o and R_o are the exit velocity and radius of the plume, and r_{max} is the largest drop radius such that $v_s \leq w_o$. Rather than evaluate (7) accurately, we approximate it by assuming all drops leave the tower with speed w_o. Then

if the fraction of the total chromium that is carried by the large drops is κ, we obtain

$$N_2 = \frac{\kappa\, Q_o}{\frac{4}{3}\pi b^4\, \rho c\, w_o\, \pi R_o^2\, 5!};$$

$$N_1 = \frac{(1 - \kappa)\, \dot{Q}_o}{\frac{4}{3}\pi a^4\, \rho c\, w_o\, \pi R_o^2\, 5!}. \qquad (8)$$

Finally, after these preliminaries we can obtain the distribution of ξ, the distances downwind from the breakaway point where the drops land (ignoring turbulence and variations in x_b and z_b). During an arbitrary time interval T, the number of r-drops that leave the tower is $f(r)\, dr\, \pi R_o^2\, w_o\, T$. After some delay time (irrelevant if steady-state conditions prevail) these specific r-drops will land at 5 to $\xi + d\xi$ where

$$\xi = \frac{\bar{u}\, z_b}{v_s(r)}. \qquad (9)$$

Thus during a time interval T (delayed from the time interval used above, but of the same length) the amount of chromium deposited at ξ to $5 + d\xi$ is just

$$4/3\, \pi r^3\, \rho c\, \pi R_o^2\, w_o\, T\, f(r)\, dr \qquad (10)$$

where r is such that (9) is satisfied.

For the large drop mode we have $v_s = sr$. Then the amount of chromium deposited by the large drops at ξ to $\xi + d\xi$ during the time interval T is

$$4/3\, \pi \left(\frac{\bar{u}\, z_b}{s\xi}\right)^3 \rho c\, \pi R_o^2\, w_o\, T\, f\left[r = r(\xi)\right] \left|\frac{dr}{d\xi}\right| d\xi. \qquad (11)$$

For the small drop mode we use (6) and obtain a similar expression.

It is convenient to nondimensionalize these two expressions for the amount of chromium deposited. The total amount of chromium released during the arbitrary time interval T is $\dot{Q}_o T$. Then the fraction of the total amount of chromium released, that lands at ξ to $5 + d\xi$ is

$$\gamma\, d\xi = \frac{\kappa}{5!}\left[\frac{\bar{u}\, z_b}{v_s(b)\, \xi}\right]^6 \exp\left[-\frac{\bar{u}\, z_b}{v_s(b)\, \xi}\right]\frac{d\xi}{\xi}$$

$$+ 1/2\, \frac{(1 - \kappa)}{5!}\left[\frac{\bar{u}\, z_b}{v_s(a)\, \xi}\right]^3$$

$$\exp\left\{-\left[\frac{\bar{u}\, z_b}{v_s(a)\, \xi}\right]^{1/2}\right\}\frac{d\xi}{\xi}. \qquad (12)$$

In Figure 13 we have plotted the nondimensional fractional flux, $z_b\gamma$ for the a and b values used in Figure 11 and for $\kappa = 0.05$ and $\bar{u} = 5$ $msec^{-1}$. The value $\kappa = 0.05$ means that 5% of the total chromium released is carried by the large-drop mode. Since $\gamma\, d\xi$ is the fraction of the flux (or amount) from the tower that lands at 5 to $\xi + d\xi$, then γ has units of m^{-1} and $z_b\, \gamma$ is dimensionless. The abscissa is also nondimensionalized with the height of the breakaway point, z_b. Upon comparing Figures 11 and 13 it is clear (and also intuitively obvious) that the wind simply "inverts" the size distribution, the larger drops being deposited closer to the tower. However, it was not immediately obvious how the relative magnitudes of the two peaks would change, and this is shown in Figure 13 for the specific choice of the free parameters.

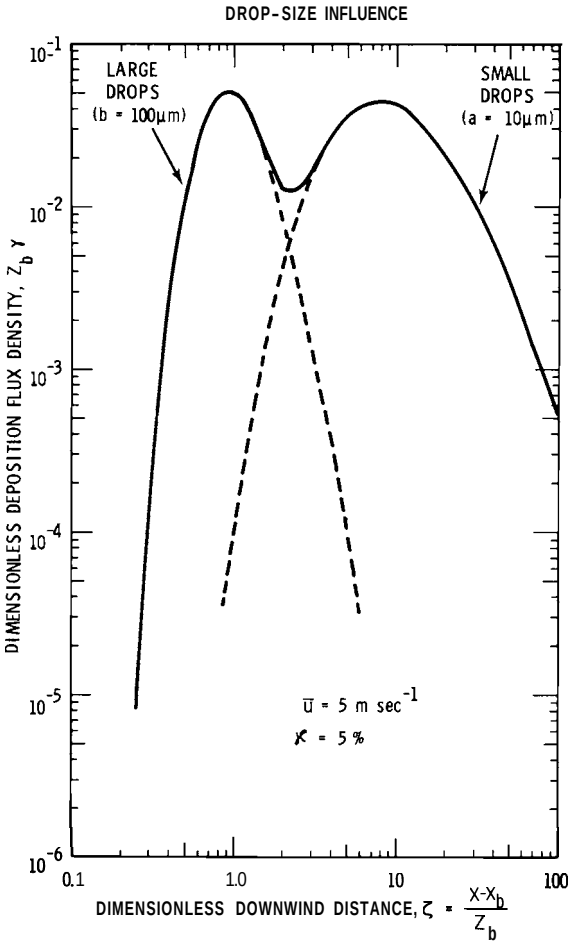

Neg 740753

FIGURE 13. The Deposition Flux as a Function of Downwind Distance when Turbulence Is Ignored as well as the Variability in the Breakaway Points

INFLUENCE OF TURBULENCE

If we now ignore the variability in the breakaway point and also just concentrate on a single drop size, then we can use the developments of others to estimate the influence of turbulence (Van der Hoven; Stewart).[19,20] We take the air concentration of drops of a specific size range to be

$$\chi(x,y,z) = \frac{\dot{Q}_r\, dl}{2\pi\, \bar{u}\, \sigma_y\, \sigma_z} \exp\left(-\$_Y\right) \left(\frac{\left\{z - \left[z_b - \frac{v_s}{\bar{u}}(x - x_b)\right]\right\}^2}{2\sigma_z^2}\right) \qquad (13)$$

where $\dot{Q}_r\, dr$ is the number of r-drops/sec that break free from the fixed breakaway point (x_b, z_b). To obtain (13) all'one does is replace the stack height, h, in the usual Gaussian plume model by the apparent stack height $z_b - v_s\, t$ where $t = (x - x_b)/\bar{u}$ is the fall time. We propose to ignore the effect discussed by Csanady,[21] namely, that large drops will not be influenced by the high frequency modes of the turbulence. That is we take'a$_Y$ and σ_z in (13) to be the values obtained for massless particles.

The number flux to the ground is just $v_s\, \chi(x,y,o)$. If (13) is integrated across the mean wind,* then the linear flux density (particles m^{-1} sec^{-1}) is just

$$\frac{v_s}{\bar{u}} \frac{\dot{Q}_r\, dr}{(2\,\pi\sigma_z^2)^{1/2}} \exp\left(-\frac{\left\{x - \left[x_b + (\bar{u}/v_s)\, z_b\right]\right\}^2}{2\left(\frac{\bar{u}}{v_s}\,\sigma_z\right)^2}\right) \qquad (14)$$

* Incidentally it is of interest to notice that almost the only stochastic process which influences the crosswind distribution is the atmospheric turbulence and therefore that one can experimentally gain an indication of the importance of diffusion to the deposition pattern.

For constant σ_z, this is a Gaussian distribution of x about the mean position

$$\langle x \rangle = x_b + \frac{\bar{u}}{v_s} z_b, \quad v_s \neq 0 \qquad (15)$$

(which is intu'itively obvious since the fall time is z_b/v_s). The variance of the distribution of the drift drops caused by turbulence is

$$\left(\sigma_x^t\right)^2 = \left(\frac{\bar{u}}{v_s} \sigma_z\right)^2, \quad v_s \neq 0, \qquad (16)$$

which, at least to this author, is not an obvious result.

Whether or not diffusion is significant depends in part on the magnitude of σ_z. If $\sigma_z \to 0$ (very stable conditions), then (14) becomes a delta function about the mean position (15). Then the same results will be obtained as were demonstrated in Figure 13. For unstable conditions, suppose we take $\sigma_z = kx$ where k is a dimensionless constant near 0.1. Diffusion will broaden the peaks of Figure 13 and the question is whether or not the breadth (σ_x^t) caused by turbulence is larger or smaller than the breadth caused by the drop-size distribution, σ_x^d.

One way to compare the stochastic influences of turbulence and of the distribution of drop sizes is to compare the variances of the two distributions. From (12) we have that the mean position of the deposition from the large drop mode is

$$\langle \xi \rangle = \frac{1}{5!} \int_0^\infty \frac{d\xi}{\xi} \xi \left[\frac{\bar{u} z_b}{v_s(b) \xi}\right]^6 \exp\left[-\frac{\bar{u} z_b}{v_s(b) \xi}\right]. \qquad (17)$$

This can be evaluated easily. Similarly the variance for the large drop distribution is found to be

$$\left(\sigma_x^d\right)^2 = \left\langle (\xi - \langle \xi \rangle) \right\rangle = \left[\frac{\bar{u}}{v_s(b)} \frac{z_b}{10}\right]^2 \qquad (18)$$

where $v_s(b)$ is the settling velocity of drops of radius b (i.e., for b = 100 μm, $v_s(b) \doteq 0.8$ msec^{-1}). Upon comparing (18) and (16) we see that the ratio of the spread caused by turbulence from some drop size, r, (and assuming that it is a Gaussian distribution even when σ_z is a variable) to that caused by the large drop size distribution is approximately

$$\frac{\sigma_x^t(r)}{\sigma_x^d(b)} = 10 \frac{v_s(b)}{v_s(r)} \frac{\sigma_z}{z_b}. \qquad (19)$$

Similarly for the small drops we obtain

$$\frac{\sigma_x^t(r)}{\sigma_x^d(b)} = \left(\frac{10}{7} 5!\right)^{1/2} \frac{v_s(a)}{v_s(r)} \frac{\sigma_z}{z_b} \qquad (20)$$

It is interesting that these ratios are independent of ϖ.

To determine whether the spread caused by turbulence or by the drop size distribution is greater, we need a specification of the breakaway point, z_b, and. of σ_z. In Figure 14 we have plotted (19) and (20) for the case $\sigma_z = k(x - x_b)$ where k is a constant, and nondimensionalized lengths with z_b. For the large-drop mode we took b = 100 μm and $v_s(r)$ to be the settling velocity of the drops at the mass peak of Figure 11, i.e., $v_s = v_s(500\ \mu m) = 4$ msec^{-1}. For the small-drop mode we took a = 10 μm and $v_s = v_s(50\ \mu m) = 0.25$

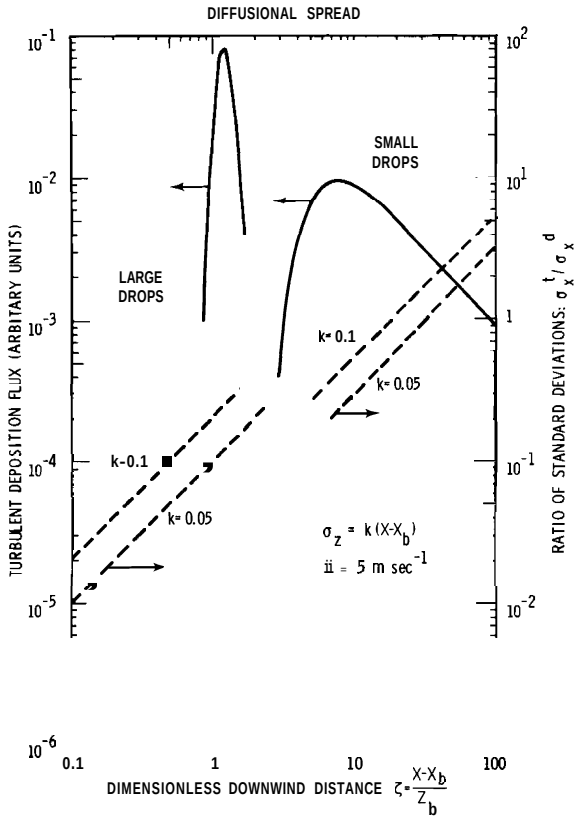

Neg 740753-3

FIGURE 14. The Deposition Flux when the Drop Size Distribution is Ignored and for a Fixed Breakaway Point. The Ordinate on the RHS is the Ratio of the Standard Deviation Caused by Turbulence to that Caused by the Drop-Size Distribution of Figure 11.

msec^{-1}. From this plot it is seen that for these particular values of the parameters, $\sigma_x^t/\sigma_x^d << 1$ for the large-drop mode. For the small-drop mode, the two variances are of comparable magnitude. In Figure 14 we have also shown the essence of the distribution (14) which reinforces the idea that the spread caused by turbulence is negligible for the large-drop mode. In this regard, compare Figures 13 and 14.

AN ESTIMATE OF THE BREAKAWAY POINTS

In the above we have ignored any variability in the points where drops break free from the influence of the plume's updraft. In fact, none of the results obtained depended explicitly upon the updraft, w_o, but the dependence is implicit in the breakaway coordinates (x_b, z_b). To specify (x_b, z_b) is not at all trivial and has resulted in a number of different assumptions in the literature. For example, Hosler et al.(") assumed that drops of a given size break free when the updraft in a vertical plume falls to v_s for this size. Further, they assumed w_o falls linearly with z. Roffman and Grimble[23] apparently take all drops to the full plume rise (assumed to be vertical) and let all drops break free from this point. Apparently Wistrom and Ovard[17] let the drops break free from the plume right at the top of the tower. In this section we present a crude model to estimate the distribution of breakaway points for different drop sizes.

Although we do not know how to determine the breakaway points accurately, it seems that other authors have omitted a fundamental feature: namely, the influence of the plume's turbulence. A vivid picture of its importance can be imagined by the reader if he will ask himself how close he would stand to a horizontal jet of sulfuric acid. To describe this semiquantitatively we write a continuity equation for the density of r-drops in the plume:

$$\frac{d}{ds}(fdr\ \pi R^2\ w)\ As\ At = -2\ \pi R\ As\ At\ (Flux) \quad (21)$$

where (Flux) is the turbulent flux of r-drops through the plume's boundary.

It seems to us that there are two components to this flux. The first is independent of the fall velocity of the drops, and we estimate it to be

$$K\nabla(fdr) \sim K\left(\frac{fdr}{R}\right) \sim \frac{\beta\ w_o\ R}{2}\left(\frac{fdr}{R}\right) \sim \frac{\beta}{2} w_\Theta\ fdr \quad (22)$$

where K is a turbulent diffusivity and $\beta/2$ is an unknown numerical factor. We envision a second component which follows from the physical fact that a drop will not exactly follow the fluid as it swirls out and then becomes re-entrained by the plume, and thereby drops will be sprayed out from the plume's boundary. We approximate this flux by $(\gamma/2)\ v_s\ fdr$ where $(\gamma/2)$ is another numerical factor.

These assumed expressions for the flux are now substituted into the continuity Equation (21). Further, recognizing the crudeness of this analysis, we approximate w d/ds by $\bar{u}$ d/dx (or by w_o d/dz if there were zero mean wind, but this is a case of little practical interest). We also treat R to be a constant: $R = R_o$, the initial plume radius. Then (21) can be integrated to give

$$f(r,x) = f_o(r)\ \exp\left[-\left(\frac{\beta\ w_o}{\bar{u}} + \frac{\gamma}{\bar{u}}\frac{v_s}{}\right)\frac{x}{R_o}\right] \quad (23)$$

where $f_o(r)$ is the drop-size distribution at the plume exit. With the above we have the flux of drops from the segment of the plume at s to s + As is

$$\left(\beta\ w_o + \gamma\ v_s\right) f(r,x)\ dr\ \pi R_o\ \Delta s \quad (24)$$

with f given by (23).

Although (24) may eventually be a useful result, it is essentially useless now, because we have found no data from which to estimate β and y. Physical intuition suggests $\beta = O(10^{-2})$ and $y = O(1)$; in other words, the large-drop mode will be sprayed out from the plume in a few plume radii downwind, and the small-drop mode will almost perfectly follow the motion of the air in the plume. Consequently, until data becomes available, we suggest that it will be within the order of magnitude of the accuracy of the entire theory to assume that the coordinates of the breakaway point for the large-drop mode is at the top of the tower: $(x_b, z_b) = (\Theta, h)$, and for the small-drop mode that most of it remains entrained with the plume. Partly just to observe the consequences of this assumption on the results, we propose to assume that a small fraction, say β, of the small-drop mode does break free from the plume right at the top of the tower.

SUMMARY STATEMENT

The goal of this study was to search for the stochastic-dominating processes in the drift deposition problem. It must be concluded that

we have been only very marginally successful in finding such processes, partly because there appears no strongly dominating process and partly because we have no adequate model to describe the breakaway process. The major positive result, though, appears to be that the drop-size distribution is the stochastic dominating process for the large- (or drift--or carry-over) drop mode. Until further progress is made with analysis of the breakaway points, we suggest that the breakaway points for the large-drop mode be taken to be at the top of the cooling tower. For the smaller drops (essentially cloud drops) in the plume, it appears that diffusion and the drop-size distribution have comparable effects on the deposition patterns, at least within the first ten or so tower heights downwind. At further distances, unless the atmosphere is very stable, turbulence will begin to dominate the deposition pattern. Again, until further progress is made with the breakaway problem, we recommend that the deposition of these small (or cloud) drops be estimated using a Gaussian plume model and assuming that the drops do not breakfree from the plume's updraft, except for some unknown fraction, β, which breaks free at the top of the tower.

ILLUSTRATIVE RESULTS

In the above analysis the main thrust was to identify the stochastic-dominating process in drift deposition. Consequently no attempt was made to display the results (however tentative they may be) in a form which might be useful for applications (or, more appropriately, for comparison with experimental data, to see if our results are correct). This omission will be partially remedied in this section by concisely presenting the formulae which have been suggested.

The problem posed is to predict the crosswind-integrated chromium deposition downwind of a single cooling tower of height h, source strength $\dot{Q}_o$ (g chromium sec^{-1}), and initial buoyancy flux F_o (see Briggs).[12] The proposed procedure is first to obtain the drop size distribution and from it identify the characteristics of the large-drop mode. Next one calculates the deposition pattern of these large drops, ignoring turbulence and assuming the breakaway point is at the top of the tower. This can be done numerically simply using a histogram fit through the drop-size distribution, or it can be done analytically.

In the latter case the number distribution of the large-drop mode might be fit, for example, by a gamma distribution

$$f(r)\ dr = N dr \left(\frac{r}{b}\right)^{\nu} \exp\left(-\frac{r}{b}\right). \qquad (25)$$

If the amount of chromium leaving the tower, during a time interval T, carried by the large drops is $\kappa \dot{Q}_o T$, then the normalization constant N is given approximately by [see (7)]

$$N = \frac{\kappa Q_o}{4/3\ \pi b^4\ \rho c\ w_o\ \pi R_o^2\ \Gamma(\nu + 4)}. \qquad (26)$$

Then the fraction of the total chromium released in the large-drop mode and deposited on the ground on a strip from x to x + dx is

$$\gamma\, dx = \frac{\kappa}{\Gamma(\nu + 4)} \left[\frac{\bar{u}\, h}{v_s(b)\, x}\right]^{\nu+4} \exp\left[-\frac{iih}{v_s(b)\, x}\right] \frac{dx}{x}. \quad (27)$$

Once the distribution of these large drops has been found it is proposed that the deposition flux of the small drops be found from $v_s(\bar{r}_m)\, \chi(x, y, o)$ where $\bar{r}_m$ is the radius of the mass peak (or the mass-average radius) and where the air concentration χ is given by some Gaussian plume model. For example, if the "2/3 law" (see Briggs)[12] is used to describe the trajectory of the plume:

$$z_p = h + 1.6\, \frac{F_o^{1/3}\, x^{2/3}}{\bar{u}}, \quad (28)$$

then the air concentration of the (cloud) drops could be taken as

$$\chi = \frac{(1 - \kappa)\, \dot{Q}_o}{2\pi\sigma_y\, \sigma_z\, \bar{u}} \exp\left\{\frac{-y^2}{2\sigma_y^2} - \frac{[z - (z_p - v_s\, x/\bar{u})]^2}{2\sigma_z^2}\right\}. \quad (29)$$

Substituting (28) into (29) and normalizing the result by the amount of chromium released we obtain the cross wind-integrated fraction of material that is deposited by the small-drop mode on a strip from x to x + dx:

$$\gamma\, dx = \frac{dx}{\sigma_z} \frac{(1 - \kappa)}{\sqrt{2\pi}} \frac{v_s(\bar{r}_m)}{\bar{u}} \exp\left\{-\frac{1}{2\sigma_z^2}\left[h + 1.6\, \frac{F_o^{1/3}\, x^{2/3}}{\bar{u}} - \frac{v_s(\bar{r}_m)\, x}{\bar{u}}\right]\right\}. \quad (30)$$

Finally we suggest that a fraction β of the small-drop mode be assumed to break free from the plume at the top of the tower and that their diffusion be ignored. In reality drops break free all along the plume's trajectory, but the details of this process are not known. Also, as we have seen, diffusion does become important at about five to ten tower heights downwind. However, since so many uncertainties enter into this aspect of the problem, we suggest that these assumptions and the presence of an "ignorance" parameter, β, can be used to remind us of the uncertainties. The resulting normalized deposition flux is [see (12)]

$$\gamma\, dx = \frac{dx}{x} \frac{\beta\,(1 - \kappa)}{5!} \left[\frac{\bar{u}h}{v_s(a)\, x}\right]^3 \exp\left\{-\left[\frac{v_s(\bar{a})\, x}{\bar{u}h}\right]^{1/2}\right\}. \quad (31)$$

Further corrections to this formalism should account for drop evaporation and for cloud depletion because of deposition, but it is the author's opinion that the theory is not yet sufficiently developed to justify these refinements.

The results (27), (30) and (31) are illustrated in Figure 15 for

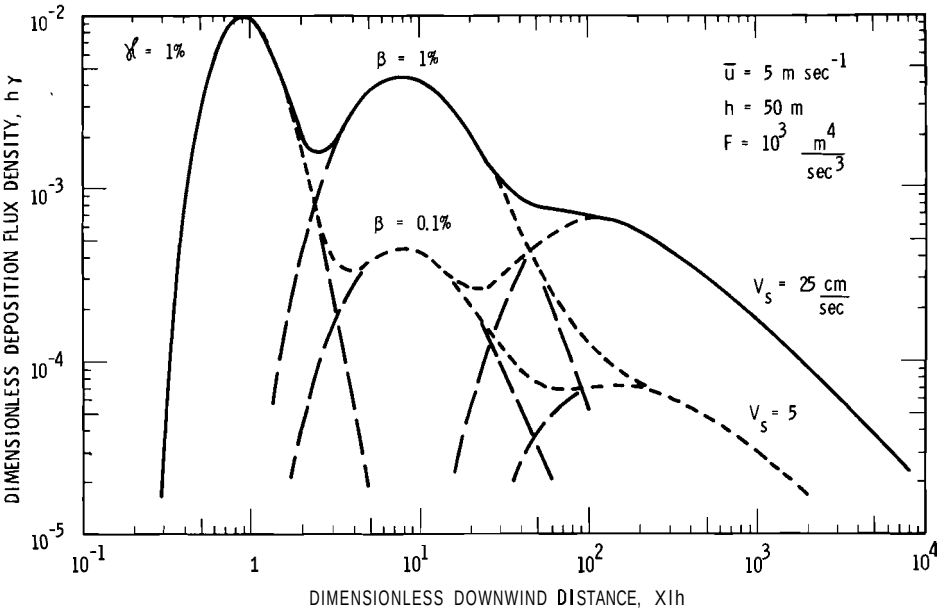

Neg 740753-5

FIGURE 15. Illustrative Results for Specific Values of the Parameters in Equations (27), (30) and (31). β is the fraction of the small drops which are assumed to break free at the top of the cooling tower. κ is the fraction of the pollutant that is in the large (drift or carry-over) drops.

1. Large-drop mode: $\nu = 2$, $b = 100\ \mu m$, $v_s(b) = 0.8\ msec^{-1}$, $\kappa = 1\%$.
2. Small-drop mode: $\bar{r}_m = 50\ \mu m$, $v_s(r_m) = 0.25\ msec^{-1}$, $(1 - \kappa) = 99\%$, $\beta = 1\%$ and 0.1%.
3. Plume: $F_o = 10^3\ m^4\ sec^{-3}$, $h = 50$ m.
4. Atmosphere: $\bar{u} = 5\ msec^{-1}$, $\sigma_z = 0.1\ x$.

In Figure 15 we have plotted the nondimensional deposition flux hy, where $\gamma\ dx$ is the fraction of the chromium released that lands at x to x + dx, against nondimensional downwind distance $\zeta = x/h$. Plotted in this way the results are almost independent of h. Figure 15 demonstrates the significant consequences if there is 1% or 0.1% of the small drops which break free at the tower top. We also show the difference which occurs if $v_s(\bar{r}_m) = 25\ cm\ sec^{-1}$ or $5\ cm\ sec^{-1}$, the latter perhaps being a reasonable deposition velocity if the drops evaporate. If the initial buoyancy flux F_o is smaller, then the small-drop peak will shift closer toward the tower.

CONCLUSIONS

Earlier in this report a summary statement of the results of this study is presented and it will not be repeated here. To put our conclusions into perspective we note that predictions of drift deposition,

especially of salt deposition downwind of proposed brackish-water cooling towers, are proliferating almost as rapidly as are cooling towers. Conclusions being reached include:

"The assessment of the environmental effects caused by drift from a salt water cooling tower was made and it was concluded that beyond some reasonable distance, usually within the plant site boundary, drift does not effect the environment" (Wistrom and Ovard). [17]

"The most important result would seem to be that, when attention is paid to actual time of flight of droplets the salt fallout is not excessive and it appears that saltwater will not be accompanied by unmanageable environmental hazards" (Hosler et al.).[22]

"The predicted salt deposition rates obtained by this model are lower than those derived by currently used models" (Roffman and Grimble, 1973). [23]

From the study presented here we conclude that drift depostion can not be predicted at all well; there are uncertainties of at least an order of magnitude, resulting in the main from the poorly answered question of where the drops break free from the influence of the plume's updraft. Consequently we are of the opinion that the calculations in the reports quoted above can not be used to justify significant conclusions with respect to environmental impact. However, as pointed out by Engelmann,[24] whether or not salt or chromium or some other pollutant from cooling towers will cause significant environmental stress is really not a meteorological problem. Meteorologists can, at best, present accurate predictions of drift deposition to ecologists or others competent in assessing the resulting environmental stress. Further, it is apparent to the author that it would be much more profitable if fewer models of drift deposition were developed and, instead, if more measurements were made. In this regard the recent data obtained by Wolf et al.[25,26] is a most welcome contribution.

ALE RESERVE CLIMATOLOGY FOR 1973

J. M. Thorp

The Arid Lands Ecology Reserve microclimatological program will encompass 5 years of monthly maximum and minimum temperatures and monthly precipitation data at the end of calendar year 1973. An interim climatological summary of these data is planned for publication in 1974. Bioyear precipitation for 1973 was the least in the 5 years of record. A range fire burned over some 9,000 acres of ALE land in August.

Precipitation measurements at 26 sites on the Arid Lands Ecology (ALE) Reserve commenced in October 1968. The data collected by the end of 1973 will thus permit 5-year precipitation statistics on both bioyear (October-May) and calendar year periods. Monthly maximum and minimum temperatures which have been tabulated for the same time period, though, are of less value in a climatological sense as they are not representative of the monthly temperature regime except in the most general way. However, since January 1971 daily data from temperature recording instruments located at nine sites on the ALE Reserve have been processed with the monthly data. Thus, at the end of 1973, 3 years of daily temperature data will be in hand. Though the period of record is too short for a valid climatology, it is felt that a so-called "interim climatology" will be of value to scientists conducting experiments and research on the ALE Reserve. This work is planned for early 1974.

On a current note is a presentation of the October 72-May 73 bioyear precipitation on the ALE Reserve (Figure 16). At the Hanford Meteorology Tower, precipitation for this period showed all months but December 1972 below normal. This apparently is consistent for the ALE Reserve also, though length of record there precludes establishment of normals for each site at this time. Of the 5 years of record, certainly Bioyear 1972-73 had the least precipitation of all.

On August 13-14, range fires set by lightning burned over about 9,000 acres at the eastern end of the ALE Reserve. Three climatological sites--Calochortus #191, Beetle Plot 5 #251 and Beetle Plot 6 #260--were within the burned area, though only site #251 was damaged. At that site, the plastic rain gage and the plastic frame for the max/min thermometer were deformed by the heat. However, the thermometer was not broken. The heat side of the thermometer is scaled to 126°F, and the resetting

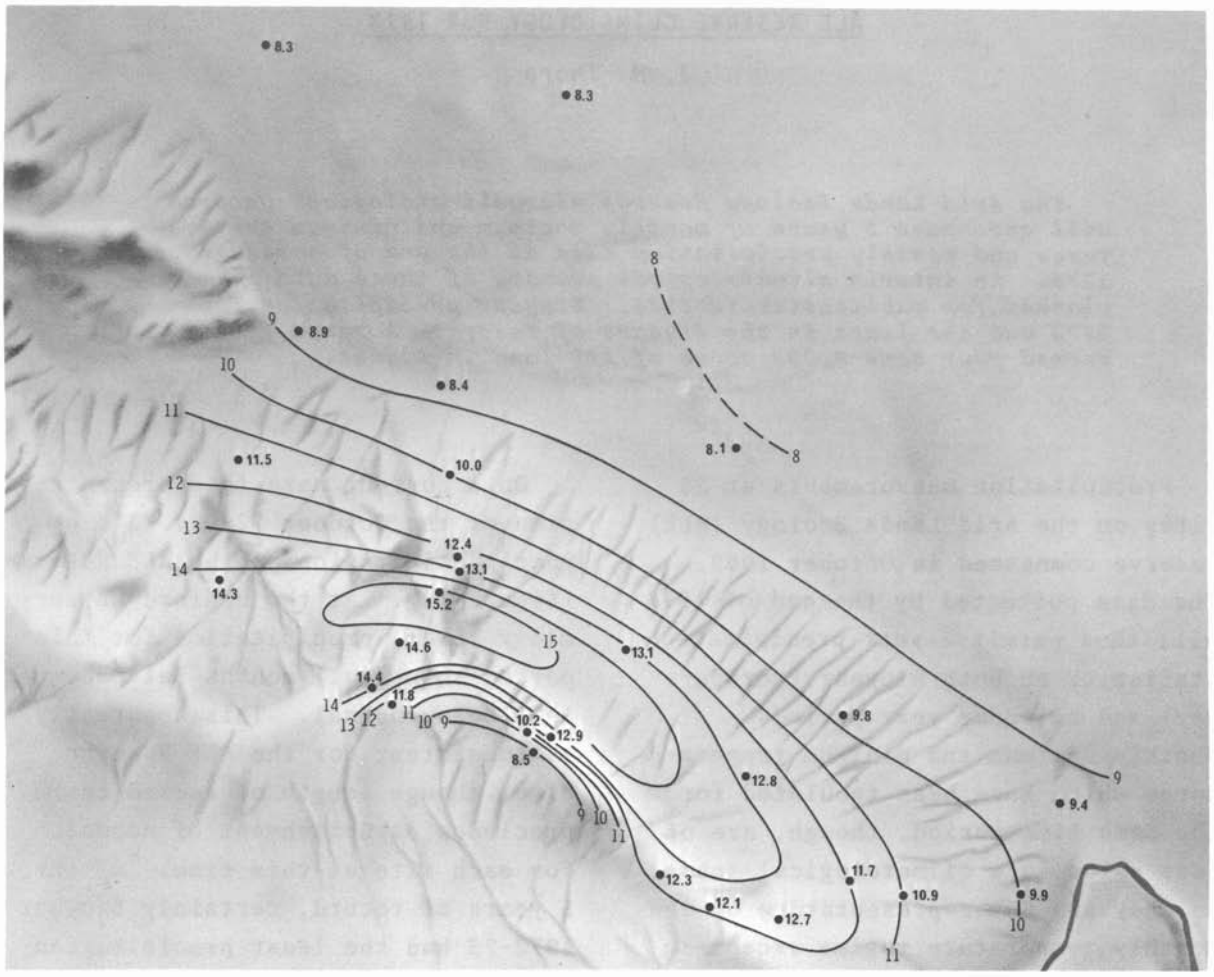

Neg 735930-1

FIGURE 16. Precipitation in Centimeters of Water as Measured at 27 Sites on or near the Arid Lands Ecology Reserve During the Bioyear October 1972 to May 1973

index was driven considerably beyond that position and into the end of the tube. Hot water tests indicate that at least 160°F is required to do this. A comparison of maximum temperatures at these sites with others at similar elevations, but in unburned areas, is given in Table 3. Judging from these temperatures, only slightly higher than normal summer maxima, it seems reasonable to expect that over much of the burned area the native grasses will survive.

TABLE 3. Comparison of Maximum Temperatures in Unburned Areas

Site NO.	Elevation, ft	Maximum Temp., °F	Comment
191	1250	113	Site near edge of burn, sparse vegetation
251	1470	160+	Plastic gages deformed, shelter smudged
260	2480	112	Site near edge of burn, sparse vegetation
141	1200	108	Unburned area
081	1600	106	Unburned area
101	2440	103	Unburned area

REFERENCES

1. Daily, Monthly and Annual Climatological Data for Oak Ridge, Tennessee, Townsite and Area Stations, January 1951 through December 1971, Air Resources Atmospheric Turbulence and Diffusion Laboratory, Oak Ridge, TN, July 1972.

2. B. R. Morton, G. I. Taylor and J. S. Turner, "Turbulent Gravitational Convection from Maintained and Instantaneous Sources," Proc. Roy. Soc., London, vol. A 23, pp. 1-23, 1956.

3. G. A. Briggs, "Some Recent Analyses of Plume Rise Observations," Presented at the 1970 International Air Pollution Conference of the IUAPPA, Reprint available from NOAA Atmospheric Turbulence and Diffusion Laboratory, Oak Ridge, TN, ATDL-38, 1970.

4. P. R. Slawson and G. T. Csanady, "The Effect of Atmospheric Conditions on Plume Rise," J. Fluid Mech., vol. 47, pp. 33-49, 1971.

5. R. S. Scorer, "Plumes, Jets and Entrainment Coefficients" in the Microphysics and Dynamics of Convective Clouds - A Colloquium, NCAR-TN-52, National Center for Atmospheric Research, Boulder, CO. 1970.

6. S. R. Hanna, "Meteorological Effects of Cooling Tower Plumes," Presented at the Cooling Tower Institute Winter Meeting, Houston, TX, January 25, 1971, available in the Proceedings or as ATDL-48, 1971.

7. B. R. Morton, "The Choice of Conservation Equations for Plume Models," J. Geophys. Res. vol. 76, pp. 7409-7416, 1971

8. W. G. N. Slinn, "Kinematically Possible Flows Exterior to Jets and Plumes," Pacific Northwest Laboratory Annual Report for 1971 to the USAEC, Division of Biology and Medicine, Volume II. Physical Sciences, Part 1, Atmospheric Sciences, Battelle, Pacific Northwest Laboratories, Richland, WA, BNWL-1651 Pt 1, 1972. Available from NTIS.

9. G. J. Haltiner and F. L. Martin. Dynamical and Physical Met., McGraw-Hill, NY, 1957.

10. J. Simpson and V. Wiggert, "Models of Precipitating Cumulus Towers," Mon. Wea. Rev., vol. 97, pp. 471-489, 1970.

11. S. R. Hanna, "Rise and Condensation of Large Cooling Tower Plumes, J. Appl. Met., vol. 11, pp. 793-799, 1972.

12. G, A. Briggs, Plume Rise, AEC Critical Review Series, available from NTIS as TID-25075, Springfield, VA, 1969.

13. D. P. Hoult, J. A. Fay and L. J. Forney, "A Theory of Plume Rise Compared with Field Observations," J. Air Pollut. Contr. Assoc., vol. 19, pp. 585-590, 1969.

14. E. J. Plate, Aerodynamic Characteristics of Atmospheric Boundary Layers, AEC Critical Review Series, available as TID-25465 from NTIS, Springfield, VA, 1971.

15. W. G. N. Slinn, "Rate Limiting Aspects of In-cloud Scavenging," BNWL-SA-3768, J. Atmos. Sciences, 1974, in press.

16. W. G. N. Slinn. "Initial Resuspension Models," Pacific Northwest Laboratory Annual Report for 1972 to the USAEC, Division of Biology and Medicine, Volume II, Physical Sciences, BNWL-1751, Pt. 1, Atmospheric Sciences, Battelle, Pacific Northwest Laboratories, Richland, WA, 1973, Available from NTIS, Springfield, VA.

17. G. K. Wistrom and J. C. Ovard, "Cooling Tower Drift--Its Measurement, Control and Environmental Effects," Presented at the Cooling Tower Institute Annual Meeting, Houston TX, January 29-31, 1973.

18. S. R. Hanna and S. G. Perry, "Meteorological Effects of the Cooling Towers at the Oak Ridge Gaseous Diffusion Plant," to be published, 1974.

19. I. Van der Hoven, "Deposition of Particles and Gases," in Meteorology and Atomic Energy 1968, D. H. Slade, ed., available from NTIS as TID-24190, Springfield, VA, 1968.

20. R. E. Stewart, "Atmospheric Diffusion of Particulate Matter Released from an Elevated Continuous Source," J. Appl. Met., vol. 7, pp. 425-432, 1968.

21. G. T. Csanady, "Turbulent Diffusion of Heavy Particles in the Atmosphere," J. Atmos. Sciences, vol. 20, pp. 201-208, 1963.

22. C. L. Hosler, J. Pena and R. Pena, Determination of Salt Deposition Rates from Drift from Evaporative Towers, Dept of Meteorology, Pennsylvania State University, May 1972.

23. A. Roffman and R. E. Grimble, "Predictions of Drift Deposition from Salt Water Cooling Towers," Presented at the annual meeting of the Cooling Tower Institute, Houston, TX, January 29-31, 1973.

24. R. J. Engelmann, USAEC, Division of Biomedical and Environmental Research, Private communication, 1973.

25. M. A. Wolf, R. N. Lee and J. W. Sloot, Measurements of Chromate Resulting from Cooling Tower Drift at the Oak Ridge Gaseous Diffusion Plant, Final Report to Union Carbide Nuclear Co., Oak Ridge, TN, Battelle, Pacific Northwest Laboratories, Richland, WA, October 1973.

26. M. A. Wolf, et al., "Measurements of Drift from a Mechanical Draft Cooling Tower," in this report, 1974.

PUBLICATIONS AND PRESENTATIONS

PUBLICATIONS AND PRESENTATIONS

DOCUMENTS

Dana, M. T., J. M. Hales, W.G.N. Slinn and M. A. Wolf, Natural Precipitation Washout of Sulfur Compounds from Plumes, EPA-R3-73-047, June 1973.

Hales, J. M., J. O. Wilkes and J. L. York, The Application of Ideal Reactors to Studies in Atmospheric Chemistry, BNWL-1773, Battelle, Pacific Northwest Laboratories, Richland, Washington, 1973.

Lee, R. N., J. W. Sloot and M. A. Wolf, Measurements of Chromate Resulting from Cooling Tower Drift at the Oak Ridge Gaseous Diffusion Plant, Subcontract No. 11K-24804, Union Carbide Nuclear Company, Oak Ridge, Tennessee, October 1973.

Mishima, J. and L. C. Schwendiman, Some Experimental Measurements of Airborne Uranium (Representing Plutonium) in Transportation Accidents, BNWL-1732, Battelle, Pacific Northwest Laboratories, Richland, Washington, August 1973.

Ramsdell, J. V. and D. C. Powell, Meteorological Information for Vertical and Short Take-Off and Landing (V/STOL) Operations in Built-up Urban Areas - An Analysis, FAA-RD-72-135, Department of Transyortation, Federal Aviation Administration, Systems Research and Development Service, Washington, D.C., September 1973.

Selby, J. M. et al., Considerations in the Assessment of the Consequences of Effluents from Mixed Oxide Fuel Fabrication Plants, BNWL-1697, Battelle, Pacific Northwest Laboratories, Richland, Washington, June 1973.

Simpson, C. L. and Staff, Pacific Northwest Laboratory Annual Report for 1972 to the USAEC Division of Biomedical and Environmental Research, Volume II: Physical Sciences, Part 1., Atmospheric Sciences, BNWL-1751 Pt. 1, Battelle, Pacific Northwest Laboratories, Richland, Washington, April 1973.

Young, J. A., N. A. Wogman, C. W. Thomas, and T. M. Tanner. Feasibility Study of the Use of Inert Tracers in the National Hail Research Experiment, BNWL-1763, final report to the National Science Foundation, June 27, 1973.

PUBLICATIONS

Alkezweeny, A. J. and L. F. Radke, "Airborne Measurements of the Size Distribution and the Condensation and Ice Nucleating Ability of Particles Produced by AgI-containing Pyrotechnics and Acetone Solution Burners," BNWL-SA-4716, Proceedings of the Eighth International Conference on Nucleation of the IAMAP (ICCP), Leningrad, U.S.S.R., September 23-29, 1973, November, 1973 (in press).

Alkezweeny, A. J., M. T. Dana, J. M. Hales, T. M. Tanner, C. W. Thomas, J. M. Thorp, J. A. Young and N. A. Wogman, "Activities of the Battelle-Northwest Laboratory in METROMEX," BNWL-SA-4822, accepted for publication in AMS Bulletin, October 1973.

Droppo, J. G., Jr. and H. L. Hamilton, Jr., "Experimental Variability in the Determination of the Energy Balance in a Deciduous Forest," J. Appl. Met., vol. 12, no. 5, pp. 781-791, August 1973.

Hadlock, R. K. et al., "The Role of Convection in Surface Property and Velocity Fluctuations," accepted for publication in J. Boundary-Layer Met., August 1973.

Hadlock, R. K. and P. H. Stone, "Direct Thermal Verification of Symmetric Baroclinic Instability," J. Atmos. Sci., vol. 30, no. 8, pp. 1702-1703, November 1973.

Hales, J. M. and S. L. Sutter, "Solubility of Sulfur Dioxide in Water at Low Concentrations," Atmos. Env., vol. 7, pp. 997-1001, 1973.

Hales, J. M., J. O. Wilkes and J. L. York, "Some Recent Measurements of H_2S Oxidation Rates and Their Implication to Atmospheric Chemistry," BNWL-SA-4512, accepted for publication in Tellus, May 1973.

Hales, J. M., M. A. Wolf and M. T. Dana, "A Linear Model for Predicting the Washout of Pollutant Gases from Industrial Plumes," AIChE Journal, vol. 19, pp. 292-297, 1973.

Hane, C. E., "The Squall Line Thunderstorm: Numerical Experimentation," J. Atmos. Sci., vol. 30, no. 8, November 1973.

Horst, T. W., "Corrections for Response Errors in a Three-Component Propeller Anemometer," J. Appl. Met., vol. 12, no. 4, pp. 716-725, June 1973.

Horst, T. W., "Spectral Transfer Functions for a Three-Component Sonic Anemometer," J. Appl. Met., vol. 12, no. 6, pp. 1072-1075, September 1973.

Nickola, P. W., "Field Measurements of the Benefits of Increased Stack Height," BNWL-SA-4744. submitted to the J. Air Poll. control Assoc., July 1973.

Sehmel, G. A., "Particle Eddy Diffusivities and Deposition Velocities for Isothermal Flow and Smooth Surfaces," Aerosol Sci., vol. 4, pp. 125-138, 1973.

Sehmel, G. A., "Particle Resuspension from an Asphalt Road Caused by Car and Truck Traffic," Atmos. Env., vol. 7, pp. 291-301, 1973.

Slinn, W.G.N., "The Redistribution of a Gas Plume Caused by Reversible Washout," BNWL-SA-4647, accepted for publication in Atmos. Env., March 1973.

Slinn, W.G.N., "Residence Time of Particles in Urban Air," Atmos. Env., vol. 7, pp. 763-765, 1973.

Slinn, W.G.N. and A. G. Gibbs, "Fluctuations in Trace Gas Concentrations in the Troposphere," J. Geophysical Research, vol. 78, pp. 574-576, 1973.

Slinn, W.G.N., "A Postulated Estimate of Wet Versus Dry Deposition Downwind of a Point Source of Pollution," BNWL-SA-4800, submitted for publication in Atmos. Env., October 1973.

Slinn, W.G.N. "Rate Limiting Aspects of In-Cloud Scavenging," BNWL-SA-3768, accepted for publication in J. Atmos. Sci., December 1973.

PRESENTATIONS

Hales, J. M., M. T. Dana and M. A. Wolf, "Advances in the Theory and Modeling of Pollutant-Gas Washout," BNWL-SA-4684, Presented at the 3rd International Clean Air Congress, Dusseldorf, Germany, October 8-12, 1973.

Hane, C. E., "A Numerical Model of the Great Plains Squall Line Thunderstorm," BNWL-SA-4684, Presented at the Eighth Conference on Severe Local Storms, Denver, Colorado, October 15-17, 1973.

Rancitelli, L. A., J. A. Cooper, and R. W. Perkins, "Multi-element Characterization of Atmospheric Aerosols by Instrumental Neutron Activation Analysis and X-ray Fluorescence Analysis," BNWL-SA-4671, Presented at FAO/IAEA/WHO Symposium on Nuclear Techniques in Comparative Studies of Food and Environmental Contamination, Otaniemi, Finland, August 27-31, 1973, Accepted for Publication in Proceedings of Conference.

Schwendiman, L. C., "Genesis of an Environmental Impact Statement," BNWL-SA-4860, Presented at the Graduate Seminar, Chemical Engineering Department, Washington State University, Pullman, Washington, December 12, 1973.

Sehmel, G. A., "Influence of Soil Erosion on the Airborne Particle Size Distribution Function," BNWL-SA-4472, Presented at the 66th Annual Meeting of the Air Pollution Control Association, Chicago, Illinois, June 24-28, 1973.

Sehmel, G. A. and S. L. Sutter, "Particle Deposition Rates on a Water Surface as a Function of Particle Diameter and Air Velocity," BNWL-SA-4755, Presented at the International Symposium on the Chemistry of Sea-Air Particulate Exchange Processes, UNESCO, IAPSO/IUGG, Nice, France, October 4-10, 1973.

Sehmel, G. A., "An Evaluation of a High-Volume Cascade Impactor System," BNWL-SA-4677, Presented at the 2nd Joint Conference on the Sensing of Environmental Pollutants, Washington, D.C., December 10-12, 1973.

Slinn, W.G.N., "Precipitation Scavenging Research at Battelle-Northwest," BNWL-SA-4258, Presented at the Rainout-Washout Meeting, Stanford Research Institute, Menlo Park, California, July 24-25, 1973.

Wendell, L. L., "Some Influences of Regional Boundary Layer Flow on Atmospheric Transport and Dispersion," BNWL-SA-4819, Presented at the 2nd Joint Conference on the Sensing of Environmental Pollutants, Washington, D.C., December 10-12, 1973.

Young, J. A., T. M. Tanner, C. W. Thomas, and N. A. Wogman, "The Use of Tracers to Measure Entrainment Around the Sides of Convective Towers in St. Louis," presented at METROMEX Scientific Conference, St. Louis, November 5-9, 1973, (unpublished data).

ORGANIZATION CHARTS

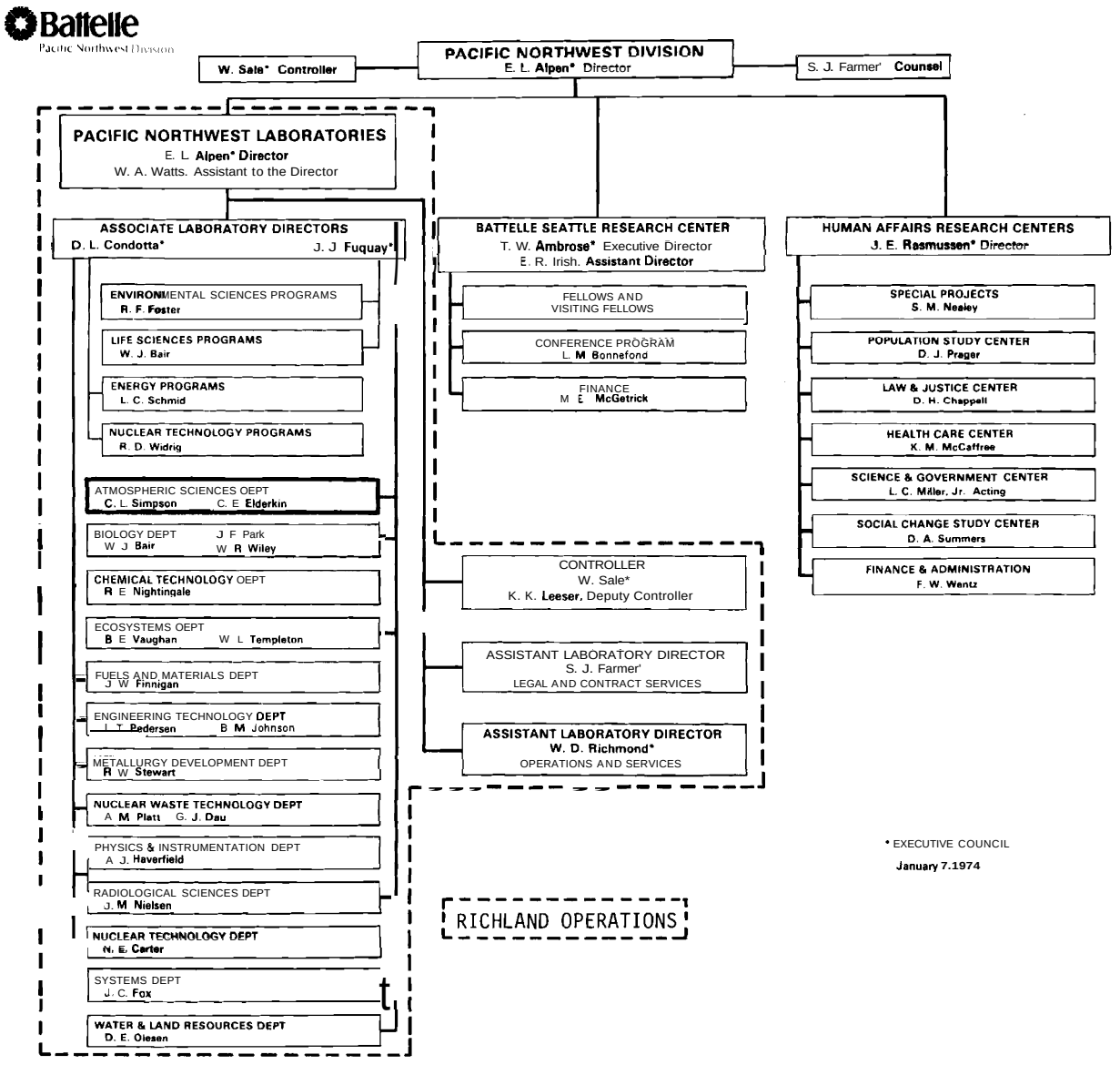
Battelle
Pacific Northwest Division
PACIFIC NORTHWEST DIVISION
E. L. Alpen* Director
W. Sale* Controller
S. J. Farmer' Counsel
PACIFIC NORTHWEST LABORATORIES
E. L. Alpen* Director
W. A. Watts. Assistant to the Director
ASSOCIATE LABORATORY DIRECTORS
D. L. Condotta*
J. J Fuquay*
ENVIRONMENTAL SCIENCES PROGRAMS
R. F. Foster
LIFE SCIENCES PROGRAMS
W. J. Bair
ENERGY PROGRAMS
L. C. Schmid
NUCLEAR TECHNOLOGY PROGRAMS
R. D. Widrig
ATMOSPHERIC SCIENCES OEPT
C. L. Simpson C. E Elderkin
BIOLOGY DEPT
W J. Bair
J F Park
W R Wiley
CHEMICAL TECHNOLOGY OEPT
R E Nightingale
ECOSYSTEMS OEPT
B E Vaughan
W L Templeton
FUELS AND MATERIALS DEPT
J W Finnigan
ENGINEERING TECHNOLOGY DEPT
I. T. Pedersen
B M Johnson
METALLURGY DEVELOPMENT DEPT
R W Stewart
NUCLEAR WASTE TECHNOLOGY DEPT
A M. Platt G. J. Dau
PHYSICS & INSTRUMENTATION DEPT
A J. Haverfield
RADIOLOGICAL SCIENCES DEPT
J. M. Nielsen
NUCLEAR TECHNOLOGY DEPT
N. E. Carter
SYSTEMS DEPT
J. C. Fox
WATER & LAND RESOURCES DEPT
D. E. Olesen
BATTELLE SEATTLE RESEARCH CENTER
T. W. Ambrose* Executive Director
E. R. Irish. Assistant Director
FELLOWS AND VISITING FELLOWS
CONFERENCE PROGRAM
L. M Bonnefond
FINANCE
M E McGetrick
CONTROLLER
W. Sale*
K. K. Leeser, Deputy Controller
ASSISTANT LABORATORY DIRECTOR
S. J. Farmer'
LEGAL AND CONTRACT SERVICES
ASSISTANT LABORATORY DIRECTOR
W. D. Richmond*
OPERATIONS AND SERVICES
RICHLAND OPERATIONS
HUMAN AFFAIRS RESEARCH CENTERS
J. E. Rasmussen* Director
SPECIAL PROJECTS
S. M. Nealey
POPULATION STUDY CENTER
D. J. Prager
LAW & JUSTICE CENTER
D. H. Chappell
HEALTH CARE CENTER
K. M. McCaffree
SCIENCE & GOVERNMENT CENTER
L. C. Miller, Jr. Acting
SOCIAL CHANGE STUDY CENTER
D. A. Summers
FINANCE & ADMINISTRATION
F. W. Wentz
* EXECUTIVE COUNCIL
January 7.1974

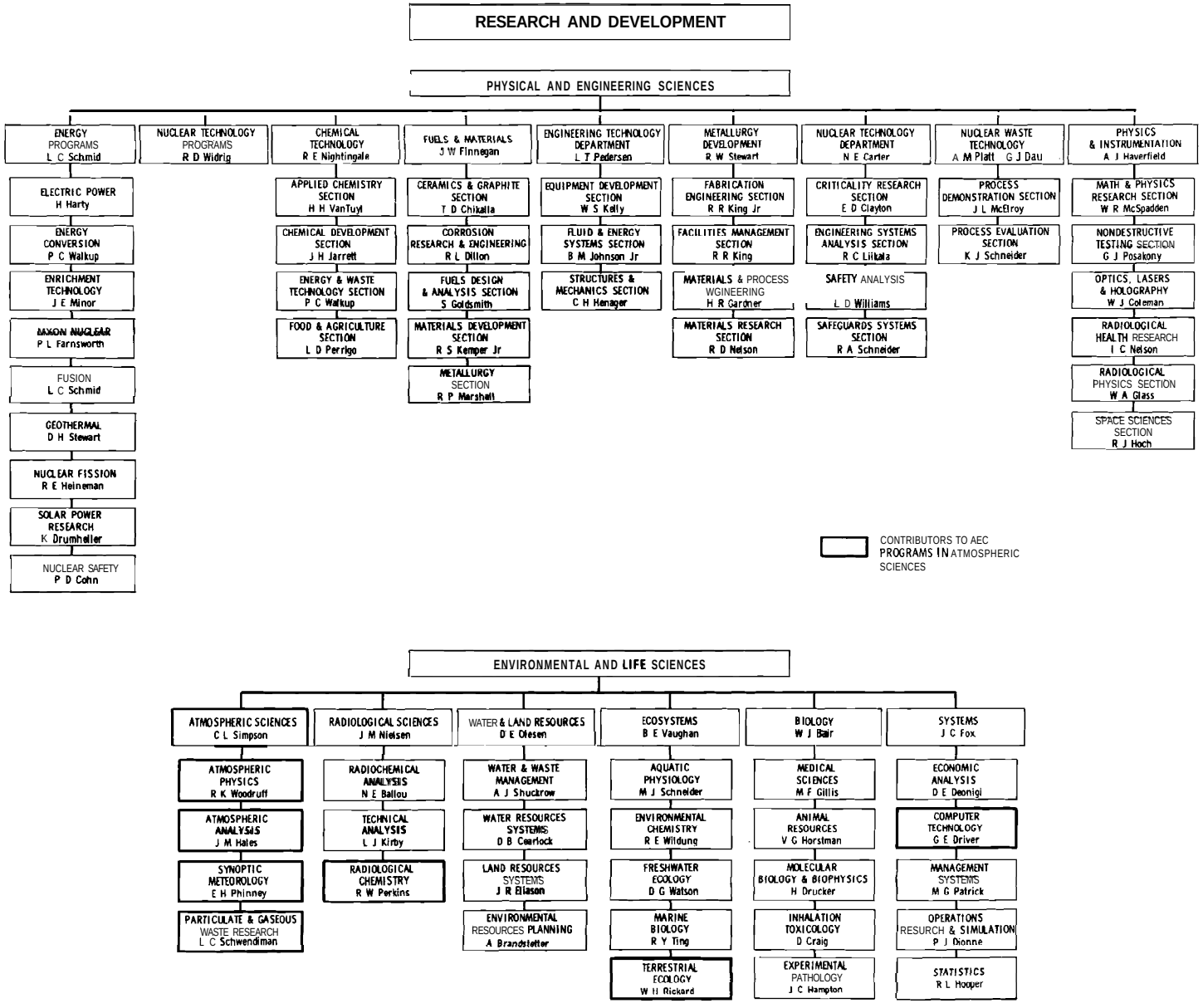
RESEARCH AND DEVELOPMENT
PHYSICAL AND ENGINEERING SCIENCES
ENERGY PROGRAMS L C Schmid
ELECTRIC POWER H Harty
ENERGY CONVERSION P C Walkup
ENRICHMENT TECHNOLOGY J E Minor
AVCO NUCLEAR P L Farnsworth
FUSION L C Schmid
GEOTHERMAL D H Stewart
NUCLEAR FISSION R E Heineman
SOLAR POWER RESEARCH K Drumheller
NUCLEAR SAFETY P D Cohn
NUCLEAR TECHNOLOGY PROGRAMS R D Widrig
CHEMICAL TECHNOLOGY R E Nightingale
APPLIED CHEMISTRY SECTION H H VanTuyl
CHEMICAL DEVELOPMENT SECTION J H Jarrett
ENERGY & WASTE TECHNOLOGY SECTION P C Walkup
FOOD & AGRICULTURE SECTION L D Perrigo
FUELS & MATERIALS J W Finnegan
CERAMICS & GRAPHITE SECTION T D Chikalla
CORROSION RESEARCH & ENGINEERING R L Dillon
FUELS DESIGN & ANALYSIS SECTION S Goldsmith
MATERIALS DEVELOPMENT SECTION R S Kemper Jr
METALLURGY SECTION R P Marshall
ENGINEERING TECHNOLOGY DEPARTMENT L T Pedersen
EQUIPMENT DEVELOPMENT SECTION W S Kelly
FLUID & ENERGY SYSTEMS SECTION B M Johnson Jr
STRUCTURES & MECHANICS SECTION C H Henager
METALLURGY DEVELOPMENT R W Stewart
FABRICATION ENGINEERING SECTION R R King Jr
FACILITIES MANAGEMENT SECTION R R King
MATERIALS & PROCESS WGINEERING H R Gardner
MATERIALS RESEARCH SECTION R D Nelson
NUCLEAR TECHNOLOGY DEPARTMENT N E Carter
CRITICALITY RESEARCH SECTION E D Clayton
ENGINEERING SYSTEMS ANALYSIS SECTION R C Liikala
SAFETY ANALYSIS L D Williams
SAFEGUARDS SYSTEMS SECTION R A Schneider
NUCLEAR WASTE TECHNOLOGY A M Platt G J Dau
PROCESS DEMONSTRATION SECTION J L McElroy
PROCESS EVALUATION SECTION K J Schneider
PHYSICS & INSTRUMENTATION A J Haverfield
MATH & PHYSICS RESEARCH SECTION W R McSpadden
NONDESTRUCTIVE TESTING SECTION G J Posakony
OPTICS, LASERS & HOLOGRAPHY W J Coleman
RADIOLOGICAL HEALTH RESEARCH I C Nelson
RADIOLOGICAL PHYSICS SECTION W A Glass
SPACE SCIENCES SECTION R J Hoch
CONTRIBUTORS TO AEC PROGRAMS IN ATMOSPHERIC SCIENCES
ENVIRONMENTAL AND LIFE SCIENCES
ATMOSPHERIC SCIENCES C L Simpson
ATMOSPHERIC PHYSICS R K Woodruff
ATMOSPHERIC ANALYSIS J M Hales
SYNOPTIC METEOROLOGY E H Phinney
PARTICULATE & GASEOUS WASTE RESEARCH L C Schwendiman
RADIOLOGICAL SCIENCES J M Nielsen
RADIOCHEMICAL ANALYSIS N E Ballou
TECHNICAL ANALYSIS L J Kirby
RADIOLOGICAL CHEMISTRY R W Perkins
WATER & LAND RESOURCES D E Olesen
WATER & WASTE MANAGEMENT A J Shuckrow
WATER RESOURCES SYSTEMS D B Cearlock
LAND RESOURCES SYSTEMS J R Eliason
ENVIRONMENTAL RESOURCES PLANNING A Brandstetter
ECOSYSTEMS B E Vaughan
AQUATIC PHYSIOLOGY M J Schneider
ENVIRONMENTAL CHEMISTRY R E Wildung
FRESHWATER ECOLOGY D G Watson
MARINE BIOLOGY R Y Ting
TERRESTRIAL ECOLOGY W H Rickard
BIOLOGY W J Bair
MEDICAL SCIENCES M F Gillis
ANIMAL RESOURCES V G Horstman
MOLECULAR BIOLOGY & BIOPHYSICS H Drucker
INHALATION TOXICOLOGY D Craig
EXPERIMENTAL PATHOLOGY J C Hampton
SYSTEMS J C Fox
ECONOMIC ANALYSIS D E Deonigi
COMPUTER TECHNOLOGY G E Driver
MANAGEMENT SYSTEMS M G Patrick
OPERATIONS RESURCH & SIMULATION P J Dionne
STATISTICS R L Hooper

ATMOSPHERIC SCIENCES PROGRAM CONTRIBUTORS

O. B. Abbey
K. H. Abel
A. J. Alkezweeny
J. M. Baily
L. L. Baker
T. J. Bander
D. L. Barrett
W. L. Butcher
L. L. Carratt
B. G. Christensen
G. H. Clark
R. L. Conley, Jr.
J. A. Cooper
M. T. Dana
W. E. Davis
J. C. Draper
J. G. Droppo
D. R. Edwards
C. E. Elderkin
O. P. Gifford
F. O. Gladfelder
D. W. Glover
R. K. Hadlock
J. M. Hales
C. E. Hane
V. T. Henderson
W. H. Hodgson
T. W. Horst
D. M. Hughey
C. E. Jenkins
R. E. Kerns
R. F. Lee
R. N. Lee
E. F. Leonard
F. D. Lloyd
J. D. Ludwick
M. C. Miller
J. Mishima
R. F. Myers
D. J. Newland
P. W. Nickola
M. M. Orgill
L. J. Parker
R. W. Perkins
M. R. Petersen
E. H. Phinney
D. C. Powell
J. A. Powell
J. V. Ramsdell
L. A. Rancitelli
J. Rosinski
R. W. Sanders
W. F. Sandusky
L. C. Schwendiman
G. A. Sehmel
C. L. Simpson
W. G. N. Slinn
J. W. Sloot
F. B. Steele
W. A. Stone
S. L. Sutter
T. M. Tanner
C. W. Thomas
J. M. Thorp
R. W. Walters
W. C. Weiner
L. L. Wendell
C. L. Wilkerson
N. A. Wogman
M. A. Wolf
R. K. Woodruff
J. A. Young

DISTRIBUTION

No. of Copies

OFFSITE

20

A. A. Churm
AEC Chicago Patent Group
U.S. Atomic Energy Commission
9800 So. Cass Avenue
Argonne, Illinois 60439

N. F. Barr
Division of Biomedical and Environmental Research
U.S. Atomic Energy Commission
Washington, D.C. 20545

R. W. Beadle
Division of Biomedical and Environmental Research
U.S. Atomic Energy Commission
Washington, D.C. 20545

W. W. Burr
Division of Biomedical and Environmental Research
U.S. Atomic Energy Commission
Washington, D.C. 20545

R. D. Cooper
Division of Biomedical and Environmental Research
U.S. Atomic Energy Commission
Washington, D.C. 20545

C. W. Edington
Division of Biomedical and Environmental Research
U.S. Atomic Energy Commission
Washington, D.C. 20545

R. J. Engelmann
Division of Biomedical and Environmental Research
U.S. Atomic Energy Commission
Washington, D.C. 20545

J. D. Goldstein
Division of Biomedical and Environmental Research
U.S. Atomic Energy Commission
Washington, D.C. 20545

H. H. Hollister
Division of Biomedical and Environmental Research
U.S. Atomic Energy Commission
Washington, D.C. 20545

J. S. Kirby-Smith
Division of Biomedical and Environmental Research
U.S. Atomic Energy Commission
Washington, D.C. 20545

No. of Copies

J. L. Liverman
Division of Biomedical and Environmental Research
U.S. Atomic Energy Commission
Washington, D.C. 20545

W. F. Marlow
Division of Biomedical and Environmental Research
U.S. Atomic Energy Commission
Washington, D.C. 20545

J. E. Miller
Division of Biomedical and Environmental Research
U.S. Atomic Energy Commission
Washington, D.C. 20545

C. L. Osterberg
Division of Biomedical and Environmental Research
U.S. Atomic Energy Commission
Washington, D.C. 20545

D. H. Slade
Division of Biomedical and Environmental Research
U.S. Atomic Energy Commission
Washington, D.C. 20545

J. Swinebroad
Division of Biomedical and Environmental Research
U.S. Atomic Energy Commission
Washington, D.C. 20545

H. Wasson
Division of Biomedical and Environmental Research
U.S. Atomic Energy Commission
Washington, D.C. 20545

J. C. Whitnah
Division of Biomedical and Environmental Research
U.S. Atomic Energy Commission
Washington, D.C. 20545

R. W. Wood
Division of Biomedical and Environmental Research
U.S. Atomic Energy Commission
Washington, D.C. 20545

W. L. Lennemann
AEC Division of Production and Materials Management
U.S. Atomic Energy Commission
Washington, D.C. 20545

No. of Copies

1 Chief, Environmental and Sanitary Engineering Branch
AEC Division of Reactor Development and Technology
U.S. Atomic Energy Commission
Washington, D.C. 20545

204 AEC Technical Information Center

21 W. Singlevich
Air Force Technical Applications Center/TD-4
Patrick Air Force Base
Florida 32925

H. Mueller, Chief
Air Resources Laboratory
National Oceanic and Atmospheric Administration
Research Laboratories
P.O. Box 14985
Las Vegas, Nevada 89114

L. Machta
Air Resources Laboratory
National Oceanic and Atmospheric Administration
8060 13th Street
Silver Spring, Maryland 20910

D. H. Pack (3)
Air Resources Laboratory
National Oceanic and Atmospheric Administration
8060 13th Street
Silver Spring, Maryland 20910

I. Van der Hoven
Air Resources Laboratory
National Oceanic and Atmospheric Administration
8060 13th Street
Silver Spring, Maryland 20910

L. Hodges
Ames Laboratory, USAEC
Iowa State University
Physics Bldg., Rm. A530
Ames, Iowa 50010

P. Frenzen
Argonne National Laboratory
9700 South Cass Avenue
Argonne, Illinois 60439

No. of Copies

F. Gustafson
Argonne National Laboratory
9700 South Cass Avenue
Argonne, Illinois 60439

J. Sedlet
Argonne National Laboratory
9700 South Cass Avenue
Argonne, Illinois 60439

G. A. Briggs
Atmospheric Turbulence and Diffusion Laboratory
NOAA, Oak Ridge, Tennessee 37830

F. I. Gifford
Atmospheric Turbulence and Diffusion Laboratory
NOAA, Oak Ridge, Tennessee 37830

S. R. Hanna
Atmospheric Turbulence and Diffusion Laboratory
NOAA, Oak Ridge, Tennessee 37830

C. A. Mawson
Atomic Energy of Canada Limited
Chalk River, Ontario, Canada

I. Ophel
Atomic Energy of Canada Limited
Chalk River, Ontario, Canada

R. V. Osborne
Atomic Energy of Canada Limited
Chalk River, Ontario, Canada

Librarian
Atomic Energy Research Establishment
Harwell, Berks, England

A.E.J. Eggleton
Atomic Energy Research Establishment
Harwell, Berks, England

D. H. Peirson
Atomic Energy Research Establishment
Harwell, Berks, England

G. H. Clark
Australian AEC
Post Office Coogee
New South Wales, 2034
Australia

No. of Copies

19

D. R. Davy
Australian AEC
Post Office Coogee
New South Wales, 2034
Australia

G. M. Watson
Australian AEC
Post Office Coogee
New South Wales, 2034
Australia

A.W.R. Wilson
Australian AEC
Post Office Coogee
New South Wales, 2034
Australia

V. V. Shirvaikar
Bhabha Atomic Research Center
Health Physics Division
Meteorology Group,
Environmental Studies Section
Bombay - 400 085 India

F. Girardi
C.C.R. EURATOM-ISPRA
(VERESE) Italy

A. Malvicini
C.C.R. EURATOM-ISPRA
(VERESE) Italy

W. Broecker
Columbia University
Lamong Geological Observatory
Palisades, New York 10964

J. Phillips
Defense Nuclear Agency
Fallout Project Officer
Thomas & Greenly Building
Washington, D.C. 20305

A. V. Dodd
Department of Army
U.S. Army Research Office
Environmental Sciences Division
Box CM Duke Station
Durham, North Carolina 27706

M. P. Measures
Department of National Health and Welfare
Radiation Protection Division
Ottawa, Canada

No. of Copies

J. Shapiro
Department of Environmental Health Sciences
School of Public Health
Harvard University
Boston, Massachusetts 02115

Department of Geography
McMaster University
Hamilton, Ontario
Canada L854M1

C. A. Bower
Deseret Test Center
Building 100
Soldier's Circle
Fort Douglas, Utah 84113

L. Jeanmaire
D.P.S. - S.C.S.
B.P. 6, Fontenay-aux-roses
(Seine) France

J. F. Willging
Dow Chemical USA, Rocky Flats Division
Box 888
Golden, Colorado 80401

T. V. Crawford
E. I. du Pont de Nemours and Co.
Savannah River Laboratories
Environmental Analysis and Planning Section
Savannah River Laboratories
Aiken, South Carolina 29801

A. R. Boulogne
E. I. du Pont de Nemours and Co.
Savannah River Plant
Health Physics Section
Aiken, South Carolina 29801

D. D. Dominick
Environmental Protection Agency
Office of Categorical Programs
Washington, D.C. 20460

Stanley M. Greenfield
Environmental Protection Agency
Washington, D.C. 20460

No. of Copies

19 W. Cotton
Experimental Meteorology Laboratory
University of Miami Branch
NOAA
P.O. Box 8044
Coral Gables, Florida 33124

R. I. Sax
Experimental Meteorology Laboratory
University of Miami Branch
NOAA
P.O. Box 8044
Coral Gables, Florida 33124

J. W. Winchester
Florida State University
Department of Oceanography
Tallahassee, Florida 32306

K. Edvarson
Forsvarets Forskningsanstalt
Research Institute of Nation Defense
Avdelning 4, Stockholm 80
Sweden

M. K. Hubbert
Geological Survey of the United States
Washington, D.C. 20460

C. R. Naeser
George Washington University
Washington, D.C. 20460

K. Samsahl
Gesellsch Strehlen Umweltforsch
8042 Neuherberg, Munich
Germany

R. G. Semonin
Illinois State Water Survey
Box 232
Urbana, Illinois 61801

C. E. Junge
Institut fur Chemie
65 Mainz
Saarstrasse 23, Postfach 3060
West Germany

S. Beilke
Institut fur Meteorologie und Geophysik der Johann Wolfgang Goethe Universitat
600 Frankfurt am Main,
Feldbergstrabe 47, Germany

No. of Copies

H. W. Georgii
Institut fur Meteorologie und Geophysik der Johann Wolfgang Goethe Universitat
600 Frankfurt am Main,
Feldbergstrabe 47, Germany

Director, Division of Health, Safety and Waste Management
International Atomic Energy Agency
Vienna 1, Kaerntnerring 11,
Austria

L. Anspaugh
Lawrence Livermore Laboratory
University of California
P.O. Box 808
Livermore, California 94550

R. E. Heft
Lawrence Livermore Laboratory
University of California
P.O. Box 808
Livermore, California 94550

G. H. Higgins
Lawrence Livermore Laboratory
University of California
P.O. Box 808
Livermore, California 94550

J. B. Knox
Lawrence Livermore Laboratory
University of California
P.O. Box 808
Livermore, California 94550

D. W. Wilson
Lawrence Livermore Laboratory
University of California
P.O. Box 808
Livermore, California 94550

S. Barr
Los Alamos Scientific Laboratory
University of California
P.O. Box 1663
Los Alamos, New Mexico 87544

J. W. Healy
Los Alamos Scientific Laboratory
University of California
P.O. Box 1663
Los Alamos, New Mexico 87544

No. of Copies

21 Librarian
Ministry of Agriculture,
Fisheries, & Food
Laboratory
Lowestoft, Suffolk, England

H. W. Kirby
Mound Laboratory
Monsanto Research Corporation
Miamisburg, Ohio 45345

P. LaFleur
National Bureau of Standards
Nuclear Reactor Laboratory
Gaithersburg, Maryland 20760

M. Saiki
National Institute of
Radiological Sciences
250, Kurosuna Cho
Chiba-shi, Japan

M. Suzuki
National Institute of
Radiological Sciences
250, Kurosuna Cho
Chiba-shi, Japan

J. Z. Holland
National Oceanic and
Atmospheric Administration
North Bethesda Office Center
11420 Rockville Heights
Rockville, Maryland 20852

S. I. Auerbach
Oak Ridge National Laboratory
P.O. Box X
Oak Ridge, Tennessee 37830

G. D. O'Kelley
Oak Ridge National Laboratory
P.O. Box X
Oak Ridge, Tennessee 37830

Kathy Sanders
Oak Ridge National Laboratory
P.O. Box X
Oak Ridge, Tennessee 37830

D. Lal
Physical Research Laboratory
Navrangpura
Ahmedabad-9, India

P. K. Kuroda
University of Arkansas
Department of Chemistry
Fayetteville, Arkansas 72701

No. of Copies

R. C. Srivastava
University of Chicago
Laboratory for Atmospheric
Probing
Geophysical Sciences
5734 So. Ellis Avenue
Chicago, Illinois 60637

F. I. Badgley
University of Washington
Department of Atmospheric
Sciences
Seattle, Washington 98195

J. E. Tillman
University of Washington
Department of Atmospheric
Sciences
Seattle, Washington 98195

E. Held
USAEC Directorate Regulatory
Standards
Washington, D.C. 20545

M. F. Milligan
USAEC Directorate Regulatory
Standards
Washington, D.C. 20545

E. P. Hardy, Jr.
USAEC Health and Safety
Laboratory
376 Hudson Street
New York, New York 10012

J. H. Harley
USAEC Health and Safety
Laboratory
376 Hudson Street
New York, New York 10012

P. W. Krey
USAEC Health and Safety
Laboratory
376 Hudson Street
New York, New York 10012

C. W. Sill
USAEC Idaho Operations
Office
Idaho Falls, Idaho 83401

C. V. Theis
U.S. Geological Survey
P.O. Box 4369
Albuquerque, New Mexico 87106

No. of Copies

3 B. Baskin
Wayne County Department of Health
Air Pollution Control Division
1311 East Jefferson
Detroit, Michigan 48207

R. L. Dobson
World Health Organization
Geneva, Switzerland

Librarian
World Meteorological Organization
Geneva, Switzerland

ONSITE

1 AEC/RL Patent Attorney
R. M. Poteat

3 AEC Richland Operations Office
P.F.X. Dunigan, Jr.
N. W. Fraser
B. J. Melton

Atlantic Richfield Hanford Co.
D. J. Brown
L. E. Bruns
R. E. Isaacson
T. R. McKenzie

1 United Nuclear Industries, Inc.
P. C. Jerman

1 Hanford Environmental Health Foundation
P. A. Fuqua

No. of Copies

193 Battelle-Northwest.
E. L. Alpen
W. J. Bair
N. E. Ballou
J. P. Corley
G. L. Culp
G. M. Dalen
R. L. Dillon
R. D. Dierks
J. J. Fuquay
A. G. Gibbs
J. M. Hales (50)
H. V. Larson
R. H. Moore
J. M. Nielsen
T. P. O'Farrell
D. E. Olesen
J. F. Park
R. W. Perkins
E. H. Phinney
A. K. Postma
L. C. Schwendiman (20)
W.G.N. Slinn
W. H. Swift
C. L. Simpson (35)
J. A. Strand
W. L. Templeton
R. C. Thompson
C. M. Unruh
B. E. Vaughan
E. C. Watson
N. A. Wogman
R. K. Woodruff (50)
J. A. Young
Biology Library (2)
Technical Information (5)
Technical publications (2)